Advances in Clinical and Experimental Medicine

MONTHLY ISSN 1899-5276 (PRINT) ISSN 2451-2680 (ONLINE) www.advances.umed.wroc.pl

2021, Vol. 30, No. 4 (April)

Impact Factor (IF) – 1.514
Ministry of Science and Higher Education – 40 pts.
Index Copernicus (ICV) – 152.95 pts

Wroclaw Medical University

Advances
in Clinical and Experimental
Medicine

Advances
in Clinical and Experimental Medicine

ISSN 1899-5276 (PRINT) ISSN 2451-2680 (ONLINE) www.advances.umed.wroc.pl

MONTHLY 2021
Vol. 30, No. 4
(April)

Advances in Clinical and Experimental Medicine (*Adv Clin Exp Med*) publishes high quality original articles, research in progress and reviews of recognized scientists that deal with all clinical and experimental medicine.

Editorial Office
ul. Marcinkowskiego 2–6
50-368 Wrocław, Poland
Tel.: +48 71 784 11 36
E-mail: redakcja@umed.wroc.pl

Publisher
Wroclaw Medical University
Wybrzeże L. Pasteura 1
50-367 Wrocław, Poland

© Copyright by Wroclaw Medical University, Wrocław 2021

Online edition is the original version of the journal

Editor-in-Chief
Prof. Donata Kurpas

Deputy Editor
Prof. Wojciech Kosmala

Managing Editor
Paulina Piątkowska

Statistical Editors
Prof. Dorota Diakowska
Dr. Lesław Rusiecki
Dr. Dominik Marciniak
Dr. Andrzej Dąbrowski

Manuscript editing
Paulina Piątkowska, Marek Misiak

Scientific Committee
Prof. Sabine Bährer-Kohler
Prof. Antonio Cano
Prof. Breno Diniz
Prof. Erwan Donal
Prof. Chris Fox
Prof. Naomi Hachiya
Prof. Carol Holland
Prof. Markku Kurkinen
Prof. Christos Lionis
Prof. Raimundo Mateos
Prof. Zbigniew W. Ras
Prof. Jerzy W. Rozenblit
Prof. Silvina Santana
Prof. James Sharman
Prof. Jamil Shibli
Prof. Michal Toborek
Prof. László Vécsei
Prof. Cristiana Vitale

Section Editors

Basic Sciences
Dr. Mateusz Olbromski

Biochemistry
Prof. Małgorzata Krzystek-Korpacka

Dentistry
Prof. Marzena Dominiak
Prof. Tomasz Gedrange
Prof. Jamil Shibli

Dermatology
Prof. Jacek Szepietowski

Emergency Medicine, Innovative Technologies
Prof. Jacek Smereka

Gynecology and Obstetrics
Prof. Olimpia Sipak-Szmigiel

Histology and Embryology
Prof. Marzenna Podhorska-Okołów

Intensive Therapy and Anesthesiology
Assoc. Prof. Barbara Adamik
Assoc. Prof. Wiesława Duszyńska
Prof. Waldemar Goździk

Internal Medicine

Angiology
Dr. Angelika Chachaj

Cardiology
Prof. Wojciech Kosmala
Dr. Daniel Morris

Endocrinology
Prof. Marek Bolanowski

Gastroenterology
Assoc. Prof. Katarzyna Neubauer

Hematology
Prof. Dariusz Wołowiec
Nephrology and Transplantology
Assoc. Prof. Dorota Kamińska
Assoc. Prof. Krzysztof Letachowicz
Pulmonology
Prof. Elżbieta Radzikowska

Microbiology
Prof. Marzenna Bartoszewicz
Assoc. Prof. Adam Junka

Molecular Biology
Dr. Monika Bielecka
Prof. Jolanta Saczko
Dr. Marta Sochocka

Neurology
Assoc. Prof. Magdalena Koszewicz
Assoc. Prof. Anna Pokryszko-Dragan
Dr. Masaru Tanaka

Oncology
Dr. Marcin Jędryka
Prof. Lucyna Kępka
Gynecological Oncology
Dr. Marcin Jędryka

Ophthalmology
Prof. Marta Misiuk-Hojło

Orthopedics
Assoc. Prof. Paweł Reichert

Otolaryngology
Assoc. Prof. Tomasz Zatoński

Pediatrics
Pediatrics, Metabolic Pediatrics, Clinical Genetics, Neonatology, Rare Disorders
Prof. Robert Śmigiel
Pediatric Nephrology
Prof. Katarzyna Kiliś-Pstrusińska
Pediatric Oncology and Hematology
Assoc. Prof. Marek Ussowicz

Pharmaceutical Sciences
Assoc. Prof. Maria Kepinska
Prof. Adam Matkowski

Pharmacoeconomics, Rheumatology
Dr. Sylwia Szafraniec-Buryło

Psychiatry
Prof. Istvan Boksay
Prof. Jerzy Leszek

Public Health
Prof. Monika Sawhney
Prof. Izabella Uchmanowicz

Qualitative Studies, Quality of Care
Prof. Ludmiła Marcinowicz

Rehabilitation
Prof. Jakub Taradaj

Surgery
Assoc. Prof. Mariusz Chabowski
Prof. Renata Taboła

Telemedicine, Geriatrics, Multimorbidity
Assoc. Prof. Maria Magdalena Bujnowska-Fedak

Editorial Policy

Advances in Clinical and Experimental Medicine (Adv Clin Exp Med) is an independent multidisciplinary forum for exchange of scientific and clinical information, publishing original research and news encompassing all aspects of medicine, including molecular biology, biochemistry, genetics, biotechnology and other areas. During the review process, the Editorial Board conforms to the "Uniform Requirements for Manuscripts Submitted to Biomedical Journals: Writing and Editing for Biomedical Publication" approved by the International Committee of Medical Journal Editors (www.ICMJE.org/). The journal publishes (in English only) original papers and reviews. Short works considered original, novel and significant are given priority. Experimental studies must include a statement that the experimental protocol and informed consent procedure were in compliance with the Helsinki Convention and were approved by an ethics committee.

For all subscription-related queries please contact our Editorial Office:
redakcja@umed.wroc.pl

For more information visit the journal's website:
www.advances.umed.wroc.pl

Pursuant to the ordinance No. 134/XV R/2017 of the Rector of Wroclaw Medical University (as of December 28, 2017) from January 1, 2018 authors are required to pay a fee amounting to 700 euros for each manuscript accepted for publication in the journal Advances in Clinical and Experimental Medicine.

Indexed in: MEDLINE, Science Citation Index Expanded, Journal Citation Reports/Science Edition, Scopus, EMBASE/Excerpta Medica, Ulrich's™ International Periodicals Directory, Index Copernicus

Typographic design: Monika Kolęda, Piotr Gil
DTP: Wydawnictwo UMW
Cover: Monika Kolęda
Printing and binding: ARGI SC

Advances
in Clinical and Experimental Medicine

MONTHLY 2021, Vol. 30, No. 4 (April)

ISSN 1899-5276 (PRINT)
ISSN 2451-2680 (ONLINE)
www.advances.umed.wroc.pl

Contents

Original papers

Multicenter study

Reviews

© Copyright by Wroclaw Medical University, Wrocław 2021

Serum hepatitis B virus ribonucleic acid and its influencing factors in chronic hepatitis B

Yifeng Zhou[A–C,F], Yameng Peng[B,C,F], Hao Yuan[A,D–F], Zhenyi Long[B,C,F], Sixian Wu[B,C,F], Jiping Yang[B,C,F]

Hunan Provincial People's Hospital, The First Affiliated Hospital of Hunan Normal University, Changsha, China

A – research concept and design; B – collection and/or assembly of data; C – data analysis and interpretation;
D – writing the article; E – critical revision of the article; F – final approval of the article

Advances in Clinical and Experimental Medicine, ISSN 1899–5276 (print), ISSN 2451–2680 (online) *Adv Clin Exp Med*. 2021;30(4):361–367

Address for correspondence
Hao Yuan
E-mail: yuanhao696@sina.com

Funding sources
This work was supported by Health Commission of Hunan Provincial Research Project (C2019052)

Conflict of interest
All authors report no potential conflicts of interest with regard to this work

Received on June 1, 2020
Reviewed on June 4, 2020
Accepted on December 17, 2020

Published online on April 30, 2021

Abstract

Background. Hepatitis B virus (HBV) remains one of the most serious and prevalent health problems in the world.

Objectives. To determine the serum hepatitis B virus (HBV) RNA levels in patients with chronic hepatitis B (CHB) with low HBV DNA levels and analyze the influencing factors.

Materials and methods. Seventy-two CHB patients with low HBV DNA levels were enrolled and divided into 2 groups according to hepatitis B e antigen (HBeAg) status; their age, sex, the incidence of HBV RNA level < lower limit of detection (LLD), and serum alanine aminotransferase (ALT), aspartate aminotransferase (AST), quantitative determination of HBsAg (qHBsAg), HBV DNA, and HBV RNA levels were compared. The factors influencing serum HBV RNA levels < LLD and the correlation between serum HBV RNA levels, and serum ALT, AST, qHBsAg and HBV DNA levels were analyzed.

Results. In HBeAg-positive patients, serum AST, qHBsAg and HBV RNA levels were higher, and serum HBV DNA levels and incidence of HBV RNA < LLD were lower than those in HBeAg-negative patients ($p < 0.05$). Multivariate linear regression analysis revealed that HBeAg is a factor that significantly influences serum HBV RNA levels in patients with CHB ($p < 0.05$). Multivariate logistic regression analysis indicated that HBeAg and qHBsAg are factors that influence serum HBV RNA levels < LLD in patients with CHB. In HBeAg-positive patients, serum HBV RNA levels were positively correlated with qHBsAg and HBeAg.

Conclusions. The serum HBV RNA levels in CHB patients with low HBV DNA levels varied according to HBeAg status. The HBeAg is a factor that significantly influences serum HBV RNA levels in patients with CHB, while HBeAg and qHBsAg are factors that significantly influence serum HBV RNA levels < LLD in patients with CHB.

Key words: chronic hepatitis B, DNA, hepatitis B virus, pre-gene RNA, serum markers

Cite as
Zhou Y, Peng Y, Yuan H, Long Z, Wu S, Yang J. Serum hepatitis B virus ribonucleic acid and its influencing factors in chronic hepatitis B. *Adv Clin Exp Med*. 2021;30(4):361–367. doi:10.17219/acem/131756

DOI
10.17219/acem/131756

Copyright
© 2021 by Wroclaw Medical University
This is an article distributed under the terms of the Creative Commons Attribution 3.0 Unported (CC BY 3.0) (https://creativecommons.org/licenses/by/3.0/)

Background

Hepatitis B virus (HBV) infection remains one of the most serious and prevalent health problems in the world.[1] Every year, 0.5–1.2 million patients die from liver decompensation, liver cirrhosis, liver failure, hepatocellular carcinoma, and other HBV-related diseases.[2,3] The underlying cause of persistent HBV infection is the constant presence of covalently closed circular DNA (cccDNA).[4] Further exacerbating the issue, existing serum markers and virological replication molecular assays are unable to accurately detect the presence of cccDNA in hepatocytes. Studies have demonstrated that despite the low concentration of HBV DNA in the serum of chronic hepatitis B (CHB) patients, cccDNA still actively replicates in vivo. This is evident through the observation of enhanced inflammation and fibrosis reported in liver histology.[5] The monitoring of cccDNA in liver tissue requires an invasive liver biopsy, which is difficult to continuously implement in clinical practice. Additionally, the uneven distribution of cccDNA in liver tissue and the presence of relaxed circular double-stranded DNA (rcDNA) also increase the difficulty of detecting HBV.[6]

In 2017, The European Association for the Study of the Liver Clinical Practice Guidelines defined serum HBV RNA as a novel marker and pointed out that pre-gene RNA (pgRNA), a major component of HBV RNA, is released into the blood as a virus-like particle.[1] The pgRNA is a direct transcript of cccDNA that accurately reflects the presence of cccDNA in hepatocytes. The ability to detect serum HBV RNA will provide more direct evidence of the status of viral replication and its therapeutic efficacy in patients with CHB.[7] To this end, this study explores the presence and influencing factors of serum HBV RNA at low replication levels in patients with CHB and aims to provide new ideas for the clinical diagnosis and treatment of CHB.

Objectives

This study explores the presence and influencing factors of serum HBV RNA at low replication levels in patients with CHB and aims to provide new ideas for the clinical diagnosis and treatment of CHB.

Materials and methods

Study criteria

Our research was a retrospective case-control study. Inclusion criteria were as follows: patients who satisfy the relevant diagnostic criteria in the Guidelines for Prevention and Control of Chronic Hepatitis B (2015 Edition) (hereinafter referred to as the "Prevention and Control Guidelines"). These criteria include: confirmed HBV infection for at least 6 months, and serum HBV DNA < 1.0×10^4 U/mL. Exclusion criteria were as follows: the diagnosis of other Hepadnaviridae infections, alcoholic liver disease, nonalcoholic fatty liver disease, drug-induced liver disease, liver injury due to metabolic and autoimmune liver disease or other causes, HIV-infected patients, and patients with primary biliary cirrhosis.[8]

Ethics approval

This study was performed according to the Declaration of Helsinki and approved by the Clinical Research Ethics Committee of Hunan Provincial People's Hospital (Ethical Application Ref: 2018S77), and each patient provided written informed consent before participation in the study. The research was conducted in compliance with institutional review board regulations.

Subjects

Patients with CHB who were definitively diagnosed in our hospital from May 2018 to July 2018 and who met the study criteria were selected. All patients had low levels of serum HBV DNA and were treated according to the Prevention and Control Guidelines[8] after admission.

Methodology

Sample collection and processing

Five milliliters of fasting venous blood was collected in the morning and added to an anticoagulation tube. After centrifugation at 4000 rpm for 10 min (centrifugation radius: 10 cm), the supernatant was collected, dispensed into 1.5-mL enzyme-free Eppendorf (EP) tubes, and stored at −80°C for further analysis.

Serum HBV DNA detection

The SLAN Real-Time PCR Detection System 96 fluorescence quantitative detector (Shanghai Hongshi Medical Technology Co., Ltd., Shanghai, China) was used to detect serum HBV DNA. The reagent was purchased from Hunan Sansure Biotech Inc. (Changsha, China) and the approved by the National Medical Products Administration (NMPA) quantitative polymerase chain reaction (qPCR) method was applied. Certified laboratory staff performed the assay in accordance with the instructions. The lower limit of detection (LLD) of the kit was 1.0×10^2 U/mL.

Detection of HBV serological markers (HBV-M)

A fully automatic chemiluminescence immunoassay analyzer, Caris200 (Beijing Wantai BioPharm Co., Ltd., Beijing, China), was used to detect HBV serological markers

(HBV-M). The reagent was a hepatitis B diagnostic kit purchased from Xiamen innoDx Biotechnology Co., Ltd (Xiamen, China). Detection was performed using the chemiluminescence microparticle immunoassay. The effective linear range of detection of hepatitis B surface antigen (HBsAg) was 0.05–250 U/mL. Hepatitis B e antigen (HBeAg) was qualitatively detected.

Detection of liver function indicators

The Beckman 5800 fully automatic biochemical analyzer and the reagent purchased from Shanghai Kehua Bio-Engineering co., Ltd (Shanghai, China) were used to detect liver function. Serum alanine aminotransferase (ALT) and aspartate aminotransferase (AST) were used as observation indicators; both were detected using the dual-reagent rate method.

Serum HBV RNA extraction and purification

For HBV RNA detection, the HBV pre-genomic RNA (pgRNA) from all samples was extracted and purified using a nucleic acid extraction (DNA/RNA) or purification kit (magnetic beads method) from Sansure Biotech Inc. (Registration certificate for medical device No. 20173401141).

The detailed protocol was as follows: 200 µL of each serum sample, 600 µL of solution 1 and 100 µL of solution 2 were added into EP tube and heated up to 60°C for 10 min. The samples were then placed at room temperature for 10 min. All tubes were placed on a magnetic rack for 3 min, after which the supernatant was discarded. Next, 600 µL of solution 3 and 200 µL of solution 4 were added to each tube. The tubes were then briefly vortexed and centrifuged. Then, they were placed on the magnetic rack for 3 min, after which the supernatant was carefully discarded. Next, 50 µL of elution solution was added to each tube. The tubes were then vortexed and centrifuged briefly for 3 min. Next, they were placed on a magnetic rack at room temperature for 10 min. The solution was then transferred to new EP tubes and stored at 4°C for further use. Before HBV RNA detection, the purified nucleic acid was treated with DNase. Briefly, 16 µL of each purified nucleic acid solution and 4 µL of DNase solution were added to each PCR tube. The tubes were sealed and placed at 37°C for 30 min and then at 75°C for 10 min. DNase-treated solutions were used for further HBV RNA detection.

Serum HBV RNA detection

The serum HBV RNA detection was processed using Hepatitis B Viral pregeno miRNA Quantitative Fluorescence Diagnostic Kit (PCR-Fluorescence Probing) from Sansure Biotech Inc. The kit's LOD was reported at 50 copies/mL.

The detailed protocol was as follows: 30 µL of HBV RNA master mix was added to each PCR tube. Then, 20 µL of purified and DNase-treated nucleic acid sample solution, purified HBV RNA quantitative reference RNA (A-B-C-D), as well as negative and positive RNA controls, were added to the PCR tubes. All PCR tubes were carefully sealed and placed into the Real-Time PCR Detection Systems (including Slan 96P (Shanghai Hongshi Medical Technology Co., Ltd., China) and ABI 7500 (Applied Biosystem, USA). The PCR program was run as follows: 95°C for 1 min, 60°C for 30 min and 95°C for 1 min, and followed as 45 thermocycles as 95°C for 15 s and 60°C for 30 s with fluorescence detection. The results were analyzed according to the kit user manual.

Observation indicators

To compare patient age, sex, the incidence of HBV RNA below the LLD, as well as serum ALT, AST, qHBsAg, HBV DNA, and HBV RNA levels, all patients were divided into HBeAg-positive and HBeAg- negative patients according to their HBeAg status. The serum HBV RNA levels in patients with CHB and factors which influence serum HBV RNA levels that were below the LLD were analyzed. The correlation of serum HBV RNA levels with serum ALT, AST, qHBsAg, and serum HBV DNA levels was also analyzed.

Statistical methods

Data were processed using the SPSS v. 19.0 statistical software (IBM Corp., Armonk, USA). Statistical graphs were plotted using GraphPad Prism 6.0 (GraphPad Software, San Diego, USA). Logarithmic transformation (log) was adopted for all laboratory data used for serum detection of patients with CHB. Quantitative data that satisfied normal distribution were expressed by $x \pm s$, and the paired t-test was used for comparison between both groups. Pearson correlation analysis was applied; non-normally distributed measurement data were expressed using M (P25, P75) after logarithmic transformation. The Mann–Whitney U test was used for intergroup comparison, and Spearman's rank correlation analysis was applied; enumeration data were expressed as percentages. The χ^2 test was used for intergroup comparison; linear regression analysis and binary logistic regression analysis were used to analyze the influencing factors of HBV RNA. A p-value <0.05 was used to indicate statistical significance.

Results

Seventy-two cases of CHB patients with low levels of HBV DNA were included in this study. The average age of the patients was 49.49 ±13.539 years. Among them, 46 were men and 26 were women. Among the 72 patients, 12 were HBeAg-positive and 60 were HBeAg-negative. There was no statistically significant difference in terms

Table 1. Comparison of clinical data between HBeAg-positive and HBeAg-negative patients

Variable	HBeAg-positive	HBeAg-negative	Test statistic	p-value
N	12	60	–	–
Age [years]	40.4 ±10.5	51.3 ±13.4	–2.649†	0.01
Sex (male/female)	9/3	37/23	0.301‡	0.58
ALT (M (P25, P75)) [U/L]	1.74 (1.44, 1.95)	1.39 (1.19, 1.70)	210§	0.23
AST (M (P25, P75)) [U/L]	1.63 (1.52, 1.94)	1.40 (1.27, 1.64)	191§	0.011
qHBsAg (M (P25, P75)) [U/mL]	3.45 (1.46, 3.77)	2.74 (1.34, 3.23)	216§	0.03
HBV DNA (M (P25, P75)) [U/mL]	2.06 (2.00, 2.88)	2.93 (2.68, 3.19)	174§	0.005
HBV RNA (M (P25, P75)) [U/mL]	2.39 (1.70, 4.69)	1.70 (1.70, 1.74)	212§	0.007
HBV RNA below the LLD, n (%)	5 (42.0)	44 (73.0)	4.613‡	0.032

Data are expressed as means ± standard deviation (SD). † t-value; ‡ χ^2-value; § Z-value; HBV – hepatitis B virus; HBeAg – hepatitis B e antigen; LLD – lower limit of detection; ALT – alanine aminotransferase; AST – aspartate aminotransferase; qHBsAg – quantitative determination of HBsAg.

of sex or serum ALT levels between HBeAg-positive and HBeAg-negative patients ($p > 0.05$). HBeAg-positive patients were younger than HBeAg-negative patients; their serum AST, qHBsAg and HBV RNA levels were higher than those in HBeAg-negative patients, while their serum HBV DNA levels and incidence of HBV RNA below the LLD were lower than those in HBeAg-negative patients. These differences were statistically significant ($p < 0.05$, Table 1).

To perform the univariate linear regression analysis, age (assigned value: continuous variable), sex (men = 1, women = 2), ALT (assigned value: continuous variable), AST (assigned value: continuous variable), qHBsAg (assigned value: continuous variable), HBeAg (assigned value: HBeAg-positive = 0, HBeAg-positive = 1), and HBV DNA (assigned value: continuous variable) were taken as independent variables. Further, serum HBV RNA (assigned value: continuous variable) was taken as the dependent variable. The results demonstrated that age, AST, qHBsAg, and HBeAg are factors that significantly influence serum HBV RNA levels in patients with CHB ($p < 0.05$). Independent variables with $p < 0.20$ in the univariate analysis were included in the multivariate linear regression analysis. The results demonstrated that HBeAg is a factor that significantly influences serum HBV RNA levels in patients with CHB ($p < 0.05$, Table 2).

To perform multivariate logistic regression analysis of the factors which influence serum HBV RNA levels to be below the LLD, age (assigned value: continuous variable), sex (men = 1, women = 2), ALT (assigned value: continuous variable), AST (assigned value: continuous variable), qHBsAg (assigned value: continuous variable), HBeAg (assigned value: HBeAg-positive = 0, HBeAg-positive = 1), and HBV DNA (assigned value: continuous variable) were taken as independent variables. Whether serum HBV RNA was below the LLD (assigned value: yes = 1, no = 0) was taken as the dependent variable. The results demonstrated that HBeAg (odds ration (OR) = 3.85, 95% confidence interval (95% CI) [1.068, 13.880], $p < 0.039$) and qHBsAg (OR = 1.682, 95% CI [1.055, 2.681], $p < 0.029$) are factors which significantly influence serum HBV RNA levels to be below the LLD in patients with CHB.

Serum HBV RNA in patients with CHB was positively correlated with qHBsAg ($r = 0.322$, $p = 0.006$) (Fig. 1A) and HBeAg ($r = 0.235$, $p = 0.047$) (Fig. 1B) but was not correlated with ALT ($r = 0.038$, $p = 0.752$), AST ($r = 0.189$, $p = 0.557$) or HBV DNA ($r = 0.058$, $p = 0.629$).

In HBeAg-positive patients, serum HBV RNA levels were positively correlated with qHBsAg ($r = 0.848$; $p \leq 0.001$) (Fig. 1C) and HBeAg ($r = 0.725$; $p = 0.008$) (Fig. 1D) but were not correlated with ALT ($r = 0.051$, $p = 0.876$), AST

Table 2. Univariate and multivariate linear regression analysis of factors influencing serum HBV RNA levels in CHB patients

Variable	B	Univariate analysis		p-value	Multivariable analysis			
		SD	t-value		B	SD	t-value	p-value
Age	–0.024	0.009	–2.770	0.007	–0.012	0.009	–1.368	0.247
Sex	–0.256	0.254	–1.007	0.317	–	–	–	–
ALT	0.292	0.300	0.976	0.332	–	–	–	–
AST	0.651	0.388	1.678	0.098	0.373	0.368	1.014	0.314
qHBsAg	0.273	0.092	2.956	0.004	0.167	0.093	1.795	0.077
HBeAg	1.164	0.299	3.897	<0.001	0.837	0.318	2.634	0.010
HBV DNA	0.05	0.224	0.222	0.825	–	–	–	–

HBV – hepatitis B virus; CHB – chronic hepatitis B; SD – standard deviation; HBeAg – hepatitis B e antigen; ALT – alanine aminotransferase; AST – aspartate aminotransferase; qHBsAg – quantitative determination of HBsAg.

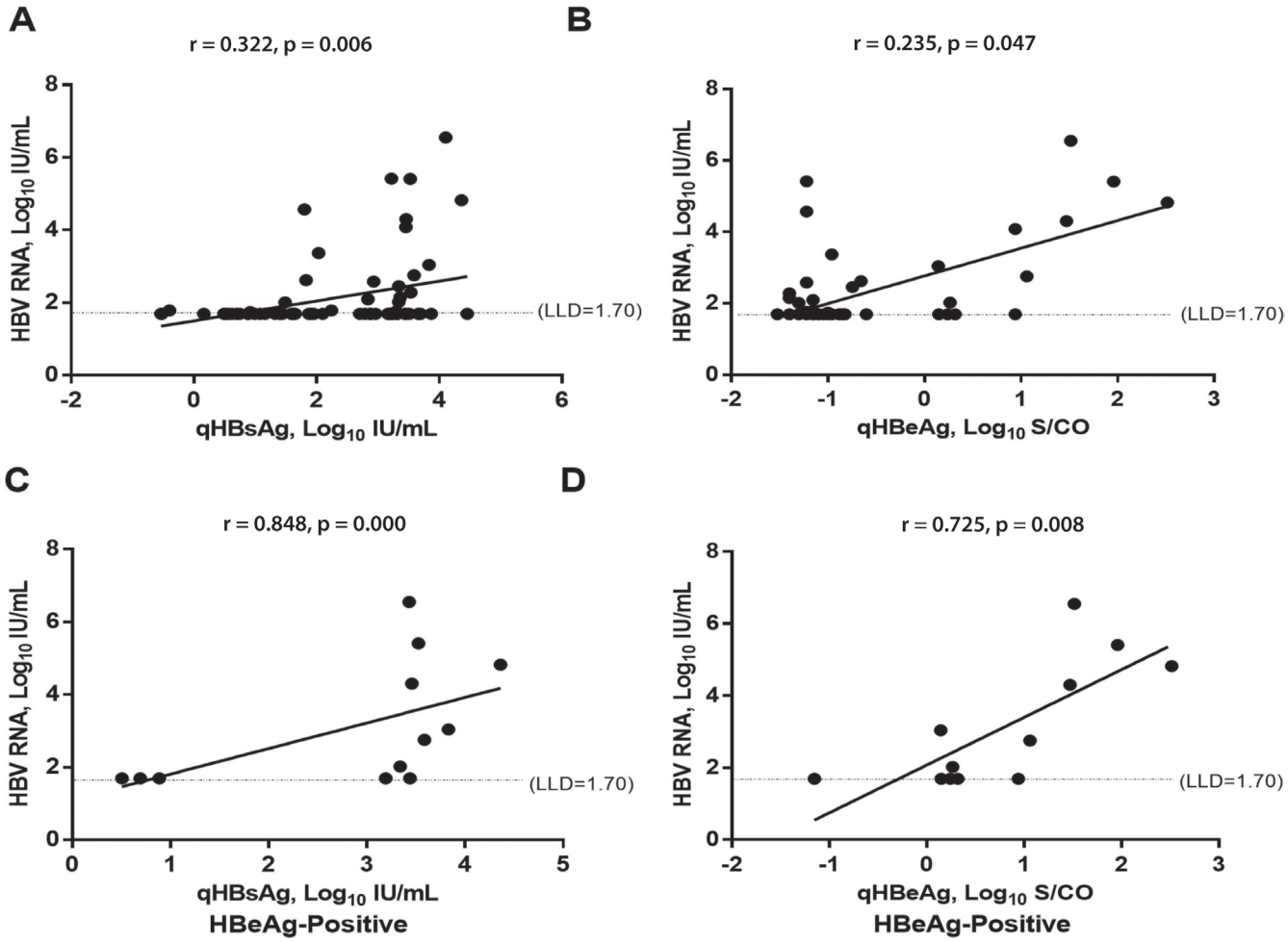

Fig. 1. Correlation of HBV RNA with serum levels of qHBsAg and HBeAg. The LLD for the HBV RNA PCR is 50 U/mL (1.70 $\log_{10}$ U/mL)

(r = 0.046, p = 0.702) or HBV DNA (r = 0.383, p = 0.219). In HBeAg-negative patients, serum HBV RNA was not significantly correlated with qHBsAg (r = 0.151, p = 0.251), HBeAg (r = 0.083, p = 0.529), ALT (r = −0.020, p = 0.878), AST (r = −0.080, p = 0.542), or HBV DNA (r = 0.145, p = 0.268).

Discussion

The current treatment of patients with CHB remains challenging, with difficulties in drug discontinuation and easy rebound among the issues. Existing serological markers do not accurately reflect the existence of cccDNA in hepatocytes.[9] In 1996, when studying whether HBV can infect human peripheral blood mononuclear cells, Kock et al.[10] detected HBV RNA in the serum of patients with CHB. In recent years, both national and international studies have conducted extensive research on continuously improving and optimizing HBV detection methods, and further exploring the clinical implications of serum HBV RNA.[7,9,11,12]

The Prevention and Control Guidelines suggest that the ideal treatment-endpoint for HBeAg-positive and HBeAg-negative patients with CHB is the clinical observation of sustained HBsAg clearance, with or without seroconversion after drug withdrawal.[8] However, HBsAg cannot accurately reflect the replication of HBV in hepatocytes. Furthermore, the HBeAg-negative conversion rate is not an ideal marker of CHB pathogenesis during the actual treatment. This study compared serum HBV RNA levels in HBeAg-positive and HBeAg-negative patients with CHB with low levels of HBV DNA replication and found significant differences in serum HBV RNA levels between both groups. The results of this study demonstrated that HBeAg-positive patients were younger than HBeAg-negative patients; this was similar to the results obtained by Yang et al.[13] In that study, the authors suggested that the incidence of negative HBeAg correlated with age. Further analysis of potential influencing factors demonstrated that HBeAg is a factor that significantly influences serum HBV RNA levels in patients with CHB. Further, we observed that serum HBV RNA was positively correlated with HBeAg in patients with CHB, and serum HBV RNA levels were positively correlated with HBeAg in HBeAg-positive patients. These data indicate that serum HBV RNA can accurately reflect the replication status of the virus

in patients with CHB. In a previous study, Huang et al.[14] found that serum HBV RNA levels may be used as a serological marker for predicting the seroconversion of HBeAg during treatment with nucleosides and nucleotides.[15]

While, to a certain extent, HBV DNA can reflect the replication activity of cccDNA in vivo, the low detection rate of HBV RNA is inconsistent with this phenomenon.[5] However, serum HBV DNA below the lower limit of detection only indicates that the reverse transcription process of the virus is inhibited and cannot reflect the transcriptional status of cccDNA. After the reverse transcription process is inhibited, cccDNA still produces progeny virus in the form of HBV RNA virus-like particles.[5] Therefore, following drug withdrawal on the premise of existing virological response, the rates of disease rebound, and recurrence are higher.[5,12,16,17] The results of this study demonstrate that there was no correlation between serum HBV DNA and HBV RNA in patients with CHB, and that serum HBV DNA was not correlated with HBV RNA in patients with different HBeAg status. These data indicate that even when HBV DNA is at a low level or below the lower limit of detection, cccDNA maintains its replication activity which results in HBV RNA being detected at a relatively high level. Thus, serum HBV RNA can reflect the presence of cccDNA more accurately than serum HBV DNA, thereby providing more powerful evidence for the efficacy of antiviral treatment in patients with CHB.[5,18,19]

The incidence of serum HBV RNA below the lower limit of detection is higher in HBeAg-negative patients than in HBeAg-positive patients. This may be due to the higher cccDNA transcriptional activity in HBeAg-positive patients compared to HBeAg-negative patients, which is consistent with findings from other studies.[20] Multivariate logistic regression analysis revealed that qHBsAg and HBeAg are factors that influence serum HBV RNA below the lower limit of detection in patients with CHB. In this study, the total detection rate of serum HBV RNA in patients with CHB was 32% (23/72), which was similar to the detection rate in the study by Huang et al.[12] However, the detection rate in the study conducted by Li et al.[21] was 85.3%. Among other factors, this difference may be due to sample selection, demographic characteristics and variable methodology.

The results of this study demonstrate that serum HBV RNA is positively correlated with HBsAg in HBeAg-positive patients; however, there is no significant correlation between the two in HBeAg-negative patients. This may be because HBsAg can be synthesized, not only from cccDNA but also from the integrated HBV gene fragments. Studies have shown that in HBV-infected patients, hepatocytes carrying integrated HBV DNA fragments account for approx. 1% of total hepatocytes and that HBV DNA is transcribed and translated into HBsAg after integration. This may be an important factor that contributes to the failure to completely clear HBeAg in clinical practice.[22,23] Therefore, HBsAg has certain shortcomings in terms of judging whether patients have reached the level of clinical cure. In contrast, serum HBV RNA is a direct transcript of cccDNA, and can more directly reflect the replication activity of cccDNA in vivo compared with HBsAg. Several studies have suggested that HBV RNA should be included in the clinical diagnosis, disease progression monitoring and the rational withdrawal of antiviral drugs.[24–26] However, its use as an established serum marker in clinical practice still requires more accurate, sensitive, and standardized detection methods, as well as more sophisticated prospective studies.

Limitations

The main limitation of our study was the size of the study sample.

Conclusions

There is a marked difference in serum HBV RNA levels in CHB patients with low HBV DNA levels and different HBeAg statuses. The HBeAg is a factor that influences serum HBV RNA levels in patients with CHB, while HBeAg and qHBsAg are factors that influence serum HBV RNA levels to be below the lower limit of detection in patients with CHB. Concurrently, serum HBV RNA levels in patients with CHB are correlated with other serological markers. This suggests that serum HBV RNA levels in patients with CHB with low HBV DNA levels can reflect virus activity to a certain extent. We, thus, believe that HBV RNA can be utilized as a novel serum marker for the detection of HBV infection.

ORCID iDs

Yifeng Zhou https://orcid.org/0000-0002-7590-4894
Yameng Peng https://orcid.org/0000-0001-5667-6702
Hao Yuan https://orcid.org/0000-0003-2573-7669
Zhenyi Long https://orcid.org/0000-0002-9078-2469
Sixian Wu https://orcid.org/0000-0002-0863-6324
Jiping Yang https://orcid.org/0000-0002-4119-6420

References

1. European Association for the Study of the Liver. EASL 2017 Clinical Practice Guidelines on the management of hepatitis B virus infection. *J Hepatol*. 2017;67(2):370–398. doi:10.1016/j.jhep.2017.03.021
2. Liaw Y, Chu C. Hepatitis B virus infection. *Lancet*. 2009;373(9663):582–592. doi:10.1016/S0140-6736(09)60207-5
3. Yim HJ, Hussain M, Liu Y, Wong SN, Fung SK, Lok ASF. Evolution of multi-drug resistant hepatitis B virus during sequential therapy. *Hepatology*. 2006;44(3):703–712. doi:10.1002/hep.21290
4. Nassal M. HBV cccDNA: Viral persistence reservoir and key obstacle for a cure of chronic hepatitis B. *Gut*. 2015;64(12):1972–1984. doi:10.1136/gutjnl-2015-309809
5. Lu F M, Wang J, Chen X M, et al. The potential use of serum HBV RNA to guide the functional cure of chronic hepatitis B. *Zhonghua Gan Zang Bing Za Zhi*. 2017;25(2):105–110. doi:10.3760/cma.j.issn.1007-3418.2017.02.005
6. Jinhong Z, Man WX. Clinical significance of serum HBV cccDNA in patients with hepatitis B. *J Pract Med*. 2013;29(3):395–397. doi:10.3969/j.issn.1006-5725.2013.03.021

7. Wang J, Shen T, Huang X, et al. Serum hepatitis B virus RNA is encapsidated pregenome RNA that may be associated with persistence of viral infection and rebound. *J Hepatol*. 2016;65(4):700–710. doi:10.1016/j.jhep.2016.05.029
8. Hou J, Wang G, Wang F, et al; Chinese Society of Hepatology and Chinese Society of Infectious Diseases (Chinese Medical Association). The guideline of prevention and treatment for chronic hepatitis B: A 2015 update. *J Clin Hepatol*. 2015;31(12):1941–1960. doi:10.14218/JCTH.2016.00019
9. Halgand B, Desterke C, Riviere L, et al. Hepatitis B virus pregenomic RNA in hepatocellular carcinoma: A nosological and prognostic determinant. *Hepatology*. 2018;67(1):86–96. doi:10.1002/hep.29463
10. Su Q, Wang SF, Chang TE, et al. Circulating hepatitis B virus nucleic acids in chronic infection: Representation of differently polyadenylated viral transcripts during progression to nonreplicative stages. *Clin Cancer Res*. 2001;7(7):2005–2015. PMID:11448918
11. Rokuhara A, Matsumoto A, Tanaka E, et al. Hepatitis B virus RNA is measurable in serum and can be a new marker for monitoring lamivudine therapy. *J Gastroenterol*. 2006;41(8):785–790. doi:10.1007/s00535-006-1856-4
12. Huang Y, Chayama K, Tsuge M, et al. Differential effects of interferon and lamivudine on serum HBV RNA inhibition in patients with chronic hepatitis B. *Antivir Ther*. 2010;15(2):177–184. doi:10.3851/IMP1508
13. Gong YJ, Bing H, Bang QJ, et al. Clinical analysis of the relationship between the incidence of hepatitis B e antigen-negative chronic hepatitis B and age. *Clin Focus*. 2008:23(7):502–503. doi:10.3969/j.issn.1004-583X.2008.07.021.
14. Huang Y, Takahashi S, Tsuge M, et al. On-treatment low serum HBV RNA level predicts initial virological response in chronic hepatitis B patients receiving nucleoside analogue therapy. *Antivir Ther*. 2015;20(4):369–375. doi:10.3851/IMP2777
15. Tsuge M, Murakami E, Imamura M, et al. Serum HBV RNA and HBeAg are useful markers for the safe discontinuation of nucleotide analogue treatments in chronic hepatitis B patients. *J Gastroenterol*. 2013;48(10):1188–1204. doi:10.1007/s00535-012-0737-2
16. Wang J, Yu Y, Li G, et al. Natural history of serum HBV-RNA in chronic HBV infection. *J Viral Hepat*. 2018;25(9):1038–1047. doi:10.1111/jvh.12908
17. Xia LR, Cheng PX, Jian G. Clinical value of serum HBV RNA. *J Clin Hepatol*. 2017;33(11):2196–2199. doi:10.3969/j.issn.1001-5256.2017.11.032
18. Butler EK, Gersch J, McNamara A, et al. Hepatitis B serum DNA and RNA levels in nucleos(t)ide analogue-treated or untreated patients during chronic and acute infection. *Hepatology*. 2018;68(6):2106–2117. doi:10.1002/hep.30082
19. Tsuge M, Chayama K. Availability of monitoring serum HBV DNA plus RNA during nucleot(s)ide analogue therapy. *J Gastroenterol*. 2013;48(6):779–780. doi:10.1007/s00535-013-0801-6
20. Lu F, Wang J, Chen X, Xu D, Xia N. Potential use of serum HBV RNA in antiviral therapy for chronic hepatitis B in the era of nucleos(t)ide analogs. *Front Med*. 2017;11(4):502–508. doi:10.1007/s11684-017-0590-z
21. Li Y, He L, Li Y, et al. Characterization of serum HBV RNA in patients with untreated HBeAg-positive and -negative chronic hepatitis B infection. *Hepatitis Monthly*. 2018,18(2):e62079. doi:10.5812/hepatmon.62079.
22. Chan HLY, Wong VWS, Chim AML, Chan HY, Wong GLH, Sung JJY. Serum HBsAg quantification to predict response to peginterferon therapy of e antigen positive chronic hepatitis B. *Aliment Pharmacol Ther*. 2010;32(11):1323–1331. doi:10.1111/j.1365-2036.2010.04474.x
23. Höner zu Siederdissen C, Maasoumy B, Cornberg M. What is new on HBsAg and other diagnostic markers in HBV infection? *Best Pract Res Clin Gastroenterol*. 2017;31(3):281–289. doi:10.1016/j.bpg.2017.04.009
24. Wang J, Yu YQ, Li GJ, et al. Relationship between serum HBV-RNA levels and intrahepatic viral as well as histologic activity markers in entecavir-treated patients. *J Hepatol*. 2018;68(1):16–24. doi:10.1016/j.jhep.2017.08.021
25. van Bommel F, van Bommel A, Krauel A, et al. Serum HBV RNA as a predictor of peginterferon alfa-2a (40KD) response in patients with HBeAg-positive chronic hepatitis B. *J Infect Dis*. 2018;218(7):1066–1074. doi:10.1093/infdis/jiy270
26. van Campenhout M, van Bommel F, Pfefferkorn M, et al. Host and viral factors associated with serum hepatitis B virus RNA levels among patients in need for treatment. *Hepatology*. 2018;68(3):839–847. doi:10.1002/hep.29872

Is low radioiodine uptake a contraindication to radioiodine therapy in patients with benign thyroid disease?

Maria Teresa Płazińska[1,A,B,D], Agata Czarnywojtek[2,3,A,B,D], Nadia Sawicka-Gutaj[3,B], Kosma Woliński[4,D], Iwona Krela-Kaźmierczak[5,A], Małgorzata Zgorzalewicz-Stachowiak[6,A,E], Izabela Miechowicz[6,B,C], Paweł Gut[3,E], Ewa Florek[7,E], Karolina Skonieczna-Żydecka[8,E], Marek Ruchała[3,E,F], Leszek Królicki[1,E,F]

[1] Department of Nuclear Medicine, Warsaw Medical University, Poland
[2] Chair and Department of Pharmacology, Poznan University of University of Medical Sciences, Poland
[3] Chair and Department of Endocrinology, Metabolism and Internal Medicine, Poznan University of University of Medical Sciences, Poland
[4] Department of Endocrinology, Metabolism and Internal Medicine, Poznan University of Medical Sciences, Poland
[5] Department of Gastroenterology, Dietetics and Internal Medicine, Poznan University of Medical Sciences, Poland
[6] Department of Computer Science and Statistics, Poznan University of Medical Sciences, Poland
[7] Laboratory of Environmental Research, Department of Toxicology, Poznan University of Medical Sciences, Poland
[8] Department of Biochemistry and Human Nutrition, Pomeranian Medical University, Szczecin, Poland

A – research concept and design; B – collection and/or assembly of data; C – data analysis and interpretation; D – writing the article; E – critical revision of the article; F – final approval of the article

Advances in Clinical and Experimental Medicine, ISSN 1899–5276 (print), ISSN 2451–2680 (online) *Adv Clin Exp Med*. 2021;30(4):369–378

Address for correspondence
Kosma Woliński
E-mail: kosma1644@poczta.onet.pl

Funding sources
None declared

Conflict of interest
None declared

Received on March 31, 2019
Reviewed on July 4, 2019
Accepted on August 11, 2020

Published online on April 29, 2021

Cite as
Płazińska MT, Czarnywojtek A, Sawicka-Gutaj N, et al. Is low radioiodine uptake a contraindication to radioiodine therapy in patients with benign thyroid disease?. *Adv Clin Exp Med*. 2021;30(4):369–378. doi:10.17219/acem/126287

DOI
10.17219/acem/126287

Copyright
© 2021 by Wroclaw Medical University
This is an article distributed under the terms of the Creative Commons Attribution 3.0 Unported (CC BY 3.0) (https://creativecommons.org/licenses/by/3.0/)

Abstract

Background. Radioiodine therapy (^{131}I) is a standard procedure in the treatment of hyperthyroidism in the course of Graves' disease or toxic nodules. However, the use of ^{131}I in patients with low radioiodine uptake (RAIU) may be controversial.

Objectives. To determine the influence of lithium carbonate (Li) on iodine kinetics.

Materials and methods. Patients with hyperthyroidism and low RAIU (< 30%) were divided into 2 groups: a Li(–) group of 305 patients not receiving Li adjuvant therapy and a Li(+) group of 264 patients receiving adjuvant therapy. The serum concentrations of free triiodothyronine (fT3), free thyroxine (fT4) and thyroid stimulating hormone (TSH) were assessed at baseline, 24 h, 48 h, 72 h and 96 h, and 1, 6 and 12 months after ^{131}I therapy. The RAIU was assessed after 5 h, 24 h, 48 h, 72 h, and 96 h.

Results. Levels of fT3 in the Li(+) group compared to the Li(–) group were significantly higher at baseline, lower after 48 h, 72 h, 96 h and 1 month, and did not differ significantly after 24 h, 6 months and 12 months. Levels of fT4 in the Li(+) group compared to the Li(–) group were significantly higher at baseline, lower after 24 h, 48 h, 72 h, 96 h and 1 month, and not differ significantly after 6 and 12 months. The RAIU in the hyperthyroidism Li(–) and Li(+) groups, respectively, was 11.9 ±5.6% compared to 23.9 ±10.1% ($p < 0.001$) after 5 h; 25.9 ±8.3% compared to 40.5 ±12.4% ($p < 0.05$) after 24 h; 7.8 ±8.1% compared to 40.9 ±13.7% ($p < 0.05$) after 48 h; 26.2 ±10.2% compared to 39.5 ±11.2% ($p < 0.01$) after 72 h; and 24.7 ±7.1% compared to 37.4 ±10.1% ($p < 0.01$) after 96 h.

Conclusions. Adjuvant therapy with Li in patients with hyperthyroidism caused a significant increase in RAIU and positive changes in the fT3 and fT4 profiles. The use of lithium carbonate prior to the inclusion of ^{131}I in hyperthyroid patients with low RAIU should be considered.

Key words: hyperthyroidism, radioiodine therapy, lithium therapy, adjuvant lithium therapy, low radioiodine uptake

Background

Lithium carbonate (Li), which is a drug known for over 100 years, is successfully used in the treatment of depression. However, various studies have shown that it can cause the emergence of goiter and even hypothyroidism in the range of 3.4–52% of treated patients[1–9] and, in extremely rare cases, hyperthyroidism.[1,10,11] The mechanism of action of Li on thyroid function seems to be similar to that of iodine. It is believed that ionized lithium inhibits thyroglobulin proteolysis which, in turn, inhibits the release of thyroid hormones into the bloodstream and leads to a prolonged biological half-life of iodine.[12] Another mechanism involves inhibition of the conversion of free thyroxine (T4) to triiodothyronine (T3) by this drug.[1] Lithium carbonate has also been shown to reduce the concentration of thyroid hormone transporter proteins in the blood serum.[1,13]

Radioiodine (^{131}I) therapy is a very popular therapeutic method in patients with hyperthyroidism,[14–18] especially in cases where antithyroid drugs (ATDs) have proved to be inefficient. The mechanism of action of ^{131}I involves the total destruction of thyroid tissues, resulting in euthyroidism or hypothyroidism.[19,20] However, it is very difficult to choose the right activity of ^{131}I to achieve euthyroidism. Several studies have attempted to determine the optimal level to treat hyperthyroidism while avoiding the development of permanent hypothyroidism. Various ^{131}I administration protocols are available, including low doses (80 MBq),[14,21,22] various fixed doses (185 MBq, 370 MBq and 555 MBq),[14,22–24] and doses calculated on the basis of thyroid size, radioactive iodine uptake (RAIU) or the turnover of ^{131}I.[14,24,25] However, our clinical experience has proven that hypothyroidism develops in approx. 80% of cases, which is not a significant problem for an experienced clinician, as it only requires the substitution of L-thyroxin.[26]

The premise for using Li is that this compound leads to the inhibition of thyroglobulin proteolysis and release of thyroid hormones.[1] Therefore, it is assumed that the administered radioactive iodine accumulates in thyroid tissue to a higher degree, and thus ^{131}I treatment is possible in patients with critically reduced RAIU at baseline. However, in the existing literature, there is relatively little data on the long-term results of the use of Li in patients with hyperthyroidism, especially those with a low radioiodine uptake (RAIU) after or during treatment with amiodarone,[1,13,26,27] after coronary angiography, or in cases using iodine-containing contrast (e.g., eye drops or multivitamin preparations). Additionally, there are few publications related to the use of this type of therapy and the available publications have too short observation period or too few patients. Therefore, a method involving the administration of Li to hyperthyroid patients was introduced.[28]

Objectives

The aim of this study was to demonstrate the usefulness and effectiveness of the administration of Li prior to the administration of ^{131}I in patients with established hyperthyroidism for whom the reduced RAIU did not allow this type of treatment.

Materials and methods

Patients and study design

This retrospective study was conducted at the Department of Nuclear Medicine in Warszawa, Poland, from January 1, 2005, to December 31, 2016. The study was approved by the local ethics committee of the county of Warszawa. Our cohort comprised 569 consecutive patients with hyperthyroidism with reduced RAIU at baseline (<30%) and 78 patients with normal or elevated RAIU (comparison group) treated with ^{131}I. Data were retrieved from the medical records of patients who were eligible for this study. Informed consent was obtained from all participants.

The patients were categorized into 3 following groups:

– group I (Li (–) group): patients with very low RAIU (<30%), with Graves' disease (GD), toxic nodular goiter (TNG) or iodine-induced toxic adenoma (TA) not treated with Li;

– group II (Li(+) group): patients who received Li in order to increase RAIU (>30%), with GD, TNG or TA; and

– group III: the comparison group comprising hyperthyroid patients with GD treated with ^{131}I with correct or elevated RAIU at baseline.

Among the included patients, low RAIU was caused by amiodarone therapy (n = 186, 32.7%), coronary angiography before the iodine uptake test (n = 281, 49.4%), iodine-containing eye drops (e.g., Iodoxouridine; n = 57, 10.0%), and multivitamin preparations containing iodine (n = 45, 7.9%).

The etiology of hyperthyroidism was established on the basis of clinical examination and history of the disease. The following diagnostic criteria for GD were applied: 1) biochemical hyperthyroidism (increased serum free T4 concentration and undetectable TSH) and diffuse goiter without nodules, with or without an isotopic scan; 2) the presence of the titer of the TSH receptor antibody (TRAb); and 3) symptoms of mild ophthalmopathy.

The TNG was defined as hyperthyroidism with the presence of nodular goiter on thyroid ultrasonography and ^{131}I scintigraphy and, in the case of toxic adenoma, clinical or subclinical hyperthyroidism and the presence of hot nodules on scintigraphy.

The diagnosis of mild GO was defined based on the following criteria: goiter on thyroid ultrasound, mild proptosis or mild exophthalmos assessed using an exophthalmometer (<18 mm), and hormonal analyses showing suppressed TSH levels, as well as an increased concentration of free T4

(fT4) and free T3 (fT3) combined with positive autoantibodies in regard to the thyrotropin receptor (TSHR-Abs).

Patients with GD for whom long-term remission did not appear following ATDs treatment, and patients with persistent hyperthyroidism due to toxic multinodular goiter or single toxic adenoma, were administered ^{131}I.

Study design

Using a thyroid uptake probe, we counted 2 capsules of 25 μCi ^{131}I, each kept in a neck phantom. A standard distance of 30 cm was maintained from the phantom for the purpose of the count. We acquired 2 readings of 100 s for each capsule and, subsequently, expressed the average of the 2 readings as counts per minute (cpm). The first capsule was administered if the average count of the 2 capsules amounted to ±10%, and the patient was asked to swallow it with plain water. The 2nd capsule, labelled the 'standard capsule', was kept in the neck phantom. Following administration of this capsule, the patient's thyroid and thigh counts were measured using a thyroid uptake probe at 5 h, 24 h, 48 h, 72 h, and 96 h at the same distance and for the same time; the results were expressed as cpm. The patient's thigh counts were used for the correction of non-thyroidal blood pool activity. The source, which was kept inside the lucite thyroid phantom, was located 30 cm from the detector (isoresponse distance). Counts were taken at specific times after each patient's readings, namely at 5 h, 24 h, 48 h, 72 h, and 96 h, with the reading expressed in the standard capsule cpm. The following formula was used to calculate the percentage uptake:

$$\text{percentage uptake} = \\ = \text{thyroid counts [cpm]} - \text{thigh counts [cpm]} \times 100.$$

Iodine sensitivity tests were performed using a Siemens ZLC gamma camera (Siemens AG, Munich, Germany).

After performing RAIU and obtaining the activity of ^{131}I, patients were scheduled to visit outpatient clinics at baseline (before radioiodine therapy (RIT)), and at 24 h, 48 h, 72 h and 96 h after the procedure, and after 1, 6 and 12 months during 1 year of follow-up after the initiation of RIT. The TSH, fT3, fT4, and thyroid autoantibodies were examined at every follow-up visit to the outpatient clinic.

Our study did not include patients with contraindications to Li, i.e., allergy to lithium, heart and kidney failure, hypothyroidism, uncontrolled arterial hypertension, water-electrolyte disorders, Addison's disease, or brain diseases with dementia.

Treatment

Antithyroid drug

The ATD therapy was discontinued in all patients before ^{131}I therapy. Most patients (83%) did not receive ATD for 5–7 days before ^{131}I treatment. The TD treatment was discontinued in all other patients for a period of more than 7 days (7–25 days).

Lithium carbonate

Oral administration of adjuvant Li (GlaxoSmithKline Pharmaceuticals SA, Poznań, Poland) was recommended for patients with low RAIU. Patients were assigned to receive a daily oral average dose of 750 mg starting 3 days prior to ^{131}I therapy and continuing for 7 days following the administration of ^{131}I.

Radioiodine therapy

Radioactive iodine was administered as a single, standard, orally administered dose of 740 MBq (20 mCi) in patients with GD and TMG (with adjuvant lithium therapy (750 mg/day for 10 days) or without lithium). The administered activity of ^{131}I in TA was 555 MBq (15 mCi), irrespective of adjuvant Li therapy.

L-thyroxine

In all patients with hypothyroidism (TSH > 4.5 mIU/L) after ^{131}I therapy, L-thyroxin therapy was applied.

Assays

A Hitachi Cobas e601 chemiluminescent analyzer (Roche Diagnostics, Basel, Switzerland) was used to diagnose serum TSH levels (normal range: 0.27–4.2 μIU/mL) and to perform the hormonal assessments fT4, normal range: 11.5–21.5 pmol/L; fT3, normal range: 3.9–6.8 pmol/L). Determination of TSH concentrations was performed using third-generation assays (sensitivity: 0.005 μIU/mL). Second-generation antibodies (RIA-2 Dynotest TRAK human; BRAHMS Diagnostica GmbH, Berlin, Germany) were the radioimmunological method used to measure the titer of the antithyroid peroxidase autoantibody (TPO-Abs, reference range: <35 IU/mL), antithyroglobulin antibody (Tg-Abs, reference range: <115 IU/mL) and TSHR-Abs (reference range: <2 IU/L).

The serum level of Li was assayed by ion-selective lithium determination using a lithium electrode and an AVL 988-3 apparatus with automatic three-point calibration. This method consists of determining the difference in the potential of the lithium level between the standard and the sample. The selective potential between the 2 different concentrations of lithium ions was automatically measured. Using this method, the measurement limit for lithium is in the range of 0.1 ±9.99 mmol/L and the sensitivity is 0.01 ±0.02 mmol/L.

Sonography and scintigraphy

An Aloka SSD-500 (Aloka Ltd., Tokyo, Japan) ultrasound machine with a 7.5-MHz linear transducer was used

to perform ultrasonography of the thyroid. Ultrasound was also used to measure the thyroid volume. The ellipsoid model (width × length × thickness × 0.52 for each lobe) was used for the calculation.[29,30]

In the case of patients with thyroid nodules, 150 MBq of ^{99m}Tc was intravenously administered and a thyroid scintiscan was performed (Nucline gamma camera; Mediso, Budapest, Hungary) 30 min later.

Statistical analyses

The thyroid hormone and TSH serum levels before and after administration of Li were assessed using Student's t-test for independent observations. Friedman's test was also used for statistical comparison of mean iodine uptake measurements before and 5 h, 24 h, 48 h, 72 h, and 96 h after administration of Li. One-way analysis of variance (ANOVA) was used to establish if there was a statistically justified division of the analyzed data into subgroups of the various clinical forms of hyperthyroidism. Variance analysis was preceded by assessment of the compatibility of the variances of the hypothetical subgroups using Levene's test. The mean uptake of ^{131}I before and after the administration of Li for particular groups at the determined measurement times was also compared using Student's t-test. Statistical analyses were performed using STATISTICA v. 12 software (StatSoft Inc. Tulsa, USA). The adopted level of statistical significance was $\alpha = 0.05$ and results were considered statistically significant when $p < \alpha$.

Table 1A. Baseline characteristic of the hyperthyroid patients (GD, TMG and TA) with reduced RAIU at baseline (<30%) according to the clinical diagnosis or the demographic, clinical and laboratory characteristics

Characteristic	GD (n = 284)		TMG (n = 231)		TA (n = 54)	
	Li(–)	Li(+)	Li(–)	Li(+)	Li(–)	Li(+)
Females (n, %)	121 (42.6)	107 (36.7)	79 (34.2)	74 (32.0)	22 (40.7)	9 (16.6)
Males (n, %)	23 (8.1)	33 (11.6)	41 (17.7)	37 (16.1)	19 (35.2)	4 (7.4)
Age of females, mean (range) [years]	49 (18–61)	45 (19–54)	51 (37–81)	54 (34–78)	54 (33–71)	55 (29–87)
Age of males, mean (range) [years]	43 (26–52)	47 (32–58)	59 (42–78)	62 (32–69)	52 (38–83)	56 (32–86)
Week of diagnosis	23	17	27	20	13	11
Mild ophthalmopathy yes (%) no (%)	 96 (67) 48 (33)	 102 (73) 38 (27)	 0 (0) 120 (52)	 0 (0) 111 (48)	 0 (0) 41 (76)	 0 (0) 13 (24)
TSH level [mIU/L] mean (SEM) range	 0.0 (0.09) 0.0–0.012	 0.0 (0.04) 0.0–0.05	 0.13 (0.04) 0.1–0.21	 0.1 (0.15) 0.01–0.20	 0.15 (0.1) 0.14–0.23	 0.18 (0.13) 0.1–0.22
Free T3 level [pmol/L] mean (SEM) range	 9.6 (3.8) 3.9–12.7	 8.7 (5.2) 4.6–11.2	 6.6 (3.1) 3.3–8.4	 4.3 (4.1) 3.6–9.6	 4.3 (3.9) 3.6–5.7	 3.9 (4.2) 4.1–6.2
Free T4 level [pmol/L] mean (SEM) range	 29.1 (5.6) 25.0–39.7	 32.2 (6.7) 24–45	 26 (3.9) 35.5–32.5	 23.91 (4.6) 22.4–32.3	 22.9 (4.1) 18.9–25.9	 21.71 (3.5) 20.4–27.1
TSHR-Abs titers [IU/L] mean (SEM) range	 12.1 (5.6) 2.1–16.7	 7.8 (4.8) 2.5–13.7	 0.9 (0.6) 0.3–2.4	 1.1 (0.5) 0.5–1.3	 1.2 (0.5) 0.4–1.7	 2.0 (0.6) 0.4–2.1
TPO-Abs titers [IU/mL] mean (SEM) range	 332.6 (349.4) 79–451	 249.4 (284.8) 134–456	 64.5 (34.1) 19.0–71.3	 56.1 (32.5) 31.0–81.7	 52.2 (22.5) 19.5–49.3	 45.7 (25.3) 28.5–47.3
Tg-Abs titer [IU/mL] mean (SEM) range	 319.2 (295.7) 214–546	 329.3 (254) 212–634	 102.9 (71.4) 49.5–183.0	 114.6 (93.5) 39.3–161.7	 91.3 (76.6) 29.5–137	 89.3 (88.3) 53.4–192.6
Thyroid volume [mL/m^2] mean (SEM) {Me; min–max}	 21.0 (3.4) {19.0; 17.8–25.4}	 24.9 (5.7) {21.8; 20.8–25.4}	 19.0 (2.4) {17.2; 15.8–21.4}	 21.6 (3.6) {18.8; 17.7–25.2}	 17.5 (2.7) {16.9; 15.1–22.3}	 20.9 (4.8) {17.6; 16.5–24.3}
Activity of ^{131}I [MBq] ([mCi])	800 (0.0) 22 (0.0)	800 (0.0) 22 (0.0)	800 (0.0) 22 (0.0)	800 (0.0) 22 (0.0)	555 (15) 555 (15)	555 (15) 555 (15)

TSH – thyroid stimulating hormone; fT4 – free tetraiodothyroxine; fT3 – free triiodothyronine; TPO-Abs – thyroperoxidase autoantibodies; Tg-Abs – thyroglobulin autoantibodies; TSHR-Abs – autoantibodies to the thyrotropin receptor; ^{131}I – radioiodine; mCi – millicurie; SEM – standard error of the mean; min – minimum; max – maximum; Me – median.
Data are given as n, mean (SEM, range, %). Normal values in our laboratory are as follows: fT4: 11.5–21.5 pmol/L; fT3: 3.9–6.8 pmol/L; TSH: 0.27–4.2 µU/mL; TSHR-Abs: <2 IU/L, TPO-Abs: 0–34 IU/mL and Tg-Abs: 10–115 IU/mL. All patients had undetectable serum Tg-Ab, TPO-Ab and TSHR-Abs. Thyroid volume was measured with ultrasonography (normal values range up to 19 mL for F and up to 25 mL for M).

Results

Of the 678 patients assessed, 109 were eligible for inclusion in this study. The reasons for ineligibility were: incomplete medical records for 38 (35%) patients (27 women and 11 men), retrosternal goiter in 35 (32%) patients (23 males and 12 females); severe Graves' ophthalmopathy in 13 (12%) female patients, and mental disease in 11 (10%) patients, while 12 (11%) patients did not agree to participate.

The demographic, clinical and laboratory characteristics of the cohort at presentation are summarized in Table 1A,1B. Between 2005 and 2016, we were able to obtain follow-up data for 569 hyperthyroid patients with reduced RAIU at baseline (<30%). Of these, 284 were classified as suffering from GD (228 women and 56 men), 231 (153 women and 78 men) developed TMG and 54 (31 women and 23 men) were assigned to the group with TA.

Adjuvant lithium increased RAIU in all hyperthyroid patients (Table 2). For the hyperthyroidism Li(–) and Li(+) groups, respectively, the RAIU at the following time points (T) was: T_{5h}, 11.9 ±5.6% compared to 23.9 ±10.1% ($p < 0.001$); T_{24h}, 25.9 ±8.3% compared to 40.5 ±12.4% ($p < 0.05$); T_{48h}, 27.8 ±8.1% compared to 40.9 ±13.7% ($p < 0.05$); T_{72h}, 26.2 ±10.2% compared to 39.5 ±11.2% ($p < 0.01$); and T_{96h}, 24.7 ±7.1% compared to 37.4 ±10.1% ($p < 0.01$). In the comparison group, RAIU was 31.3% ±10.2% at T_{5h}, 52.3% ±6.9% at T_{24h}, 54.9 ±12.7% at T_{48h}, 47.5 ±10.8% at T_{72h}, and 38.5 ±9.2% at T_{96h}.

In the Li(+) group, the RAIU before administration of lithium was 12.0 ±4.4% at T_{5h}, 25.0 ±5.4% at T_{24h} and 24.0 ±6.0% at T_{96h} ($p > 0.05$ for all 3 time points in comparison to the Li(–) group).

Table 1B. Clinical and biochemical characteristic of the Li(–) and Li(+) and comparison groups at baseline

Characteristic	Examined groups		Comparison group
	Li(–)	Li(+)	
Females (n, %)	222 (39.0)	190 (33.4)	57 (37.0)
Males (n, %)	83 (14.9)	74 (13.00)	21 (27.0)
Age of females, mean (range) [years]	52 (32–81)	53 (29–87)	51 (19–59)
Age of males, mean (range) [years]	51 (26–83)	55 (27–86)	47 (21–52)
Week of diagnosis	13–27	11–20	12–25
Mild ophthalmopathy yes (%) no (%)	 96 (17) 209 (37)	 102 (18) 162 (28)	 46 (59) 32 (41)
TSH level [mIU/L] mean (SEM) range	 0.09 (0.07) 0.0–0.23	 0.0 (0.12) 0.01–0.22	 0.0 (0.04) 0.00–0.19
Free T3 level [pmol/L] mean (SEM) range	 5.6 (3.6) 3.3–12.7	 8.2 (4.1) 3.9–6.2	 5.6 (3.3) 3.1–7.4
Free T4 level [pmol/L] mean (SEM) range	 26.0 (4.5) 25–32.5	 29.3 (5.8) 20.4–32.3	 27.4 (6.7) 21.9–33.6
TSHR-Abs titers [IU/L] mean (SEM) range	 4.7 (2.2) 0.9–13.4	 3.6 (1.9) 1.1–5.7	 6.7 (2.8) 2.4–11.2
TPO-Abs titers [IU/mL] mean (SEM) range	 149.7 (135.3) 39.1–190.5	 117.0 (114.2) 64.5–195.0	 189 (345.8) 116.0–1285.0
Tg-Abs titer [IU/mL] mean (SEM) range	 171.1 (147.9) 97.6–307.2	 177.3 (145.3) 113.2–329.4	 231.7 (198.4) 98.2–1121.0
Thyroid volume [mL/m^2] mean (SEM) {Me; min–max}	 15.6 (2.9) {15.7; 14.1–54.1}	 18.9 (3.6) {16.5; 13.4–43.3}	 21.5 (4.7) {17.5; 16.4–42.3}
Activity of ^{131}I [MBq] ([mCi])	814 (22)	814 (22)	185.0–814.0 (5–22)

TSH – thyroid stimulating hormone; fT4 – free tetraiodothyroxine; fT3 – free triiodothyronine; TPO-Abs – thyroperoxidase autoantibodies; Tg-Abs – thyroglobulin autoantibodies; TSHR-Abs – autoantibodies to the thyrotropin receptor; ^{131}I – radioiodine; mCi – millicurie; SEM – standard error of the mean; min – minimum; max – maximum; Me – median.

Data are given as n, mean (SEM, range, %). Normal values in our laboratory are as follows: fT4: 11.5–21.5 pmol/L; fT3: 3.9–6.8 pmol/L; TSH: 0.27–4.2 µU/mL; TSHR-Abs: <2 IU/L, TPO-Abs: 0–34 IU/mL and Tg-Abs: 10–115 IU/mL. All patients had undetectable serum Tg-Ab, TPO-Ab and TSHR-Abs. Thyroid volume was measured with ultrasonography (normal values range up to 19 mL for F and up to 25 mL for M).

Table 2. The mean iodine uptake values (RAIU) in all studied groups

Time of observation of RAIU [h]	5	24	48	72	96
Li (–) group [%]	11.9 ±5.6	25.9 ±8.3	27.8 ±8.1	26.2 ±10.2	24.7 ±7.1
Li (+) group [%]	23.9 ±10.1	40.5 ±12.4	40.9 ±13.7	39.5 ±11.2	37.4 ±10.1
Comparison group [%]	31.3 ±10.2	52.3 ±6.9	54.9 ±12.7	47.5 ±10.8	38.5 ±9.2

Thyroid hormone concentrations

For the Li(–) and Li(+) groups, differences in the serum level of fT3 (Fig. 1) were recorded at most time points ($p = 0.001$), except at 48 h and after 6 and to 12 months of follow-up. The initial concentration of fT3 in Li(+) patients was 8.2 ±4.1 pmol/L, while that in ^{131}I Li(–) patients was significantly lower at 5.6 ±3.6 pmol/L ($p < 0.001$). The fT3 level in ^{131}I Li(–) and ^{131}I Li(+) patients at each time point was as follows: after 24 h, 8.1 ±3.9 pmol/L compared to 6.2 ±3.2 pmol/L; after 48 h, 8.1 ±3.9 pmol/L compared to 7.8 ±4.1 pmol/L; after 72 h, 8.3 ±4.4 pmol/L compared to 6.3 ±3.9 pmol/L; after 96 h, 8.4 ±3.4 pmol/L compared to 6.0 ±3.1 pmol/L; after 1 month, 8.7 ±4.5 pmol/L compared to 7.1 ±5.1 pmol/L; after 6 months, 4.9 ±3.1 compared to 5.1 ±3.9 pmol/L; and after 1 year, 3.1 ±3.7 pmol/L compared to 3.8 ±3.9 pmol/L.

The baseline serum fT4 concentration in Li(+) patients was 29.3 ±5.8 pmol/L, which was significantly higher than in Li(–) patients (26.0 ±4.5 pmol/L; $p = 0.001$). However, after 24 h and up to 1 month into the observation period, the fT4 concentration was significantly lower in the ^{131}I Li(+) group compared to the ^{131}I Li(–) group ($p < 0.001$). After 24 h, it was 27.9 ±3.9 pmol/L compared to 34.2 ±7.4 pmol/L; after 48 h, it was 27.3 ±3.8 pmol/L compared to 38.2 ±5.2 pmol/L; after 72 h, it was 25.7 ±4.8 pmol/L compared to 38.2 pmol/L ±5.2; after 96 h, it was 24.8 ±5.0 pmol/L compared to 38.2 ±5.2 pmol/L; after 1 month, it was 29.3 ±4.2 pmol/L compared to 39.7 ±6.7 pmol/L; after 6 months, it was 21.2 ±7.5 pmol/L compared to 19.5 ±6.1 pmol/L; and after 1 year, it was 19.6 ±6.4 pmol/L compared to 18.1 ±3.9 pmol/L (Fig. 2).

Therefore, a significant reduction of fT4 and fT3 was observed in the Li(+) group compared to the Li(–) and comparison groups. This significant reduction was observed at each subsequent time point following ^{131}I.

Comparison of the mean TSH serum concentrations of patients before and after administration of Li did not show a statistically significant difference ($p > 0.05$). The average TSH level before administration of Li was 0.3 mIU/L, and after administration of Li it was 0.45 mIU/L. All patients who received Li underwent analysis of serum concentrations on the 7th day of application, obtaining values from 0.34 mmol/L to 0.49 mmol/L, with a mean value of 0.5 ±0.06 mmol/L.

Clinical thyroid status

At 1 year, 462 patients (81.2%) were successfully treated (hypothyroid or euthyroid) and 107 (18.8%) remained hyperthyroid. Euthyroid status was achieved by about 10% of patients, including approx. 70% of Li(+) group patients with GD. In the group with TNG, this percentage was 43%, including 74.7% in the Li(+) group; in the TA group, this percentage was approx. 76%, including 71% in the Li(+) group. In addition, clinical signs were less pronounced during follow-up in patients in the Li(+) group. Among Li(+) group patients with GD, recurrent hyperthyroidism was observed in approx. 31% of patients with GD and 29% of patients with TMG, whereas no cases of recurrent hyperthyroidism were diagnosed in patients with TA, as judged from biochemical analysis, clinical symptoms and reduced demand for antithyroid medications (Table 3).

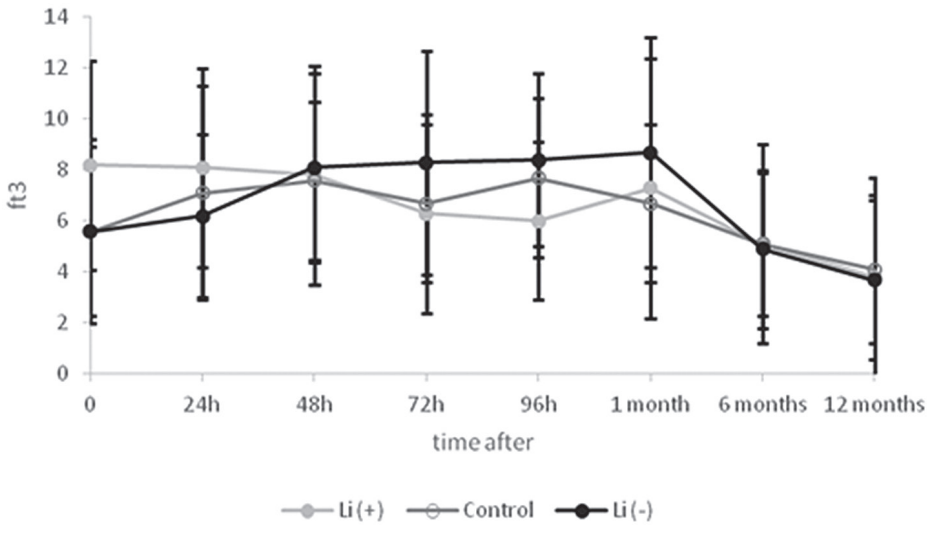

Fig. 1. Serum fT3 concentrations for the Li(–) and Li(+) groups and the comparison group at baseline and at each subsequent time point following ^{131}I administration

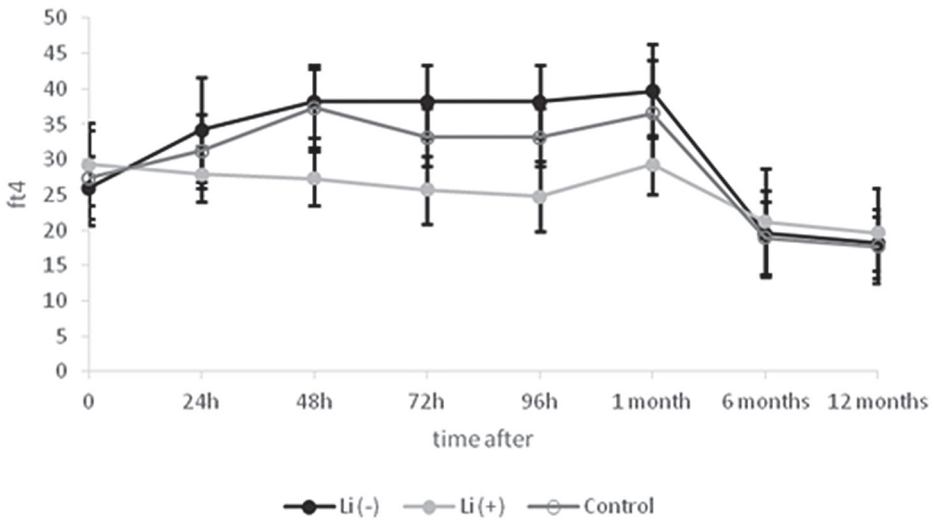

Fig. 2. Serum fT4 concentrations for the Li(–) and Li(+) groups and the comparison group at baseline and at each subsequent time point following ^{131}I administration

Table 3. Clinical outcome of a single fixed dose (555(15mCi)* MBq or 740 MBq (20mCi)) of radioiodine for all patients

[Empty cell]	Euthyroid (n, %) (Li(–), %/ Li(+), %)	Hypothyroidism (n,%) (Li(–), %/ Li(+), %)	Hyperthyroidism (n,%) (Li(–), %/ Li(+), %)	Treated with 1st dose of ^{131}I (n, %) (Li(–), %/ Li(+), %)	Treated with 2nd dose of ^{131}I (n, %) (Li(–), %/ Li(+), %)
GD (n = 284)	28 (9.8) 9 (32.1)/ 19 (67.9)	195 (68.6) 84 (43.1)/ 111 (56.9)	61 (21.6) 42 (68.8)/ 19 (31.2)	238 (83.8) 187 (78.6)/ 51 (21.4)	46 (16.2) 28 (60.9)/ 18 (39.1)
TMG (n = 231)	99 (42.8) 25 (25.3)/ 74 (74.7)	90 (39.0) 27 (30.0)/ 63 (70.0)	42 (18.2) 30 (71.4)/ 12 (28.6)	193 (33.9) 151 (78.2)/ 42 (21.8)	38 (6.7) 31 (81.6)/ 7 (18.4)
TA* (n = 54)	41 (75.9) 12 (29.3)/ 29 (70.7)	9 (16.7) 2 (22.2)/ 7 (77.8)	4 (7.4) 4 (100)/ –(–)	49 (8.6)* 29 (59.2)/ 20 (40.8)	5 (87.8) 3 (60)/ 2 (40)
All (mean) (n = 569)	168 (29.5) 46 (27.4)/ 122 (72.6)	294 (51.7) 113 (38.4)/ 181 (61.6)	107 (18.8) 76 (71.0)/ 31 (29.0)	480 (84.3) 367 (76.5)/ 113 (23.5)	89 (15.6) 62 (69.7)/ 27 (30.3)
Comparison group (n = 78)	21 (26.9)	40 (51.3)	17 (21.8)	63 (80.8)	15 (19.2)

* Administered activity of ^{131}I in patients with toxic adenoma was in each case equal to 555 MBq (15mCi), while in other cases an "ablative" dose of 740 MBq (20mCi) of ^{131}I was used.

Discussion

Li is as a normothymic drug widely used in psychiatry, thyrology and therapy for hyperthyroidism. Its mechanism of action is not fully understood, although it is believed to work similarly to iodine. Moreover, ionized lithium inhibits proteolysis of thyroglobulin,[12] inhibits T4 to T3 conversion,[1,9] and reduces the concentration of thyroid hormone transport proteins in the blood serum.[1,32] The data on the effect of Li on thyroid iodine in the literature is divergent. An increase in iodine uptake after administration of Li was described by Sedvall et al.[32] The authors demonstrated that Li administered for 12 consecutive days resulted in a decrease in the level of protein-bound iodine in all 7 patients, alongside an increase in iodine uptake from 26% to 36.7% after 24 h. Similar results were obtained in animals by Berens et al.[33] These authors also found that the increased ability of the thyroid to accumulate iodine during Li administration is independent of the degree of prolonged iodine retention in the thyroid. In our study, administration of Li according to the proposed regimen caused a significant increase of RAIU in all patients after adjuvant therapy, and iodine uptake increased from approx. 12% to 24% and from 25% to 41% after 24 h in comparison to RAIU after 5 h. The results of our research, which are consistent with most of the data available in the literature, have demonstrated the significant role of lithium adjuvant therapy in increasing RAIU.

Different results were presented by Temple et al.[34] and Turner at al.[35] Temple et al. studied, among other things, the effect of Li on thyroid RAIU in 11 patients with hyperthyroidism. The initial iodine uptake of T_{24h} in this group was 33 ±88% and did not change during administration of 900 ±1500 mg of Li for 10 days. Turner et al.,[35] on the other hand, administered 400 mg of Li for 1 week before and continued for 1 week after administration

of a standard therapeutic dose of radioiodine (5 mCi). The T_{24h} at baseline in this group was approx. 70%, while after administration of Li it was 67%. Summarizing the obtained results, the authors emphasized the fact that Li only affected the effective half-life of iodine, but did not affect iodine uptake. The basic difference between the groups studied by Sedvall et al.,[32] Turner at al.[35] and Temple et al.[34] concerns the initial iodine uptake. In a study by Sedvall et al.,[32] it amounted to 26%, as mentioned above, while in a study by Turner et al.,[35] it was 70%.

In the paper by Bogazzi et al. additional studies were carried out on a group of patients for whom the iodine uptake T_{24h} was at least 30%.[13] The administration of Li to this group did not significantly increase iodine uptake. Given the literature data and our own observations, it should be assumed that the Li effect depends on the initial value of T_{24h}. If the initial iodine uptake is relatively high, Li may not affect this parameter; however, if it is lower, it should be assumed that Li will likely cause it to increase. As noted above, this is certainly not the only parameter determining the effect of Li. In some patients with reduced T_{24h}, the administration of Li may not have the desired effect. The basic condition for conducting radioisotope treatment of patients with hyperthyroidism is adequately high retention of radioiodine in the thyroid gland. In some patients, it is so low that the use of radioactive iodine is impossible or involves a much higher dose of radioactivity, especially after treatment with amiodarone[26] or shading agents.[36]

The results of our study confirm the present observations[29] and indicate that even a few days of administration of Li results in favorable changes in thyroid hormone levels in blood serum, such as decreases in the fT3 and fT4 levels, and has no effect on the TSH level. This result certainly depends on the inhibitory effect of Li on thyroglobulin proteolysis and the secretion of thyroid hormones into the bloodstream. In our study, the serum level of fT3 at baseline in the Li(+) group was 8.2 ±4.1 pmol/L and after T_{96h} it was fT3 6.0 ±3.1 pmol/L; fT4 at baseline was 29.3 ±5.8 pmol/L and after T_{96h} it was 24.8 ±5.0 pmol/L. The significant effect of short-term administration of Li on the T3 level can result from a decrease in the concentration of transport proteins (TBG), which was previously described, but mainly results from inhibition of the conversion of T4 to T3. Jarlov et al.[24] concluded that administration of Li at a dose of 32.4 mEq/day led to a decrease in the level of T4 by 13% on the 3rd day of the regimen and a 27% decrease by the 10th day, whereas the decrease in the concentration of T3 in the blood serum (resin test) was 16% and 38% on the 3rd and 10th day, respectively.

Data concerning changes in the concentration of thyroid hormones 1 week after administration of a radioisotope can be found in a publication by Bogazzi et al.[13] and our earlier research.[21] Bogazzi et al.[13] evaluated the effect of the administration of Li on the course of treatment with ^{131}I in patients with GD. The authors observed a transient increase in fT3 and fT4 and an increase in the thyroglobulin level in patients who did not take Li. These changes are likely caused by the direct destructive action of ionizing radiation on follicular cells. This phenomenon was not observed in patients additionally treated with Li. Similar observations were reported by Martin et al.[27] In our results, which do not deviate significantly from that study, the levels of thyroid hormones after administration of ^{131}I were evaluated after 1, 6 and 12 months. It was shown that in this period, the group of patients receiving Li was characterized by significantly lower levels of thyroid hormones. This phenomenon is extremely beneficial in the initial period of radioiodine treatment as it allows for faster euthyreosis than in patients who do not receive Li. Furthermore, it likely allows for avoiding transient increases in thyroid hormone levels as a result of ionizing radiation in the initial period after the administration of ^{131}I.

Our findings indicate that the administration of Li for a short period of time does not cause significant changes in serum TSH levels. The TSH was normalized only a few months after the administration of ^{131}I. Similar results have been reported by other authors.[31,33,37]

This paper presents a different method of determining the therapeutic activity of radioiodine than used in previous publications on the therapeutic effects of ^{131}I and Li. The recommended dose determination method has now been adopted in clinical practice. The administered ^{131}I activity of ^{131}I in patients with toxic adenoma was in each case equal to 555 MBq (15 mCi), while in other cases, an "ablative" dose of 740 MBq (20 mCi) of ^{131}I was used. Despite the use of such a high ^{131}I activity for ^{131}I, 22% of patients should have been treated with the second activity of ^{131}I. Previous studies used the standard dose[38] or calculated the radioactivity used per 1 g of tissue.[31] Despite these methodological differences, the curative effects shown in the cited works and in our study are similar. The administration of Li had a positive effect on the efficacy of radioisotope treatment in the early period after the administration of ^{131}I.

At one-year follow-up, in the group of patients with GD with Li(+), hyperthyroidism persisted in approx. 31% of patients after administration of Li, while remission euthyroidism and hypothyroidism were obtained in 67% and 57% of patients, respectively (Table 3). In the Li(+) group with TMG, recurrent hyperthyroidism was observed in 28.6% of patients, whereas in patients with TA, no cases of recurrent hyperthyroidism were diagnosed, as judged from biochemical analysis, clinical symptoms and reduced demand for ATD. In the group with toxic nodular goiter, the percentage of successfully treated patients in the Li(+) group was approx. 25% (euthyroidism) and 70% had hypothyroidism; in the toxic adenoma group, it was approx. 70% (euthyroidism) and in the Li(+) group of patients, it was approx. 78% (hypothyroidism). Additionally, clinical signs were less pronounced during follow-up in patients with

Li(+). Similar percentages were observed for the control group, with hyperthyroidism found in 21.8% of patients and remission in 78.2% of patients. Our observations were confirmed by Bogazzi et al.,[31] who demonstrated that adjuvant lithium therapy is more effective, as evidenced by the fact that much better theranostic effects were obtained. Most patients (approx. 84%, with Li(+)) were given a single therapeutic dose of radioiodine.

No significant side effects (e.g., nausea, diarrhea and anorexia) were reported in the studied group of patients after administration of Li. Bogazzi et al.[31] used a similar treatment protocol (298 patients treated with combined ^{131}I and Li therapy) and reported nausea in 19.4% of patients and polyuria in 23.9% of patients, although these changes were not statistically significant.

Burrow et al.[39] observed side effects in only 2 of 13 patients receiving 900 mg of Li per day. The side effects consisted mainly of enlargement of the thyroid gland. However, goiter regressed after cessation of treatment. In 2015, the European Medicine Agency announced that long-term use of lithium might induce renal tumors. However, a recent study by Ambrosiani et al.[40] based on 33 years of observation of 1871 lithium patients (clinical records) clearly demonstrated low rates of and mortality due to thyroid or renal cancers in patients receiving permanent adjuvant lithium therapy.

In our study, due to the therapeutic activity of ^{131}I, no thyroid goiter was observed in any case. In all cases, goiter was significantly reduced, which was the aim of this treatment.

Limitations

Our study has some limitations. Firstly, we could not study the level of urinary iodine excretion in this group of patients as an indicator of the overall iodine pool in the body. Therefore, it is assumed that a significant reduction in thyroid iodine uptake capacity as a result of the increased overall pool of iodides in the body might be a possible determinant of Li inefficiency. Secondly, our study did not analyze the titer of the thyroid antibodies in serum; however, it has not been previously observed that short-term administration of Li results in intensification of clinical symptoms (e.g., infiltrative exophthalmos).

Conclusions

The results of this study of a large cohort of patients with different types of hyperthyroidism (GD, TMN and TA) suggest that a short course of adjuvant lithium and ^{131}I therapy is feasible, highly effective and safe, particularly in patients with low RAIU. Lithium therapy may be a valuable adjunct in this group of patients to reduce thyroid hormone levels.

ORCID iDs

Maria Teresa Płazińska https://orcid.org/0000-0002-2605-917X
Agata Czarnywojtek https://orcid.org/0000-0003-3595-8449
Nadia Sawicka-Gutaj https://orcid.org/0000-0003-1510-4702
Kosma Woliński https://orcid.org/0000-0001-9800-7881
Iwona Krela-Kaźmierczak https://orcid.org/0000-0001-5122-8003
Małgorzata Zgorzalewicz-Stachowiak https://orcid.org/0000-0001-9260-3674
Izabela Miechowicz https://orcid.org/0000-0003-0751-4867
Paweł Gut https://orcid.org/0000-0002-1661-175X
Ewa Florek https://orcid.org/0000-0002-2689-3009
Karolina Skonieczna-Żydecka https://orcid.org/0000-0002-3430-9079
Marek Ruchała https://orcid.org/0000-0002-6296-7220
Leszek Królicki https://orcid.org/0000-0002-7117-9621

References

1. Lazarus JH. Lithium and thyroid. *Best Pract Res Clin Endocrinol Metab*. 2009;23(6):723–733. doi:10.1016/j.beem.2009.06.002
2. Ozpoyraz N, Tamam L, Kulan E. Thyroid abnormalities in lithium-treated patients. *Adv Ther*. 2002;19(4):176–184. doi:10.1007/BF02848693
3. Deodhar SD, Singh B, Pathak CM, Sharan P, Kulhara P. Thyroid functions in lithium-treated psychiatric patients: A cross-sectional study. *Biol Trace Elem Res*. 1999;67(2):151–163. doi:10.1007/BF02784070
4. Kallner G, Petterson U. Renal, thyroid and parathyroid function during lithium treatment: Laboratory tests in 207 people treated for 1–30 years. *Acta Psychiatr Scand*. 1995;91(1):48–51. doi:10.1111/j.1600-0447.1995.tb09741.x
5. Kirov G. Thyroid disorders in lithium-treated patients. *J Affect Disord*. 1998;50(1):33–40. doi:10.1016/s0165-0327(98)00028-7
6. Johnston AM, Eagles JM. Lithium-associated clinical hypothyroidism: Prevalence and risk factors. *Br J Psychiatry*. 1999;175:336–339. doi:10.1192/bjp.175.4.336
7. Fagiolini A, Kupfer DJ, Scott J, et al. Hypothyroidism in patients with bipolar I disorder treated primarily with lithium. *Epidemiol Psichiatr Soc*. 2006;15(2):123–127. doi:10.1017/s1121189x00004322
8. Shine B, McKnight RF, Leaver L, Geddes JR. Long-term effects of lithium on renal, thyroid, and parathyroid function: A retrospective analysis of laboratory data. *Lancet*. 2015;386(9992):461–468. doi:10.1016/S0140-6736(14)61842-0
9. Suwansaksri N, Preechasuk L, Kunavisarut T. Nonthionamide drugs for the treatment of hyperthyroidism: From present to future. *Int J Endocrinol*. 2018;4:5794054. doi:10.1155/2018/5794054
10. Livingstone C, Rampes H. Lithium: A review of its metabolic adverse effects. *J Psychopharmacol*. 2006;20(3):347–355. doi:10.1177/0269881105057515
11. Mizukami Y, Michigishi T, Nonomura A, Nakamura S, Noguchi M, Takazakura E. Histological features of the thyroid gland in a patient with lithium induced thyrotoxicosis. *J Clin Pathol*. 1995;48(6):582–584. doi:10.1136/jcp.48.6.582
12. Robbins J. *The Role of TRH and Lithium in the Management of Thyroid Cancer*. Rome, Italy: Field Educational Italia; 1981:233–234.
13. Bogazzi F, Bartalena L, Brogioni S, et al. Comparison of radioiodine with radioiodine plus lithium in the treatment of Graves' hyperthyroidism. *J Clin Endocrinol Metab*. 1999;84(2):499–503. doi:10.1210/jcem.84.2.5446
14. Franklyn JA. The management of hyperthyroidism. *N Engl J Med*. 1994;330(24):1731–1738. doi:10.1056/NEJM199406163302407
15. Chouhan A, Abhyankar A, Basu S. The feasibility of low-dose oral lithium therapy and its effect on thyroidal radioiodine uptake, retention, and hormonal parameters in various subcategories of hyperthyroid patients: A pilot study. *Nucl Med Commun*. 2016;37(1):74–78. doi:10.1097/MNM.0000000000000414
16. Bonnema SJ, Hegedüs L. Radioiodine therapy in benign thyroid diseases: Effects, side effects, and factors affecting therapeutic outcome. *Endocr Rev*. 2012;33(6):920–980. doi:10.1210/er.2012-1030
17. Płazińska MT, Królicki L, Bąk M. Lithium carbonate pre-treatment in 131-I therapy of hyperthyroidism. *Nucl Med Rev Cent East Eur*. 2011;14(1):3–8. doi:10.5603/nmr.2011.0002
18. Sawicka-Gutaj N, Ziółkowska P, Sowiński J, et al. Recurrent goiters: Risk factors, patient quality of life, and efficacy of radioiodine therapy. *Pol Arch Intern Med*. 2019;129(1):22–27. doi:10.20452/pamw.4383

19. Franklyn JA, Daykin J, Drolc Z, Farmer M, Sheppard MC. Long-term follow-up of treatment of thyrotoxicosis by three different methods. *Clin Endocrinol (Oxf)*. 1991;34(1):71–76. doi:10.1111/j.1365-2265.1991.tb01738.x
20. Allahabadia A, Daykin J, Holder RL, Sheppard MC, Gough SC, Franklyn JA. Age and gender predict the outcome of treatment for Graves' hyperthyroidism. *J Clin Endocrinol Metab*. 2000;85(3):1038–1042. doi:10.1210/jcem.85.3.6430
21. Lowdell CP, Dobbs HJ, Spathis GS, McCready VR, Cosgrove DO, Harmer CL. Low-dose 131I in treatment of Graves' disease. *J Royal Soc Med*. 1985;78(3):197–202. doi:10.1177/014107688507800305
22. Nordyke RA, Gilbert FI Jr. Optimal iodine-131 dose for eliminating hyperthyroidism in Graves' disease. *J Nucl Med*. 1991;32(3):411–416. PMID:2005449
23. Watson AB, Brownlie BE, Frampton CM, Turner JG, Rogers TG. Outcome following standardized 185 MBq dose 131I therapy for Graves' disease. *Clin Endocrinol (Oxf)*. 1988;28(5):487–496. doi:10.1111/j.1365-2265.1988.tb03683.x
24. Jarlov AE, Hegedus L, Kristensen LO, Nygaard B, Hansen JM. Is calculation of the dose in radioiodine therapy of hyperthyroidism worthwhile? *Clin Endocrinol (Oxf)*. 1995;43(3):325–329. doi:10.1111/j.1365-2265.1995.tb02039.x
25. Sridama V, McCormick M, Kaplan EL, Fauchet R, DeGroot L. Long term follow-up study of compensated low-dose 131I therapy for Graves' disease. *N Engl J Med*. 1984;311(7):426–432. doi:10.1056/NEJM198408163110702
26. Czarnywojtek A, Płazińska MT, Zgorzalewicz-Stachowiak M, et al. Dysfunction of the thyroid gland during amiodarone therapy: A study of 297 cases. *Risk Ther Clin Manag*. 2016;4:505–513. doi:10.2147/TCRM.S96606
27. Martin NM, Patel M, Nijher GM, Misra S, Murphy E, Meeran K. Adjuvant lithium improves the efficacy of radioactive iodine treatment in Graves' and toxic nodular disease. *Clin Endocrinol (Oxf)*. 2012;77(4):621–627. doi:10.1111/j.1365-2265.2012.04385.x
28. Ruchała M, Sowiński J, Dolata M, Junik R, Gembicki M, Skiba A. Radioiodine treatment of hyperthyroidism in patients with low thyroid uptake. *Nucl Med Rev Cent East Eur*. 2005;8(1):28–32. PMID:15977144
29. Ruchała M, Szczepanek E. Thyroid ultrasound: A piece of cake? [in Polish]. *Endokrynol Pol*. 2011;62(Suppl 1):8–24. PMID:22125105
30. Mosteller RD. Simplified calculation of body-surface area. *N Engl J Med*. 1987;317(17):1098. doi:10.1056/NEJM198710223171717
31. Bogazzi F, Giovannetti C, Fessehatsion R, et al. Impact of lithium on efficacy of radioactive iodine therapy for Graves' disease: A cohort study on cure rate, time to cure, and frequency of increased serum thyroxine after antithyroid drug withdrawal. *J Clin Endocrinol Metab*. 2010;95(1):201–208. doi:10.1210/jc.2009-1655
32. Sedvall G, Jonsson B, Petterson V. Evidence of an altered thyroid function in man during treatment with lithium carbonate. *Acta Psychiatr Scand*. 1969;207(Suppl):59–66. https://doi.org/10.1111/j.1600-0447.1969.tb02045.x
33. Berens SC, Bernstein RS, Robbins J, Wolff J. Antithyroid effects of lithium. *J Clin Invest*. 1970;49(7):1357–1367.
34. Temple R, Berman M, Robbins J, Wolff J. The use of lithium in the treatment of thyreotoxicosis. *J Clinical Invest*. 1972;51(10):2746–2756. doi:10.1172/JCI107094
35. Turner JG, Brownlie BEW, Rogers TGH. Lithium as an adjunct to radioiodine therapy for thyrotoxicosis. *Lancet*. 1976;1(7960):614–615. doi:10.1016/s0140-6736(76)90419-0
36. Lee SY, Chang DLF, He X, Pearce EN, Braverman LE, Leung AM. Urinary iodine excretion and serum thyroid function in adults after iodinated contrast administration. *Thyroid*. 2015;25(5):471–477. doi:10.1089/thy.2015.0024
37. Berens SC, Wolff J, Murphy DL. Lithium concentration by the thyroid. *J Endocrinol*. 1970;87(5):1085–1091. doi:10.1210/endo-87-5-1085
38. Werner SC, Ingbar DH. *The Thyroid*. Philadelphia, USA: Lippincott Williams & Wilkins (LWW); 1991:578–585.
39. Burrow GN, Burke WR, Himmelhoch JM, et al. Effect of lithium on thyroid function. *J Clin Endocrinol Metab*. 1971;32(5):647–652. doi:10.1210/jcem-32-5-647
40. Ambrosiani L, Pisanu C, Deidda A, Chillotti C, Stochino ME, Bocchetta A. Thyroid and renal tumors in patients treated with long-term lithium: Case series from a lithium clinic, review of the literature and international pharmacovigilance reports. *Int J Bipolar Disord*. 2018;6(1):17. doi:10.1186/s40345-018-0125-9

Treatment results and safety assessment of the LARS system for the reconstruction of the anterior cruciate ligament

Maciej Kentel[1,A,C,E,F], Michał Barnaś[1,A–F], Jarosław Witkowski [2,E,F], Paweł Reichert[3,A,D–F]

[1] Orthopaedics and Traumatology Department, eMKa MED Medical Centre, Wrocław, Poland
[2] Division of Sports Medicine, Department of Physiotherapy, Faculty of Health Sciences, Wroclaw Medical University, Poland
[3] Department of Trauma and Hand Surgery, Faculty of Medicine, Wroclaw Medical University, Poland

A – research concept and design; B – collection and/or assembly of data; C – data analysis and interpretation;
D – writing the article; E – critical revision of the article; F – final approval of the article

Advances in Clinical and Experimental Medicine, ISSN 1899–5276 (print), ISSN 2451–2680 (online) *Adv Clin Exp Med*. 2021;30(4):379–386

Address for correspondence
Pawel Reichert
E-mail: pawelreichert74@gmail.com

Funding sources
None declared

Conflict of interest
None declared

Received on December 23, 2020
Reviewed on December 24, 2020
Accepted on December 30, 2020

Published online on April 28, 2021

Abstract

Background. Anterior cruciate ligament (ACL) reconstruction is the prevailing procedure in cases of ACL rupture.

Objectives. To assess the long-term safety of implementing a synthetic ligament with the Ligament Advanced Reinforcement System (LARS) in primary reconstruction of the ACL.

Material and methods. The retrospective analysis involved 403 patients who had undergone ACL reconstruction with the same results in clinical and functional assessments. The patients comprised 2 groups. In group I, a LARS graft was implemented, while in group II, an autograft was used. The Lachman test, anterior drawer test, pivot-shift test, Lysholm scale, IKDC 2000, pain posited to be experienced, the possibility of postoperative complications, the time required to return to work, and revision surgery were all considered and analyzed.

Results. The visual analogue scale (VAS) pain score in group I ranged from 37.34 ±8.22 mm on day 3 to 17.21 ±5.45 mm on day 28. In group II, it ranged from 64.72 ±10.20 mm on day 3 ($p < 0.05$) to 18.67 ±6.57 mm on day 28. The period of time taken to return to office work in group I was 7.04 ±1.82 weeks, and 9.21 ±1.75 weeks in group II ($p < 0.05$). The time taken to return to physical work in group I was 20.50 ±2.91 weeks, and 21.12 ±3.12 weeks in group II. Postoperative scar and local complications were statistically less prominent in group I. The cost and number of revision surgeries were greater in the first group.

Conclusions. Reconstruction of the ACL using a synthetic graft such as LARS yields similar results to an autograft in a cohort follow-up. Long-term results show a large number of revision surgeries when LARS is used. This method should be used with caution.

Key words: ACL reconstruction, LARS graft, arthroscopy, synthetic graft, autograft

Cite as
Kentel M, Barnaś M, Witkowski J, Reichert P. Treatment results and safety assessment of the LARS system for the reconstruction of the anterior cruciate ligament. *Adv Clin Exp Med*. 2021;30(4):379–386. doi:10.17219/acem/132037

DOI
10.17219/acem/132037

Copyright
© 2021 by Wroclaw Medical University
This is an article distributed under the terms of the Creative Commons Attribution 3.0 Unported (CC BY 3.0) (https://creativecommons.org/licenses/by/3.0/)

Background

The anterior cruciate ligament (ACL) is recognized as the most regularly injured ligament in the human knee.[1] In the USA, the average frequency of ACL injury incidence numbers 200,000 cases per year.[2] The injury most commonly occurs in individuals who are physically active and engage in dynamic sports.[1] For patients seeking to return to such physical activity, the standard treatment for ACL injury is ligament reconstruction,[3] followed by a postoperative physiotherapeutic procedure.[4,5] Restoring knee stability is the goal of reconstruction, and in turn aims to reduce the risk of secondary injuries such as further damage to the menisci and degenerative osteoarthritis.[6,7] An analysis of epidemiological data points to an increase in the incidence of ACL ruptures and ensuing reconstructions.[8] During the reconstruction, the torn ligament can usually be replaced with an autograft or allograft. Synthetic ligament usage is also a possible graft option. Autograft choices are the patellar, hamstring and quadriceps tendons, while the allograft options consist of the quadriceps, patellar, Achilles, hamstrings, anterior and posterior tibialis tendons, and the fascia lata.[9–11] Truncated surgical and anesthesia time, fewer postoperative complications, lower chance of morbidity at the harvest site, quicker postoperative recovery, less incidence of postoperative arthrofibrosis, and a lower amount of postoperative pain experienced are among the main advantages of allograft usage for ACL replacement.[4,5] In contrast, autograft usage may lead to higher rates of re-rupture, have limited availability, delay the process of healing and ligamentization when compared to autografts, have a higher risk of transmitting disease, and result in greater overall costs.[7,12,13] The synthetic materials being used in ACL reconstruction were introduced in hope of improving the firmness and stability of the graft after reconstruction, reducing instances of donor site morbidity, and eliminating the potential for disease transmission.[14] That being said, the first artificial grafts were plagued by high rates of failure and synovitis reactivation,[15] thus, with constantly advancing technology, new synthetic materials have been and are being developed for ACL reconstruction grafts.[16] The emergence of synthetic materials in ACL deficient knee treatment came at the beginning of the 20th century with the usage of silk and silver fibers. New synthetic materials being proposed for torn ACL replacements proliferated in the second half of the 20th century. These materials include Supramid®, Teflon® or Dacron®, Proplast®, carbon fiber graft, ABC graft, Kennedy-LAD®, Trevia, Leeds-Keio, Gore-Tex®, PDS®, EULIT®, and Polyflex®, Ligament Advanced Reinforcement System, and Ligament Advanced Reinforcement System (LARS)®.[17,18] Artificial ligaments have piqued surgeons' interest for all these years because of the optimism for grafts that are easily available and stronger than soft tissue "off-the-shelf" grafts, simplification of surgery, and avoidance of graft harvesting and donor site morbidity. However, most of the artificial grafts have been beset with high failure rates. One of the very few synthetic grafts gaining widespread popularity has been LARS®. It is suggested, however, that the ligament not be considered a potential graft for primary reconstruction of the ACL, and should be treated as an alternative graft in special cases, so the optimal synthetic graft material remains controversial.[19–21]

Objectives

The aim of this study was to assess the long-term safety of implementing the LARS synthetic ligament in the primary reconstruction of the ACL.

Materials and methods

The reported study was a retrospective cohort study. The sample was composed of patients who had undergone primary ACL reconstruction at the Trauma and Orthopedics Department of eMKaMED Hospital in Wrocław, Poland. Out of the 572 male patients treated from 2012 to 2018 with a partial lesion of the ACL involving anteromedial bundle damage requiring primary unilateral intra-articular ACL reconstruction, 403 patients homogeneous in terms of age and gender met the inclusion criteria for the study. Group I consisted of 46 patients aged 33.2 ±10.6 years who underwent primary unilateral ACL reconstruction of the knee using LARS graft; group II consisted of 357 patients aged 29.4 ±16.5 years who underwent primary unilateral ACL reconstruction of the knee with the use of autograft.

The study was carried out in accordance with the principles of the Declaration of Helsinki and was given approval by the Bioethics Committee of the Wroclaw Medical University. Each participant was informed of the aim of the study and the applied approach, and each signed to indicate their informed consent for participation in the study. An additional goal of the evaluation was to present the patient with the technique that was to be applied. The ACL capacity was analyzed with the 3 tests that are most frequently applied in clinical practice. The orthopedic assessment dealt with the range of motion (ROM) in the knee joint and included the Lachman test, anterior drawer test and pivot-shift test. The analysis was combined with a subjective evaluation using the International Knee Documentation Committee (IKDC) 2000 and Lysholm scales. Special attention was focused on complication and revision surgery. The follow-up was carried out over the course of 3 years.

The first limb assessed was the non-traumatic limb in order to evaluate its ROM and stability, and to make the patient familiar with the technique of the examination.

The examination was performed at 3, 7, 14 and 28 days post-surgery, and then at 12, 24 and 36 months post-surgery.

The ROM measurement of the knee was taken bilaterally using a standard goniometer. The inter-limb difference in anterior tibial dislocation taken from the Lachman test and anterior drawer test was judged normal (0; 0–2 mm), nearly normal (1+; 3–5 mm), abnormal (2+; 6–10 mm), or severely abnormal (3+; > 10 mm).[22] Anterolateral rotational knee stability was evaluated manually utilizing the pivot-shift test. The pivot-shift test was deemed negative when, referencing the ligament examination section of the 2000 IKDC, the anterolateral rotational dislocation of the tibia relative to the femur was equal in both lower limbs and positive when the difference between the limbs was judged + (glide), ++ (clunk) or +++ (gross). Moreover, early and late complications eventually requiring revision surgery were also analyzed.

Surgical technique

Each of the patients was operated on by the same team, employing the same surgical technique and autograft (hamstring; Fig. 1) or LARS (synthetic graft) (Fig. 2). The graft was secured using the Endobutton (Smith–Nephew, Warszawa, Poland) on the femur and the ComposiTCP30 interference screw (Biomet, Warszawa, Poland) on the tibia. It was constructed using the "outside-in" technique with the aimer device.

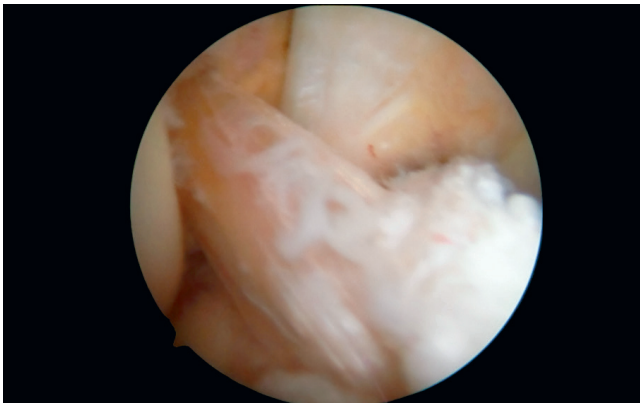

Fig. 1. Right knee ACL reconstruction using autograft

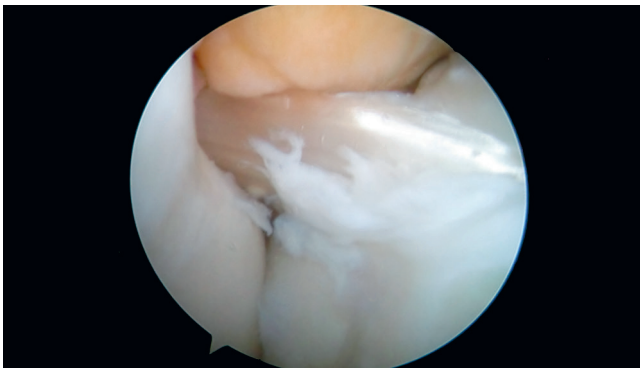

Fig. 2. Right knee ACL reconstruction using LARS

Postoperative management

Postoperative management was carried out according to ACL reconstruction protocol over a period of 6 months.

Statistical analysis

Statistical analysis was interpreted using TIBCO Statistica™ (TIBCO Software Inc., Palo Alto, USA) and Microsoft Office Excel 365 Personal (Microsoft Corporation, Redmond, USA). As for characteristics of the sample and the survey of the knee "giving way", as it is colloquially referred to, the results of Lachman test, anterior drawer test and pivot-shift test were used and the number of patients (n) who obtained a given result in each group established. The arithmetic mean (AM) and standard deviation (SD) were calculated for the following parameters: active extension and flexion range in both the involved and the uninvolved leg (°), and the total scores obtained on the Lysholm scale (n points) and IKDC 2000 questionnaire. The Shapiro–Wilk test was conducted to determine the normality of distribution for the parameters. Statistical significance was set at $p < 0.05$.

The visual analogue scale (VAS) was applied on days 3, 7, 14, and 28 post-surgery (VAS is a scaled ruler from 0 to 100 mm with an accuracy of 1 mm). Complications were then noted (hematomas at the collection site and intra-articular hematomas, skin sensation disturbances, pain in and around the back of the thigh). During the check-ups at 12, 24 and 36 months post-surgery, complications were noted (skin sensation disturbance, pain in the back of the thigh).

Choosing of the type of transplant by the patient

After qualifying the patient for surgery on the basis of the abovementioned diagnostics and their acceptance of this method of treatment, the graft choice was explored with the patient. The ultimate decision as to the choice of graft, after the operating physician discussed the available options along with their benefits and drawbacks, was made by the patient.

Results

There was no statistical difference considering clinical examination and subjective and objective scales (i.e., Lachman test, anterior drawer test, pivot-shift test, Lysholm scale, and IKDC 2000 evaluation). Statistical differences were found when referring to return to work and to physical activity, and to resulting complications.

Patients after undergoing surgery utilizing LARS returned more quickly to work and physical activity. On the other hand, the main complications also concern

the LARS group. Revision surgery was performed much more often in the LARS group than in the autograft group (50% compared to 4.5%). Moreover, revision operations in the LARS group were much more difficult to perform due to the greater damage to the knee.

Functional assessment results

Within 24 months of the reconstruction of the ACL, the average total number of points obtained on the Lysholm scale in group I was 98.65 ±4.25 points. In group II, patients obtained an average of 97.42 ±4.28 points in the same period after the surgery (Fig. 3). Comparative analyses of the results of the functional assessment based on the Lysholm scale did not show statistically significant differences in the examined groups ($p = 0.212$).

Within 24 months of the reconstruction of the ACL, the average total number of points on the IKDC 2000 scale obtained in group I was 96.79 ±6.54 points. In group II, patients obtained an average of 95.21 ±5.36 points in the same period since surgery (Fig. 3). Comparative analyses of the results of the functional assessment did not show statistically significant differences in the examined groups ($p = 0.886$).

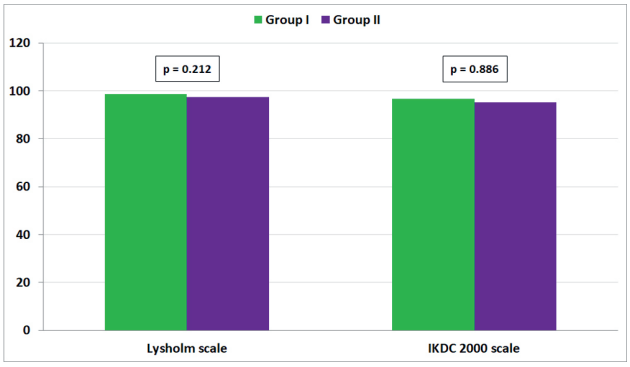

Fig. 3. Comparative analysis of the total number of points on the Lysholm scale and on the IKDC 2000 scale obtained in group I and group II

Results of pain assessment

The pain felt on a daily basis in the operated limb in group I can be interpreted as mild and at a maximum on the 3rd day post-operation (AM = 37.34 ±8.22 mm). A comparative inspection of the results of the assessment of the extremity of daily pain in the operated limb in group I exhibited statistically significant differences ($p \leq 0.001$) between the results acquired successively on postoperative days 3, 7, 14, and 28 (Fig. 4). The intensity of pain felt on a daily basis in the operated limb in group I was significantly lower ($p \leq 0.001$) on postoperative day 7 (AM = 29.22 ±7.67 mm) than on postoperative day 3 (AM = 37.34 ±8.22 mm). Pain experienced also significantly decreased ($p \leq 0.001$) on the 14th postoperative day (AM = 20.67 ±6.66 mm) compared to the 7th postoperative day. The intensity of pain sensations in the operated limb on the 28th postoperative day (AM = 17.21 ±5.45 mm) was comparable to the pain experienced on the 14th day after surgery ($p = 0.448$). The pain experienced in the operated limb in group II on the 3rd postoperative day was moderate in nature (AM = 64.72 ±10.20 mm). In the subsequent postoperative days, the values did not exceed 49.54 mm, and can therefore be considered mild pain. Comparative analyses of the evaluation results of the intensity of pain experienced on a daily basis in the operated limb in group II, similarly to group I, showed statistically significant differences ($p \leq 0.001$) between the results obtained successively on 3, 7, 14, and 28 days post-surgery (Fig. 4). The intensity of daily pain in the operated limb in group II significantly ($p \leq 0.001$) decreased on day 7 after the surgery (AM = 49.54 ±9.33 mm) when compared to day 3 after surgery (AM = 64.72 ±10.20 mm). Between days 7 and 14 post-surgery (AM = 32.42 ±8.20 mm), the intensity of pain also decreased significantly ($p \leq 0.001$). Pain felt in the operated limb on day 28 after the operation (AM = 18.67 ±6.57 mm) was significantly ($p \leq 0.001$) less intense than on the 14th day after the operation. Comparing results of the assessment of the intensity of pain experienced daily in the operated limb showed that in group I, the level of pain was significantly lower than in group II (from $p \leq 0.001$ to $p = 0.28$). A comparative analysis of the results obtained in both examined groups is shown in Fig. 4.

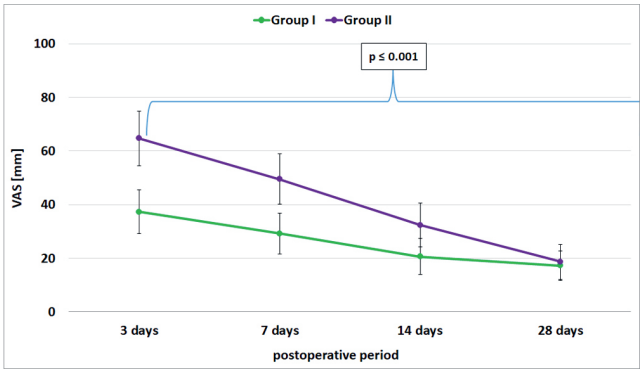

Fig. 4. Results of the assessment of the intensity of daily pain experienced in the operated limb in groups I and II on subsequent postoperative days

Results of the return to work evaluation

The patients from group I were able to return to office work significantly ($p \leq 0.001$) earlier (AM = 7.04 ±1.82 weeks) than to physical work (AM = 20.50 ±2.91 weeks). In group II, patients were also able to return to office work significantly ($p \leq 0.001$) more quickly (AM = 9.21 ±1.75 weeks) than to physical work (AM = 21.12 ± 3.12 weeks) (Fig. 5). Patients from group I returned to office work significantly earlier ($p \leq 0.001$) than patients from group II. The time necessary in order to return to physical work was similar in both groups ($p = 0.904$) (Fig. 5).

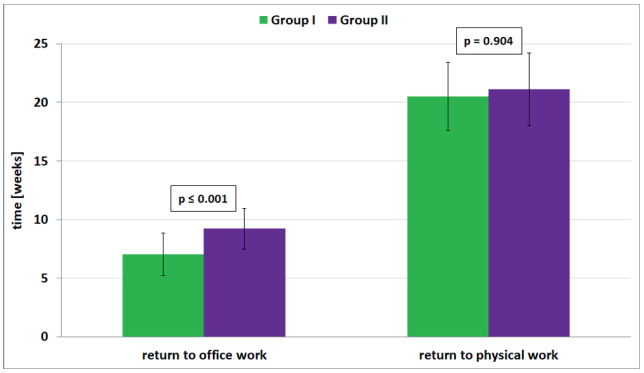

Fig. 5. Comparison of time taken to return to office work and to physical work in both groups

Local postoperative complications

Skin hypoesthesia was not present in any of the patients in group I. In contrast, it was present in 187 patients in group II, accounting for 52% of patients in this group. Symptoms of skin hypoesthesia subsided in less than 6 months after reconstruction of the ACL in 52% of the patients. Symptoms of skin hypoesthesia subsided within 12 months of surgery in 6% of the patients. No patients in group I complained of discomfort in the posterior thigh of the operated limb. However, 84 patients from group II reported this symptom, which accounted for 24% of the patients from this group. Thigh pain resolved in less than 1 month of reconstruction of the ACL in 88% of the patients. In the remaining 12% of patients, discomfort in the posterior thigh of the operated limb lingered for more than 12 months post-surgery. Twenty-four patients from group II had a hematoma at the graft site, which made up 6% of group II. Three out of 24 patients with hematoma received conservative treatment, and 1 patient out of the 4 with hematoma required surgical intervention.

Late complications

Revision surgery in autograft group was required in 21 cases (5.6%) because of: secondary instability (loosening graft) – 4 cases, secondary instability (graft rupture) – 14 cases, arthrofibrosis – 2 cases, and joint infection – 1 case.

Revision surgery in LARS group was performed in 23 cases (50%) because of: secondary instability (loosening graft) – 1 case, secondary instability (graft rupture) – 18 cases, arthrofibrosis – 2 cases, joint infection – 1 case, synovitis – 2 cases, cartilage lesion – 2 case, and synovial cyst – 5 cases (Fig. 6–11).

Discussion

The ACL reconstruction in adults using the LARS technique yields good results in short-term postoperative observations. The main advantages are: the possibility

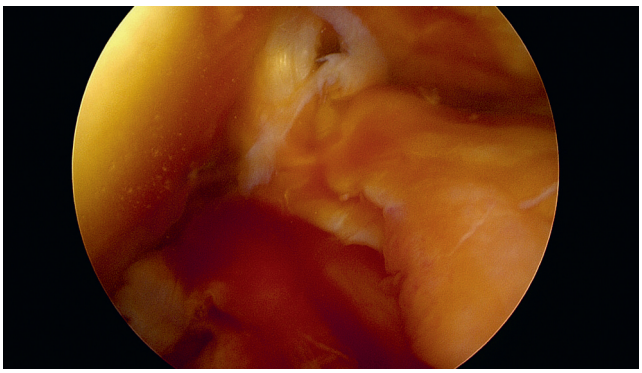

Fig. 6. LARS rupture after 12 months

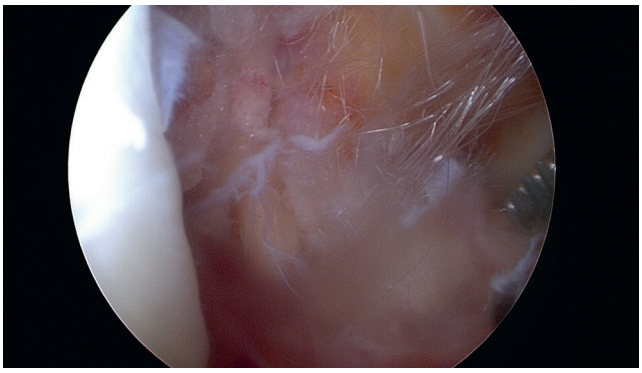

Fig. 7. Partial LARS rupture after 12 months – synthetic components

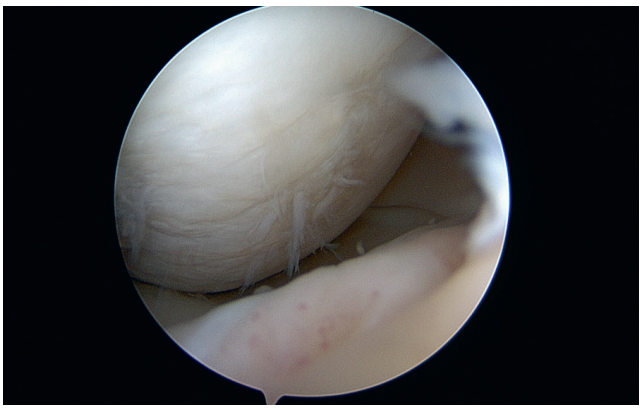

Fig. 8. Cartilage damage

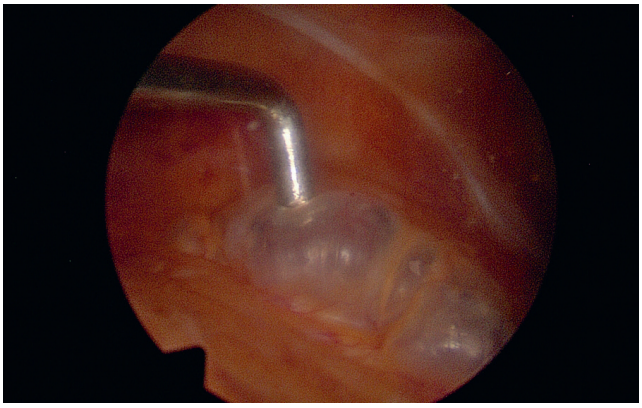

Fig. 9. Synovitis

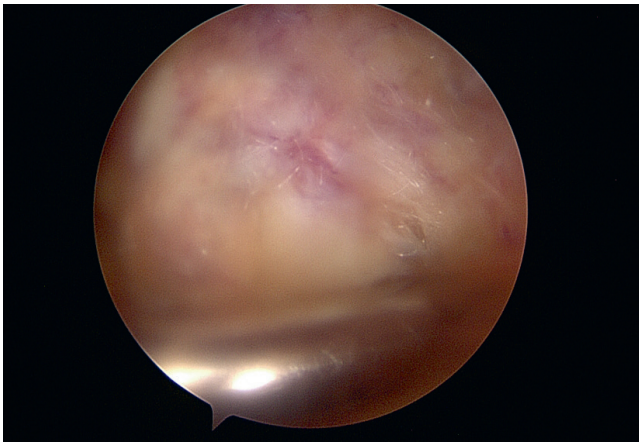

Fig. 10. Partial LARS rupture after 24 months – synthetic components

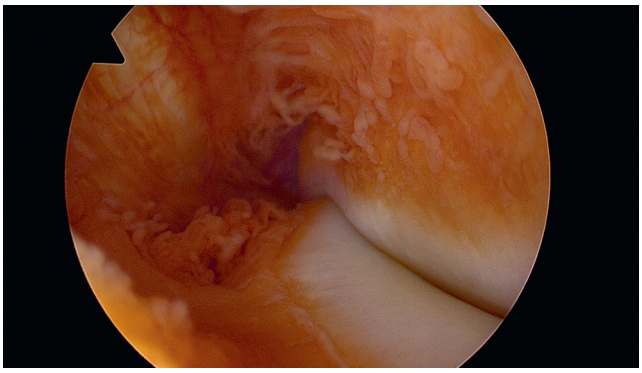

Fig. 11. Synovitis after 24 months

of increased load on the limb in a shorter time compared to natural grafts, increased mechanical strength, no local complications related to graft collection, and overall lower cost than autograft.[23–26] This was also confirmed in our research.[27–29]

Despite the existence of the LARS technique since the 1990s, it is a rarely performed procedure compared to natural transplants. There are also few long-term postoperative follow-ups.[25,26,30]

The gold standard in ACL reconstruction is still reconstruction with the use of autogenous transplant. The LARS method is intended for people who require revision reconstructions, with limited possibilities of obtaining an autogenous transplant. It is not recommended for very young people. In our study, we also did not qualify such people for surgery. This technique is intended for elderly patients who want to quickly regain their fitness with the possibility of full load on the knee joint shortly after the procedure.[31]

One of the synthetic material grafts introduced in the 2nd half of the 20th century was a graft made of polyester, which evolved into a non-absorbable synthetic ligament device made of terephthalic polyethylene polyester fibers – LARS.[32] It is intensively cleaned with the aim to remove potential machining residues and oils to further encourage soft tissue in-growth and reduce the risk of reactive synovitis. The LARS consists of 2 parts: an intra-articular part and an extra-articular part. The ligament intra-articular portion/scaffold is built of multiple parallel fibers that are twisted at 90° angle.[32] The part is composed of 2 longitudinal external rotation fibers without transverse fibers, being designed as an imitation of ACL anatomic structure. The extra-articular part is waved using longitudinal and transverse fibers with the aim to avoid ligament deformation. The short-term postoperative results of patients after ACL reconstruction with the use of LARS are very satisfying.[33] A mean 2.5-year follow-up carried out by Dericks revealed encouraging results of treatment with the use of LARS.[32] Also, a follow-up at a mean of 8 years reported by Parchi et al. showed satisfying results reflected in no postoperative complication occurrences and only 1 case of LARS rupture.[34] On the other hand, the ten-year postoperative follow-up carried out by Tiefenboeck et al. revealed a lack of subjective satisfaction in ½ of patients treated with the use of LARS; thus, the authors suggested not to consider the ligament system as a potential graft for primary reconstruction of the ACL and to treat it as an alternative graft in special cases.[35] In our study, a very large number of revisions occurred after only 36 months.

Many studies have compared the results of ACL treatment using autografts and the synthetic LARS ligament. The most frequently compared autograft is the four-fold hamstring transplant. Patellar ligament (B-PT-B) and quadriceps tendon (QT) grafts have been studied less frequently.[35–39]

Zhong conducted a four-year follow-up study on a group of 60 patients (32 autografts and 28 synthetic grafts). The results were as follows: the difference in anterior tibia translation (ATT) of the operated and healthy limbs was on average 2.4 ±0.5 mm for the natural graft and 1.2 ±0.3 mm for the synthetic graft. A translation difference of more than 5 mm occurred in 3 patients operated on with hamstrings and in none in the LARS group. In terms of the IKDC 2000 rating, 87.5% of the hamstrings group and 92.9% of the LARS group achieved a normal or near-normal result. The mean values of the Lysholm scale were 92.1 ±7.9 and 94.6 ±9.2, and for the Tegner scale they were 6.2 ±1.6 and 6.6 ±1.8, respectively, for autograft and synthetic graft group. In the 4SGH (hamstrings) group, 6.25% of respondents complained of a 5° flexion deficit in the operated knee joint, and 3.13% suffered complications due to arthrofibrosis. In the LARS group, no complications related to limited ROM in the knee were observed.[36] In terms of the IKDC 2000 and Lysholm scale, the results are similar to the results of our research.

Bianchi in his eight-year meta-analysis of the effectiveness of the 4SHG (25 patients) and LARS (25 patients) methods, assessed the occurrence of Lachman's symptom, which was 56% for LARS and 24% for 4SHG, with the anterior drawer test at 68% for LARS and 16% for 4SHG.[37]

Xiaoyu and Yecheng compared the effectiveness of treating ACL lesions using the technique of transplantation from the patellar tendon (BTB) and LARS in independent

studies on groups of 62 patients (30 BTB and 32 LARS) and 50 patients (26 BTB and 24 LARS), with a four-year postoperative follow-up in both studies.[38,39]

All researchers, regardless of the type of material used as an autograft, draw the same conclusions: They emphasize significantly better ligamentous stability of the knee in physical examinations of LARS groups. We did not see a similar relationship. At the same time, the cited researchers describe the results of the IKDC 2000, Lysholm and Tegner tests, and subjective complaints about the knee joint without statistically significant differences in the compared groups. They write about significantly less pain and earlier stress on the limb in the LARS groups compared to the groups subjected to ACL reconstructions with the use of natural transplants. They note, however, that this effect is observed only in the early postoperative period up to 1 year (it is associated with the time of ligamentization – that is, reconstruction of natural grafts).[36–40]

Despite better results in the LARS treatment of ACL injuries, scientists agree that autograft augmentation remains the method of choice. They support this decision with a lack of documented long-term observations. The longest follow-up after the LARS procedure, which we found in the literature, was 11.6 years.[24]

In our opinion, such a large number of revision surgeries and complications do not justify the use of this method. To date, no published studies have directly compared the results of ACL reconstruction treatment with the LARS technique and allografts.

Limitations

The most obvious drawback of this study is the short-term follow-up. In the future, studies involving long-term follow-up with patients that have undergone fully supervised physiotherapeutic procedures and comprehensive clinical and functional evaluations need to be taken into account.

Conclusions

Currently, numerous studies are being conducted that emphasize genetic predisposition to cruciate ligament injuries. The ACL "suture" techniques need additional testing and studies, and require much more scientific material. Research on the application of stem cells, scaffolds, plasma rich platelets, and xenografts are also breaking ground. These trends in the constant progression of ACL surgery will make way for a far more individualized method of operation and treatment.

Reconstruction of the ACL using a synthetic graft such as LARS gives similar results as autograft in a cohort follow-up. Long-term results show a large number of revision surgeries when using LARS. Using this method should be employed with caution.

ORCID iDs

Maciej Kentel https://orcid.org/0000-0002-7610-5410
Michał Barnaś https://orcid.org/0000-0003-2148-844X
Jarosław Witkowski https://orcid.org/0000-0002-2754-1339
Paweł Reichert https://orcid.org/0000-0002-0271-4950

References

1. Anderson MJ, Browning WM III, Urband CE, Kluczynski MA, Bisson LJ. A systematic summary of systematic reviews on the topic of the anterior cruciate ligament. *Orthop J Sports Med*. 2016;4(3):232596711663 4074. doi:10.1177/2325967116634074
2. Prodromos CC, Han Y, Rogowski J, Joyce B, Shi K. A meta-analysis of the incidence of anterior cruciate ligament tears as a function of gender, sport, and a knee injury-reduction regimen. *Arthroscopy*. 2007;23(12):1320–1325.e6. doi:10.1016/j.arthro.2007.07.003
3. Ekstrand J. A 94% return to elite level football after ACL surgery: A proof of possibilities with optimal caretaking or a sign of knee abuse? *Knee Surg Sports Traumatol Arthrosc*. 2011;19(1):1–2. doi:10.1007/s00167-010-1300-4
4. Czamara A, Królikowska A, Szuba Ł, Widuchowski W, Kentel M. Single- vs. double-bundle anterior cruciate ligament reconstruction: A new aspect of knee assessment during activities involving dynamic knee rotation. *J Strength Cond Res*. 2015;29(2):489–499. doi:10.1519/JSC.0000000000000638
5. Królikowska A, Sikorski Ł, Czamara A, Reichert P. Effects of postoperative physiotherapy supervision duration on clinical outcome, speed, and agility in males 8 months after anterior cruciate ligament reconstruction. *Med Sci Monit*. 2018;24:6823–6831. doi:10.12659/MSM.912162
6. Zeng C, Gao SG, Li H, et al. Autograft versus allograft in anterior cruciate ligament reconstruction: A meta-analysis of randomized controlled trials and systematic review of overlapping systematic reviews. *Arthroscopy*. 2016;32(1):153–163.e18. doi:10.1016/j.arthro.2015.07.027
7. Samuelsson K, Andersson D, Ahldén M, Fu FH, Musahl V, Karlsson J. Trends in surgeon preferences on anterior cruciate ligament reconstructive techniques. *Clin Sports Med*. 2013;32(1):111–126. doi:10.1016/j.csm.2012.08.011
8. Buller LT, Best MJ, Baraga MG, Kaplan LD. Trends in anterior cruciate ligament reconstruction in the United States. *Orthop J Sports Med*. 2014;3(1):2325967114563664. doi:10.1177/2325967114563664
9. Chen H, Chen B, Tie K, Fu Z, Chen L. Single-bundle versus double-bundle autologous anterior cruciate ligament reconstruction: A meta-analysis of randomized controlled trials at 5-year minimum follow-up. *J Orthop Surg Res*. 2018;13(1):50. doi:10.1186/s13018-018-0753-x
10. Bieri KS, Scholz SM, Kohl S, Aghayev E, Staub LP. Dynamic intraligamentary stabilization versus conventional ACL reconstruction: A matched study on return to work. *Injury*. 2017;48(6):1243–1248. doi:10.1016/j.injury.2017.03.004
11. Brown MJ, Carter T. ACL allograft: Advantages and when to use. *Sports Med Arthrosc Rev*. 2018;26(2):75–78. doi:10.1097/JSA.0000000000000194
12. Barrera Oro F, Sikka RS, Wolters B, et al. Autograft versus allograft: An economic cost comparison of anterior cruciate ligament reconstruction. *Arthroscopy*. 2011;27(9):1219–1225. doi:10.1016/j.arthro.2011.04.008
13. Cooper MT, Kaeding C. Comparison of the hospital cost of autograft versus allograft soft-tissue anterior cruciate ligament reconstructions. *Arthroscopy*. 2010;26(11):1478–1482. doi:10.1016/j.arthro.2010.04.004
14. Debieux P, Franciozi CE, Lenza M, et al. Bioabsorbable versus metallic interference screws for graft fixation in anterior cruciate ligament reconstruction. *Cochrane Database Syst Rev*. 2016;7(7):CD009772. doi:10.1002/14651858.CD009772.pub2
15. Herz M. Die chirurgische Behandlung paralytischer Schlotterelenke-Seitenligamente oder Arthrodese? [The surgical treatmentof paralytic flail knees: Silk ligaments or arthrodesis]. *Munch Med Wschr*. 1906;51:2527–2529.
16. Schindler OS. Surgery for anterior cruciate ligament deficiency: A historical perspective. *Knee Surg Sports Traumatol Arthrosc*. 2012;20(1):5–47. doi:10.1007/s00167-011-1756-x
17. West RV, Harner CD. Graft selection in anterior cruciate ligament reconstruction. *J Am Acad Orthop Surg*. 2005;13(3):197–207. doi:10.5435/00124635-200505000-00006

18. Zoltan DJ, Reinecke C, Indelicato PA. Synthetic and allograft anterior cruciate ligament reconstruction. *Clin Sports Med*. 1988;7(4):773–784. PMID:3052882
19. Wilk RM, Richmond JC. Dacron ligament reconstruction for chronic anterior cruciate ligament insufficiency. *Am J Sports Med*. 1993;21(3): 374–380. doi:10.1177/036354659302100308
20. Maletius W, Gillquist J. Long-term results of anterior cruciate ligament reconstruction with a Dacron prosthesis: The frequency of osteoarthritis after seven to eleven years. *Am J Sports Med*. 1997;25(3):288–293. doi:10.1177/036354659702500303
21. Drogset JO, Grøntvedt T, Robak OR, Mølster A, Viset AT, Engebretsen L. A sixteen-year follow-up of three operative techniques for the treatment of acute ruptures of the anterior cruciate ligament. *J Bone Joint Surg Am*. 2006;88(5):944–952. doi:10.2106/JBJS.D.02876
22. Girgis FG, Marshall JL, Monajem A. The cruciate ligaments of the knee joint: Anatomical, functional and experimental analysis. *Clin Orthop Relat Res*. 1975;(106):216–231. doi:10.1097/00003086-197501000-00033
23. Cieślik-Bielecka A, Reichert P, Skowroński R, Królikowska A, Bielecki T. A new aspect of in vitro antimicrobial leukocyte- and platelet-rich plasma activity based on flow cytometry assessment. *Platelets*. 2019; 30(6):728–736. doi:10.1080/09537104.2018.1513472
24. Parchi PD, Ciapini G, Paglialunga C, et al. Anterior cruciate ligament reconstruction with LARS artificial ligament: Clinical results after a long-term follow-up. *Joints*. 2018;6(2):75–79. doi:10.1055/s-0038-1653950
25. Cerulli G, Antinolfi P, Bruè S, et al. Esperienza clinica nell'utilizzo di biomateriali nel ginocchio. *GIOT*. 2011;37(Suppl 1):159–166.
26. Jia Z, Xue C, Wang W, Liu T, Huang X, Xu W. Clinical outcomes of anterior cruciate ligament reconstruction using LARS artificial graft with an at least 7-year follow-up. *Medicine (Baltimore)*. 2017;96(14):e6568. doi:10.1097/MD.0000000000006568
27. Czamara A, Markowska I, Królikowska A, Szopa A, Domagalska-Szopa M. Kinematics of rotation in joints of the lower limbs and pelvis during gait: Early result of SB ACLR approach versus DB ACLR approach. *Biomed Res Int*. 2015;2015:707168. doi:10.1155/2015/707168
28. Królikowska A, Reichert P, Czamara A, Krzemińska K. Peak torque angle of anterior cruciate ligament-reconstructed knee flexor muscles in patients with semitendinosus and gracilis autograft is shifted towards extension regardless of the postoperative duration of supervised physiotherapy. *PLoS One*. 2019;14(2):e0211825. doi:10.1371/journal.pone.0211825
29. Królikowska A, Sikorski Ł, Czamara A, Reichert P. Are the knee extensor and flexor muscles isokinetic parameters affected by the duration of postoperative physiotherapy supervision in patients eight months after ACL reconstruction with the use of semitendinosus and gracilis tendons autograft? *Acta Bioeng Biomech*. 2018;20(4):89–100.
30. Wang CL, Hsiao CK, Ku MC, Chang CH. Arthroscopic anterior cruciate ligament reconstruction with LARS artificial ligament: An 8–15-year follow-up. *J Mech Med Biol*. 2013;13(2):1350046.
31. Seil R, Weitz FK, Pape D. Surgical-experimental principles of anterior cruciate ligament (ACL) reconstruction with open growth plates. *J Exp Orthop*. 2015;2(1):11. doi:10.1186/s40634-015-0027-z
32. Dericks G. Ligament advanced reinforcement system anterior cruciate ligament reconstruction. *Oper Tech Sports Med*. 1995;3(3):187–205. doi:10.1016/S1060-1872(95)80009-3
33. Jia ZY, Zhang C, Cao SQ, et al. Comparison of artificial graft versus autograft in anterior cruciate ligament reconstruction: A meta-analysis. *BMC Musculoskelet Disord*. 2017;18(1):309. doi:10.1186/s12891-017-1672-4
34. Parchi PD, Gianluca C, Dolfi L, et al. Anterior cruciate ligament reconstruction with LARS™ artificial ligament results at a mean follow-up of eight years. *Int Orthop*. 2013;37(8):1567–1574. doi:10.1007/s00264-013-1917-2
35. Tiefenboeck TM, Thurmaier E, Tiefenboeck MM, et al. Clinical and functional outcome after anterior cruciate ligament reconstruction using the LARS™ system at a minimum follow-up of 10 years. *Knee*. 2015;22(6):565–568. doi:10.1016/j.knee.2015.06.003
36. Liu ZT, Zhang XL, Jiang Y, Zeng BF. Four-strand hamstring tendon autograft versus LARS artificial ligament for anterior cruciate ligament reconstruction. *Int Orthop*. 2010;34(1):45–49. doi:10.1007/s00264-009-0768-3
37. Bianchi N, Sacchetti F, Bottai V, et al. LARS versus hamstring tendon autograft in anterior cruciate ligament reconstruction: A single-centre, single surgeon retrospective study with 8 years of follow-up. *Eur J Orthop Surg Traumatol*. 2019;29(2):447–453. doi:10.1007/s00590-018-2304-x
38. Li Y, Zhang W, Wu Y, et al. A comparison of effectiveness between ligament advanced reinforcement system and bone-patellar tendon-bone autograft for anterior cruciate ligament reconstruction [in Chinese]. *Zhongguo Xiu Fu Chong Jian Wai Ke Za Zhi*. 2012;26(9):1045–1050.
39. Pan X, Wen H, Wang L, Ge T. Bone-patellar tendon-bone autograft versus LARS artificial ligament for anterior cruciate ligament reconstruction. *Eur J Orthop Surg Traumatol*. 2013;23(7):819–823. doi:10.1007/s00590-012-1073-1
40. Lavoie P, Fletcher J, Duval N. Patient satisfaction needs as related to knee stability and objective findings after ACL reconstruction using the LARS artificial ligament. *Knee*. 2000;7(3):157–163. doi:10.1016/s0968-0160(00)00039-9

The effect of different storage times on the oxygen-carrying capacity of the exosomes of red blood cells

Li-Shuang Duan[1,A–D,F], Yang Liu[2,A–D,F], Zhen-Zhou Li[1,B,C,E,F], Huan Wang[1,B,C,F], Xiao-Fang Zhou[1,B,C,F], Xiao-Xiao Wang[1,B,C,F], Zi-Wei Zhang[1,C,F], Yi-Qun Kang[1,C,F], Yong-jun Su[3,C,F], Jian-Rong Guo[1,2,C,E,F]

[1] Department of Anesthesiology, Shanghai Gongli Hospital, The Second Military Medical University, China
[2] Ningxia Medical University, Gongli Hospital of Shanghai Pudong New Area Training Base, China
[3] Department of Anesthesiology, Fujian Provincial Hospital South Branch, Fuzhou, China

A – research concept and design; B – collection and/or assembly of data; C – data analysis and interpretation; D – writing the article; E – critical revision of the article; F – final approval of the article

Advances in Clinical and Experimental Medicine, ISSN 1899–5276 (print), ISSN 2451–2680 (online) *Adv Clin Exp Med*. 2021;30(4):387–394

Address for correspondence
Jian-Rong Guo
E-mail: jr_guo@yeah.net

Funding sources
This work has been supported by the Key Disciplines Group Construction Project of Pudong Health Bureau of Shanghai (grant No. PWZxq2017-10) and National Natural Science Foundation of China (grant No. 81870147).

Conflict of interest
None declared

Received on June 2, 2020
Reviewed on June 3, 2020
Accepted on December 26, 2020

Published online on April 28, 2021

Abstract

Background. After storing blood for a period of time, the structure and properties of the red blood cells (RBC) will change, which results in a decrease in the oxygen-carrying capacity, and further has a certain impact on their exosomes.

Objectives. Effective oxygen uptake (Q), P50, 2,3-DPG, and Na^+-K^+-ATP of RBC after different storage times were detected. Electron microscopy was used to observe the morphology of RBC and the characteristics of secreting exosomes. Western blot was used to detect the expression of phenotypes CD63 and CD81 of exosomes, and the expression of mitochondrial riboprotein MRPS35 of exosomes was also detected to explore the mechanism of decreased function of RBC with the extension of preservation time.

Materials and methods. After the RBC suspension was prepared, the effective oxygen-carrying capacity (Q) and P50, as well as 2,3-DPG and Na^+-K^+-ATP were prepared. This was followed by morphology observation of erythrocyte exosomes using transmission electron microscope (TEM), and by western blot analysis of exosome phenotypes CD63 and CD81.

Results. Erythrocytes secrete exosomes, which results in abnormal expression of related proteins in mitochondria. This leads to increased ROS production, mitochondrial apoptosis and, finally, changes in or damage to erythrocytes.

Conclusions. Changes in the rheological properties and oxygen-carrying functions of erythrocytes during preservation are all observable manifestations, underlying which lie mechanisms of damage at the molecular level of erythrocytes. Erythrocytes secrete exosomes, which results in abnormal expression of related proteins in mitochondria, increasing ROS production, mitochondrial apoptosis and, finally, changes or damage to erythrocytes.

Key words: exosomes, red blood cells, storage time, oxygen-carrying capacity

Cite as
Duan L-S, Liu Y, Li Z-Z, et al. The effect of different storage times on the oxygen-carrying capacity of the exosomes of red blood cells. *Adv Clin Exp Med*. 2021;30(4):387–394. doi:10.17219/acem/131962

DOI
10.17219/acem/131962

Copyright
© 2021 by Wroclaw Medical University
This is an article distributed under the terms of the Creative Commons Attribution 3.0 Unported (CC BY 3.0) (https://creativecommons.org/licenses/by/3.0/)

Background

Blood is a fluid tissue composed of blood cells and plasma. Its main physiological functions include transporting oxygen, nutrients and metabolites for tissues and organs of the body. The body takes the oxygen needed for metabolism from the atmosphere through breathing and expels carbon dioxide produced by metabolism. In the human body, the respiratory process includes 3 processes that are conducted at the same time, namely, external respiration, transportation of gas in blood and internal respiration, while red blood cells (RBC) are the main means of gas transportation.[1] The amount of oxygen physically dissolved in the blood only accounts for 1.5% of the total oxygen and 98.5% of oxygen is transported by binding to the hemoglobin of RBC.[2] In a sense, RBC are able to distinguish active and inactive cells that take part in metabolism and release oxygen to active cells.

In modern medicine, it is very common therapeutic practice to transfer blood or blood components to patients, which can increase blood volume and plasma protein, improve circulation, change blood composition, and improve blood oxygen-carrying capacity. Due to the widespread using of blood transfusion in clinical practice, the function of blood preservation has been reconsidered. The structure and properties of RBC will change and their oxygen-carrying capacity will decrease after preservation for a period of time. However, the influence of changes in oxygen-carrying capacity on their erythrocyte exosomes has not been reported.

Objectives

Our research aimed to detect some relative parameters of oxygen-carrying activity and exosomes of erythrocyte storing in different storage time to explore the mechanism of erythrocyte function decline.

Materials and methods

Materials

Flow meter (Changzhou Chengfeng Flow Meter Company, Changzhou, China); pressure gauge (Yangquan Precision Instrument Factory, China); Cy-3 digital oxygen analyzer (Shanghai Huaguang Instrument Factory, Shanghai, China); BC-2800 blood count instrument (Mindray Medical International, Shenzen, China); 37°C constant temperature water bath (GSY-II; Beijing Medical Equipment Factory, Beijing, China); low speed M109077 automatic centrifuge (Zhongxi, Shanghai, China); 200 L and 1000 L samplers (Eppendorf, Hamburg, Germany); AB fresh/frozen plasma and defoaming agent were donated from blood bank; 2,3-DPG detection kit (Wuhan Huamei Biotechnology Company, Wuhan, China); Na^+-K^+-ATPase assay kit (Nanjing Jiancheng Biological Company, Nanjing, China); rabbit anti-human CD63 antibody, rabbit anti-human CD81 antibody (System Biosciences, Palo Alto, USA); H7600 transmission electron microscope (TEM) (Hitachi, Tokyo, Japan); and exosome extraction kit (Sigma-Aldrich, St. Louis, USA).

Preparation of RBC suspension

A total of 400 mL whole blood were collected from 5 healthy blood donors and all blood samples were examined to confirm that they accord with the national blood and component blood quality requirements.[3] When they passed the examination and conformed to the operation procedures of blood station technical operation regulations (2012 edition), the blood samples were prepared into suspended RBC.[4] Suspended RBC were divided into 5 empty bags using sterile bonder, and named 1 day group, 7 day group, 14 day group, 21 day group, and 28 day group. Q, P50, 2,3-DPG and Na^+-K^+-ATP in suspension of RBC and whole blood were observed. This research has been authorized for ethical review by hospital committees, and all volunteers agree to sign the informed consent.

Measurement of effective oxygen-carrying capacity (Q) and P50

The blood samples were centrifuged with 3696 × g/min at 4°C for 10 min after conventional anticoagulant treatment. Then plasma was removed and CPDA-1 erythrocyte preservation fluid was added to prepare suspended RBC. Suspended RBC coming from the same patient were divided into 5 copies and restored at 4°C. The blood samples were tested at 1, 7, 14, 21, and 28 days. Arterial oxygen partial pressure was simulated under the following test conditions: O_2 = 16 mL/min, CO_2 = 3 mL/min, N_2 = 120 mL/min, flow rate: 100 mL/min, 37°C to sample inflatable for 9 min. Finally, 1 mL of the sample was extracted for blood gas analysis. The charging conditions were adjusted to O_2 = 6 mL/min, CO_2 = 3 mL/min, N_2 = 160 mL/min, and the flow rate was 100 mL/min. Samples were inflated for 6 min at 37°C after being balaced for 10 min. Finally, 1 mL of the sample was also extracted for sexual blood gas analysis. According to the calculation formula of effective oxygen-carrying capacity of erythrocytes, Q = 20 × (S1-S2). When the oxygen partial pressure rose to 100 mm Hg (pulmonary arterial partial oxygen pressure) and stabilized, the oxygen saturation of hemoglobin in the solution was measured and recorded as S1. When the oxygen partial pressure of mixed gas was 40 mm Hg (oxygen partial pressure of pulmonary venous blood), the oxygen saturation of hemoglobin was measured and recorded as S2. P50 value was calculated according to the blood gas analysis results when the oxygen partial pressure reached 100 mm Hg.[5]

Measurement of 2,3-DPG and Na^+-K^+-ATP

Suspended erythrocytes obtained from 1 patient were divided into 5 portions and measured at 1, 7, 14, 21, and 28 days according to the 2,3-DPG and Na^+-K^+-ATP kit instructions.[6]

Morphology observation of erythrocyte

Morphology of erythrocytes was characterized on H7600 TEM at 0, 7, 14, 21, and 28 days after the storage of erythrocytes.

Observation of erythrocyte exosomes

Extraction of exosomes

RBC solution (1 mL) was put into a centrifuge tube and 7.5 mL of phosphae-buffered saline (PBS) was added. Organelles were removed after centrifuging for 30 min at 10,000 × g at 4°C. Then, supernatant was centrifuged and concentrated by using a 100 kDa Millipore ultrafiltration centrifugal pipe (Merck Millipore, Burlington, USA) at 1000 × g at 4°C for 30 min. The concentrate was filtered with 0.22 μm according to operating instructions for tissue culture medium and precipitation liquid was added into the supernatant in a proportion of 5 : 1 at 4°C overnight for precipitation (>12 h). Exosome suspension was obtained after centrifuging at 1000 × g at 4°C for 30 min and stored at −80°C.[7]

Morphology observation of exosome with TEM

One drop of erythrocyte exosomes suspended in PBS was taken and dropped onto the copper sample carrier network with a diameter of 2 nm. After staying at room temperature for 2 min, the edge liquid was gently absorbed with filter paper. Then, 3% phosphotungstic acid solution (pH = 6.8) was retained at room temperature for 5 min. The morphology of exosomes was observed using TEM.

Western blot analysis of exosome phenotypes CD63 and CD81

Extraction of exosome protein

The PBS resuspended exosomes were mixed with RIPA at a ratio of 1:1 according to an appropriate volume, and then the exosomes were allowed to rest on ice to shake violently for 1 min. This procedure was repeated 5 times to fully crack the exosomes. The concentration of exosome protein was determined using BCA method and a third volume of 4 × SDS buffer was added to samples, which were boiled at 100°C for 5 min and preserved at −80°C.

Western blot analysis of protein CD63 and CD81

SDS-PAGE was prepared with a concentration of 10–12%, and the sample was loaded at a total protein mass of 50 μg per well. SDS-PAGE was performed at a voltage of 80 V and 100 V for the laminated and separated gels, respectively. The protein was transferred to polyvinylidene fluoride (PVDF) membrane after electrophoresis under 350 mA constant current condition for 2 h. The PVDF membrane was incubated shaking for 1 h in 5% skimmed milk, then rabbit anti-human CD81 antibody (1 : 500) or CD63 antibody (1 : 500) were added to incubate at 4°C overnight. The film was washed 3 times with 1 × Tris-buffered saline with Tween (TBST). Horseradish peroxidase (HRP)-labeled rabbit anti-sheep (1 : 1500) was added to incubate at 37°C for 1 h. The film was washed 5 times with 1 × TBST and exposed to analysis.[8]

Western blot

Western blot was used to detect MRPS35 expression. A total of 40 μg protein were extracted from each cell, analyzed using 10% SDS-PAGE and transferred to nitrocellulose membrane. With sealing fluid containing 5% skimmed milk powder, the membrane was incubated at 37°C for 1 h, then MRPS35 antibodies (1 : 500) were added to incubate at 4°C overnight. After enhanced chemiluminescence (ECL) developing, the gray value was analyzed using the analysis system of electrophoresis gel imaging.

Statistical analysis

All data were processed using the SPSS v. 19.0 statistical software (IBM Corp., Armonk, USA) and expressed as mean ± standard deviation (SD). A paired t-test was performed to compare the 2 groups. Statistical significance was defined as $p < 0.05$.

Results and discussion

Effective oxygen-carrying capacity and P50

Effective oxygen-carrying capacity (Q) of whole blood and RBC suspensions had declined with the enhancement of storage time, as shown in Table 1. Figure 1A shows that Q decreased sharply in the first 14 days and gently after further 14 days. The Q of suspension RBC decreased by 54.4% at 14 days and 62.7% at 28 days, while that of whole blood decreased by 39.1% at 14 days and 52.1% at 28 days. P50 of RBC decreased gradually as the storage days increased as shown in Fig. 1B. It shows that the P50 of suspension RBC decreased by 11.6% at 14 days and 25.1% at 28 days. Whole blood P50 was reduced by 16.1% at 14 days and 28.6% at 28 days.

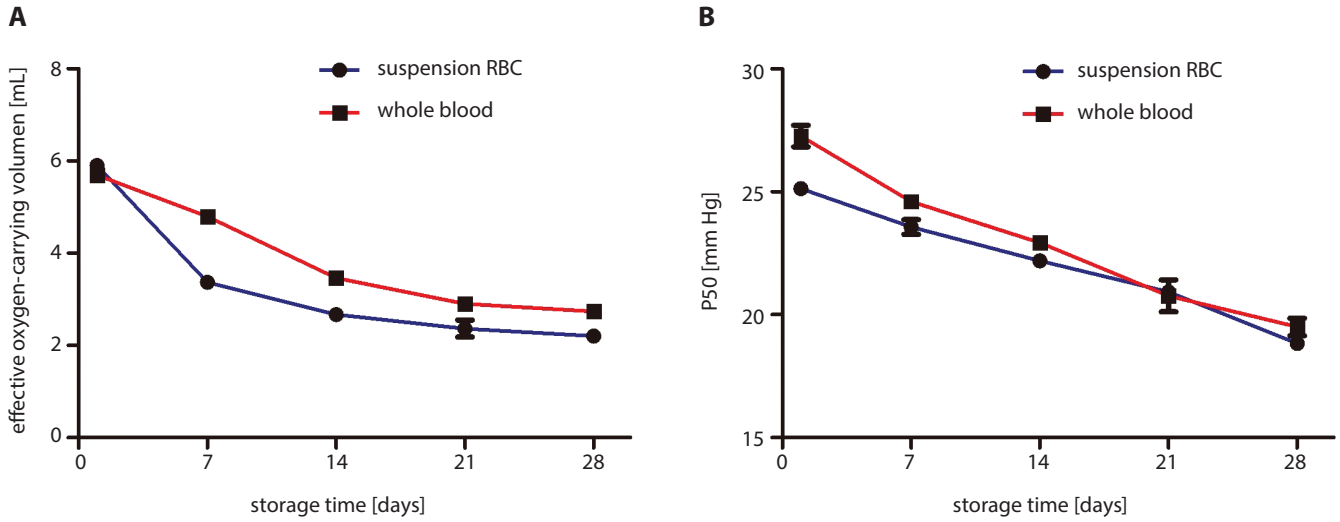

Fig. 1. Changes in oxygen-carrying capacity in whole blood and suspension RBC

A – effective oxygen-carrying volume of whole blood and suspension RBC; B – P50 of whole blood and suspension RBC.

Table 1. Changes of RBC oxygen-carrying capacity at different storage time

Group	(d)	1	7	14	21	28
Whole blood	Q [mL]	5.70 ±0.08	4.80 ±0.08	3.47 ±0.12	2.90 ±0.08	2.73 ±0.12
	P50 [mm Hg]	27.3 ±0.6	24.6 ±0.4	22.9 ±0.3	20.8 ±0.9	19.5 ±0.5
Suspension RBC	Q [mL]	5.90 ±0.08	3.37 ±0.12	2.67 ±0.12	2.37 ±0.26	2.20 ±0.16
	P50 [mm Hg]	25.1 ±0.2	23.6 ±0.4	22.2 ±0.2	20.9 ±0.2	18.8 ±0.3

Hamasaki et al.[9] first used the method of measuring Q to evaluate the change of erythrocyte oxygen-carrying capacity. They found that Q had a linear relationship with storing time and gradually declined with the enhancement of storage time. The lower the P50, the greater the affinity between RBC and oxygen, and the greater the ability to bind with oxygen, which is not conducive to oxygen release.[10] It can be demonstrated from the results of decreased Q and P50 that the ability of releasing oxygen of RBC was also decreased.

2,3-DPG and Na^+-K^+-ATP

At the first 14 days, the concentration of 2,3-DPG in RBC declined sharply and then leveled off after 14 days. The data showed that it decreased by 63.0% at the 7th storage day and by 91.7% at the 14th storage day (Table 2). The concentration of 2,3-DPG in whole blood gradually decreased with the increase of storage days, which was not as dramatic as that of RBC (Fig. 2A). The concentration of Na^+-K^+-ATP in erythrocytes decreased gently in the first 7 days, and then decreased sharply from 7 to 14 days. The concentration of Na^+-K^+-ATP decreased by 53.8% in 7 days after storage and 69.5% in 14 days after storage. The concentration of Na^+-K^+-ATP in the whole blood decreased by 41.2% after 7 days and by 63.3% after 14 days (Fig. 2B).

2,3-DPG is the unique glycolytic intermediate of RBC, which can reduce the affinity between hemoglobin and oxygen, and is one of the important factors to regulate the physiological function of oxygen transport in the body. In some physiological and pathological conditions, such as mountaineering, plateau, anemia and congenital heart disease, the level of 2,3-DPG in RBC is significantly increased to compensate for the ability of hemoglobin to release oxygen for tissue metabolism. On the contrary, in some pathological conditions, the decreased content of 2,3-DPG is not conducive for utilization of oxygen in tissue cells, such as acidosis or shock.[11,12] The lower content of 2,3-DPG makes it difficult to release oxygen, which indicated that the oxygen-carrying capacity of RBC is decreased and the physiological function of RBC is variable.

Red blood cells regulate cell volume mainly by regulating intracellular Na^+ and K^+ content through membrane Na^+-K^+-ATP, and maintaining this function requires about 30% of RBC's ATP production.[13,14] Na^+-K^+-ATP changes its conformation through phosphorylation and dephosphorylation, which lead to changes in its affinity with Na^+ and K^+. The role of "sodium-potassium pump" is to maintain cell permeability and cell volume.[15,16] Under normal physiological conditions, Na^+ (1.0–2.0 mmol/L) in RBC was slightly higher than K^+ (0.8–1.5 mmol/L) when it was passively transported into the cytoplasm. Both the increase of Na^+ and the decrease of K^+ in RBC can activate Na^+-K^+-ATP. Na^+-K^+-ATP is involved in the active transmembrane transport of Na^+ and K^+ inside and outside the cell to maintain the balance of ions.[17] Na^+-K^+-ATP also plays

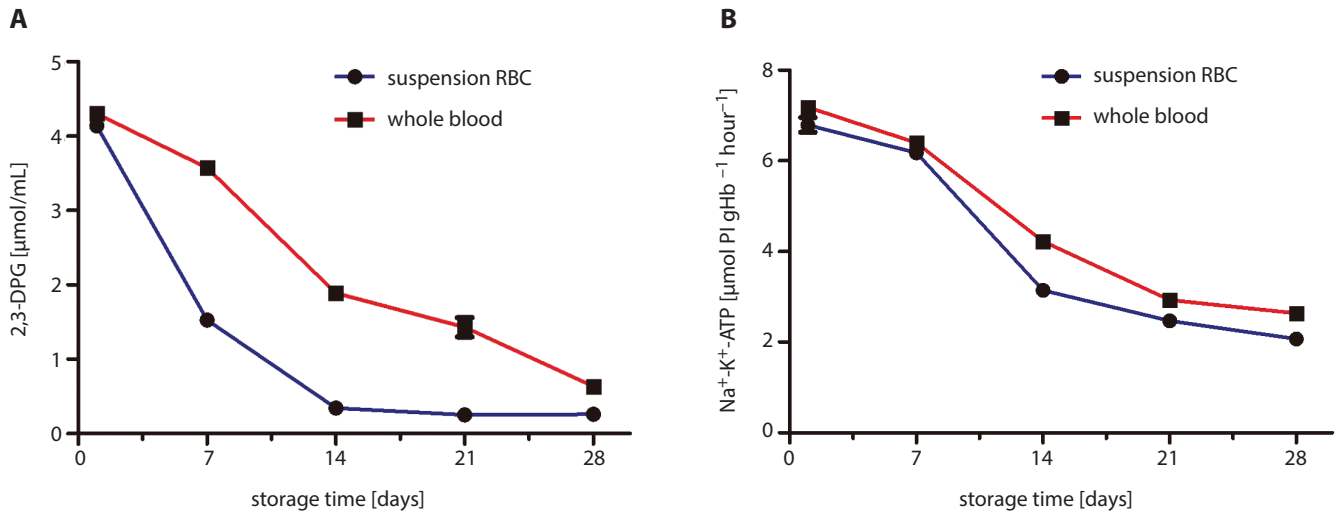

Fig. 2. Changes in 2,3-DPG, Na^+-K^+-ATP in RBC and whole blood in different storage times

A – the concentration of 2,3-DPG; B – the content of Na^+-K^+-ATP.

Table 2. Changes of erythrocyte oxygen-carrying capacity at different storage time

(d)	Group	1	7	14	21	28
2,3-DPG [µmol/mL]	suspension RBC	4.14 ±0.07	1.53 ±0.03	0.34 ±0.02	0.25 ±0.02	0.26 ±0.01
2,3-DPG [µmol/mL]	whole blood	4.3 ±0.07	3.57 ±0.11	1.89 ±0.10	1.43 ±0.18	0.63 ±0.10
Na^+-K^+-ATP [µmol PI.gHb^{-1}hour^{-1}]	suspension RBC	6.79 ±0.23	6.17 ±0.04	3.14 ±0.06	2.47 ±0.08	2.07 ±0.03
Na^+-K^+-ATP [µmol PI.gHb^{-1}hour^{-1}]	whole blood	7.18 ±0.12	6.39 ±0.04	4.22 ±0.13	2.93 ±0.07	2.63 ±0.07

an important role in maintaining the normal morphology of cells, and the survival of RBC depends on the energy provided by ATP.[18] However, decreased activity of Na^+-K^+-ATP will reduce the release of ATP energy and affect the normal metabolism of RBC.

Observation of erythrocyte morphology

The first 14 days of storage were characterized by cell morphology, defined as double concave disc, thick edge, round or oval, nucleate-free, dense, and with a diameter of 15–25 µm. The number of cells decreased after 14 days, and the TME images of RBC at storage days 21 and 28 were sparse and irregular. Therefore, the storage time has a certain effect on the morphology of erythrocytes, which can further cause the decline of erythrocyte function and increased damage (Fig. 3).

Observation of exosomes in RBC

As it can be seen from the electron microscope images, the particle size of the material ranges from 30 to 100 nm and the morphology is vesicular. After 7 days of storage, in the electron micrograph, exosomes appeared as black spots as shown in Fig. 4. The black spots gradually increased after 14 days and increased more by the 14th and 21st days. These 2 time points showed the most number and clearest exosome morphology.

Previous studies have confirmed that the vesicles in vivo are divided into 3 categories: 1) vesicles released by apoptosis with micron-scale particle sizes; 2) vesicles formed by budding of the cell membrane, with particle sizes of several hundred nanometers; 3) exosomes, with micron-scale particle size below 100 nm. Therefore, we believed that the vesicles in TEM images were exosomes.

Western blot analysis of protein CD63 and CD81

Western blot analysis probing for 2 exosome marker proteins, CD81 and CD63, was performed. As shown in Fig. 5, both CD63 and CD81 proteins were absent or hardly detectable in the isolated vesicles at a storage time of 7 days, but the expression of CD63 and CD81 proteins could be clearly detected at a storage time of 14 days. Western blot analysis probing for 2 exosome marker proteins, CD81, CD63, and MPRS35 were performed, as shown in Fig. 5 and 6. The increased expression of CD81/CD63 protein indicates that exosomes secreted were increased by RBC.

Minetti et al.[19] discovered a membranous vesicle from the culture medium of reticulocyte. These vesicles were exosomes, and many kinds of cells could secrete exosomes under normal and pathological conditions. The exosomes were discoid vesicles with a diameter of 40–100 nm, which were mainly derived from polyvesicles formed by intracellular lysosomal microparticles, and these were released into

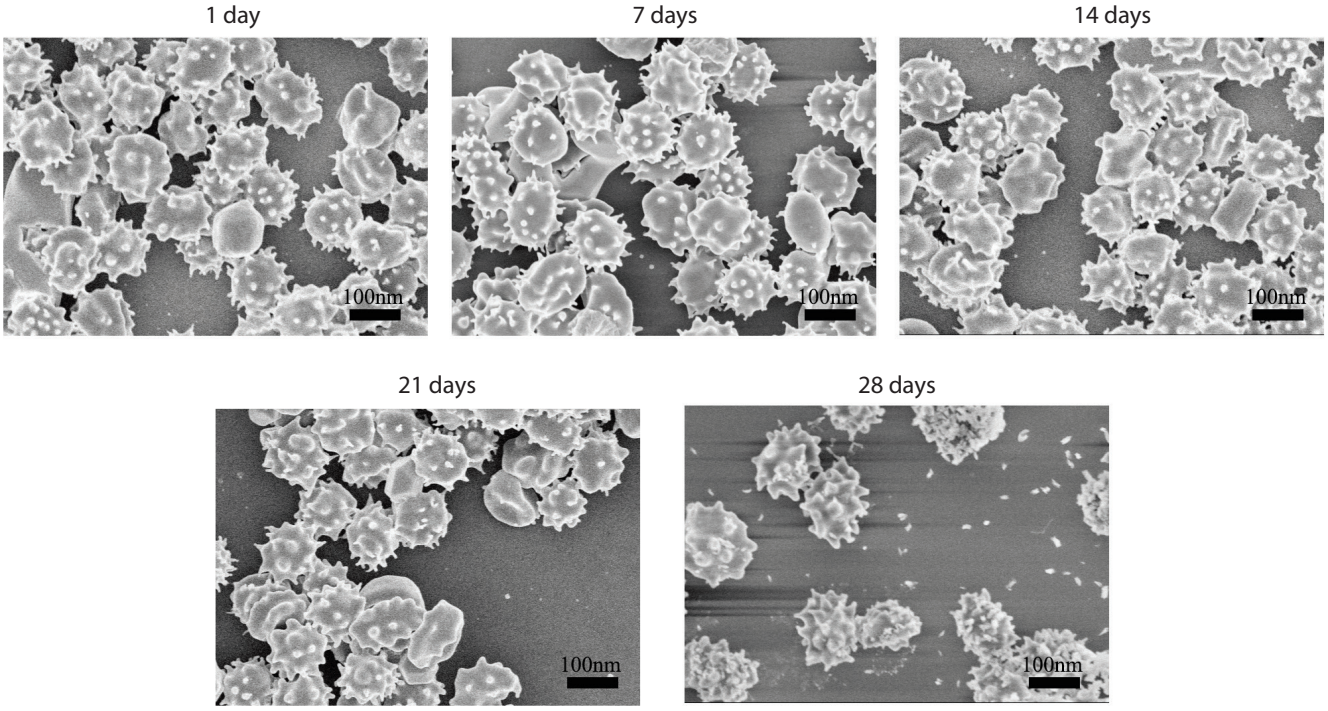

Fig. 3. Changes in erythrocyte morphology after different storage times. The scale bar was 100 nm

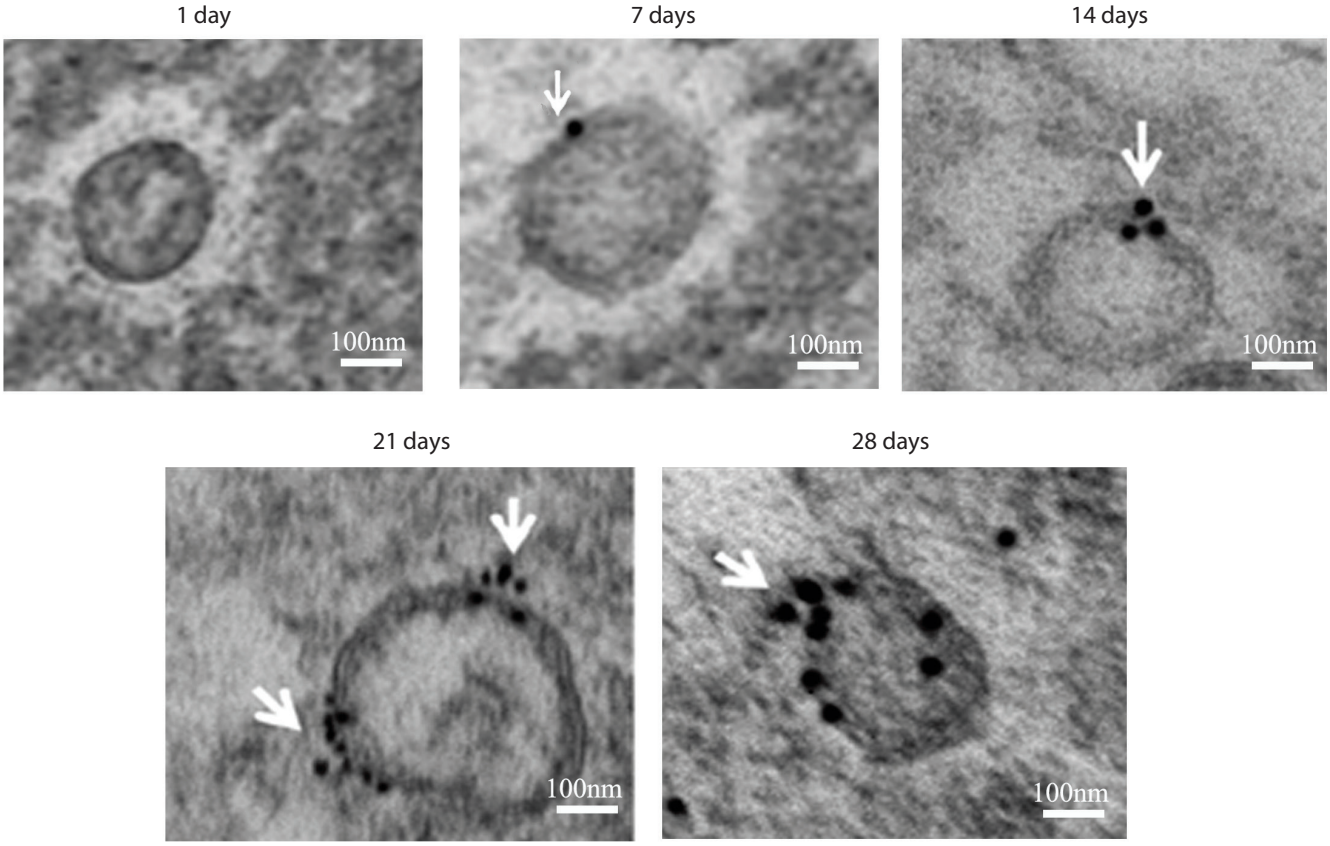

Fig. 4. TEM imaging of exosome in RBC in different storage times. Exosome was marked with arrow. The scale bar was 100 nm

the extracellular matrix after the fusion of the extracellular membrane of polyvesicles with the cell membrane. Exosomes were identified as nano-level vesicles secreted by living cells, and included proteins, nucleic acids, metabolites and other components from the mother cells. They not only carried the information of the mother cells, but also directly or indirectly regulated the functions and phenotypes of the receiving cells.[20] Exosomes played an important role

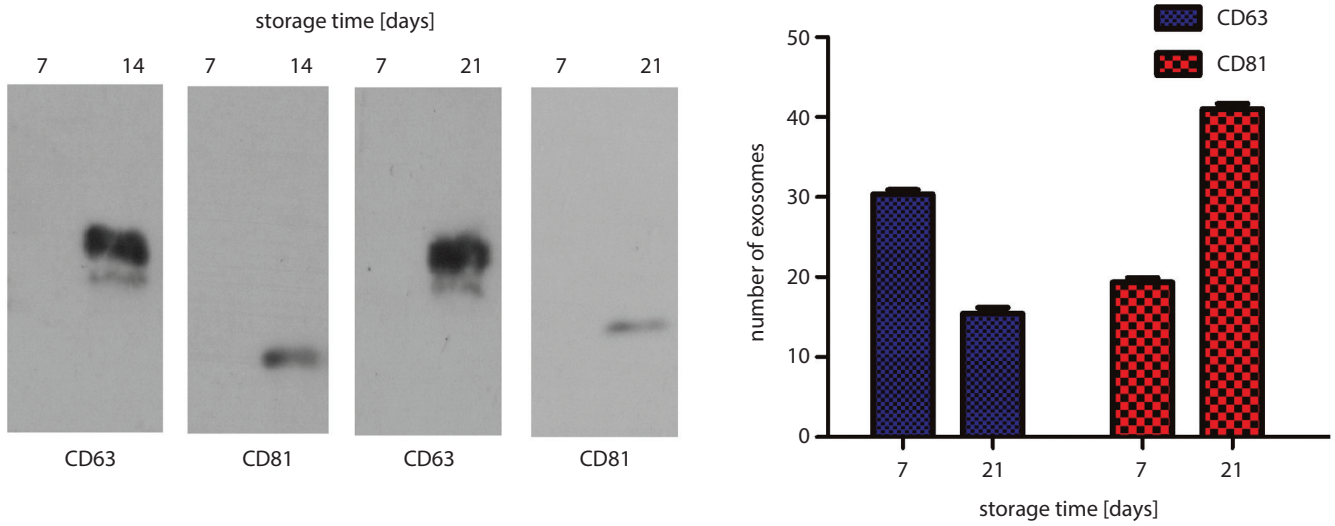

Fig. 5. Western blot analysis of expression levels of exosome-associated proteins CD63 and CD81

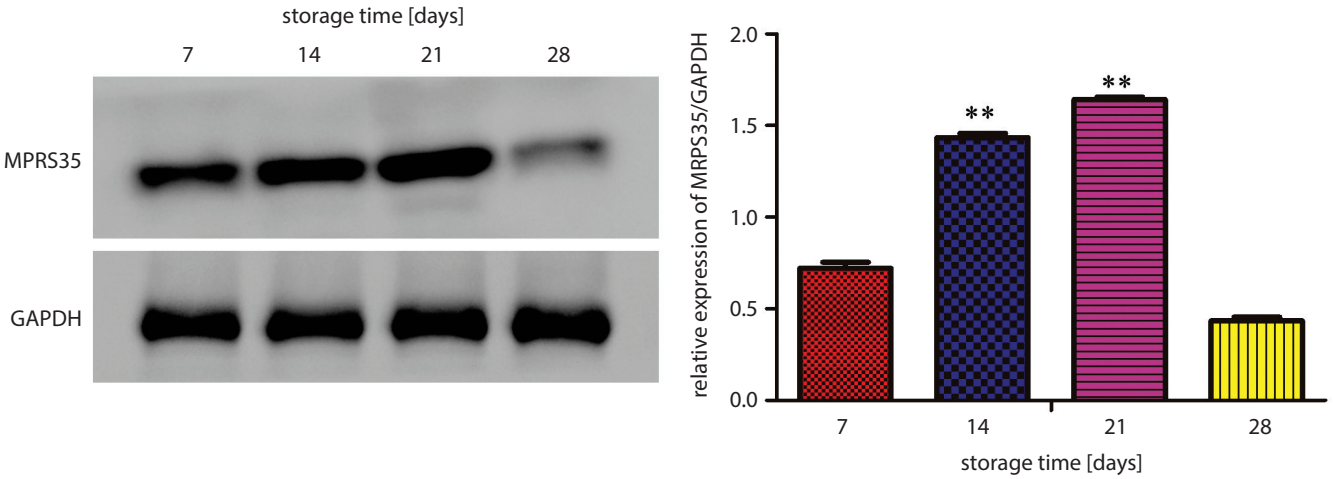

Fig. 6. Protein level of MRPS35 in RBC after different storage times, determined with western blotting (mean ±SD, n = 3. **p < 0.01 compared to 7 days group)

in immunopathology, such as antigen presentation, tumor growth and migration, tissue damage repair etc. Exosomes played an irreplaceable role in signal transduction in vivo, and also played an extremely important role in numerous physiological and pathological processes, including cardiovascular diseases,[21] nervous system diseases,[22,23] and therapy.[24,25] Meanwhile, exosomes secreted by different cells had different components and functions, which could be used as biomarkers for disease diagnosis.

Western blot analysis of exosome protein MRPS35 expression

The expression of MRPS35 increased from the 7th day to the 21st day after storage, and the relative expression of MRPS35 was significantly different from that at the storage time of day 14 and day 21. However, the expression of MRPS35 in erythrocyte mitochondria was significantly reduced at the storage time of 28 days. Abnormal expression of MRPS35 protein can induce apoptosis of normal cells. Relevant studies have proved that MRPS35 is a key protein which affects mitochondrial function, and plays a very important role in the occurrence of apoptosis. Mitochondria are an important organelle in eukaryotic cells. They can provide ATP which are the main source of energy and heat for life by oxidative phosphorylation of the electron transport chain in their inner membrane. In addition, mitochondria also played a key role in the process of apoptosis regulation. The abnormal expression of MRPS35 can make the mitochondrial electron transport barriers, and induce the production of free radicals increases, which leads to mitochondrial structure and function damage and the decrease of membrane potential, further to activate mitochondrial mediated apoptosis pathway and accelerate the apoptosis of RBC.

Conclusions

Changes in the rheological properties and oxygen-carrying functions of erythrocytes during the preservation process are manifestations, which lie in the mechanisms of damage at the molecular level of erythrocytes.

ORCID iDs

Li-Shuang Duan https://orcid.org/0000-0002-5111-058X
Yang Liu https://orcid.org/0000-0003-4743-1193
Zhen-Zhou Li https://orcid.org/0000-0003-4306-2036
Huan Wang https://orcid.org/0000-0001-8785-6124
Xiao-Fang Zhou https://orcid.org/0000-0002-4241-0521
Xiao-Xiao Wang https://orcid.org/0000-0003-4764-2281
Zi-Wei Zhang https://orcid.org/0000-0002-2140-4886
Yi-Qun Kang https://orcid.org/0000-0002-5717-4576
Yong-jun Su https://orcid.org/0000-0003-3600-3361
Jian-Rong Guo https://orcid.org/0000-0002-1759-6619

References

1. Yoshida T, Prudent M, D'Alessandro A. Red blood cell storage lesion: Causes and potential clinical consequences. *Blood Transfus*. 2019; 17(1):27–52. doi:10.2450/2019.0217-18
2. Shah A, Brunskill SJ, Desborough MJ, Doree C, Trivella M, Stanworth SJ. Transfusion of red blood cells stored for shorter versus longer duration for all conditions. *Cochrane Database Syst Rev.* 2018;12(12):Cd0 10801. doi:10.1002/14651858.CD010801.pub3
3. Lagerberg JW, Salado-Jimena JA, Löf H, et al. Evaluation of the quality of blood components obtained after automated separation of whole blood by a new multiunit processor. *Transfusion*. 2013;53(8): 1784–1807. doi:10.1111/trf.12010
4. Pasqualetti D, Ghirardini A, Arista MC, et al. Blood component fractionation: Manual versus automatic procedures. *Transfus Apher Sci*. 2004;30(1):23–28. doi:10.1016/j.transci.2003.07.002
5. Timmerman LA, Holton T, Yuneva M, et al. Glutamine sensitivity analysis identifies the xCT antiporter as a common triple-negative breast tumor therapeutic target. *Cancer Cell*. 2013;24(4):450–465. doi:10.1016/j.ccr.2013.08.020
6. Aktaran Bala D, Ozcan M. The effects of freezing on long-term storage of canine erythrocytes. *Pol J Vet Sci*. 2016;19:401–406. doi:10. 1515/pjvs-2016-0050
7. Mao JH, Liang ZF, Tian YQ, et al. Effects of different states of p53 on the exosomes secreted by mouse bone marrow mesenchymal stem cells. *Journal of Jiangsu University*. 2017;27:103–106. http://en.cnki.com.cn/Article_en/CJFDTotal-ZJYZ201702003.htm
8. Klymiuk MC, Balz N, Elashry MI, Heimann M, Wenisch S, Arnhold S. Exosomes isolation and identification from equine mesenchymal stem cells. *BMC Vet Res*. 2019; 15(1):42–49. doi:10.1186/s12917-019-1789-9
9. Hamasaki N, Yamamoto M. Red blood cell function and blood storage. *Vox Sang*. 2000;79(4):191–197. doi:10.1159/000056729
10. Dinkla S, Peppelman M, van der Raadt J, Atsma F. Phosphatidylserine exposure on stored red blood cells as a parameter for donor-dependent variation in product quality. *Blood Transfus*. 2014;12(2):204–209. doi:10.2450/2013.0106-13
11. Xiong Y, Xiong Y, Wang Y, et al. Exhaustive-exercise-induced oxidative stress alteration of erythrocyte oxygen release capacity. *Can J Physiol Pharmacol*. 2018;96(9):953–962. doi:10.1139/cjpp-2017-0691
12. Luisada-Opper AV. Colorimetric determination of 2,3-diphosphoglycerate in whole blood. *Clin Chem*. 2020;19(1):118–120. PMID:4683355
13. Cetinkaya CD, Gurbilek M, Koc M. Evaluation of the relationship of erythrocyte membrane Na^+/K^+-ATPase enzyme activity and tumor response to chemoradiotherapy in patients diagnosed with locally advanced nonsmall cell lung cancer and glioblastoma multiforme. *J Cancer Res Ther*. 2018;14(9): 450–457. doi:10.4103/jcrt.JCRT_675_15
14. Deryugina AV, Boyarinov GA, Simutis IS, Nikosiskiy VO. Correction of metabolic indicators of erythrocytes and myocardium structure with ozonized red blood-cell mass. *Cell Tissue Biol*. 2018;12(3): 207–212. doi:10.1134/S1990519X18030033
15. Mackay A, Davies DL, Horton PW. Is thallium-201 of use in the measurement of total exchangeable potassium in man? *Eur J Clin Invest*. 2008;8(4):261–262. https://doi.org/10.1111/j.1365-2362.1978.tb00863.x
16. Patrick J. The relationship between intracellular and extracellular potassium in normal and malnourished subjects as studied in leukocytes. *Pediatr Res*. 1978;12(7):767–770. doi:10.1203/00006450-197807000-00005
17. Yi J, Zhang XQ, Mu SJ. Effects of high dose rate and low dose radiation on human erythrocyte atpase. *Clinical Blood Transfusion and Examination*. 2009;11:25–26. doi:10.1016/j.ijrobp.2009.07.1273
18. Dai XF, Huang SF; Clinical Laboratory Department. Relevant research on potassium in plasma and erythrocyte,blood pH,and enzymatic activity of Na^+-K^+-ATP in patients with hypokalaemic periodic paralysis. *China Modern Medicine*. 2013;31:29–31.
19. Minetti G, Achilli C, Perotti C, Ciana A. Continuous change in membrane and membrane-skeleton organization during development from proerythroblast to senescent red blood cell. *Front Physiol*. 2018; 9:286. doi:10.3389/fphys.2018.00286
20. Li D, Ren H, Liu C, Wang F, Zhang L. A study on the invention and experiments of a new type of blood preservation liquid. *Chin J Blood Transfus*. 2013;09:841–842. doi:10.1016/j.ijpe.2014.12.013
21. Ong SG, Lee WH, Huang M, et al. Cross talk of combined gene and cell therapy in ischemic heart disease: Role of exosomal micro-RNA transfer. *Circulation*. 2014;130(11 Suppl 1):S60–69. doi:10.1161/CIRCULATIONAHA.113.007917
22. Haney MJ, Klyachko NL, Zhao Y, et al. Exosomes as drug delivery vehicles for Parkinson's disease therapy. *J Control Release*. 2015;207:18–30. doi:10.1016/j.jconrel.2015.03.033
23. Yuyama K, Sun H, Mitsutake S, Igarashi Y. Sphingolipid-modulated exosome secretion promotes clearance of amyloid-beta by microglia. *J Biol Chem*. 2012;287(14):10977–10989. doi:10.1074/jbc.M111.324616
24. Zhang L, Zhang S, Yao J, et al. Microenvironment-induced PTEN loss by exosomal microRNA primes brain metastasis outgrowth. *Nature*. 2015;527(7576):100–104. doi:10.1038/nature15376
25. Yuan FL, Wu QY, Miao ZN, et al. Osteoclast-derived extracellular vesicles: Novel regulators of osteoclastogenesis and osteoclast-osteoblasts communication in bone remodeling. *Front Physiol*. 2018;30:1–6. doi:10.3389/fphys.2018.00628
26. Bardyn M, Rappaz B, Jaferzadeh K, et al. Red blood cells ageing markers: A multi-parametric analysis. *Blood Transfus*. 2017;15(3):239–248. doi:10.2450/2017.0318-16
27. Kim JK, Park J-H, Han S-B, Cho IY, Jang K-M. Allogeneic blood transfusion is a significant risk factor for surgical-site infection following total hip and knee arthroplasty: A meta-analysis. *J Arthroplasty*. 2017;32(1):320–325. doi:10.1016/j.arth.2016.08.026

LncRNA NORAD regulates scar hypertrophy via miRNA-26a mediating the regulation of TGFβR1/2

Jun Qi[A–F], Yangyang Wu[B,C,E,F], Haijian Zhang[B,C,F], Yifei Liu[B,C,F]

Department of Burns and Plastic Surgery, Affiliated Hospital of Nantong University, China

A – research concept and design; B – collection and/or assembly of data; C – data analysis and interpretation;
D – writing the article; E – critical revision of the article; F – final approval of the article

Advances in Clinical and Experimental Medicine, ISSN 1899–5276 (print), ISSN 2451–2680 (online) *Adv Clin Exp Med*. 2021;30(4):395–403

Address for correspondence
Jun Qi
E-mail: qijun2a@163.com

Funding sources
None declared

Conflict of interest
None declared

Received on June 12, 2020
Reviewed on August 11, 2020
Accepted on February 19, 2021

Published online on April 15, 2021

Abstract

Background. Transforming growth factor-β (TGF-β) pathway presents dysregulation in pathological scarring and mediates hypertrophic scar (HS) formation.

Objectives. The study aims to analyze the potential mechanism of long non-coding RNA NORAD (LncRNA NORAD) and microRNA (miR-26a) regulation of the TGF-β pathway in hypertrophic scar fibroblasts (HSFs).

Materials and methods. Hypertrophic scar tissues were collected and assayed for LncRNA NORAD, miR-26a, transforming growth factor β receptor I (TGF-βR1) and TGF-βR2, with enzyme-linked immunosorbent assay (ELISA) or qualitative polymerase chain reaction (qPCR). LncRNA NORAD interfering plasmids were transfected into HSFs and induced with TGF-β1. Cell Counting Kit-8 (CCK-8) assays were performed to assess HSF proliferation, and flow cytometry to analyze apoptosis and the cell cycle. TGF-βR1, TGF-βR2, Smad2, and p-Smad2 levels were detected using western blot (WB). The related proteins (p21, cyclin D1 and cyclin-dependent kinase 4 (CDK4)) regulating the cell cycle, and apoptosis-related proteins (caspase-3 and Bcl-2) were also detected using WB. The binding sites of miRNA-26a and LncRNA NORAD, TGF-βR2, or UBE3A were predicted using Starbase and confirmed with dual luciferase reporter assay. RNA immunoprecipitation (RIP) was utilized to explore the interplay of miR-26a with its target genes.

Results. LncRNA NORAD is decreased, miR-26a is increased and TGF-β receptors show abnormal expression in scar tissue. LncRNA NORAD knockdown inhibits proliferation of HSF cells induced by TGF-β1 treatment. In addition, cell apoptotic levels are markedly increased and cell numbers in G0/G1 phase are increased. Moreover, the TGF-β/Smad pathway is regulated by decreasing endogenous LncRNA NORAD levels, possibly by affecting the relative levels of TGF-βR1. p21 is notably upregulated, while cyclin D1 and CDK4 are downregulated. Apoptosis-related proteins are significantly affected. LncRNA NORAD may act as a sponge, binding miR-26a and changing its expression. Finally, RIP shows that miR-26a targets the 3'UTRs of TGF-βR2 and UBE3A.

Conclusions. LncRNA NORAD regulates HSF proliferation via miR-26a mediating the regulation of TGF-βR2/R1. LncRNA NORAD/miR-26a could be a potential target for treating HS.

Key words: hypertrophic scarring, miRNA-26a, LncRNA NORAD, TGFβR1, TGFβR2

Cite as
Qi J, Wu Y, Zhang H, Liu Y. LncRNA NORAD regulates scar hypertrophy via miRNA-26a mediating the regulation of TGFβR1/2. *Adv Clin Exp Med*. 2021;30(4):395–403. doi:10.17219/acem/133482

DOI
10.17219/acem/133482

Copyright
© 2021 by Wroclaw Medical University
This is an article distributed under the terms of the Creative Commons Attribution 3.0 Unported (CC BY 3.0) (https://creativecommons.org/licenses/by/3.0/)

Background

Hypertrophic scarring (HS) is a common skin disorder, mostly following burns or skin trauma, or after an operation.[1] The process of collagen secretion and the metabolism of fibroblasts are strictly modulated during skin wound healing. However, the formation of HS could disrupt this balance. Hypertrophic scarring occurs under excess proliferation of fibroblasts and massive collagen deposition.[2] TGF-β signaling affects cell proliferation and extracellular matrix (ECM) production in the process of wound healing. There is interaction between the Smad signaling pathway and non-Smad pathways, mediated by TGF-β; TGF-β homodimers interact with TGF-β receptors (TGF-βRI and TGFβ-RII), activating the Smad pathway. Phosphorylation of TGF-βR1 is necessary for this activation,[3] while its ubiquitination contributes to its degradation and thus inactivates the Smad pathway. TGF-β signaling has been demonstrated to be dysregulated in pathological scarring,[4,5] and TGF-βR2 expression is increased in keloid fibroblasts.[6]

The TGF-β1/Smad pathway mediates the formation of HS[7]; suppression of the TGF-β1/Smad pathway is involved in reducing collagen deposition and inhibiting hypertrophic scar fibroblast (HSF) proliferation.[8,9] Anti-TGFβ treatment reduces ECM synthesis and Smad-3 phosphorylation in irradiated rat tissue.[10] In addition, HS is markedly decreased via targeting of TGF-β2R or TGFβ-R1.[11,12] In cancer studies, the classical TGF-β/Smad signaling pathway regulates the cell cycle from G1 to S, and subsequently affects cell apoptosis.[13] MicroR-26a (miRNA-26a) has been indicated to promote wound healing in fracture patients and regulate cell apoptosis in coronary heart disease.[14,15] It also has an anti-tumor effect.[16] A previous study has shown that miRNA-26a causes downregulation in HS patients and suppresses the formation of hyperplastic scars.[17] LncRNA-NORAD shows increased levels in breast cancer tissue and mediates the activation of TGF-β.[18] Thus, TGF-β and TGF-β2R/1R expression in modulating the Smad signaling pathway plays a crucial role in the formation and development of HS. However, how the TGF-β pathway is regulated is still unexplored.

Objectives

This study intends to interrogate how LncRNA and miRNA regulate the TGF-β pathway to affect HSF formation. This study was designed to investigate the role of LncRNA NORAD in scar hypertrophy. Additionally, we also investigated whether TGF-β pathway is involved in the molecular mechanism of LncRNA NORAD.

Materials and methods

Specimen collection

Hypertrophic scar tissues and adjacent normal skin tissues (total number of cases in both groups n = 20) were surgically removed and collected, as shown in Table 1. Scar tissues included peripheral and central tissues, with intact surfaces, no rupture and covering an area of more than 3 × 2 cm. Hypertrophic scar formation was confirmed during postoperative pathological examination. The scar tissues were assayed to detect the levels of LncRNA NORAD, miR-26a, TGF-βR1 and TGF-βR2 through quantitative polymerase chain reaction (qPCR) and enzyme-linked immunosorbent assay (ELISA). Patients did not receive any treatment before the operation. Tissue collection was conducted with the informed consent of patients signed before the operation. All experimental operations were approved by the ethics committee of the Affiliated Hospital of Nantong University, China. The scar tissue samples were obtained according to the Declaration of Helsinki.

Cells

Hypertrophic scar fibroblasts (Jennio, Guangzhou, China) were cultured in RPMI 1640 medium containing 10% fetal-inactivated bovine serum (FBS; Gibco, Waltham, USA) at 5% CO_2 and 37°C. Cells of the 3rd–5th passage were used in further experiments. The HSFs were cultured in serum-free medium overnight before recombinant human TGF-β1 treatment (R&D Systems, Minneapolis, USA), and then cultured in medium containing TGF-β1 (5 ng/mL) for 24 h.

qPCR

Total RNA was extracted with RNAiso Plus (TaKaRa, Tokyo, Japan). RNA was quantified using SYBR®Premix Ex Taq™ (TaKaRa), with GADPH used as the reference. Total miRNA was extracted with the mirVana™ miRNA Isolation Kit (Invitrogen, Carlsbad, USA). Concentrations of RNA and miRNA were detected using a Microplate Reader (Invitrogen). MiRNA was transcribed into cDNA using the TaqMan® MicroRNA Reverse Transcription Kit (Invitrogen). MiRNA levels were detected using TaqMan® MicroRNA Assays (Invitrogen), with U6 as a reference. Relative levels of LncRNA NORAD, TGF-βR1, TGF-βR2, and miRNA were calculated using the $2^{-\Delta\Delta Ct}$ method.

ELISA

Cells were lysed with RIPA lysis buffer and centrifuged at 12,000 rpm/min for 15 min. TGFβR1 (Zhen Shanghai and Shanghai Industrial, Shanghai, China), TGF-βR2 (ab193715; Abcam, Cambridge, UK) and TGF-β (Mlbio, Shanghai,

Table 1. Clinical characteristics of patients with HS

No. of patient	Sex	Age [years]	Biopsy site	Duration of lesion [months]	Etiology
1	male	23	shoulder	10	burn
2	male	40	back	18	scald
3	male	33	chest	15	electric injury
4	male	27	chest	16	post-operation
5	male	24	arm	36	burn
6	male	39	shoulder	20	scald
7	male	36	buttock	17	post-operation
8	male	41	cheek	22	electric injury
9	male	29	chest	20	electric injury
10	male	30	arm	9	burn
11	female	29	back	17	electric injury
12	female	42	shoulder	11	scald
13	female	43	arm	10	trauma
14	female	25	arm	7	burn
15	female	26	back	15	trauma
16	female	22	cheek	24	electric injury
17	female	38	cheek	21	electric injury
18	female	36	arm	33	trauma
19	female	45	chest	28	post-operation
20	female	32	shoulder	15	burn

China) levels were detected using corresponding ELISA kits according to the respective manufacturer's protocol.

Western blot

Cells were lysed with RIPA lysis buffer and then centrifuged at 12,000 rpm/min for 15 min. Total protein concentration was measured with the BCA method (Beyotime, Shanghai, China). Target proteins were separated using 10% SDS-PAGE electrophoresis and transferred onto a polyvinylidene fluoride (PVDF) membrane. The bands were incubated with the following primary antibodies (all from Abcam): Rabbit anti-TGF-βR1 (ab235178), Rabbit anti-TGF-βR2 (ab184948), Rabbit anti-Smad2 (ab40855), Rabbit anti-p21 (ab109520), Rabbit anti-Cyclin D1 (ab40754), Rabbit anti-CDK4 (ab108357), Rabbit anti-Bcl-2 (ab32124) (all at 1:1000 dilution), Rabbit anti-p-Smad2 (ab216482; 1:300 dilution), Mouse anti-GADPH (ab8245; 1:5000 dilution), and Rabbit anti-Caspase-3 (ab13847; 1:500 dilution) at 4°C overnight, which then were washed with Tris-buffered saline with Tween (TBST) twice. A secondary antibody (Goat Anti-Rabbit IgG (ab6721) or Rabbit Anti-Mouse IgG (ab6728); 1:10000 dilution; Abcam) was then applied and the bands incubated for 2 h. After the bands were washed twice, electrochemiluminescence (ECL) was used to develop the color. ImageJ software (National Institutes of Health, Bethesda, USA) detected the gray value of each protein band. The relative expression of protein was calculated, taking GADPH as a reference.

Plasmids transfection

NORD knockdown plasmids (sh-NORD) or a negative control (sh-NC) were transfected into cells using Lipofectamine 2000 (Invitrogen) according to the manufacturer's protocol. LncRNA NORAD overexpression vectors (LncRNA NORAD vector) or a control (empty vector) were transfected into cells. MiRNA-26a mimic or a control mimic (mimic NC) were also transfected into cells. All plasmids and mimics were purchased from IGE Biotechnology (Guangzhou, China). Forty-eight hours after transfection, the cells were used in further experiments.

Dual luciferase reporter assay

The HSF cells were seeded into a six-well plate (5 × 10^4 cells/well). Culture medium without antibiotics was added to each well and the same number of cells were inoculated in each well. The confluent degree of cells should reach approx. 85–90% during transfection. Luciferase reporter vectors were constructed through respective cloning of LncRNA NORAD, TGF-R2 or UBE3A into pmirGLO plasmids. The putative binding sites of miR-26a on the corresponding pmirGLO-WT plasmids were mutated using a QuikChange Lightning Site-Directed Mutagenesis Kit (Stratagene, San Diego, USA) and construct pmirGLO-Mut plasmids. A miR-26a mimic or miR-NC was transfected into HSF cells.

Forty-eight hours after transfection, luciferase activity was detected using Dual Luciferase® Reporter Assay System kits (Promega, Madison, USA).

CCK-8

TGF-β1 (5 ng/mL) peptides were used to activate HSF cells. Cell proliferation was detected using a Cell Counting Kit-8 (CCK-8) assay (Sigma-Aldrich, St. Louis, USA). The HSF cells were seeded into 96-well plates (5 × 10^3 cells/well) and treated using CCK-8 solution (10 μL/well; Beyotime). After incubation at 37°C for 2 h, the absorbance at 490 nm was detected using a microplate reader.

Flow cytometry

Forty-eight hours after transfection, the cells seeded into a six-well plate were digested with trypsin and centrifuged at 1000 rpm/min for 10 min. The supernatant was discarded and the cells were washed with pre-cold phosphate-buffered saline (PBS) 3 times. Annexin V assay was used in combination with PI labeled HSF cells to distinguish apoptosis and death at different stages of the cell cycle. Annexin V–/PI– and Annexin V+/PI– fluorescence assays were used to indicate living cells and early apoptotic cells respectively, whereas Annexin V+/PI+ fluorescence assay indicated dead cells and apoptotic cells in the middle and advanced stages. Cells were stained using FITC-Annexin V and propidium iodide (Becton Dickinson Bioscience, San Jose, USA) according to the manufacturer's guidance. All assays were performed in triplicate.

Cell cycle analysis

Cells were seeded into a six-well plate and digested using trypsin. The cell suspension was collected and centrifuged at 1000 rpm/min for 10 min. The supernatant was discarded and cells were incubated with 70–80% pre-cold ethanol (5 mL) at 4°C overnight. The cells were centrifuged at 1000 rpm/min for 10 min; then, the ethanol was flushed out using PBS or staining solution. Afterwards, the cells were suspended into 0.5 mL PI/RNase solution (Becton Dickinson Bioscience) and incubated without light for 15 min. The cell cycle was detected with flow cytometry within 1 h.

RIP

Cells were washed twice using cold-PBS, then centrifuged at 1000 rpm at 4°C for 10 min. Afterwards, cells were lysed using RIP lysis buffer and centrifuged at 14,000 rpm at 4°C for 10 min. The supernatant was incubated with anti-Ago antibody or lgG (Merck Millipore, Burlington, USA) as a control at 4°C. Magnetic beads conjugated with protein A/G (Thermo Fisher Scientific, Waltham, USA) were added into the supernatant. Proteinase K Buffer was used to resuspend the beads and antibody complex. The related RNA in the immunoprecipitation was collected and detected using quantitative reverse-transcription PCR (qRT-PCR).

Statistical analysis

Data were analyzed using GraphPad Prism software (GraphPad Software, San Diego, USA). Comparison among groups was analyzed using one-way analysis of variance (ANOVA), followed by Tukey's test. Data are expressed as mean ± standard deviation (SD). A value of $p < 0.05$ was considered statistically significant.

Results

LncRNA NORAD and miR-26a show dysregulation in HS tissue

The qPCR results showed that LncRNA NORAD was significantly upregulated and miR-26a was downregulated in intermediate scar tissues compared to adjacent normal tissues. TGF-βR2 levels were increased, as demonstrated by qPCR and ELISA (Fig. 1A,B). However, TGF-βR1 levels were reduced. TGF-β showed no significant change in the HTS group compared to the control group.

LncRNA NORAD knockdown suppresses cell proliferation and facilitates cell apoptosis

TGF-β1 was used to induce HSF proliferation, and qPCR was used to evaluate the transfection efficacy of shRNA-NORAD-1 or shRNA-NORAD-2. The results showed that shRNA-NORAD-1 has a greater inhibitory effect on NORAD expression than shRNA-NORAD-2 (Fig. 2A). Thus, shRNA-NORAD-1 was used in all further experiments. Additionally, the CCK-8 assay demonstrated that cell proliferation ability was markedly decreased by silencing LncRNA NORAD (Fig. 2B). Silencing LncRNA NORAD promotes cell apoptosis, as shown by comparing to results from the ShRNA-NC group (Fig. 2C,D).

The results of flow cytometry revealed that decreasing endogenous LncRNA NORAD significantly increased the proportion of cells in G0/G1 phase compared with the control group. Simultaneously, the proportion of cells in S and G2/M phase was reduced (Fig. 2E,F). These results imply that LncRNA NORAD affects the G1 arrest of HSFs treated with TGF-β1. That is to say, G1 arrest is significantly promoted by a decrease in endogenous LncRNA NORAD expression (Fig. 2E,F). TGF-βR1 levels were significantly increased, while TGF-βR2 and p-Smad2 were markedly decreased (Fig. 3A). These results suggest that decreasing endogenous LncRNA NORAD levels may suppress the TGF-β pathway. Proteins regulating cell cycle and cell apoptosis-related proteins were also significantly

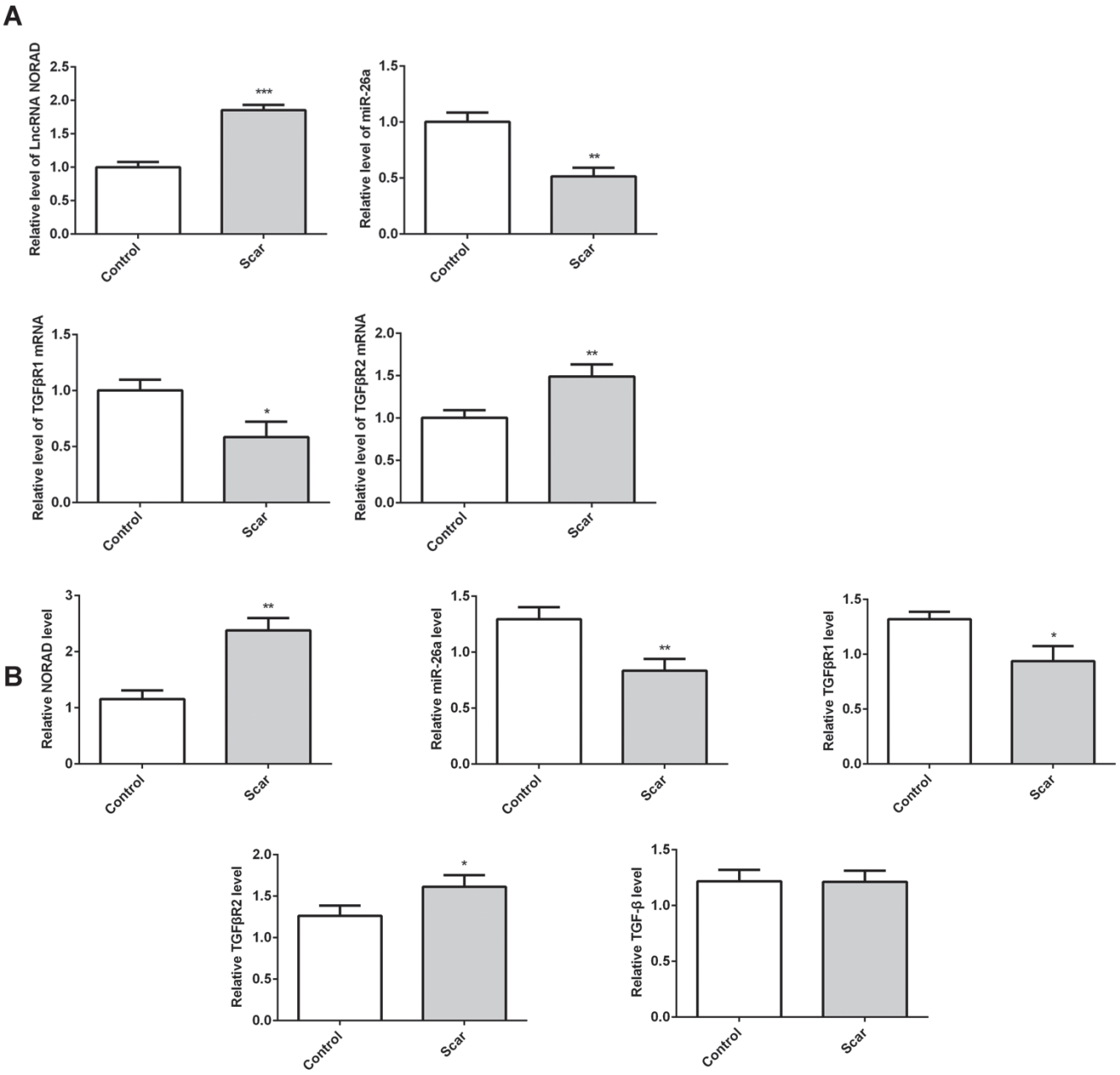

Fig. 1. A. NORAD, miR-26a, TGF-βR1, and TGF-βR2 are detected with qPCR in intermediate scar tissues; B. TGFβ-R1, TGF-βR2 and TGF-β are detected with ELISA. Data is shown as mean ±SD

affected (Fig. 3B). The above findings indicate that LncRNA NORAD knockdown promotes G1 arrest by regulating p21/cyclin D1/CDK4, and by modulating the apoptosis pathway by increasing pro-apoptosis protein caspase-3 and decreasing anti-apoptosis protein Bcl-2.

LncRNA NORAD as a sponge regulates miR-26a level

The Starbase database (http://starbase.sysu.edu.cn/) predicts that miR-26a could target LncRNA NORAD (Fig. 4A). Therefore, a cell experiment was performed to investigate whether miR-26a could bind to LncRNA NORAD, and whether LncRNA NORAD could act as a sponge of miR-26a and regulate its biological function. The sequence of LncRNA NORAD was inserted downstream of a luciferase gene to establish wt-NORAD plasmids. In HSF cells co-transfected with wt-NORAD and a miR-26a mimic, luciferase activity was significantly decreased compared to the mut-NORAD and miR-26a treatment groups, suggesting an interaction between miR-26a and NORAD (Fig. 4B). Also, the RIP assay showed the LncRNA NORAD level in the miR-26a mimic group was significantly higher than that of the miR-26a-NC group when anti-Ago2 antibody was used to treat the supernatant (Fig. 4C). In addition, LncRNA NORAD markedly affects miR-26a level (Fig. 4D,E). Thus, LncRNA NORAD functions as a sponge of miR-26a to inhibit miR-26a expression.

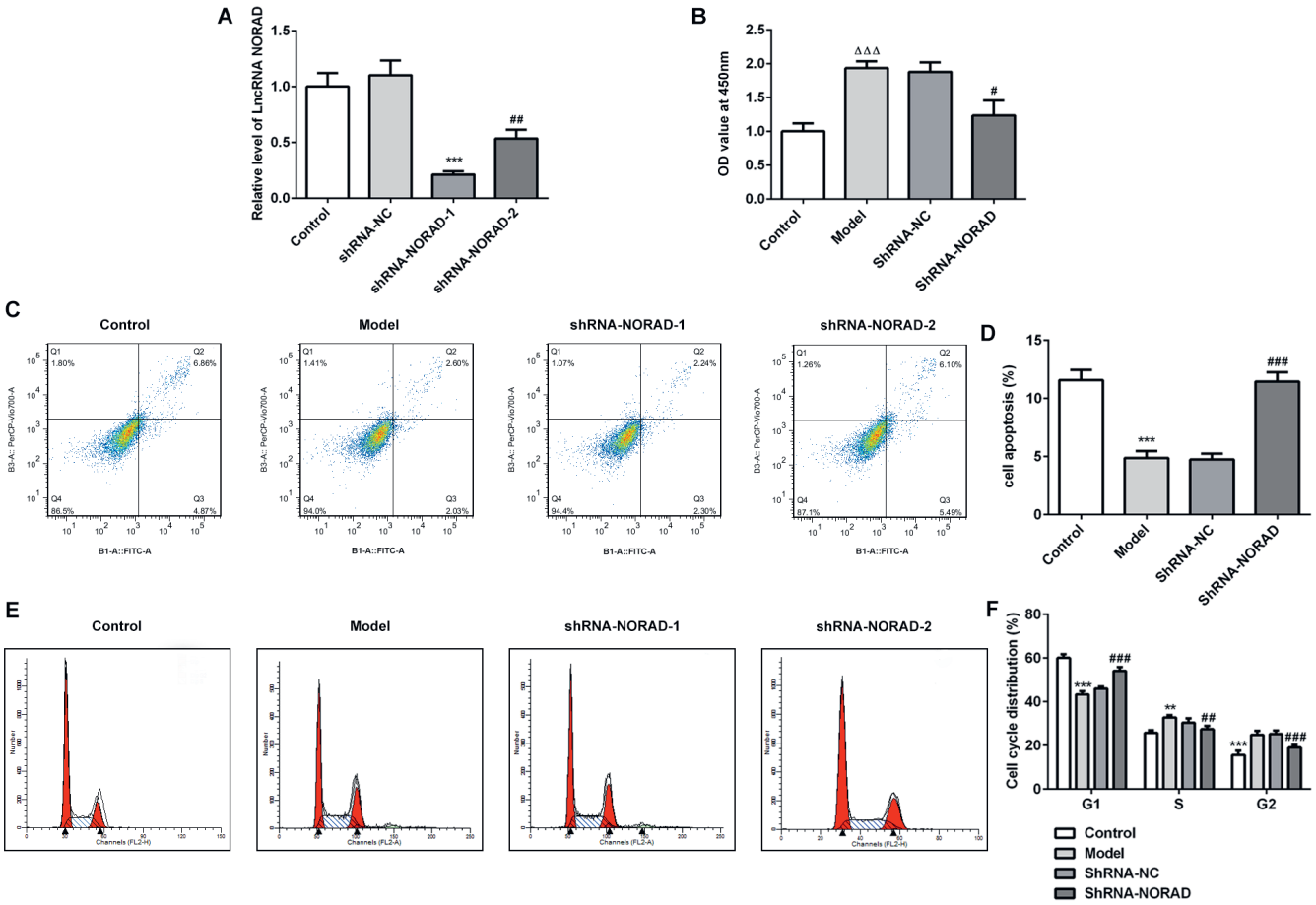

Fig. 2. A. shRNA-NORAD-1 or shRNA-NORAD-2 are respectively transfected into cells to enable evaluation of transfection efficacy; B. A CCK-8 assay is used to assess the proliferation of HSF induced by TGF-β1; C and D. Flow cytometry demonstrates cell apoptosis levels; E and F. Flow cytometry is used to analyze the cell cycle. Data is shown as mean ±SD

miR-26a binds to the 3'UTR of TGF-βR2

We analyzed whether miRNA-26a targets the TGF-β pathway. Starbase predicts that miR-26a could bind to the 3'UTRs of TGF-β2 and UBE3A (Fig. 5A,D). The luciferase reporter assay revealed miR-26a can bind to the 3'UTR of either TGFR2 or UBE3A, as it reduces the luciferase activity of both wt-TGFR2 and UBE3A (Fig. 5B,E). The RIP assay demonstrated that TGF-βR2 and UBE3A levels in the miR-26a mimic group were distinctly higher than in the miR-26a-NC group when anti-Ago2 antibody was added to the supernatant (Fig. 5C,F). These data imply that miRNA-26a post-transcriptionally regulates TGF-βR2 and UBE3A.

Discussion

Our data showed that LncRNA NORAD exhibited a significant increase and miR-26 showed an obvious decrease in scar tissues. We also found reduced TGFβ-R1 and enhanced TGFβ-R2 expression in scar tissues relative to a control group. The involvement of LncRNA in the activation of TGFβ signals has previously been investigated.[18] Further investigation of the mechanism of LncRNA NORAD in HSF cells revealed that decreasing endogenous expression of LncRNA NORAD significantly increased p21, and downregulated cyclin D1 and CDK4 levels. Cyclin D1 and CDK4 could form a complex and allow cells to bypass G1 phase, whereas p21 could also suppress cells from entering S phase via inhibition of cyclin dependent kinase (CDK) activity. The CDK activity is positively regulated by cyclin D and negatively regulated by cyclin dependent kinase inhibitor (CKI). Thus, LncRNA NORAD silence facilitates G1 arrest, possibly via upregulating p21 levels, and downregulating CDK4 and cyclin D1 expression. A study has shown that inhibition of cyclin D1 and CDK4 could mediate G1 arrest in HSF cells.[19] Additionally, upregulation of p21 expression contributes to the suppression of apoptosis in HSF.[20] Collectively, these results indicate that LncRNA NORAD knockdown significantly boosts apoptosis and G1 arrest in TGF-β-stimulated HSF.

In this study, we discovered that LncRNA NORAD was dramatically enriched in the complex precipitated by anti-Ago2 in HSF cells overexpressing miR-26a-5p, suggesting an interactive relationship between LncRNA NORAD and miR-26a-5p. In addition, LncRNA NORAD overexpression or silence markedly regulated miR-26a-5p. Therefore,

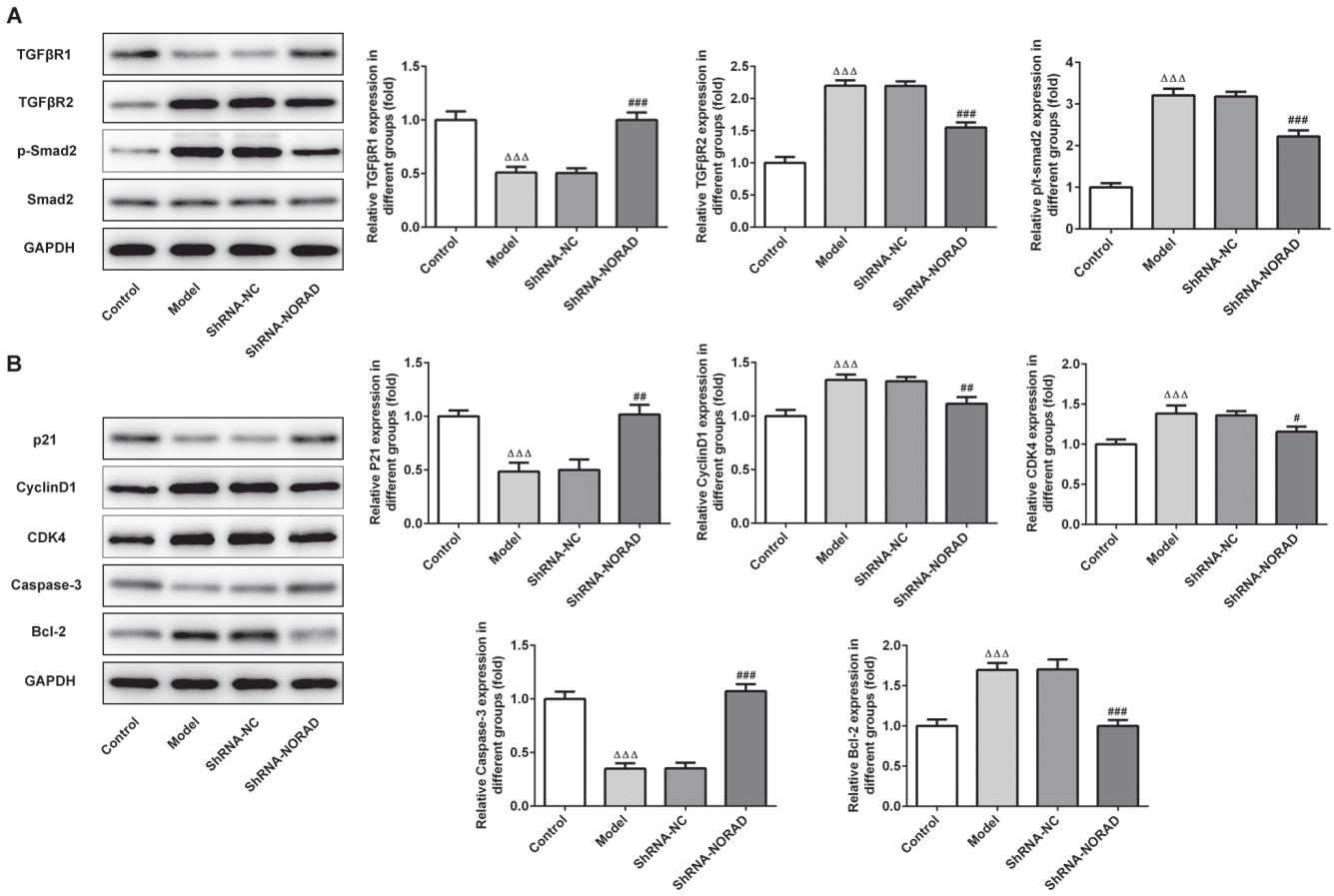

Fig. 3. A. TGF-β pathway-related proteins are detected with WB; B. Proteins regulating the cell cycle and cell apoptosis-related proteins are detected with WB. Data are shown as mean ±SD

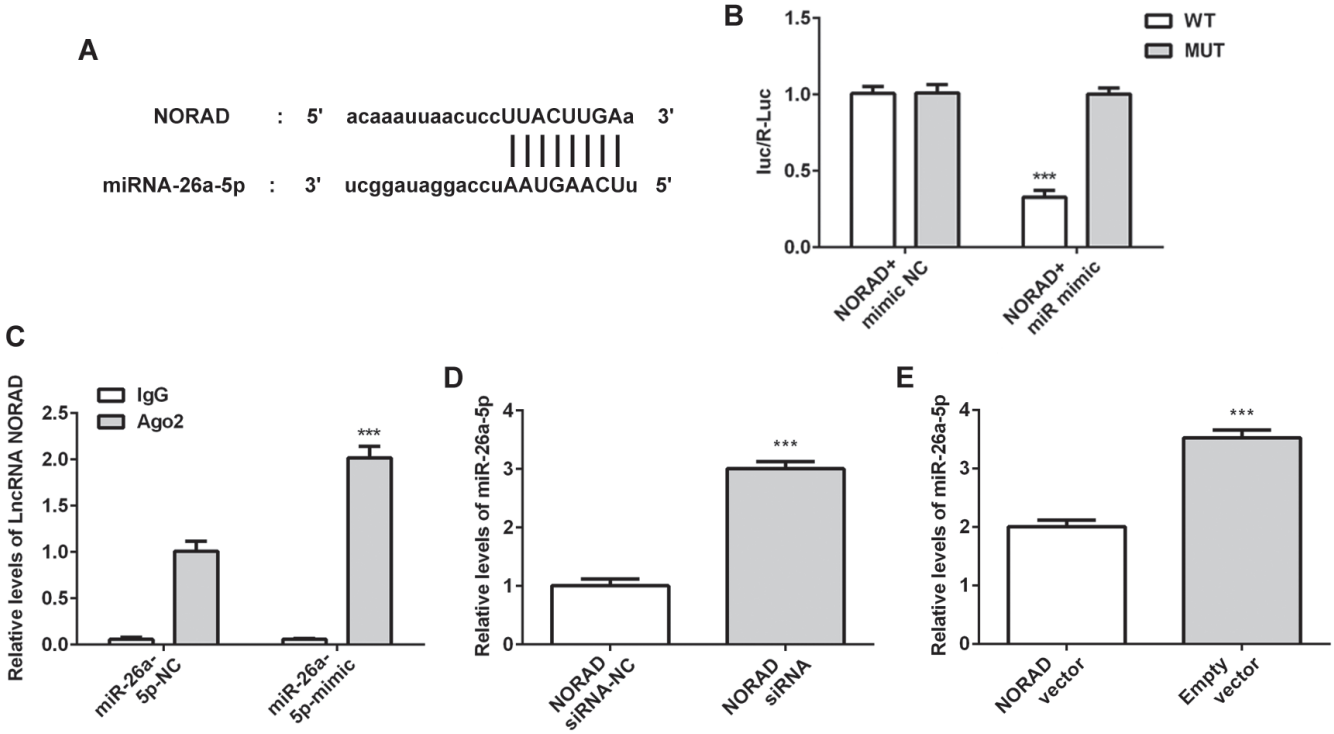

Fig. 4. A. The binding sites of miR-26a and NORAD are predicted using the Starbase database; B. A luciferase report assay shows that miR-26a binds to NORAD; C. A RIP assay indicates that NORAD is enriched in anti-Ago2 antibody-induced immunoprecipitation in the miR-26 mimic transfection group; D and E. NORAD markedly regulates miR-26 levels. Data are shown as mean ±SD

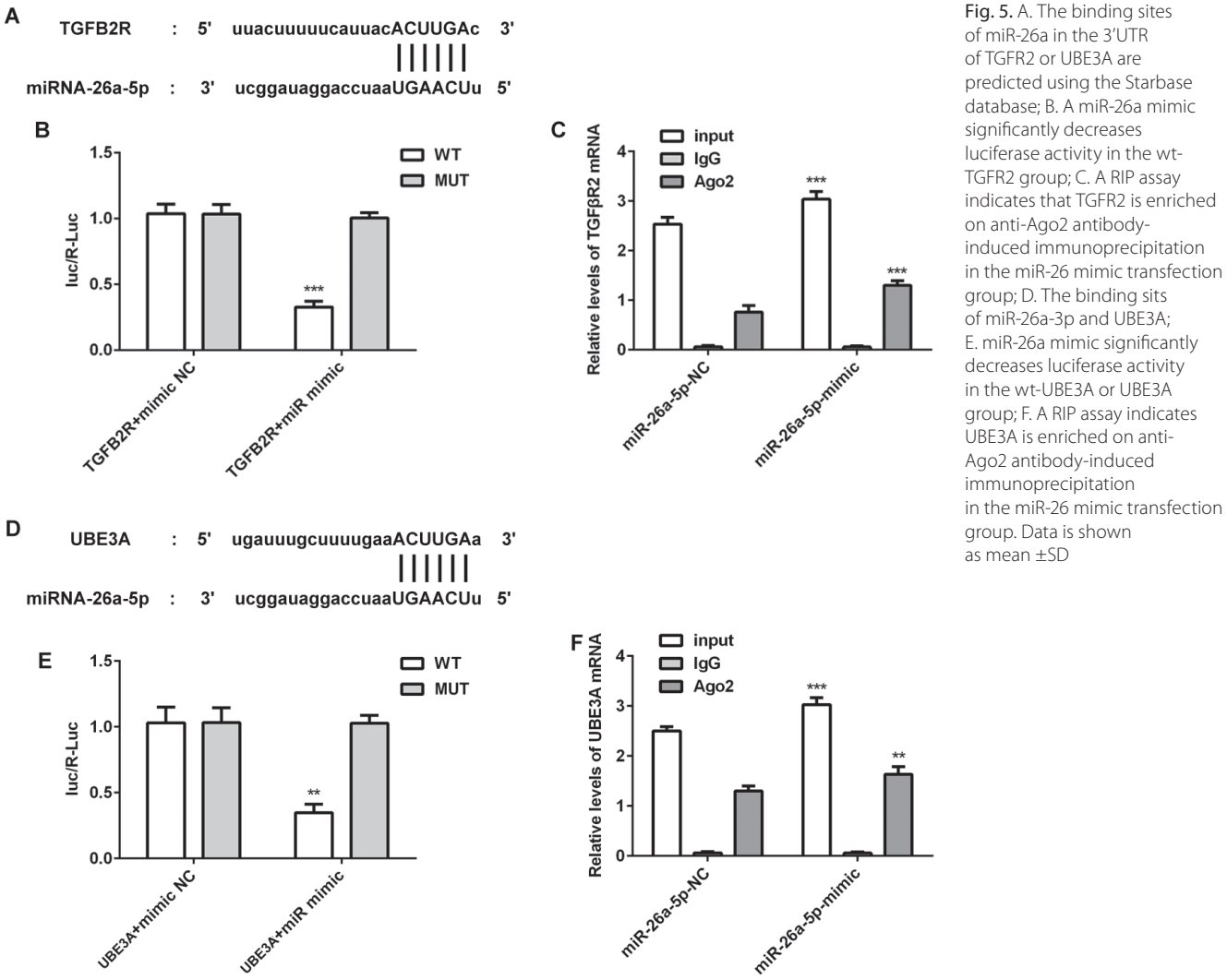

Fig. 5. A. The binding sites of miR-26a in the 3'UTR of TGFR2 or UBE3A are predicted using the Starbase database; B. A miR-26a mimic significantly decreases luciferase activity in the wt-TGFR2 group; C. A RIP assay indicates that TGFR2 is enriched on anti-Ago2 antibody-induced immunoprecipitation in the miR-26 mimic transfection group; D. The binding sits of miR-26a-3p and UBE3A; E. miR-26a mimic significantly decreases luciferase activity in the wt-UBE3A or UBE3A group; F. A RIP assay indicates UBE3A is enriched on anti-Ago2 antibody-induced immunoprecipitation in the miR-26 mimic transfection group. Data is shown as mean ±SD

LncRNA NORAD could be a sponge of miR-26a-5p in that it regulates the biological activity mediated by miRNA-26a.

A luciferase reporter assay was applied to confirm our prediction that miRNA-26a targets the 3'UTR of TGF-βR2 and UBE3A, proving that miRNA-26a could regulate TGFβ-R2 and UBE3A expression, and in turn influence cell proliferation and apoptosis. The excessive proliferation of HSF causes abnormal ECM synthesis.[21] TGF-β has been demonstrated to be involved in the process of wound repair and healing, which includes extravagant proliferation of fibroblasts.[22] The TGF-β1/TGF-βR1/Smad3 pathway is reported to promote HTS formation.[23] Medicine targeting the TGF-β/Smad pathway could suppress fibroblast proliferation or reduce scar formation.[24] Changing the expression of endogenous miRNA regulates apoptosis, possibly by affecting the TGF-β pathway in HSF.[25] Smad ubiquitination regulatory factor 2 (Smurf2), known as one of the homologous to the E6-AP carboxyl terminus (HECT) family E3 ligase members, is involved in the ubiquitination of TGF-βR1.[26] Ubiquitin and proteasome degradation of TGF-β receptors negatively regulates the TGF-β pathway.[27] Therefore, Smurf2 could negatively regulate TGFβ-R1 levels through ubiquitin induction. Research has demonstrated that the degradation of TGFβ-R1 induced by Smurf ameliorates TGF-β signals,[28] thereby affecting the development of HTS.[29] A study has shown that miRNAs enhance the TGF-β signal pathway through targeting Smurf2 mRNA and inhibiting its translation.[30] Therefore, it follows that miR-26a could regulate TGFβ-R1 though Smurf2 and affect TGF-β signals based on the experimental data and published studies.

Limitations

There is still lacking in vivo evidence to support this conclusion about the regulatory mechanism of LncRNA NORAD in scar hypertrophy in vitro, which requires further study.

Conclusions

TGF-β signals have been shown to be transmitted through the engagement of TGFβR2,[31] and TGF-β signaling can be significantly activated with the deubiquitination of a TGF-β receptor.[32] Collectively, TGFβ-R1/R2

plays a substantial role in regulating the TGF-β pathway, and miRNA-26a could be a potential target for treating HTS. In this study, we show that miRNA-26a can regulate the expression of TGF-βR2 and Smurf2 by binding to their 3'UTRs. Previous studies have indicated that miRNA regulates the expression of protein through suppressing its translation and recruiting other proteins to induce degradation. Our study confirms that LncRNA NORAD regulates HSF proliferation and apoptosis, possibly via miR-26a mediating TGF-βR2/R1, which provides a novel insight for understanding the pathological mechanism of HTS. In conclusion, LncRNA NORAD/miR-26a could be utilized as potential targets for new HS treatment.

ORCID iDs

Jun Qi https://orcid.org/0000-0002-7394-0621
Yangyang Yangyang Wu https://orcid.org/0000-0002-2047-3257
Haijian Zhang https://orcid.org/0000-0002-5135-3354
Yifei Liu https://orcid.org/0000-0001-7223-0196

References

1. Li Z, Liu Q, Wang X, Luan J. The characteristics of blood supply and tissue hypoxia in pathological scars. *Chin Med Sci J*. 201;32(2):113–118. https://doi.org/10.24920/J1001-9294.2017.014
2. El Hallani S, Boisselier B, Peglion F, et al. A new alternative mechanism in glioblastoma vascularization: Tubular vasculogenic mimicry. *Brain*. 2010;133(Pt 4):973–982. doi:10.1093/brain/awq044
3. Kiritsi D, Nystrom A. The role of TGFbeta in wound healing pathologies. *Mech Ageing Dev*. 2018;172:51–58. doi:10.1016/j.mad.2017.11.004
4. Finnson KW, Arany PR, Philip A. Transforming growth factor beta signaling in cutaneous wound healing: Lessons learned from animal studies. *Adv Wound Care (New Rochelle)*. 2013;2(5):225–237. doi:10.1089/wound.2012.0419
5. Finnson KW, McLean S, Di Guglielmo GM, Philip A. Dynamics of transforming growth factor beta signaling in wound healing and scarring. *Adv Wound Care (New Rochelle)*. 2013;2(5):195–214. doi:10.1089/wound.2012.0419
6. Chin GS, Liu W, Peled Z, et al. Differential expression of transforming growth factor-beta receptors I and II and activation of Smad 3 in keloid fibroblasts. *Plast Reconstr Surg*. 2001;108(2):423–429. doi:10.1097/00006534-200108000-00022
7. He S, Liu X, Yang Y, et al. Mechanisms of transforming growth factor beta(1)/Smad signalling mediated by mitogen-activated protein kinase pathways in keloid fibroblasts. *Br J Dermatol*. 2010;162(3):538–546. doi:10.1111/j.1365-2133.2009.09511.x
8. Li H, Yang L, Zhang Y, Gao Z. Kaempferol inhibits fibroblast collagen synthesis, proliferation and activation in hypertrophic scar via targeting TGF-beta receptor type I. *Biomed Pharmacother*. 2016;83:967–974. doi:10.1016/j.biopha.2016.08.011
9. Ji X, Tang Z, Shuai W, et al. Endogenous peptide LYENRL prevents the activation of hypertrophic scar-derived fibroblasts by inhibiting the TGF-beta1/Smad pathway. *Life Sci*. 2019;231:116674. doi:10.1016/j.lfs.2019.116674
10. Schultze-Mosgau S, Blaese MA, Grabenbauer G, et al. Smad-3 and Smad-7 expression following anti-transforming growth factor beta 1 (TGFbeta1)-treatment in irradiated rat tissue. *Radiother Oncol*. 2004;70(3):249–259. doi:10.1016/j.radonc.2004.01.010
11. Reid RR, Roy N, Mogford JE, Zimmerman H, Lee C, Mustoe TA. Reduction of hypertrophic scar via retroviral delivery of a dominant negative TGF-beta receptor II. *J Plast Reconstr Aesthet Surg*. 2007;60(1):64–72, discussion 73–74. doi:10.1016/j.bjps.2005.12.026
12. Liu YL, Liu WH, Sun J, et al. Mesenchymal stem cell-mediated suppression of hypertrophic scarring is p53 dependent in a rabbit ear model. *Stem Cell Res Ther*. 2014;5(6):136. doi:10.1186/scrt526
13. Meulmeester E, Ten Dijke P. The dynamic roles of TGF-beta in cancer. *J Pathol*. 2011;223(2):205–218. doi:10.1002/path.2785
14. Xiong Y, Cao F, Hu L, et al. miRNA-26a-5p Accelerates healing via downregulation of PTEN in fracture patients with traumatic brain injury. *Mol Ther Nucleic Acids*. 2019;17:223–234. doi:10.1016/j.omtn.2019.06.001
15. Jing R, Zhong QQ, Long TY, Pan W, Qian ZX. Downregulated miRNA-26a-5p induces the apoptosis of endothelial cells in coronary heart disease by inhibiting PI3K/AKT pathway. *Eur Rev Med Pharmacol Sci*. 2019:23(11):4940–4947. doi:10.26355/eurrev_201906_18084
16. Miyamoto K, Seki N, Matsushita R, et al. Tumour-suppressive miRNA-26a-5p and miR-26b-5p inhibit cell aggressiveness by regulating PLOD2 in bladder cancer. *Br J Cancer*. 2016;115(3):354–363. doi:10.1038/bjc.2016.179
17. Qi J, Liu Y, Hu K, Zhang Y, Wu Y, Zhang X. MicroRNA-26a inhibits hyperplastic scar formation by targeting Smad2. *Exp Ther Med*. 2018;15(5):4332–4338. doi:10.3892/etm.2018.5984
18. Zhou K, Ou Q, Wang G, Zhang W, Hao Y, Li W. High long non-coding RNA NORAD expression predicts poor prognosis and promotes breast cancer progression by regulating TGF-beta pathway. *Cancer Cell Int*. 2019;19:63. doi:10.1186/s12935-019-0781-6
19. Kavsak P, Rasmussen RK, Causing CG, et al. Smad7 binds to Smurf2 to form an E3 ubiquitin ligase that targets the TGF beta receptor for degradation. *Mol Cell*. 2000;6(6):1365–1375. doi:10.1016/s1097-2765(00)00134-9
20. Izzi L, Attisano L. Regulation of the TGFbeta signalling pathway by ubiquitin-mediated degradation. *Oncogene*. 2004;23(11):2071–2078. doi:10.1038/sj.onc.1207412
21. Derynck R, Zhang YE. Smad-dependent and Smad-independent pathways in TGF-beta family signalling. *Nature*. 2003;425(6958):577–584. doi:10.1038/nature02006
22. Wang B, Xu X, Yang Z, et al. POH1 contributes to hyperactivation of TGF-beta signaling and facilitates hepatocellular carcinoma metastasis through deubiquitinating TGF-beta receptors and caveolin-1. *EBioMedicine*. 2019;41:320–332. doi:10.1016/j.ebiom.2019.01.058
23. Li Y, Cui C, Xie F, et al. VprBP mitigates TGF-beta and Activin signaling by promoting Smurf1-mediated type I receptor degradation. *J Mol Cell Biol*. 2020;12(2):138–151. doi:10.1093/jmcb/mjz057
24. Tracy LE, Minasian RA, Caterson EJ. Extracellular matrix and dermal fibroblast function in the healing wound. *Adv Wound Care (New Rochelle)*. 2016;5(3):119–136. doi:10.1089/wound.2014.0561
25. Pakyari M, Farrokhi A, Maharlooei MK, Ghahary A. Critical role of transforming growth factor beta in different phases of wound healing. *Adv Wound Care (New Rochelle)*. 2013;2(5):215–224. doi:10.1089/wound.2012.0406
26. Qian W, Li N, Cao Q, Fan J. Thrombospondin-4 critically controls transforming growth factor beta1-induced hypertrophic scar formation. *J Cell Physiol*. 2018;234(1):731–739. doi:10.1002/jcp.26877
27. Ye X, Pang Z, Zhu N. Dihydromyricetin attenuates hypertrophic scar formation by targeting activin receptor-like kinase 5. *Eur J Pharmacol*. 2019;852:58–67. doi:10.1016/j.ejphar.2019.02.039
28. Zhou X, Xie Y, Xiao H, et al. MicroRNA-519d inhibits proliferation and induces apoptosis of human hypertrophic scar fibroblasts through targeting Sirtuin 7. *Biomed Pharmacother*. 2018;100:184–190. doi:10.1016/j.biopha.2018.01.158
29. Chae DK, Park J, Cho M, et al. MiR-195 and miR-497 suppress tumorigenesis in lung cancer by inhibiting SMURF2-induced TGF-beta receptor I ubiquitination. *Mol Oncol*. 2019;13(12):2663–2678. doi:10.1002/1878-0261.12581
30. Zhang Z, Finnerty CC, He J, Herndon DN. Smad ubiquitination regulatory factor 2 expression is enhanced in hypertrophic scar fibroblasts from burned children. *Burns*. 2012;38(2):236–246. doi:10.1016/j.burns.2011.08.012
31. Gong YF, Zhang XM, Liu F, et al. Inhibitory effect of recombinant human endostatin on the proliferation of hypertrophic scar fibroblasts in a rabbit ear model. *Eur J Pharmacol*. 2016;791:647–654. doi:10.1016/j.ejphar.2016.09.034
32. Liu B, Guo Z, Gao W. miR-181b-5p promotes proliferation and inhibits apoptosis of hypertrophic scar fibroblasts through regulating the MEK/ERK/p21 pathway. *Exp Ther Med*. 2019;17(3):1537–1544. doi:10.3892/etm.2019.7159

Eplerenone inhibits oxidized low-density lipoprotein-induced proliferation and migration of vascular smooth muscle cells by downregulating GPER expression

Dandan Wang[1,A–D,F], Minglei Wang[2,B,C,F], Pingping Sun[1,C,F], Qiaoyan Gao[3,A,E,F]

[1] Nursing Department, Weihai Central Hospital, China
[2] Pharmacy Department, Weihai Central Hospital, China
[3] Nursing Department, Weihai Central Hospital, China

A – research concept and design; B – collection and/or assembly of data; C – data analysis and interpretation; D – writing the article; E – critical revision of the article; F – final approval of the article

Advances in Clinical and Experimental Medicine, ISSN 1899–5276 (print), ISSN 2451–2680 (online) *Adv Clin Exp Med*. 2021;30(4):405–412

Address for correspondence
Qiaoyan Gao
E-mail: qiaoyang55@126.com

Funding sources
None declared

Conflict of interest
None declared

Received on July 16, 2020
Reviewed on August 4, 2020
Accepted on February 19, 2021

Published online on April 29, 2021

Abstract

Background. Excessive proliferation and migration of vascular smooth muscle cells (VSMCs) are associated with the pathogenesis of atherosclerosis (AS). Eplerenone (EPL), a novel selective aldosterone receptor blocker, plays a substantial role in the treatment of cardiovascular disease. The G protein-coupled estrogen receptor (GPER) is a target of EPL as the STITCH website predicated.

Objectives. We aimed to investigate the roles of EPL in AS and identify its potential mechanisms of action.

Materials and methods. Oxidized low-density lipoprotein (ox-LDL) was employed to stimulate VSMCs to establish a cellular model of AS. The ability of cell proliferation was examined using a Cell Counting Kit-8, and the expression of proliferation-related proteins was tested using immunofluorescence staining and western blot analysis. Subsequently, cell migration and the expression of migration-associated proteins were evaluated with a wound healing assay, transwell assay and western blot analysis. Then, GPER expression was determined using western blot analysis in the absence or presence of EPL. To explore the regulatory mechanisms of EPL in ox-LDL-stimulated VSMCs, GPER was overexpressed, followed by measurement of cell proliferation and migration.

Results. The Ox-LDL stimulation notably upregulated GPER expression, whereas EPL treatment down-regulated GPER expression in a dose-dependent manner. Additionally, EPL markedly inhibited proliferation and migration of VSMCs, and the highest dose of EPL resulted in the most marked effect. By contrast, GPER overexpression reversed the inhibitory effects of EPL on proliferation and migration of VSMCs.

Conclusions. Eplerenone suppressed ox-LDL-induced proliferation and migration of VSMCs partly through downregulation of GPER, providing a new mechanism of support for EPL use in the clinical treatment of AS.

Key words: atherosclerosis, proliferation, migration, vascular smooth muscle cells, eplerenone

Cite as
Wang D, Wang M, Sun P, Gao Q. Eplerenone inhibits oxidized low-density lipoprotein-induced proliferation and migration of vascular smooth muscle cells by downregulating GPER expression. *Adv Clin Exp Med*. 2021;30(4):405–412. doi:10.17219/acem/133484

DOI
10.17219/acem/133484

Copyright
© 2021 by Wroclaw Medical University
This is an article distributed under the terms of the Creative Commons Attribution 3.0 Unported (CC BY 3.0) (https://creativecommons.org/licenses/by/3.0/)

Background

Atherosclerosis (AS), a chronic degenerative disease of the arterial wall, is the leading cause of peripheral vascular disease and cardiac-cerebral vascular disease.[1] It is well known to cause high morbidity and mortality in aged individuals worldwide.[2,3] Vascular smooth muscle cells (VSMCs) are involved in the reconstruction of arterial wall by maintaining blood flow in affected vessels due to atherosclerotic alteration.[4] A growing body of literature has shown that abnormal proliferation and migration of VSMCs are closely associated with AS progression.[5,6] Oxidized low-density lipoprotein (ox-LDL), a well-established risk factor for AS, can induce proliferation and migration of VSMCs, thereby contributing to atherosclerotic plaque formation and progression.[7] Therefore, ox-LDL was employed in the present study to stimulate VSMCs to establish an AS cell model, providing a similar environment to explore the regulatory mechanisms involved in AS.

Eplerenone (EPL), a selective aldosterone receptor antagonist, is approved by Federal Drug Administration (FDA) for the treatment of left-sided heart failure and systemic hypertension.[8] Compelling evidence has indicated that EPL is effective in remedying cardiovascular diseases secondary to hypertension.[9] One report supports the notion that EPL inhibits Tregs by inactivation of Kv1.3 channel to reverse cardiac fibrosis.[10] Additionally, EPL can suppress proliferation of contralateral renal cells in rats with unilateral ureteral obstruction.[11] What is more, EPL has been affirmed to reduce renal inflammation, interstitial cell proliferation and phenotypic changes of interstitial cells.[12] The STITCH website (http://stitch.embl.de) predicts that the G protein-coupled estrogen receptor (GPER), a G protein-coupled receptor coupled with Gs proteins, is a target of EPL. It has been reported that GPER promotes proliferation, invasion and migration of triple-negative breast cancer cells.[13] Furthermore, blocking the function of GPER can alleviate the bisphenol A-induced proliferation of VSMCs.[14] However, the role of EPL in AS and whether it functions through targeting GPER remain to be elucidated.

Objectives

In the present study, we probed the impacts of EPL on proliferation and migration of VSMCs stimulated by ox-LDL, as well as its underlying molecular mechanism. This study is of great significance since it provides experimental support for EPL therapy in the clinical treatment of AS.

Materials and methods

Cell culture and treatment

Human VSMCs were purchased from China Center for Type Culture Collection (Wuhan, China) and cultured in Dulbecco's modified Eagle's medium (DMEM) containing 10% fetal bovine serum (FBS; Gibco, Grand Island, USA) at 37°C in fully humidified air of 95% air and 5% CO_2. The VSMCs were seeded in six-well plates at the density of 1×10^5 cells/well. To construct the AS model in vitro, 100 μg/mL of ox-LDL (Yiyuan Biotech, Guangzhou, China) were utilized to treat cells for 48 h. After that, the cells were treated with 0.3 μM, 1 μM and 3 μM EPL (Pfizer, New York, USA) for 24 h to evaluate the effects of EPL on ox-LDL-induced VSMCs.

Cell transfection

Cells were plated into six-well plates (1×10^6 cells per well) and transfection was performed once cells in the logarithmic growth phase reached 80% confluence. The overexpression plasmids of GPER (Oe-GPER-1 and Oe-GPER-2) and empty vector (Oe-NC) were designed and synthesized by RiboBio Co., Ltd. (Guangzhou, China). Transfection experiments were carried out with Lipofectamine 3000 (Invitrogen, Carlsbad, USA) following manufacturer's recommendations. At 24 h after transfection, VSMCs were collected and the successful transfection was determined using reverse transcription-quantitative polymerase chain reaction (RT-qPCR) analysis.

Cell viability assay

A Cell Counting Kit-8 (CCK-8; Shanghai Yi Sheng Biotechnology Co. Ltd., Shanghai, China) was adopted for detecting cell viability after appropriate treatments according to standard techniques. In brief, VSMCs (about 5×10^3 cells/per well) were seeded in a 96-well plate. After exposure to EPL or ox-LDL, a volume of 10 μL of CCK-8 solution was added to each well. Following further incubation at 37°C for 1 h, the absorbance was determined at the wavelength of 450 nm using a microplate reader (Molecular Devices, Sunnyvale, USA).

Immunofluorescence staining

The VSMCs were plated on coverslips in 24-well plates following transfection and cultured until 80% confluence was reached. After different treatments, cells were fixed with 4% paraformaldehyde for 15 min, followed by permeabilization with 0.05% Triton X-100 for 20 min at room temperature. After blocking in 5% bovine serum albumin for 30 min, cells were cultivated with a primary antibody against Ki67 (Cell Signaling Technology, Inc., Boston, USA) overnight at 4°C. Following three-time washing with phosphate-buffered saline (PBS), cells were incubated DyLight™ 488-conjugated secondary antibody (Thermo Fisher Scientific, Inc., Waltham, USA) for 1 h at room temperature. Subsequently, the nuclei were stained with 4',6-diamidino-2-phenylindole (DAPI; Sigma-Aldrich, Merck KGaA, St. Louis, USA) for 5 min and then washed 3 times with PBS in the dark. Immunofluorescence was detected under a fluorescence microscope (Olympus Corp., Tokyo, Japan).

Wound healing assay

The VSMCs (2×10^5 cells/well) were placed in six-well plates and cultured overnight at 37°C. Thereafter, cells were incubated with serum-free medium for 12 h prior to the experiment. Afterwards, a wound was gently created by a 10 µL sterile pipette tip and the cell debris was washed twice with PBS. Wound closure was monitored by comparing digital photographs of the same region of interest taken at 0 h and 24 h time points using a fluorescence microscope (Olympus Corp.). Quantitative analysis of the wound healing area was performed using ImageJ software (National Institutes of Health (NIH), Bethesda, USA).

Transwell migration assay

For the transwell migration assay, serum-free media containing 5×10^4 VSMCs were placed into the upper chamber of a 24-well transwell filter with 8 µm pore size. The lower chamber was filled with media supplemented with 10% FBS. Migratory cells would transgress through the porous filters at 37°C within 24 h. Then, VSMCs were fixed with 4% paraformaldehyde for 20 min. Cells that migrated through the pores of the filters were stained with 1% crystal violet for 30 min. The images were photographed under a fluorescence microscope (Olympus Corp.) and the number of migrated cells was calculated using ImageJ software.

RT-qPCR analysis

Total RNA was isolated from VSMCs using TRIzol reagent (Invitrogen) according to standard techniques. The complementary DNA (cDNA) was synthesized using a PrimeScript RT Reagent Kit (TaKaRa, Tokyo, Japan). The PCR then was performed with 2 µg cDNA as the templet using Power SYBR Master Mix (Applied Biosystems, Foster City, USA) on the ABI 7500 PCR system (Applied Biosystems). The following thermocycling conditions were used: initial denaturation at 95°C for 7 min; 40 cycles of 95°C for 15 s and 60°C for 30 s; and a final extension at 72°C for 30 s. Sequences of the gene-specific primers were synthesized by Ribobio Co., Ltd. (Guangzhou, China). Relative expression was calculated using the $2^{-\Delta\Delta Ct}$ method. Gene expression was normalized to that of glyceraldehyde 3-phosphate dehydrogenase (GAPDH).

Western blot analysis

Whole proteins were extracted using a protein lysis buffer in the presence of a protease inhibitor cocktail (Beyotime, Shanghai, China), which were further quantified using a bicinchoninic acid protein assay kit (Beyotime). Then, equal amount of total protein (50 µg) was subjected to 10% SDS-PAGE electrophoresis and transferred onto polyvinylidene fluoride (PVDF) membranes (Millipore, Billerica, USA). The membranes were subsequently blocked with 5% non-fat milk for 1 h at room temperature and incubated with primary antibodies (Santa Cruz Biotechnology, Dallas, USA) overnight at 4°C. Following this, the membranes were further probed with horseradish peroxidase (HRP)-conjugated secondary antibody (Cell Signaling Technology) for 1.5 h at room temperature. The immunoreactive protein bands on the membranes were visualized using the Odyssey Infrared Imaging System (LI-COR Biosciences, Lincoln, USA). ImageJ software was used for quantitative analysis of the gray values of protein bands. The relative expression was normalized to the internal control GAPDH.

Statistical analyses

All data are represented as mean values ± standard deviation (SD) from at least 3 independent experiments. Statistical analysis was conducted with GraphPad Prism v. 6 (GraphPad Software, Inc., San Diego, USA). Student's t-test was utilized to analyze data between 2 groups. Comparisons involving multiple samples were conducted using one-way analysis of variance (ANOVA) followed by Tukey's post hoc test. The acceptable value of significance was $p < 0.05$.

Results

EPL dose-dependently inhibited cell proliferation in ox-LDL-stimulated VSMCs

Firstly, a CCK-8 assay was used to assess cell viability after VSMCs were treated with increasing EPL. As displayed in Fig. 1A, there was no significant effect on cell viability in response to EPL treatment (0.3 µM, 1 µM and 3 µM) relative to the control group. By contrast, ox-LDL challenge significantly enhanced cell viability, which was reduced with EPL co-treatment in a dose-dependent manner (Fig. 1B). Additionally, notably elevated Ki67 expression was observed in ox-LDL-stimulated VSMCs relative to the untreated group, whereas EPL intervention significantly decreased Ki67 expression, especially under co-treatment with 3 µM EPL (Fig. 1C). Consistently, EPL markedly downregulated the expression of minichromosome maintenance-2 (MCM-2) and proliferating cell nuclear antigen (PCNA), which are key proliferation-related proteins, in ox-LDL-exposed VSMCs (Fig. 1D). These results implicate that EPL attenuates proliferation of VSMCs stimulated by ox-LDL.

EPL treatment suppressed migration of VSMCs induced by ox-LDL

The influence of EPL on cell migration in ox-LDL-induced VSMCs was explored in the following experiments. Results presented in Fig. 2A,B show that ox-LDL challenge

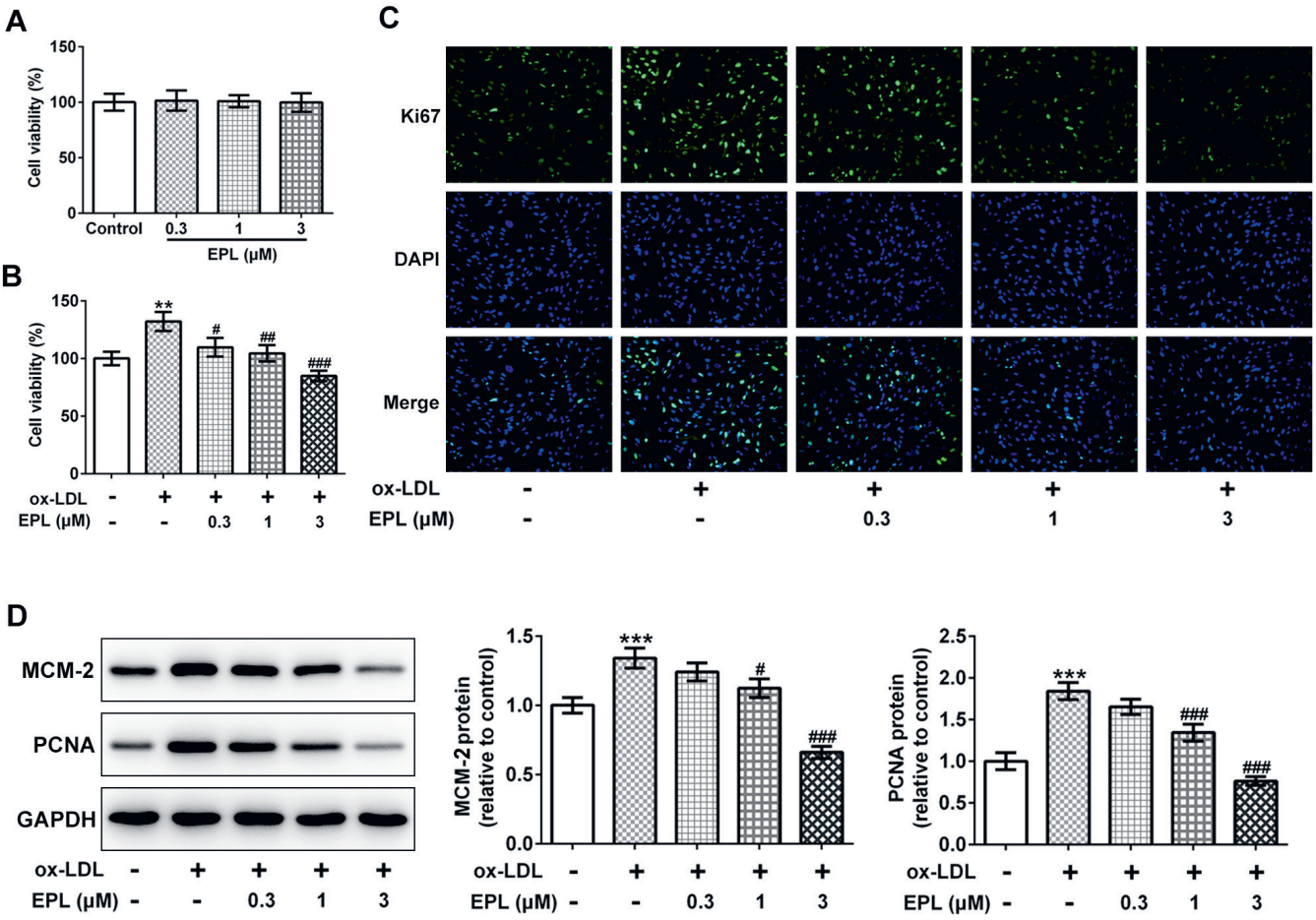

Fig. 1. EPL dose-dependently inhibited cell proliferation in ox-LDL-stimulated VSMCs

A. Cell viability was detected using a CCK-8 assay when VSMCs were treated with different concentrations of EPL; B. CCK-8 assay was employed to determine viability of VSMCs in the presence or absence of ox-LDL and EPL; C. The expression of Ki67 was measured using immunofluorescence staining (magnification ×200); D. Western blot analysis was used to analyze the levels of MCM-2 and PCNA. All experiments were repeated 3 times independently (n = 3). **$p < 0.01$, ***$p < 0.001$ compared to control; #$p < 0.05$, ##$p < 0.01$ and ###$p < 0.001$ compared to ox-LDL; EPL – eplerenone; ox-LDL – oxidized low-density lipoprotein; VSMCs – vascular smooth muscle cells; CCK-8 – cell counting kit-8; MCM-2 – minichromosome maintenance-2; PCNA – proliferating cell nuclear antigen.

remarkably promoted the migration of VSMCs relative to the control group. Conversely, EPL dose-dependently declined the ox-LDL-promoted ability of cell migration. As expected, results of transwell migration assay presented the same trends with those of the scratch wound healing assay (Fig. 2C,D). Simultaneously, EPL dramatically downregulated the expression of migration-associated proteins including MMP2 and MMP9 in a dose-dependent manner (Fig. 2E). Overall, these data suggest that EPL treatment represses migration of VSMCs boosted by ox-LDL.

EPL downregulated the expression of GPER in VSMCs exposed to ox-LDL

To uncover the potential mechanisms of EPL in VSMCs under ox-LDL exposure, the STITCH website (http://stitch.embl.de) was applied to search the potential proteins interacting with EPL. The GPER was assumed to combine with EPL (Fig. 3A). It is observable in Fig. 3B that GPER expression was gradually enhanced with the increased concentrations of ox-LDL. Moreover, under exposure to 100 μg/mL of ox-LDL at time points from 12 h to 72 h, the level of GPER in VSMCs was markedly upregulated compared with the control group, and the highest level of GPER was noted at 48 h (Fig. 3C). Afterwards, the effect of EPL on GPER expression was assessed using western blot analysis. Figure 3D displays that EPL dose-dependently lowered the level of GPER induced by ox-LDL. To sum up, these observations reveal that EPL can inhibit GPER expression in VSMCs exposed to ox-LDL.

GPER overexpression reversed the inhibitory impacts of EPL exposure on proliferation and migration of VSMCs treated with ox-LDL

Subsequently, to study the exact regulatory mechanisms of EPL on GPER, GPER was overexpressed by transfection with overexpression plasmids. Successful transfection was presented in Fig. 4A, and VSMCs transfected with Oe-GPER-1 were selected for the following experiments due to Oe-GPER-1 producing higher expression of GPER.

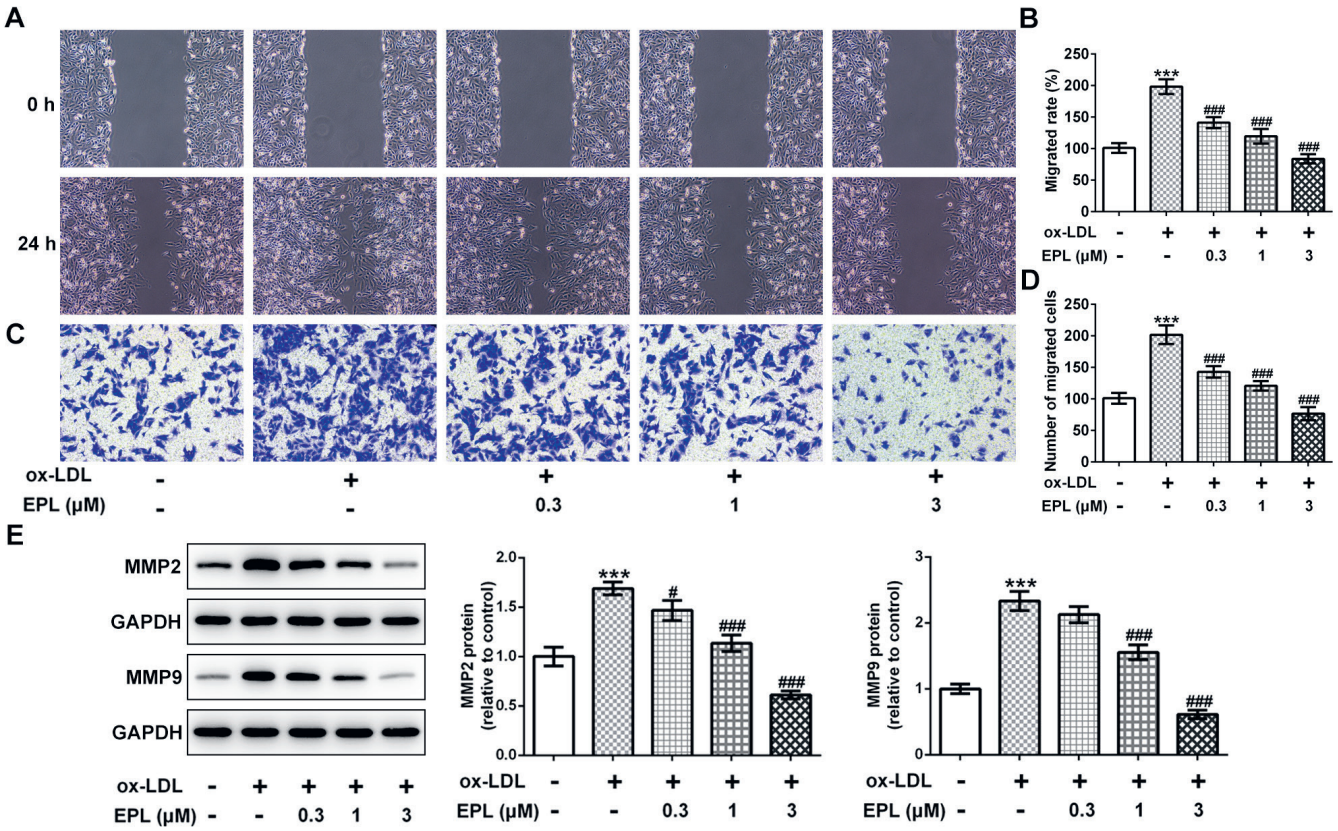

Fig. 2. EPL treatment suppressed migration of VSMCs induced by ox-LDL

A and B. Cell migration was determined using scratch wound healing assay (magnification ×100); C and D. Cell migration was assessed using transwell migration assay (magnification ×200); E. The expression of MMP2 and MMP9 was examined using western blot analysis. The experiments were generated from 3 independent repeats (n = 3). ***p < 0.001 compared to control; #p < 0.05 and ###p < 0.001 compared to ox-LDL. EPL – eplerenone; ox-LDL – oxidized low-density lipoprotein; VSMCs – vascular smooth muscle cells; MMP – matrix metalloproteinase.

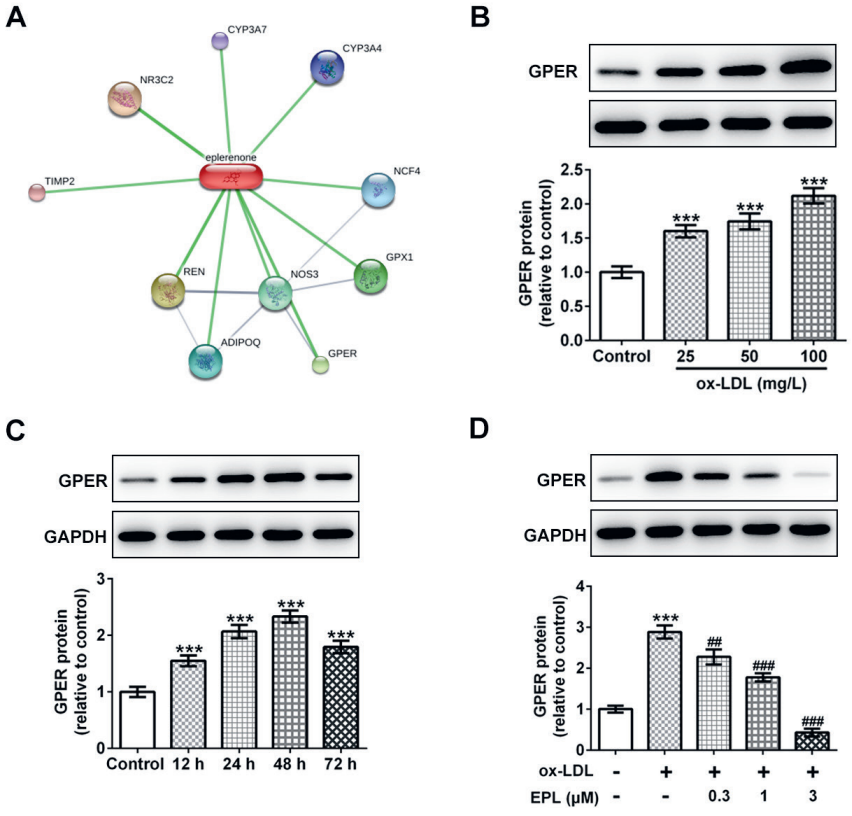

Fig. 3. EPL decreased GPER expression in ox-LDL-treated VSMCs

A. The EPL-protein interaction network was predicted using the STITCH website; B. Western blot analysis of the expression of GPER when VSMCs were exposed to 25 mg/L, 50 mg/L and 100 mg/L of ox-LDL, respectively; C. The level of GPER was examined using western blot analysis in VSMCs stimulated by 100 mg/L of ox-LDL for 12 h, 24 h, 48 h, and 72 h, respectively. The experiments were generated from 3 independent repeats (n = 3); D. GPER expression was measured using western blot analysis when VSMCs were treated with a series of concentrations of EPL. All experiments were repeated 3 times independently (n = 3). ***p < 0.001 compared to control; ##p < 0.01 and ###p < 0.001 compared to ox-LDL; EPL – eplerenone; ox-LDL – oxidized low-density lipoprotein; VSMCs – vascular smooth muscle cells; GPER – G protein-coupled estrogen receptor.

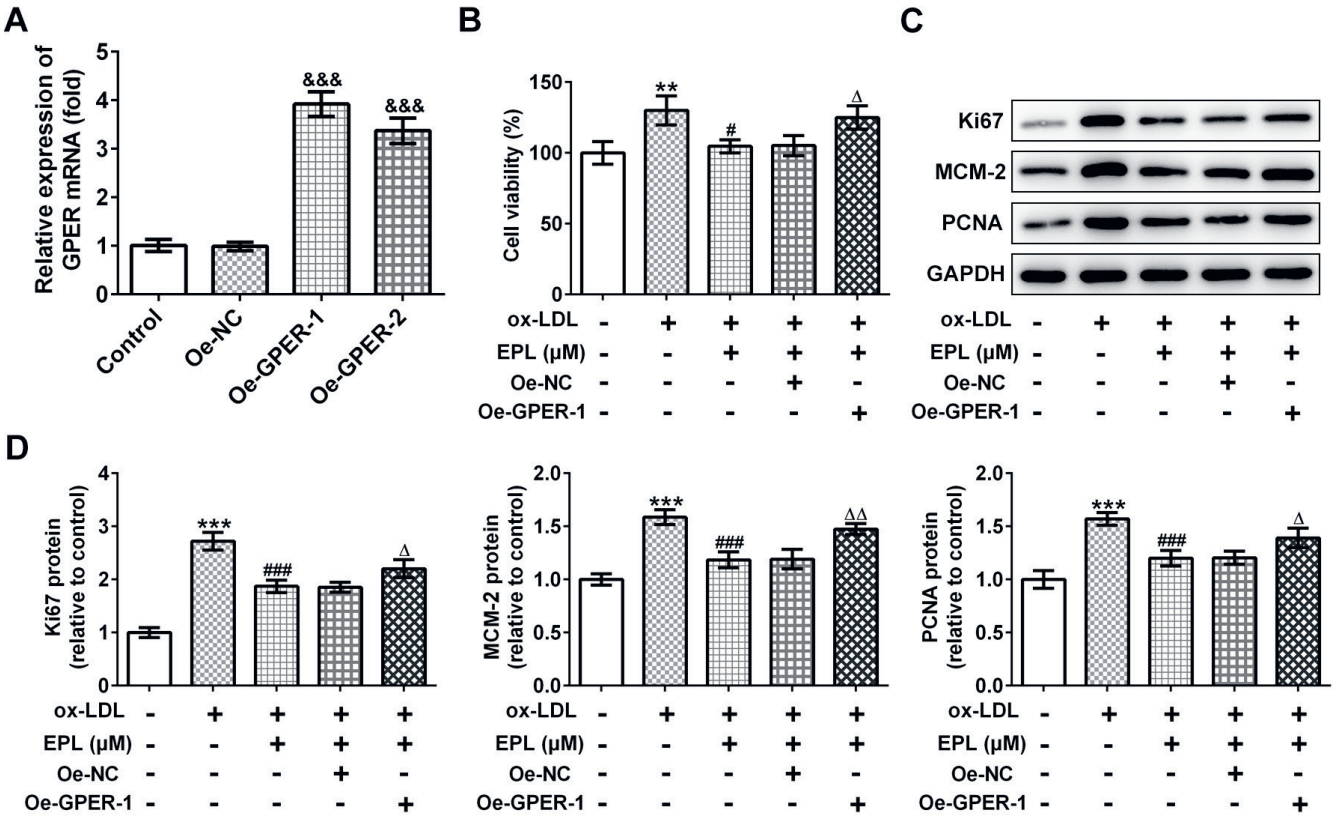

Fig. 4. GPER overexpression alleviated the inhibitory effect of EPL exposure on proliferation of VSMCs induced by ox-LDL

A. The expression of GPER was determined using RT-qPCR after transfection with Oe-GPER-1 or Oe-GPER-2. The experiments were generated from 3 independent repeats (n = 3). $^{\&\&\&}p < 0.001$ compared to Oe-NC; B. Cell viability was evaluated using a CCK-8 Kit; C and D. Western blot analysis was employed to assess the expression of proliferation-related proteins. The experiments were generated from 3 independent repeats (n = 3). $^{**}p < 0.01$ and $^{***}p < 0.001$ compared to control; $^{\#}p < 0.05$ and $^{\#\#\#}p < 0.001$ compared to ox-LDL; $^{\Delta}p < 0.05$ and $^{\Delta\Delta}p < 0.01$ compared to ox-LDL + EPL + Oe-NC; EPL – eplerenone; ox-LDL – oxidized low-density lipoprotein; Oe-NC – empty vector; VSMCs – vascular smooth muscle cells; GPER – G protein-coupled estrogen receptor; CCK-8 – cell counting kit-8; MCM-2 – minichromosome maintenance-2; PCNA – proliferating cell nuclear antigen.

As shown in Fig. 4B, GPER overexpression significantly elevated cell viability relative to the Oe-NC group. Meanwhile, as compared to VSMCs transfected with Oe-NC, the decrease of Ki67, MCM-2 and PCNA was notably reversed after GPER overexpression (Fig. 4C,D). Results presented in Fig. 5A–D revealed that the ability of cell migration was remarkably enhanced in the GPER overexpression group compared with the empty vector group. Moreover, GPER-upregulation conspicuously increased the levels of MMP2 and MMP9. Through the above findings, we prove that GPER overexpression abolished the suppressive effects of EPL exposure on proliferation and migration of VSMCs treated by ox-LDL.

Discussion

It is well known that AS is a chronic degenerative disease and has become a major cause of cardiovascular morbidity and mortality.[15] Aging, obesity, diabetes mellitus, chronic inflammation, and elevated plasma ox-LDL are risk factors for the disease process.[16,17] Moreover, postoperative care, rehabilitation training and health education after AS bypass grafting is important in improving the quality of life of patients and preventing the occurrence of poor prognostic event. Existing studies have demonstrated that EPL possesses protective functions against cardiovascular disease.[18] The present study was the first to explore the roles of EPL in the functions of VSMCs as applied to AS.

The VSMCs are the major cell type observed in blood vessel walls that play considerable roles in the regulation of multiple physiological and pathological situations.[19] Aberrant proliferation and migration of VSMCs are the key events in the progression of AS and restenosis after percutaneous coronary intervention.[20] An increasing number of studies have reported that ox-LDL exerts a promotion effect in the development of AS by stimulating the proliferation of VSMCs within the vessel wall.[21,22] Therefore, agents blocking or inhibiting proliferation and migration of VSMCs induced by ox-LDL may contribute to the identification of therapeutic strategies. Eplerenone is a newly found novel selective aldosterone receptor antagonist.[8,9] Additionally, it has been reported to alleviate hepatocellular carcinoma growth and angiogenesis in mice.[23] Adriamycin nephropathy rats treated with EPL exhibit obvious

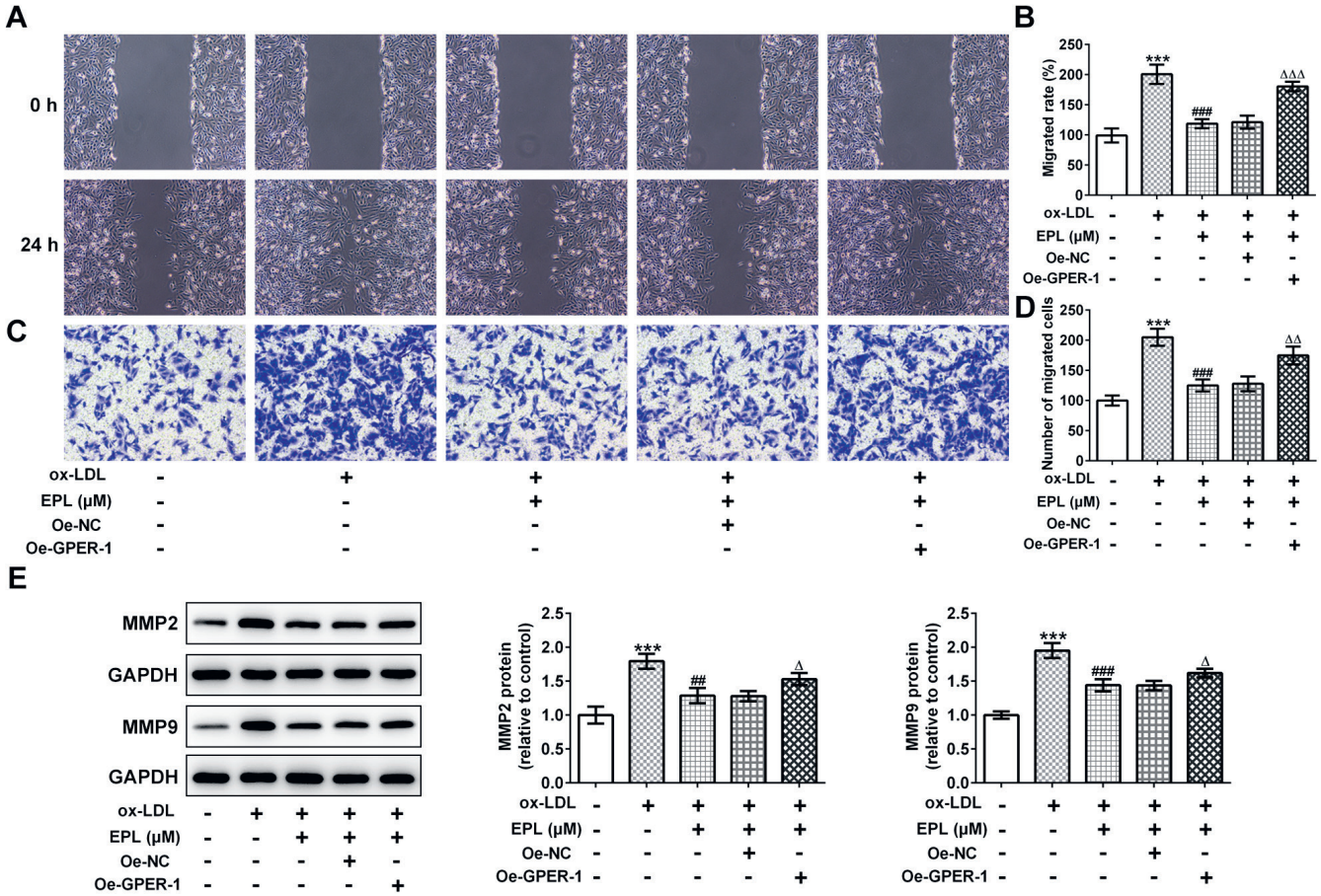

Fig. 5. GPER overexpression attenuated the inhibitory effect of EPL treatment on migration of VSMCs induced with ox-LDL

A and B. Cell migration was determined using scratch wound healing assay (magnification ×200); C and D. Cell migration was assessed using transwell migration assay (magnification ×200); E. The expression of MMP2 and MMP9 was examined using western blot analysis. The experiments were generated from 3 independent repeats (n = 3). ***p < 0.001 compared to control; $^{\#}$p < 0.05 and $^{\#\#\#}$p < 0.001 compared to ox-LDL; Oe-NC – empty vector; EPL – eplerenone; ox-LDL – oxidized low-density lipoprotein; VSMCs – vascular smooth muscle cells; GPER – G protein-coupled estrogen receptor; MMP – matrix metalloproteinase.

attenuation of mesangial cell proliferation and matrix expansion.[24] Moreover, EPL can inhibit neointimal formation after coronary stent implantation in swine by decreasing collagen accumulation.[25] The present study suggested that EPL treatment significantly hampered proliferation and migration of VSMCs treated with ox-LDL, suggesting a promising therapeutic agent in the treatment of AS.

We further explored the molecular mechanisms underlying the inhibitory roles of EPL on ox-LDL-stimulated VSMCs. The STITCH website (http://stitch.embl.de) was used to detect the potential proteins that could partake in the regulation of EPL. Thereafter, GPER, a G protein-coupled receptor coupled with Gs proteins, was discovered as one binding point of EPL. According to published studies, GPER promotes cell proliferation and migration of triple-negative breast cancer, renal cell carcinoma and ovarian cancer.[26–28] Furthermore, activation of the GPER can increase neurogenesis and alleviate neuroinflammation in the hippocampus of male spontaneously hypertensive rats.[29] Also, blocking of GPER function mitigates the bisphenol A-stimulated proliferation of VSMCs.[14] Results of the current work indicated that GPER expression was markedly upregulated in ox-LDL-induced VSMCs and the elevation was abolished under treatment with EPL. Importantly, GPER overexpression dramatically reversed the inhibitory effects of EPL intervention on proliferation and migration of VSMCs stimulated by ox-LDL, which was accompanied by the expression changes of proliferation- and migration-associated proteins.

Conclusions

To the best of our knowledge, the present study was the first to investigate the pivotal roles of EPL on VSMCs function. These findings demonstrate that EPL restricts proliferation and migration of VSMCs stimulated by ox-LDL partly by downregulating GPER expression, providing experimental and mechanistic support for EPL use in the clinical treatment of AS. However, a lack of the study in vivo is a limitation of the present research, and therefore, a comprehensive analysis is required in the future.

ORCID iDs

Dandan Wang https://orcid.org/0000-0003-0808-5419
Minglei Wang https://orcid.org/0000-0002-6819-0571
Pingping Sun https://orcid.org/0000-0001-9954-0303
Qiaoyan Gao https://orcid.org/0000-0002-7941-3099

References

1. Zhang B, Dong Y, Zhao Z. LncRNA MEG8 regulates vascular smooth muscle cell proliferation, migration and apoptosis by targeting PPA-Ralpha. *Biochem Biophys Res Commun*. 2019;510(1):171–176. doi:10.1016/j.bbrc.2019.01.074
2. Luscher TF. Atherosclerosis and CAD. *Eur Heart J*. 2015;36(8):457–459. doi:10.1093/eurheartj/ehv002
3. Torres N, Guevara-Cruz M, Velazquez-Villegas LA, Tovar AR. Nutrition and atherosclerosis. *Arch Med Res*. 2015;46(5):408–426. doi:10.1016/j.arcmed.2015.05.010
4. Chistiakov DA, Orekhov AN, Bobryshev YV. Vascular smooth muscle cell in atherosclerosis. *Acta Physiol (Oxf)*. 2015;214(1):33–50. doi:10.1111/apha.12466
5. Chen Z, Pan X, Sheng Z, Yan G, Chen L, Ma G. Baicalin suppresses the proliferation and migration of Ox-LDL-VSMCs in atherosclerosis through upregulating miR-126-5p. *Biol Pharm Bull*. 2019;42(9):1517–1523. doi:10.1248/bpb.b19-00196
6. Zheng J, Chen K, Wang H, et al. SIRT7 regulates the vascular smooth muscle cells proliferation and migration via Wnt/beta-catenin signaling pathway [erratum published in: *Biomed Res Int*. 2019;2019:8014381. doi:10.1155/2019/8014381]. *Biomed Res Int*. 2018;2018:4769596. doi:10.1155/2018/4769596
7. Wang B, Ge Z, Cheng Z, Zhao Z. Tanshinone IIA suppresses the progression of atherosclerosis by inhibiting the apoptosis of vascular smooth muscle cells and the proliferation and migration of macrophages induced by ox-LDL. *Biol Open*. 2017;6(4):489–495. doi:10.1242/bio.024133
8. Craft J. Eplerenone (Inspra), a new aldosterone antagonist for the treatment of systemic hypertension and heart failure. *Proc (Bayl Univ Med Cent)*. 2004;17(2):217–220. doi:10.1080/08998280.2004.11927973
9. Dizaye K, Mustafa ZA. The effect of eplerenone on the renin-angiotensin-aldosterone system of rats with thyroid dysfunction. *J Pharm Pharmacol*. 2019;71(12):1800–1808. doi:10.1111/jphp.13168
10. Shao PP, Liu CJ, Xu Q, et al. Eplerenone reverses cardiac fibrosis via the suppression of Tregs by inhibition of Kv1.3 channel. *Front Physiol*. 2018;9:899. doi:10.3389/fphys.2018.00899
11. Wang CH, Wang Z, Liang LJ, et al. The inhibitory effect of eplerenone on cell proliferation in the contralateral kidneys of rats with unilateral ureteral obstruction. *Nephron*. 2017;136(4):328–338. doi:10.1159/000473702
12. Chen H, Sun F, Zhong X, Shao Y, Yoshimura A, Liu Y. Eplerenone-mediated aldosterone blockade prevents renal fibrosis by reducing renal inflammation, interstitial cell proliferation and oxidative stress. *Kidney Blood Press Res*. 2013;37(6):557–566. doi:10.1159/000355736
13. Yang K, Yao Y. Mechanism of GPER promoting proliferation, migration and invasion of triple-negative breast cancer cells through CAF. *Am J Transl Res*. 2019;11(9):5858–5868. PMID:31632554
14. Gao F, Huang Y, Zhang L, Liu W. Involvement of estrogen receptor and GPER in bisphenol A induced proliferation of vascular smooth muscle cells. *Toxicol In Vitro*. 2019;56:156–162. doi:10.1016/j.tiv.2019.01.012
15. Yu MH, Lin MC, Huang CN, Chan KC, Wang CJ. Acarbose inhibits the proliferation and migration of vascular smooth muscle cells via targeting Ras signaling. *Vascul Pharmacol*. 2018;103–105:8–15. doi:10.1016/j.vph.2018.02.001
16. Anogeianaki A, Angelucci D, Cianchetti E, et al. Atherosclerosis: A classic inflammatory disease. *Int J Immunopathol Pharmacol*. 2011;24(4):817–825. https://doi.org/10.1177/039463201102400401
17. Huang YL, Hu YZ, Mai WY, et al. Plasma oxidized low-density lipoprotein is an independent risk factor in young patients with coronary artery disease. *Dis Markers*. 2011;31(5):295–301. doi:10.3233/DMA-2011-0832
18. Stewart Coats AJ, Shewan L. Eplerenone's role in the management of complex cardiovascular disorders. *Int J Cardiol*. 2015;200:1–2. https://doi.org/10.1016/j.ijcard.2015.05.128
19. Eun SY, Ko YS, Park SW, Chang KC, Kim HJ. IL-1beta enhances vascular smooth muscle cell proliferation and migration via P2Y2 receptor-mediated RAGE expression and HMGB1 release. *Vascul Pharmacol*. 2015;72:108–117. doi:10.1016/j.vph.2015.04.013
20. Fan TF, He JH, Yin YQ, et al. Dioscin inhibits intimal hyperplasia in rat carotid artery balloon injury model through inhibition of the MAPK-FoxM1 pathway. *Eur J Pharmacol*. 2019;854:213–223. doi:10.1016/j.ejphar.2019.03.050
21. Pirillo A, Norata GD, Catapano AL. LOX-1, OxLDL, and atherosclerosis. *Mediators Inflamm*. 2013;2013:152786. doi:10.1155/2013/152786
22. Yang N, Dong B, Song YQ, et al. Downregulation of miR-637 promotes vascular smooth muscle cell proliferation and migration via regulation of insulin-like growth factor-2. *Cell Mol Biol Lett*. 2020;25(1):12. doi:10.1186/s11658-020-00222-z
23. Kaji K, Yoshiji H, Kitade M, et al. Selective aldosterone blocker, eplerenone, attenuates hepatocellular carcinoma growth and angiogenesis in mice. *Hepatol Res*. 2010;40(5):540–549. doi:10.1111/j.1872-034X.2010.00636.x
24. Fang Z, Zhang C, He FF, et al. Protective effects of eplerenone on podocyte injury in adriamycin nephropathy rats. *J Huazhong Univ Sci Technolog Med Sci*. 2011;31(3):329–334. doi:10.1007/s11596-011-0376-5
25. Wakabayashi K, Suzuki H, Sato T, Iso Y, Katagiri T, Takeyama Y. Eplerenone suppresses neointimal formation after coronary stent implantation in swine. *Int J Cardiol*. 2006;107(2):260–266. doi:10.1016/j.ijcard.2005.03.078
26. Guan BZ, Yan RL, Huang JW, et al. Activation of G protein coupled estrogen receptor (GPER) promotes the migration of renal cell carcinoma via the PI3K/AKT/MMP-9 signals. *Cell Adhes Migr*. 2018;12(2):109–117. doi:10.4161/19336918.2014.990781
27. Wang Y, Peng ZQ, Meng R, et al. NHERF1 inhibits proliferation of triple-negative breast cancer cells by suppressing GPER signaling. *Oncol Rep*. 2017;38(1):221–228. doi:10.3892/or.2017.5649
28. Yan Y, Jiang XL, Zhao Y, Wen HX, Liu GY. Role of GPER on proliferation, migration and invasion in ligand-independent manner in human ovarian cancer cell line SKOV3. *Cell Biochem Funct*. 2015;33(8):552–559. doi:10.1002/cbf.3154
29. Correa J, Ronchetti S, Labombarda F, De Nicola AF, Pietranera L. Activation of the G protein-coupled estrogen receptor (GPER) increases neurogenesis and ameliorates neuroinflammation in the hippocampus of male spontaneously hypertensive rats. *Cell Mol Neurobiol*. 2020;40(5):711–723. doi:10.1007/s10571-019-00766-5

P2Y12 inhibition in macrophages reduces ventricular arrhythmias in rats after myocardial ischemia-reperfusion

Lu Wang[1,2,A–F], Na Li[3,B,C,E,F], Fei Wang[2,B,C,E,F], Lianqun Cui[1,A,F]

[1] Department of Cardiology, Shandong Provincial Hospital, Cheeloo College of Medicine, Shandong University, Jinan, China
[2] Department of Internal Medicine, Shandong Corps Hospital of Chinese People's Armed Police Forces, Jinan, China
[3] Outpatient Department, Shandong Corps Hospital of Chinese People's Armed Police Forces, Jinan, China

A – research concept and design; B – collection and/or assembly of data; C – data analysis and interpretation;
D – writing the article; E – critical revision of the article; F – final approval of the article

Advances in Clinical and Experimental Medicine, ISSN 1899–5276 (print), ISSN 2451–2680 (online) *Adv Clin Exp Med*. 2021;30(4):413–420

Address for correspondence
Lianqun Cui
E-mail: cuilianqunsdslyy@163.com

Funding sources
None declared

Conflict of interest
None declared

Received on October 20, 2020
Reviewed on December 28, 2020
Accepted on February 7, 2021

Published online on April 28, 2021

Abstract

Background. Myocardial ischemia-reperfusion (I/R) injury is still thought to be an unsolved puzzle that may lead to reperfusion arrhythmias and sudden cardiac death. Inflammation plays a key role in myocardial I/R. Studies have indicated that purinoceptor 2Y12 (P2Y12) antagonists have anti-inflammatory properties that are cardioprotective.

Objectives. In this study, we explored whether inhibition of P2Y12 in macrophages could reduce cardiac inflammation and attenuate reperfusion arrhythmias after myocardial I/R.

Materials and methods. Rats were randomly divided into 4 groups: group A (control + vehicle); group B (control + P2Y12 shRNA lentiviral vector); group C (myocardial I/R + vehicle); and group D (myocardial I/R + P2Y12 shRNA lentiviral vector). Infarct size, reperfusion arrhythmias, and P2Y12 and platelet endothelial cell adhesion molecule-1 (CD31) protein expression were measured.

Results. The incidence of reperfusion ventricular tachycardia and fibrillation (VT/VF) was 90% in the I/R group, while it was reduced to 50% by P2Y12 shRNA treatment. Ionized calcium binding adapter molecule 1 and P2Y12 immunoreactivity in the myocardial I/R + P2Y12 shRNA group was lower compared to the myocardial I/R group. P2Y12 shRNA treatment increased α-smooth muscle actin (α-SMA) and CD31 protein expression, as evidence by western blot and immunohistochemistry analyses (0.31 ±0.01 compared to 0.26 ±0.008, group D compared to group C, $p < 0.05$).

Conclusions. Inhibition of P2Y12 in macrophages improved reperfusion arrhythmias in our rat I/R model, suggesting that blocking P2Y12 could decrease the inflammatory response after cardiac perfusion.

Key words: macrophages, inflammation, P2Y12, myocardial ischemia-reperfusion, reperfusion arrhythmia

Cite as
Wang L, Li N, Wang F, Cui L. P2Y12 inhibition in macrophages reduces ventricular arrhythmias in rats after myocardial ischemia-reperfusion. *Adv Clin Exp Med*. 2021;30(4):413–420. doi:10.17219/acem/133139

DOI
10.17219/acem/133139

Copyright
© 2021 by Wroclaw Medical University
This is an article distributed under the terms of the Creative Commons Attribution 3.0 Unported (CC BY 3.0) (https://creativecommons.org/licenses/by/3.0/)

Background

Acute myocardial infarction (AMI) is one of the most common causes of cardiovascular death worldwide. Reperfusion is the primary mechanism to restore blood flow to the heart in the treatment of AMI. However, myocardial ischemia-reperfusion (I/R) can cause a variety of injuries through a number of processes, such as cell and organelle membrane injury, oxidative stress, endothelial injury, vasoconstriction, and pro-inflammatory immune responses.[1] Accordingly, reperfusion can cause heart tissue damage, electrophysiological dysfunction and heart failure.[2,3] One example are reperfusion arrhythmias, particularly ventricular tachycardia and fibrillation (VT/VF), which are serious events that complicate reperfusion therapies, like coronary interventions and thrombolytic therapy, in patients with AMI.[4] Sympathetic over-stimulation and inflammation are 2 major mediators of reperfusion arrhythmias.[5] Therefore, reducing cardiac inflammation could be an effective means to prevent myocardial I/R injury and the occurrence of reperfusion arrhythmias. Inflammation is a part of the physiological wound-healing response after mechanical injuries. At the onset of an infarction, a strong inflammatory response is initiated,[6] which involves macrophage activation.[7] Macrophages play an important role in myocardial repair and remodeling after myocardial infarction. However, the role of macrophages in I/R injury remains unclear. Previous studies have shown that the platelet P2Y12 (P2Y12) receptor plays a central role in platelet function, hemostasis and thrombosis, but there have only been a few studies that have explored the non-platelet effects of P2Y12 in cardiovascular diseases.[8,9] One study demonstrated that inhibiting the P2Y12 receptor reduced the increase in pro-inflammatory mediators, pointing to the cardioprotective properties of P2Y12 antagonists.[9] In our study, we investigated the role and mechanism of P2Y12 inhibition in I/R injury.

Materials and methods

Animals

Sixty 8-week-old male Sprague Dawley rats weighing 200–270 g were purchased from the Vital River Laboratory (Beijing, China). The protocols was approved by the Ethics Committee of Shandong Corps Hospital of Chinese People's Armed Police Forces, Jinan, China, and rats received humane care conforming to the National Institutes of Health Guide for the Care and Use of Laboratory Animals. Rats had free access to normal rat chow and drinking water.

Experimental design

A total of 60 rats were randomly divided into 4 groups: group A (control + vehicle); group B (control + P2Y12 shRNA lentiviral vector (Santa Cruz Biotechnology, Santa Cruz, ISA); group C (myocardial I/R + vehicle); and group D (myocardial I/R + P2Y12 shRNA lentiviral vector). Rats received P2Y12 shRNA lentiviral vector via tail vein injection starting 5 days before myocardial I/R surgery. Rats in the sham control groups were administered vehicle. After the shRNA expression vector enters the cytoplasm, the vector needs to be transported to the cytoplasmic nucleus for transcription. ShRNAs are synthesized in the nucleus, processed and transported to the cytoplasm, and finally incorporated into the RNA-interfering silencing complex. Mature shRNA provides RNA interference through mRNA cleavage and degradation.[10] The incidence and duration of VT/VF in the reperfusion period were recorded to evaluate reperfusion arrhythmias. After sacrifice, heart tissues were collected for western blot and immunohistochemistry analyses.

Myocardial I/R surgery

Myocardial I/R surgery was performed 5 days after P2Y12 shRNA lentiviral vector injection. After anesthetizing with 3% pentobarbital sodium (30 mg/kg; intraperitoneal), intubating via tracheotomy and ventilating with a small animal ventilator, a 3-cm left thoracotomy was performed through the left 4th intercostal space. The left anterior descending (LAD) coronary branch was ligated with 6/0 silk sutures for 30 min to induce myocardial ischemia. During the procedure, we monitored cardiac function using electrocardiogram (ECG) recordings (BL-420S; TaiMeng, Dongguan, China). Myocardial ischemia was confirmed with ST-segment elevation and tall T-waves. Rats in the sham surgery groups underwent only thoracotomy and the LAD coronary was not ligated. After 30 min of ligation, the LAD coronary was reperfused for 2 h.

Evaluation of arrhythmias

Arrhythmias were assessed according to the diagnostic criteria of the Lambeth Conventions.[9,11] Ventricular arrhythmia parameters, including percent incidence of VT/VF and duration of VT/VF, were quantified during the whole reperfusion period. Ventricular tachycardia refers to the occurrence of 4 or more consecutive ventricular premature beats in a row. Ventricular fibrillation is defined as a signal whose individual QRS wave deflections are no longer distinguishable from each other (meaning morphological instability) and whose frequency can no longer be measured.

Determination of myocardial injury

Myocardial ischemic size was determined using Evans blue/triphenyltetrazolium chloride (TTC) staining. After reperfusion, 1% Evans blue staining solution (0.3 mL) was injected to determine the ischemic area. The tissues were then incubated in a 2% TTC solution (Sigma Aldrich, St.

Louis, USA) for 30 min at 37°C, and fixed in 4% paraformaldehyde solution overnight. After storing at –20°C for 20 min, the heart was cut into 1-mm thick slices. The myocardium in the ischemic area and infarction area was stained blue and light yellow, respectively.

Immunofluorescence

Hearts were sectioned into approx. 7-μm slices for immunofluorescence assays using a freezing microtome. The sections were incubated with anti-ionized calcium binding adapter molecule 1 (Iba1) (1 : 100; Abcam, Cambridge, UK) and anti-P2Y12 (1 : 50, Novus, Centennial, USA) as primary antibodies diluted in phosphate-buffered saline (PBS) overnight at 4°C. After washing 3 times with PBS, the sections were incubated with Alexa 546-conjugated donkey anti-rabbit (1 : 200; Thermo Fisher Scientific, Waltham, USA) and Alexa 488-conjugated donkey anti-goat (1 : 200, Thermo Fisher Scientific) antibodies for 2 h. The sections were counterstained with 4',6-diamidino-2-phenylindole (DAPI; Life Technologies, Grand Island, USA) to identify nuclei. Olympus LCX100 Imaging System (Olympus Corp., Tokyo, Japan) and ImageJ software (National Institutes of Health, Bethesda, USA) were used for image acquisition and analysis.

Western blot analysis

Heart tissue was homogenized in radioimmunoprecipitation assay (RIPA) lysis buffer containing 1% phenylmethanesulfonyl fluoride (PMSF), and the supernatants were collected after centrifugation at 4°C and processed for western blot analysis. A BCA assay kit (Pierce Protein Biology, St. Louis, USA) was used to determine protein concentration. Approximately 70 μg of total protein from each sample was resolved on 8–10% polyacrylamide gels and transferred to polyvinylidene fluoride (PVDF) membranes (BioRad, Richmond, USA). The membranes were incubated at 4°C overnight with anti-P2Y12 (1 : 2000; Abcam; ab184411), anti-platelet endothelial cell adhesion molecule-1 (CD31) (1 : 1000; Abcam; ab64543), anti-glyceraldehyde-3-phosphate dehydrogenase (anti-GAPDH) (1 : 5000; CoWin Bioscience, Beijing, China) antibodies diluted in general antibody dilution buffer. The blots were detected with an enhanced chemiluminescence (ECL) detection kit (Merck Millipore, Burlington, USA) and visualized using a FluorChem E Imager (Protein-Simple, Santa Clara, USA). The protein expression relative to GAPDH was analyzed using ImageJ software.

Statistical analysis

Data are presented as means ± standard deviations (SD). Unpaired t-tests were used to compare values between 2 groups. Analysis of variance (ANOVA) and Tukey's test were used to compare the differences among multiple groups. The SPSS v. 17.0 software (SPSS Inc., Chicago, USA) was used for the analysis. A p-value less than 0.05 was considered significant in all statistical tests.

Results

P2Y12 inhibition in macrophages attenuates infarct size following myocardial I/R injury in rats

As shown in Fig. 1A,B, P2Y12 shRNA treatment significantly reduced ischemia size, as evidenced by Evans blue staining ($p < 0.05$). The ECGs were examined to elucidate the physiological effect of I/R injury and the incidence rate of reperfusion arrhythmias. Successful ischemia injury was confirmed by ST-segment elevation, and reperfusion injury was confirmed by reduced ST-segment elevation and tall T-waves after ischemia. P2Y12 knockdown (I/R + P) significantly reduced the incidence rates of reperfusion arrhythmias are shown in Fig. 1C, and the duration of VT when compared with I/R + V as shown in Fig. 1D (23.07 ±4.32 compared to 55.83 ±11.3, $p < 0.05$). The incidence of reperfusion VT/VF was 90% in the I/R group; it was reduced to 50% following P2Y12 shRNA treatment.

P2Y12 inhibition in macrophages attenuates inflammation induced by myocardial I/R injury in rats

We used P2Y12 shRNA to determine the role of P2Y12R in macrophages following myocardial I/R injury in rats. As shown in Fig. 2, immunohistochemical analysis of heart sections demonstrated a strong immunoreactive signal for Iba1 in the I/R areas in the control groups, which was significantly attenuated by P2Y12 shRNA treatment ($p < 0.05$).

P2Y12 inhibition in macrophages attenuates cardiac remodeling in rats

To assess the role of P2Y12 in myocardial I/R injury, we employed the following strategies. To evaluate the efficacy of cardiac remodeling, we measured protein expression of α-smooth muscle actin (α-SMA) and CD31 using immunohistochemistry and western blot analyses, respectively. We found that α-SMA staining was significantly higher in the I/R + P2Y12 shRNA group compared to the I/R group (Fig. 3A). CD31 protein expression in the I/R areas was significantly upregulated in the I/R + P2Y12 shRNA group compared to the other groups (Fig. 3B, 3C 0.31 ±0.01 compared to 0.26 ±0.008 (I/R + P compared to I/R + V); $p < 0.05$). The α-SMA and CD31 staining also revealed increased vessel formation in the I/R areas.

As shown in Fig. 3D, we observed that P2Y12 protein expression in the I/R areas was significantly increased compared to the control groups (0.23 ±0.01, 0.17 ±0.007

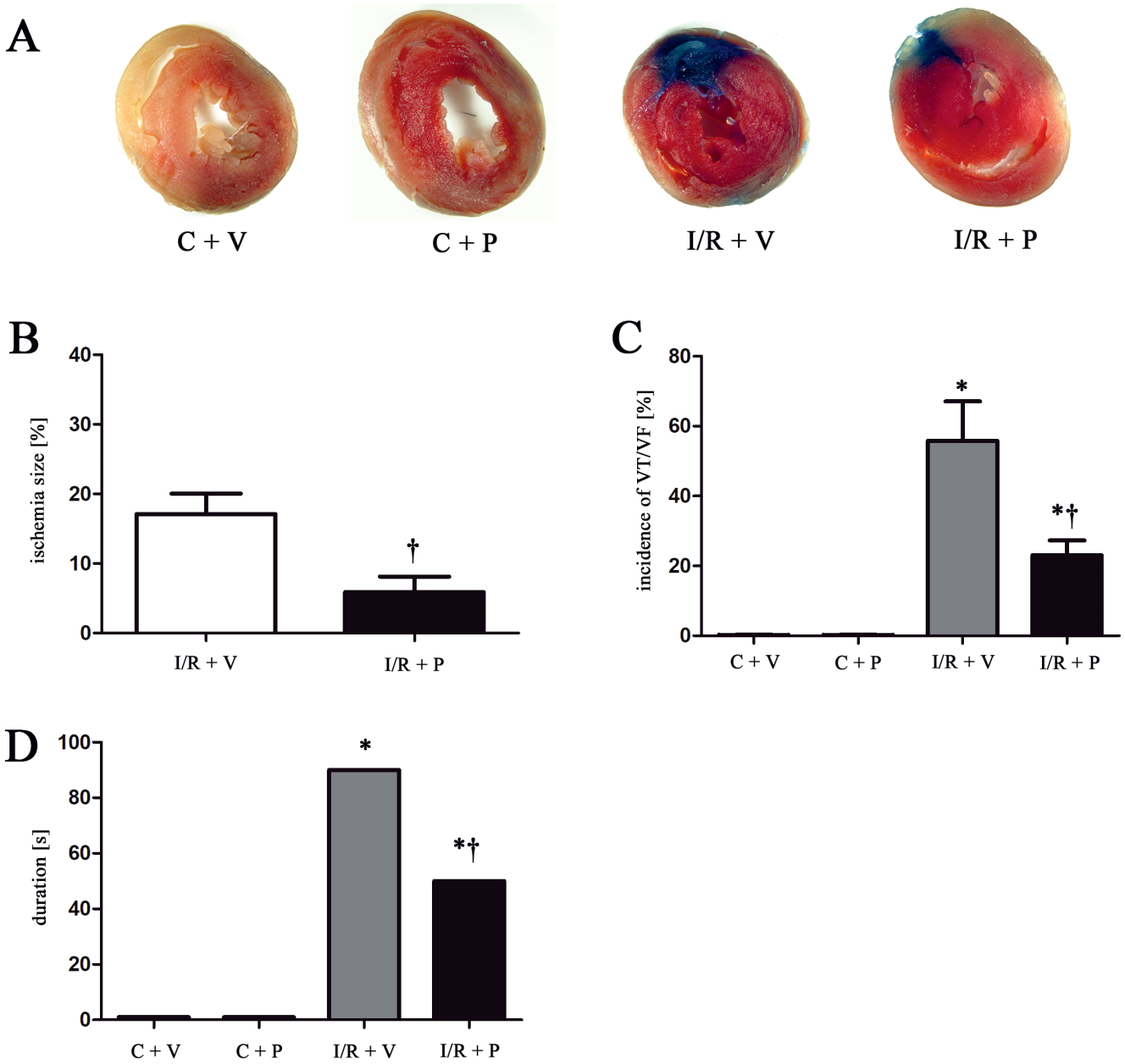

Fig. 1. A. Infarct and ischemic area as determined using Evans blue dye and TTC staining; B. Percent ischemic area after reperfusion; C. Comparisons of VT duration between the 4 groups after reperfusion; D. Comparisons of the incidence rates of reperfusion arrhythmias between the 4 groups after reperfusion; *p < 0.01 compared with C + V; †p < 0.05 compared with I/R + V. C + V; control + vehicle; C + P, control + P2Y12 shRNA lentiviral vector; I/R + V, myocardial I/R + vehicle; and I/R + P, myocardial I/R + P2Y12 shRNA lentiviral vector

compared to 0.150 ±0.007, 0.16 ±0.009 (I/R + V and I/R + P compared to C + V and C + P); $p < 0.05$). The I/R + P2Y12 shRNA group had significantly lower P2Y12 protein expression compared to the I/R group (0.17 ±0.007 compared to 0.23 ±0.01 (I/R + P compared to I/R + V); $p < 0.05$).

Discussion

The present study was designed to investigate the role of P2Y12 in macrophages following myocardial I/R injury in rats. The primary findings of our study are as follows: 1) P2Y12 shRNA lentiviral vector reduced P2Y12 protein expression in macrophages; 2) reperfusion treatment significantly increased the incidence of arrhythmias, and inhibiting P2Y12 in macrophages improved the duration and incidence of arrhythmias; and 3) inhibiting P2Y12 reduced inflammation associated with reperfusion.

Myocardial ischemia can lead to cardiovascular disease and AMI, which is the major cause of death worldwide. Reperfusion is the primary treatment for AMI, and timely and successful reperfusion can reduce myocardial ischemia injury, limit infarct areas and improve ventricular function. However, tissue ischemia often occurs despite the fact that the flow of blood is restored, resulting in myocardial I/R injury, which is characterized by endothelial cell

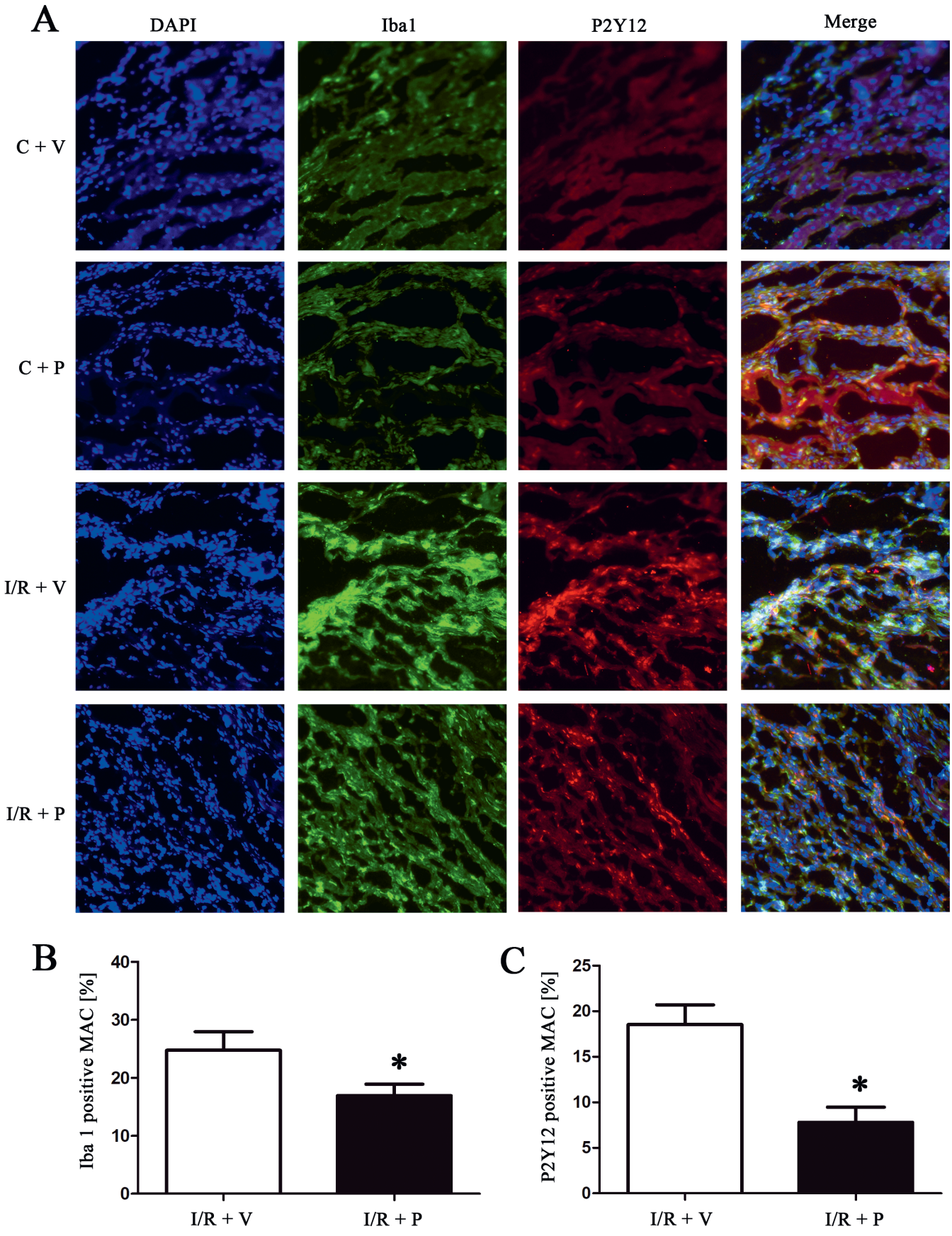

Fig. 2. A. Representative double-immunostained images of the macrophage marker Iba1 (green) and P2Y12 (red); last column shows merged images of all staining in the 4 groups after reperfusion; B. Percent of Iba1 expressed in the ischemic areas; C. Percent of P2Y12 expressed in the ischemic area. Values shown are the mean ±SD; *p < 0.01 compared with I/R + V; C + V, control + vehicle; C + P, control + P2Y12 shRNA lentiviral vector; I/R + V, myocardial I/R + vehicle; and I/R + P, myocardial I/R + P2Y12 shRNA lentiviral vector

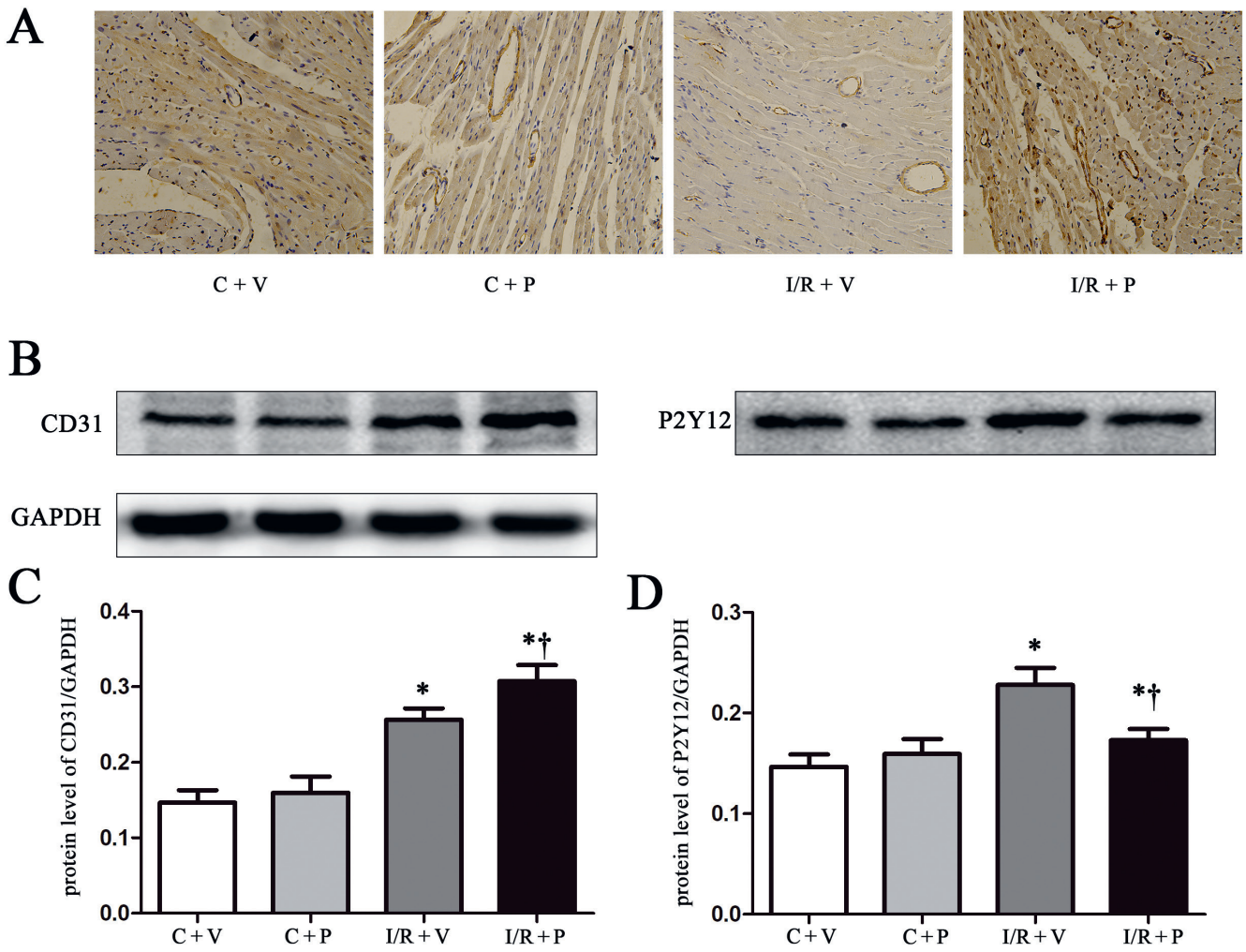

Fig. 3. A. Immunohistochemical staining of α-SMA in the 4 groups after reperfusion; B. Representative western blot images of CD31, P2Y12 and GAPDH expression in the 4 groups after reperfusion; C. Quantified CD31 expression relative to GAPDH expression in the 4 groups; D. Quantified P2Y12 expression relative to GAPDH expression in the 4 groups; *$p < 0.01$ compared with C + V; †$p < 0.05$ compared with I/R + V

dysfunction, DNA damage and inflammation.[9] A variety of clinical conditions can cause I/R injury, such as myocardial injury, stroke, organ transplantation, limb ischemia, and multiple organ system dysfunction. In the last 20 years, it has been confirmed that inflammation plays a vital role in the pathophysiological process of I/R injury. Inflammation may induce ectopic triggers, leading to the occurrence of arrhythmias.[9,12] Recent studies provide evidence that immune cells are involved in I/R-induced wound healing.[13–18] Macrophages are the primary inflammatory cell responders, and they play an important role in myocardial healing following infarction,[19] as well as the inflammatory response after I/R injury.[20]

The P2Y12 receptor is composed of 2 parts: seven-transmembrane (7-TM) α-helix bundle and a carboxyl terminal helix.[20] P2Y12 is expressed in platelets, where it stabilizes platelet aggregation induced by thrombin and thromboxane A2 (TXA2) and other agonists, and also plays an important role in thrombosis in vivo.[21–24] Activation of the ADP-P2Y12 pathway can induce an inflammatory state in vascular smooth muscle and lead to atherosclerosis.[25] A series of studies have shown that P2Y12 antagonists have cardioprotective properties that are independent of their anti-thrombotic actions.[26] This protective effect is mainly due to adenosine receptor activation and downstream phosphorylation of protein kinase B and endothelial nitric oxide synthase, and activation of cyclooxygenase-2.[27] Adenosine plays a key protective role during myocardial I/R injury.[28–31] Blocking the P2Y12 receptor can increase extracellular adenosine levels by inhibiting the reuptake of interstitial adenosine in cells.[32,33] The present study intended to investigate the cardioprotective effects of P2Y12 in the context of inflammation.

P2Y12 is also expressed on macrophages. A P2Y12 antagonist has been shown to attenuate atherogenesis and reduce accumulation of macrophages in ApoE-deficient mice.[34] A recent study demonstrated that P2Y12 expression in macrophages was involved in the modulation of the immune microenvironment in various pathological inflammatory conditions, a fact that indicates that P2Y12 is an important immunomodulatory receptor on macrophages.[35] In the present study, shRNA was used to knock down

P2Y12 expression in macrophages. Systemic administration of P2Y12 shRNA had no effect on platelet expression, given that platelets lack nuclei. Thus, we were able to rule out the effect of blocking P2Y12 in platelets in our I/R model. Our immunofluorescence staining of P2Y12 in macrophages demonstrated that P2Y12 plays an anti-inflammatory role in I/R injury. Activation of P2Y12 in macrophages could induce cell proliferation and lamellar foot formation, and inhibiting P2Y12 could reduce chemotaxis.[36] Our results suggest that regulating P2Y12 in macrophages could improve the duration and incidence rates of reperfusion arrhythmias through 2 possible mechanisms.

Downregulating P2Y12 in macrophages could ameliorate the immune microenvironment and exert anti-inflammatory effects in the I/R injury area. Furthermore, since cardiac tissue inflammation is related to cardiovascular sympathetic tone, sympathetic overstimulation and inflammation could be 2 major mediators of reperfusion arrhythmias.[5]

Another possibility is that reperfusion arrhythmias were obviously correlated with myocardial I/R injury. Our results showed that systemic administration of P2Y12 shRNA could significantly reduce the ischemia area, altering the release of oxygen free radicals and inflammatory factors.

In our study, we only carried out animal experiments to investigate the cardioprotective effect of P2Y12 on macrophages. However, determination of the effect of P2Y12 inhibition on macrophages in clinical scenarios and the exact mechanism underlying the effect requires further research. Ticagrelor is a P2Y12 receptor antagonist with proven clinical benefits in patients with myocardial infarction and acute coronary syndrome.[37] This experiment elaborated upon the mechanism of potential cardioprotective effects outside of the antiplatelet actions of ticagrelor, particularly from the perspective of inflammation regulation.

Limitations

In our study, we only carried out animal experiments to investigate the cardioprotective effect of P2Y12 on macrophages. However, determination of the effect of P2Y12 inhibition on macrophages in clinical scenarios and the exact mechanism underlying the effect requires further research. Ticagrelor is a P2Y12 receptor antagonist with proven clinical benefits in patients with myocardial infarction and acute coronary syndrome.[37] This experiment elaborated upon the mechanism of potential cardioprotective effects outside of the antiplatelet actions of ticagrelor, particularly from the perspective of inflammation regulation.

Conclusions

Knockdown of P2Y12 in macrophages was a main mechanism in improving the duration and incidence of arrhythmias after reperfusion in a I/R rat model. In addition, blocking P2Y12 could decrease the inflammatory response after cardiac reperfusion, which may be a new mechanism to target in the development of new cardioprotective therapeutics.

ORCID iDs

Lu Wang https://orcid.org/0000-0003-2076-0624
Na Li https://orcid.org/0000-0001-7087-6495
Fei Wang https://orcid.org/0000-0001-5817-2161
Lianqun Cui https://orcid.org/0000-0003-2888-0639

References

1. Park ES, Kang DH, Kang JC, et al. Cardioprotective effect of KR-33889, a novel PARP inhibitor, against oxidative stress-induced apoptosis in H9c2 cells and isolated rat hearts. *Arch Pharm Res*. 2017;40(5):640–654. doi:10.1007/s12272-017-0912-3
2. Di Lisa F, Bernardi P. Mitochondria and ischemia-reperfusion injury of the heart: Fixing a hole. *Cardiovasc Res*. 2006;70(2):191–199. doi:10.1016/j.cardiores.2006.01.016
3. Chen YF, Chen WY, Chung CH, Kuo CL, Lee AS. Cardiac protection of *Bauhinia championii* against reperfusion injury. *Environ Toxicol*. 2020;35(7):774–782. doi:10.1002/tox.22912
4. Mehta RH, Starr AZ, Lopes RD, et al. Relationship of sustained ventricular tachyarrhythmias to outcomes in patients undergoing primary percutaneous coronary intervention with varying underlying baseline risk. *Am Heart J*. 2011;161(4):782–789. doi:10.1016/j.ahj.2011.01.005
5. Wang S, Wu L, Li X, et al. Light-emitting diode therapy protects against ventricular arrhythmias by neuro-immune modulation in myocardial ischemia and reperfusion rat model. *J Neuroinflammation*. 2019;16(1):139. doi:10.1186/s12974-019-1513-5
6. Troidl C, Mollmann H, Nef H, et al. Classically and alternatively activated macrophages contribute to tissue remodelling after myocardial infarction. *J Cell Mol Med*. 2009;13(9B):3485–3496. doi:10.1111/j.1582-4934.2009.00707.x
7. Outtz HH, Wu JK, Wang X, Kitajewski J. Notch1 deficiency results in decreased inflammation during wound healing and regulates vascular endothelial growth factor receptor-1 and inflammatory cytokine expression in macrophages. *J Immunol*. 2010;185(7):4363–4373. doi:10.4049/jimmunol.1000720
8. Zhang K, Zhang J, Gao ZG, et al. Structure of the human P2Y12 receptor in complex with an antithrombotic drug. *Nature*. 2014;509(7498):115–118. doi:10.1038/nature13083
9. Ye Y, Birnbaum GD, Perez-Polo JR, Nanhwan MK, Nylander S, Birnbaum Y. Ticagrelor protects the heart against reperfusion injury and improves remodeling after myocardial infarction. *Arterioscler Thromb Vasc Biol*. 2015;35(8):1805–1814. doi:10.1161/ATVBAHA.115.305655
10. Rao DD, Vorhies JS, Senzer N, Nemunaitis J. siRNA vs. shRNA: Similarities and differences. *Adv Drug Deliv Rev*. 2009;61(9):746–759. doi:10.1016/j.addr.2009.04.004
11. Liverani E, Rico MC, Garcia AE, Kilpatrick LE, Kunapuli SP. Prasugrel metabolites inhibit neutrophil functions. *J Pharmacol Exp Ther*. 2013;344(1):231–243. doi:10.1124/jpet.112.195883
12. Nicoletti A, Michel JB. Cardiac fibrosis and inflammation: Interaction with hemodynamic and hormonal factors. *Cardiovasc Res*. 1999;41(3):532–543. doi:10.1016/s0008-6363(98)00305-8
13. Dong X, Swaminathan S, Bachman LA, Croatt AJ, Nath KA, Griffin MD. Resident dendritic cells are the predominant TNF-secreting cell in early renal ischemia-reperfusion injury. *Kidney Int*. 2007;71(7):619–628. doi:10.1038/sj.ki.5002132
14. Walsh SK, Kane KA, Wainwright CL. Mast cells, peptides and cardioprotection: An unlikely marriage? *Auton Autacoid Pharmacol*. 2009;29(3):73–84. doi:10.1111/j.1474-8673.2009.00436.x
15. Meldrum DR. Tumor necrosis factor in the heart. *Am J Physiol*. 1998;274(3):R577–R595. doi:10.1152/ajpregu.1998.274.3.R577
16. Levick SP, Gardner JD, Holland M, Hauer-Jensen M, Janicki JS, Brower GL. Protection from adverse myocardial remodeling secondary to chronic volume overload in mast cell deficient rats. *J Mol Cell Cardiol*. 2008;45(1):56–61. doi:10.1016/j.yjmcc.2008.04.010
17. Linfert D, Chowdhry T, Rabb H. Lymphocytes and ischemia-reperfusion injury. *Transplant Rev (Orlando)*. 2009;23(1):1–10. doi:10.1016/j.trre.2008.08.003

18. Lahat N, Rahat MA, Ballan M, Weiss-Cerem L, Engelmayer M, Bitterman H. Hypoxia reduces CD80 expression on monocytes but enhances their LPS-stimulated TNF-alpha secretion. *J Leukoc Biol*. 2003;74(2):197–205. doi:10.1189/jlb.0303105
19. Frantz S, Hofmann U, Fraccarollo D, et al. Monocytes/macrophages prevent healing defects and left ventricular thrombus formation after myocardial infarction. *FASEB J*. 2013;27(3):871–881. doi:10.1096/fj.12-214049
20. Pruenster M, Vogl T, Roth J, Sperandio M. S100A8/A9: From basic science to clinical application. *Pharmacol Ther*. 2016;167:120–131. doi:10.1016/j.pharmthera.2016.07.015
21. Cattaneo M. P2Y12 receptors: Structure and function. *J Thromb Haemost*. 2015;13(Suppl 1):S10–S16. doi:10.1111/jth.12952
22. Crepaldi P, Cacciari B, Bonache MC, et al. 6-amino-2-mercapto-3H-pyrimidin-4-one derivatives as new candidates for the antagonism at the P2Y12 receptors. *Bioorg Med Chem*. 2009;17(13):4612–4621. doi:10.1016/j.bmc.2009.04.061
23. Cattaneo M, Canciani MT, Lecchi A, et al. Released adenosine diphosphate stabilizes thrombin-induced human platelet aggregates. *Blood*. 1990;75(5):1081–1086. PMID:2137716
24. Eckly A, Gendrault JL, Hechler B, Cazenave JP, Gachet C. Differential involvement of the P2Y1 and P2YT receptors in the morphological changes of platelet aggregation. *Thromb Haemost*. 2001;85(4):694–701. PMID:11341507
25. Rauch BH, Filep JG. Purinergic receptors and atherosclerosis: Emerging role for vessel wall P2Y12. *Cardiovasc Res*. 2014;102(3):339–341. doi:10.1093/cvr/cvu108
26. Yang XM, Liu Y, Cui L, et al. Platelet P2Y(1)(2) blockers confer direct postconditioning-like protection in reperfused rabbit hearts. *J Cardiovasc Pharmacol Ther*. 2013;18(3):251–262. doi:10.1177/1074248412467692
27. Nanhwan MK, Ling S, Kodakandla M, Nylander S, Ye Y, Birnbaum Y. Chronic treatment with ticagrelor limits myocardial infarct size: An adenosine and cyclooxygenase-2-dependent effect. *Arterioscler Thromb Vasc Biol*. 2014;34(9):2078–2085. doi:10.1161/ATVBAHA.114.304002
28. Armstrong D, Summers C, Ewart L, Nylander S, Sidaway JE, van Giezen JJ. Characterization of the adenosine pharmacology of ticagrelor reveals therapeutically relevant inhibition of equilibrative nucleoside transporter 1. *J Cardiovasc Pharmacol Ther*. 2014;19(2):209–219. doi:10.1177/1074248413511693
29. Bonello L, Laine M, Kipson N, et al. Ticagrelor increases adenosine plasma concentration in patients with an acute coronary syndrome. *J Am Coll Cardiol*. 2014;63(9):872–877. doi:10.1016/j.jacc.2013.09.067
30. van Giezen JJ, Sidaway J, Glaves P, Kirk I, Bjorkman JA. Ticagrelor inhibits adenosine uptake in vitro and enhances adenosine-mediated hyperemia responses in a canine model. *J Cardiovasc Pharmacol Ther*. 2012;17(2):164–172. doi:10.1177/1074248411410883
31. Cattaneo M, Schulz R, Nylander S. Adenosine-mediated effects of ticagrelor: Evidence and potential clinical relevance. *J Am Coll Cardiol*. 2014;63(23):2503–2509. doi:10.1016/j.jacc.2014.03.031
32. Kitakaze M, Minamino T, Node K, et al. Adenosine and cardioprotection in the diseased heart. *Jpn Circ J*. 1999;63(4):231–243. doi:10.1253/jcj.63.231
33. Kloner RA. Current state of clinical translation of cardioprotective agents for acute myocardial infarction. *Circ Res*. 2013;113(4):451–463. doi:10.1161/CIRCRESAHA.112.300627
34. Ganbaatar B, Fukuda D, Salim HM, et al. Ticagrelor, a P2Y12 antagonist, attenuates vascular dysfunction and inhibits atherogenesis in apolipoprotein-E-deficient mice. *Atherosclerosis*. 2018;275:124–132. doi:10.1016/j.atherosclerosis.2018.05.053
35. Kloss L, Dollt C, Schledzewski K, et al. ADP secreted by dying melanoma cells mediates chemotaxis and chemokine secretion of macrophages via the purinergic receptor P2Y12. *Cell Death Dis*. 2019;10(10):760. doi:10.1038/s41419-019-2010-6
36. Kronlage M, Song J, Sorokin L, et al. Autocrine purinergic receptor signaling is essential for macrophage chemotaxis. *Sci Signal*. 2010;3(132):ra55. doi:10.1126/scisignal.2000588
37. Moulias A, Xanthopoulou I, Alexopoulos D. Does ticagrelor improve endothelial function? *J Cardiovasc Pharmacol Ther*. 2019;24(1):11–17. doi:10.1177/1074248418786936

miR-874 ameliorates retinopathy in diabetic rats by NF-κB signaling pathway

Rui Li[1,A,D], Huimin Yuan[1,A,E], Tao Zhao[2,A,E], Yimin Yan[2,C,D], Zhaochen Liu[1,C,D], Jiayu Cai[1,B,D], Chunli Qiu[1,B,D], Chuanjing Li[2,A,E,F]

[1] Department of Ophthalmology, Xiaogan Hospital Affiliated to Wuhan University of Science and Technology, China
[2] Department of Endocrinology, Xiaogan Hospital Affiliated to Wuhan University of Science and Technology, China

A – research concept and design; B – collection and/or assembly of data; C – data analysis and interpretation; D – writing the article; E – critical revision of the article; F – final approval of the article

Advances in Clinical and Experimental Medicine, ISSN 1899–5276 (print), ISSN 2451–2680 (online) *Adv Clin Exp Med*. 2021;30(4):421–430

Address for correspondence
Chuanjing Li
E-mail: lichuanjing35gh@163.com

Funding sources
None declared

Conflict of interest
None declared

Received on June 10, 2020
Reviewed on June 18, 2020
Accepted on November 18, 2020

Published online on April 29, 2021

Abstract

Background. Increased activity of the NF-κB signaling pathway boosts the progression of retinopathy in diabetic rats.

Objectives. Using a bioinformatics website, we identified a site where *miR-874* binds to the NF-κB p65. Therefore, we speculated that *miR-874* might improve retinopathy in diabetic rats by inhibiting the NF-κB signaling pathway.

Materials and methods. Ten healthy rats were taken as the control group. Sixty streptozotocin (STZ; 60 mg/kg)-induced diabetes model rats were randomly divided into the model group (injection of normal saline), negative control (NC) agomir group (injection of NC mimic), *miR-874* agomir group (injection of *miR-874* mimic), *miR-874* anti-agomir group (injection of *miR-874* inhibitor), EVP4593 group (injection of NF-κB signaling pathway antagonist EVP4593), and *miR-874* anti-agomir+EVP4593 group (injection of *miR-874* inhibitor and EVP4593). All injections were administered into the caudal vein.

Results. *miR-874* could target the degradation of p65. Compared with the control group, model rats had reduced *miR-874* expression, increased vascular endothelial growth factor (VEGF) and Ang2 protein expression, lowered end-diastolic velocity (EDV) and peak systolic velocity (PSV) of the central retinal artery (CRA) and blood velocity of central retinal vein (CRV) and CRA, heightened plasma viscosity (PV), blood viscosity (BV) and erythrocyte sedimentation rate (ESR) at all shear rates, decreased capillary pericytes (IPCs), increased vascular endothelial cells (VECs), and ascended p65 expression in the retina (all $p < 0.05$). Thus, it was shown that pathological changes appeared in the retina of diabetic rats. These indices improved in diabetic rats injected with the *miR-874* mimic or EVP4593, but deteriorated in those injected with *miR-874* inhibitor (all $p < 0.05$). EVP4593 also could alleviate the aggravation of retinopathy that was caused by *miR-874* inhibition in diabetic rats.

Conclusions. *miR-874* modulates the NF-κB signaling pathway by targeting the degradation of p65 to further improve the retina of diabetic rats, thus demonstrating the beneficial effect of *miR-874* on diabetic retinopathy in rats.

Key words: diabetic retinopathy, NF-κB, Rela, *miR-874*

Cite as
Li R, Yuan H, Zhao T, et al. *miR-874* ameliorates retinopathy in diabetic rats by NF-κB signaling pathway. *Adv Clin Exp Med*. 2021;30(4):421–430. doi:10.17219/acem/130602

DOI
10.17219/acem/130602

Copyright
© 2021 by Wroclaw Medical University
This is an article distributed under the terms of the Creative Commons Attribution 3.0 Unported (CC BY 3.0) (https://creativecommons.org/licenses/by/3.0/)

Background

Diabetes is a prevalent disease that occurs worldwide. The incidence of diabetes is high in China and there are over 100 million patients diagnosed with this condition. Neuropathy, microangiopathy and macroangiopathy are some of the primary complications of diabetes. However, diabetic retinopathy (DR) is the most common complication and can cause visual disturbances and blindness.[1–3] Indeed, DR is the leading cause of blindness in the working-age population. It is primarily triggered by the leakage of retinal capillary walls induced by hyperglycemia. However, the pathogenesis of this condition is complicated and not fully understood. Previous studies have suggested that a series of pathophysiological changes in the retina that occur in the presence of persistent hyperglycemia contribute to the etiology of DR.[4–8]

NF-κB is a nuclear transcription factor that participates in the generation process of multiple cytokines.[9,10] This protein complex plays a leading role in various biological processes, including immune function and inflammation. The NF-κB protein complex comprises 5 members including RelB, RelA (also known as p65), c-Rel, p100/p52, and p105/p50. p65-50 is the most widespread and important NF-κB heterodimer.[11–13] The retina is affected by many metabolic disorders that can induce changes in local gene expression, and the progression of diabetes is associated with retinal capillary cell death and histopathological changes. Diabetic rats show abnormal activation of the NF-κB signaling pathway. This process can augment the generation of reactive oxygen species (ROS), leading to the occurrence of microaneurysms, retinal neovascularization and vitreous hemorrhage, consequently boosting the progression of retinopathy.[14–16]

Encoded by an endogenous gene, microRNA (miRNA) is a non-coding single-stranded RNA molecule that shows a high degree of conservation, time sequence and tissue specificity.[17,18] The miRNAs can regulate the protein expression of a specific target gene by interacting with the 3'UTR region of its mRNA through a sequence-specific interaction. Recent studies have revealed that miRNAs participate in the development and progression of DR, and are involved in the multiple pathogenic mechanisms of this disorder.[19–21] Using a bioinformatics website (www.targetscan.org), we identified a site where *miR-874* can bind to NF-κB p65. It has previously been reported that the downregulation of *miR-874* expression in rats with myocardial ischemia/reperfusion injury exerts an inhibitory effect on inflammation and injury.[22,23] However, no study has examined the relationship between *miR-874* and DR, and it is unknown whether this miRNA regulates DR, or if NF-κB p65 acts as a downstream regulatory element for *miR-874*.

Therefore, in the current study, DR rat models were treated with a genetic intervention to explore the effects of *miR-874* on this condition, and to examine the regulatory relationship between *miR-874* and the NF-κB signaling pathway. The results deepen our understanding of the pathogenesis of DR and provide a theoretical foundation for establishing *miR-874* as a potential drug target for the treatment of this disorder.

Materials and methods

Cell culture

HEK293T cells from the American Type Culture Collection (ATCC, Manassas, USA) were used in the dual-luciferase reporter assay (Promega, Madison, USA). Using routine methods, HEK293T cells were cultured in Dulbecco's modified Eagle's medium (DMEM) containing 10% fetal bovine serum (FBS). Cells were passaged and cultured in fresh complete medium every 3 days.

Dual-luciferase reporter system assay

A bioinformatics website (www.targetscan.org) was used to identify a potential binding site between *miR-874* and Rela (p65), which was then verified using a dual-luciferase reporter system assay. Reporter plasmids containing the target gene *Rela* (pmirGLO-Rela wild-type (wt)) or a mutated target gene (*pmirGLO-Rela mut*) were constructed. These 2 reporter plasmids were co-transfected with a negative control (NC) mimic or a *miR-874* mimic into HEK293T cells. Twenty-four hours after transfection, the dual-luciferase reporter assay was performed according to the manufacturer's instructions. Relative luciferase activity was calculated as firefly luciferase activity/renilla luciferase activity.

Establishment of the diabetic rat model

Streptozotocin (STZ) administration was used to induce diabetes in rats. Ninety male Sprague Dawley rats (200–250 g, 8 weeks old, from the Laboratory Animal Center of Chongqing Medical University, Chongqing, China) were fed with standard chew and water, and housed under specific pathogen-free conditions. Ten rats were randomly selected as the control group, and the rest were used to construct the diabetic models. Citrate buffer solutions (pH 4.5) were used to prepare fresh STZ solutions. A single intraperitoneal injection of 60 mg/kg of STZ was administered to induce diabetes. One week later, rats with a fasting blood glucose above 250 mg/dL were considered to be diabetic.[24] In total, 71 rats met this criteria. All procedures employed were approved by the Ethics Committee of Xiaogan Hospital Affiliated to Wuhan University of Science and Technology (China) and are in compliance with the Association for Research in Vision and Ophthalmology's statement for the care and use of laboratory animals in ophthalmology and vision studies.

Nine weeks after grouping, rats were anesthetized by intraperitoneal injection of 3% pentobarbital sodium (30 mg/kg). The retinal hemodynamic and central artery hemorheology indices of the left eyeball of all rats were detected using a color Doppler ultrasound. Following this, blood samples and retinal tissue or the whole eyeballs were collected for the subsequent experiments. All animals were then killed by cervical dislocation and death was confirmed by the absence of respiration.

Treatment

Sixty diabetic rats were randomly selected and divided into 6 groups of 10 rats each. The remaining animals were euthanatized as outlined above. In total, there were 7 groups in this study: control group (healthy rats), model group (diabetic rats injected with normal saline through the caudal vein), negative control (NC) agomir group (diabetic rats injected with the NC mimic through the caudal vein), *miR-874* agomir group (diabetic rats injected with the *miR-874* mimic through the caudal vein), *miR-874* anti-agomir group (diabetic rats injected with a *miR-874* inhibitor through the caudal vein), EVP4593 group (diabetic rats injected with EVP4593 through the caudal vein), and *miR-874* anti-agomir+EVP4593 group (diabetic rats injected with a *miR-874* inhibitor and EVP4593). The details of the groupings are shown in Table 1. EVP4593 is a NF-κB signaling pathway antagonist. The above agents, at a concentration of 4.5 nM, were injected into rats at a dose of 80 mg/kg through the caudal vein, once every 3 days for 4 weeks.[25] Eight weeks later, the rats were fasted for 8 h and blood was then drawn through caudal vein to measure blood glucose with the One Touch II glucometer (LifeScan, Malvern, USA). Rats were also weighed at this point. The experimental design is shown in Fig. 1.

Measurement of retinal hemodynamic and central artery hemorheology indices

Nine weeks after grouping, the left eye of each rat was examined using a color Doppler ultrasound, and hemodynamic indices such as end-diastolic velocity (EDV), peak systolic velocity (PSV) and central retinal vein (CRV) were measured. After the rats were fasted for 20 h, the animals were anesthetized by intraperitoneal injection of 3% pentobarbital sodium (30 mg/kg) and anticoagulated blood was drawn from the abdominal aorta. Plasma viscosity (PV), blood viscosity (BV) and erythrocyte sedimentation rate (ESR) at different shear rates were measured with a blood viscometer. Each measurement was performed in triplicate.

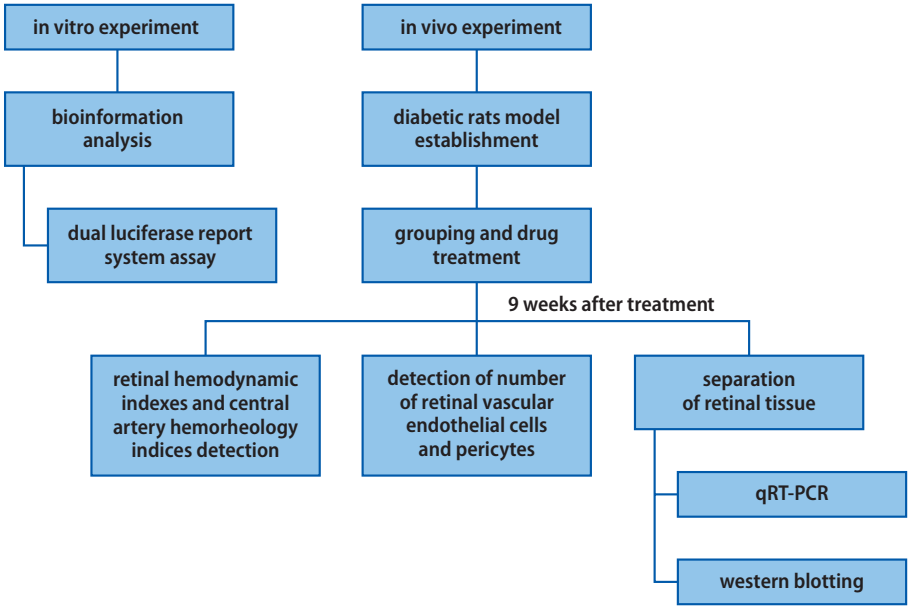

Fig. 1. Experimental design flow diagram

qRT-PCR – real-time fluorescence quantitative polymerase chain reaction.

Table 1. Grouping methods of rats

Group	Rat type	Treatment
Control	healthy	normal saline
Model	diabetic	streptozotocin
Negative control agomir	diabetic	streptozotocin + negative control mimic
miR-874 agomir	diabetic	streptozotocin + *miR-874* mimic
miR-874 anti-agomir	diabetic	streptozotocin + *miR-874* inhibitor
EVP4593	diabetic	streptozotocin + EVP4593 (NF-κB signaling pathway antagonist)
miR-874 anti-agomir + EVP4593	diabetic	streptozotocin + *miR-874* inhibitor + EVP4593

Measurement of the number of retinal vascular endothelial cells and pericytes

The eyeballs of all rats were fixed and retinal vascular digest preparations were performed. The numbers of retinal vascular endothelial cells (VECs) and capillary pericytes (IPCs) were counted using a microscope. All measurements were performed in triplicate.

Separation of retinal tissue

The eyeballs were extirpated under aseptic conditions and the bulbar conjunction was removed. The cornea was separated at 1 mm from the posterior of corneoscleral limbus, followed by evisceration of the crystalline lens and removal of the vitreous body under a stereomicroscope. The retina was isolated along with the under part of the retina, and the optic nerve was cut off. The retina was dissociated and cut into pieces.

Quantitative real-time fluorescence polymerase chain reaction

Total RNA in the retinal tissue was extracted using the Trizol method (Invitrogen, Calsbad, USA). After purity determination, the RNA was reverse transcribed into cDNA according to the manufacturer's instructions (TaqMan MicroRNA Assays Reverse Transcription primer, 4427975; Applied Biosystems, Waltham, USA), with reaction conditions of 37°C for 30 min and 85°C for 5 s. Primers were synthesized by the Wuhan Branch of Sangon Biotech Co. Ltd. (Shanghai, China) and the sequences are listed in Table 2. The reaction conditions for quantitative real-time polymerase chain reaction (qRT-PCR) were pre-denaturation at 95°C for 10 min followed by 40 cycles of denaturation at 95°C for 10 s, annealing at 60°C for 20 s, and extending at 72°C for 34 s. The reagents used for the qRT-PCR were 10 μL of SYBR Premix Ex Taq^{TM} II, 0.8 μL of PCR forward primer (10 μM), 0.8 μL of PCR reverse primer (10 μM), 0.4 μL of ROX Reference Dye II, 2.0 μL of cDNA templates, and 6.0 μL of sterilized distilled water. GAPDH was the internal reference for CD40, RORyt, Foxp3, interleukin (IL)-17, IL-10, tumor necrosis factor (TNF)-α, IL-23 and IL-8. The reactions were performed with an ABI7500 quantitative PCR amplifier (7500; Applied Biosystems). $2^{-\Delta\Delta Ct}$ showed the relative expression of the target gene. Each measurement was performed in triplicate.

Table 2. Primer sequence

Gene	Primer sequence (5′-3′)
miR-874	Forward: GGGCGGCCCCACGCACCA
	Reverse: GTGCAGGGTCCGAGGT
U6	Forward: CTCGCTTCGGCAGCACA
	Reverse: AACGCTTCACGAATTTGCGT

Western blotting

RIPA buffer (Beyotime Biotechnology Co. Ltd., Shanghai, China) was mixed with protease inhibitors and phenylmethylsulfonyl fluorid (PMSF) to lyse cells on ice for 30 min. Protein concentration was measured using a BCA protein assay kit (Beijing Dingguo Changsheng Biotechnology Co. Ltd., Beijing, China). Protein was separated using SDS-PAGE for 2 h and transferred to polyvinylidene fluoride (PVDF) membranes. The membrane was sealed with 5% milk for 2 h and incubated at 4°C with various primary antibodies, including rabbit anti-human angiopoietin2 (Ang2; 1 : 2500, ab155106; Abcam, Cambridge, USA), p65 (1 : 2500, ab32536; Abcam), vascular endothelial growth factor (VEGF; 1 : 2500, ab1316; Abcam) and *GAPDH* (1 : 2500, ab9485; Abcam). After the membrane was washed with Tris-buffered saline with Tween (TBST) 3 times, horseradish peroxidase (HRP)-labeled IgG (1 : 10,000, ab6721; Abcam) was added and incubated at room temperature for 1 h. The membrane was then washed with TBST 3 times. Color development was carried out by electrogenerated chemiluminescence solutions. The relative expression of each protein was calculated using the gray value of the target protein band divided by the gray value of the *GAPDH* band. Each measurement was performed in triplicate.

Statistical analysis

Data analysis was performed using SPSS v. 11.5 software (SPSS Inc., Chicago, USA) and the data are expressed as mean ± standard deviation (SD). Comparisons among groups were performed using one-way analysis of variance (ANOVA) followed by post hoc least significant difference (LSD) tests. An α value of $p < 0.05$ was considered statistically significant.

Results

miR-874 targets regulating the expression of p65

The bioinformatics website predicted that there was a binding site between *miR-874* and Rela (p65; Fig. 2A), which was verified using the dual-luciferase reporter system assay. The results showed that there were no significant differences in luciferase activity between the pmirGLO-Rela mut+NC mimic and the pmirGLO-Rela mut+*miR-874* mimic. However, the pmirGLO-Rela wt+*miR-874* mimic group had a significantly reduced luciferase activity compared to the pmirGLO-Rela mut+*miR-874* mimic group (Fig. 2B), indicating a targeted regulation of *miR-874* on p65.

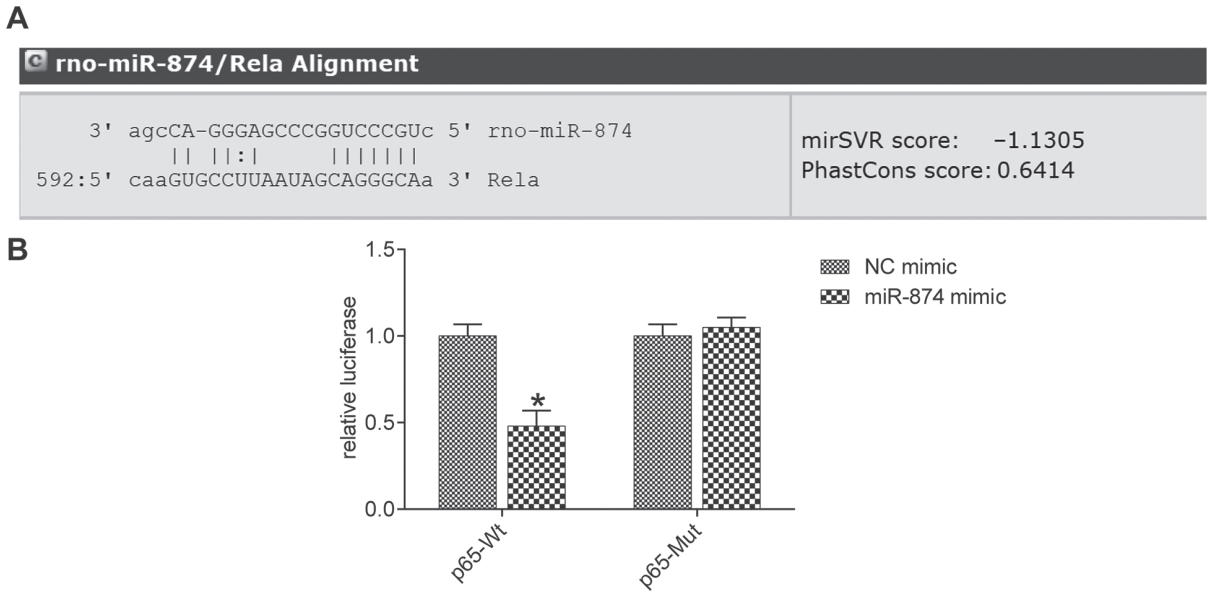

Fig. 2. Bioinformatics prediction and dual-luciferase reporter assay results

A. There was the binding site between *miR-874* and p65 predicted using a bioinformatics website; B. Dual-luciferase reporter system assay verified the target relationship between *miR-874* and p65 in a HEK293T cell line. The experiment was independently repeated 3 times. Compared with the NC mimic group *p < 0.05; NC – negative control; Wt – wild type; Mut – mutant.

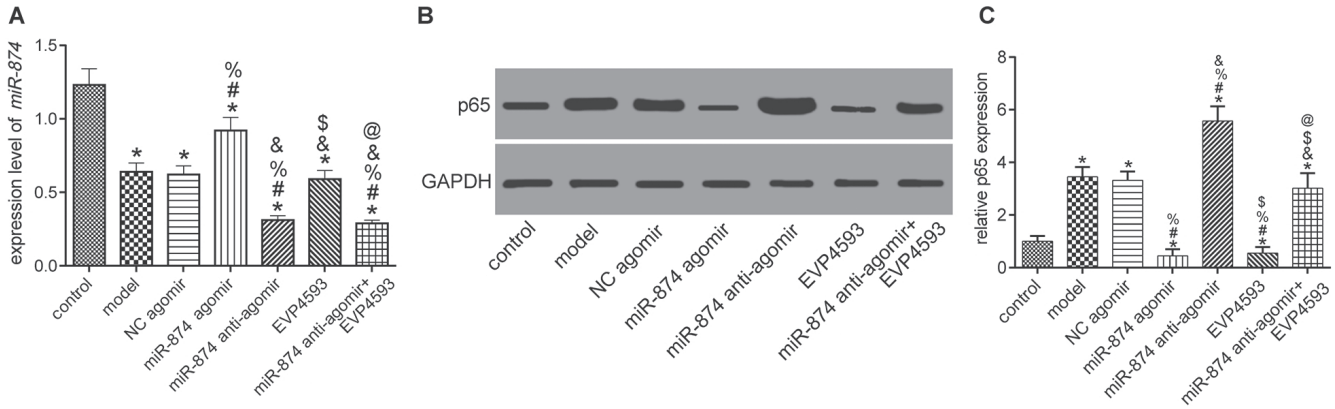

Fig. 3. The expression of *miR-874* and p65 in the retina

A. *miR-874* expression; B. Protein bands of p65; C. Protein expression histogram. Compared with the control group *p < 0.05; compared with the model group $^{\#}$p < 0.05; compared with the NC agomir group $^{\%}$p < 0.05; compared with the *miR-874* agomir group $^{\&}$p < 0.05; compared with the *miR-874* anti-agomir group $^{\$}$p < 0.05; compared with the EVP4593 group $^{@}$p < 0.05; NC – negative control.

p65 expression in the retina of diabetic rats is affected by *miR-874*

miR-874 expression in the retina was measured using qRT-PCR and Rela (p65) protein expression was measured with western blot (Fig. 3). Compared with the control group, retinal *miR-874* expression was significantly decreased and p65 expression significantly increased in the model group. The *miR-874* agomir group and EVP4593 group had increased *miR-874* expression and inhibited p65 expression, while the *miR-874* anti-agomir group showed opposite effects. EVP4593 reversed the promoting effect of *miR-874* anti-agomir on p65 expression. These results suggest that *miR-874* inhibits the NF-κB signaling pathway by suppressing p65 in the retina of diabetic rats.

Retinal injury associated with STZ-induced diabetes in rats and the ameliorative effects of *miR-874*

After STZ treatment, blood glucose levels were significantly higher in the model group than in the control group (4 mmol/L). *miR-874* agomir and EVP4593 treatment slowed the soaring increase of blood glucose in model rats, but *miR-874* anti-agomir exacerbated this effect. EVP4593 neutralized the effect of *miR-874* anti-agomir on blood glucose levels in diabetic rats (Fig. 4A).

Rats in the control group exhibited typical weight gain. Compared with the control group, rats in the model group weighed significantly less. *miR-874* agomir and EVP4593 treatment increased the weight of the rats, and the *miR-874*

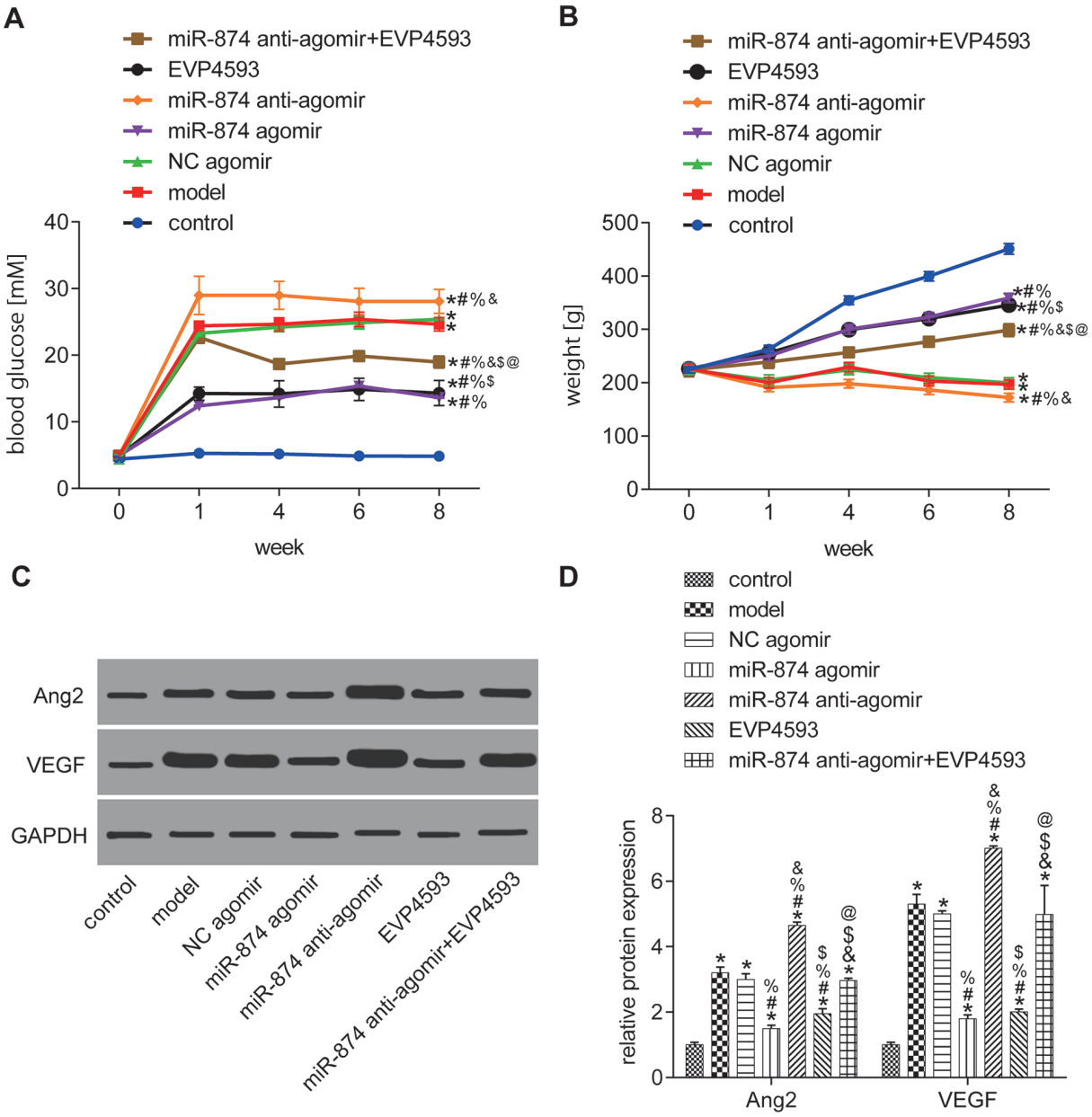

Fig. 4. Retinal pathological changes detection

A. Blood glucose; B. Weight; C. Protein bands of Ang2 and VEGF in the retina of STZ-induced diabetes rat model; D. Protein expression histogram. Compared with the control group *p < 0.05; compared with the model group $^{\#}$p < 0.05; compared with the NC agomir group $^{\%}$p < 0.05; compared with the *miR-874* agomir group $^{\&}$p < 0.05; compared with the *miR-874* anti-agomir group $^{\$}$p < 0.05; compared with the EVP4593 group $^{@}$p < 0.05; NC – negative control; VEGF – vascular endothelial growth factor; Ang2 – angiopoietin2; STZ – streptozotocin.

anti-agomir treatment resulted in lower weight. EVP4593 reduced the weight loss caused by the *miR-874* anti-agomir in diabetic rats (Fig. 4B).

Abnormal expression of Ang2 and VEGF could cause retinal VEC damage and a pro-inflammatory response. Thus, the protein expression levels of VEGF and Ang2 were measured using western blotting (Fig. 4C,D). The expression of VEGF and Ang2 was significantly increased in the retinas of diabetic rats ($p < 0.05$), indicating that pathological changes occurred in the retina. The increases in VEGF and Ang2 protein expression were inhibited in the *miR-874* agomir and EVP4593 groups, and promoted in the *miR-874* anti-agomir group. EVP4593 neutralized the promoting effect of *miR-874* anti-agomir on VEGF and Ang2 protein expression.

Retinopathy relief in diabetic rats administered *miR-874*

Hemodynamic indices in diabetic rats were measured to detect retinal blood perfusion and blood supply (Fig. 5). Compared with the control group, EDV, PSV and CRV values in the model group were decreased by varying degrees, indicating insufficient retinal blood perfusion and

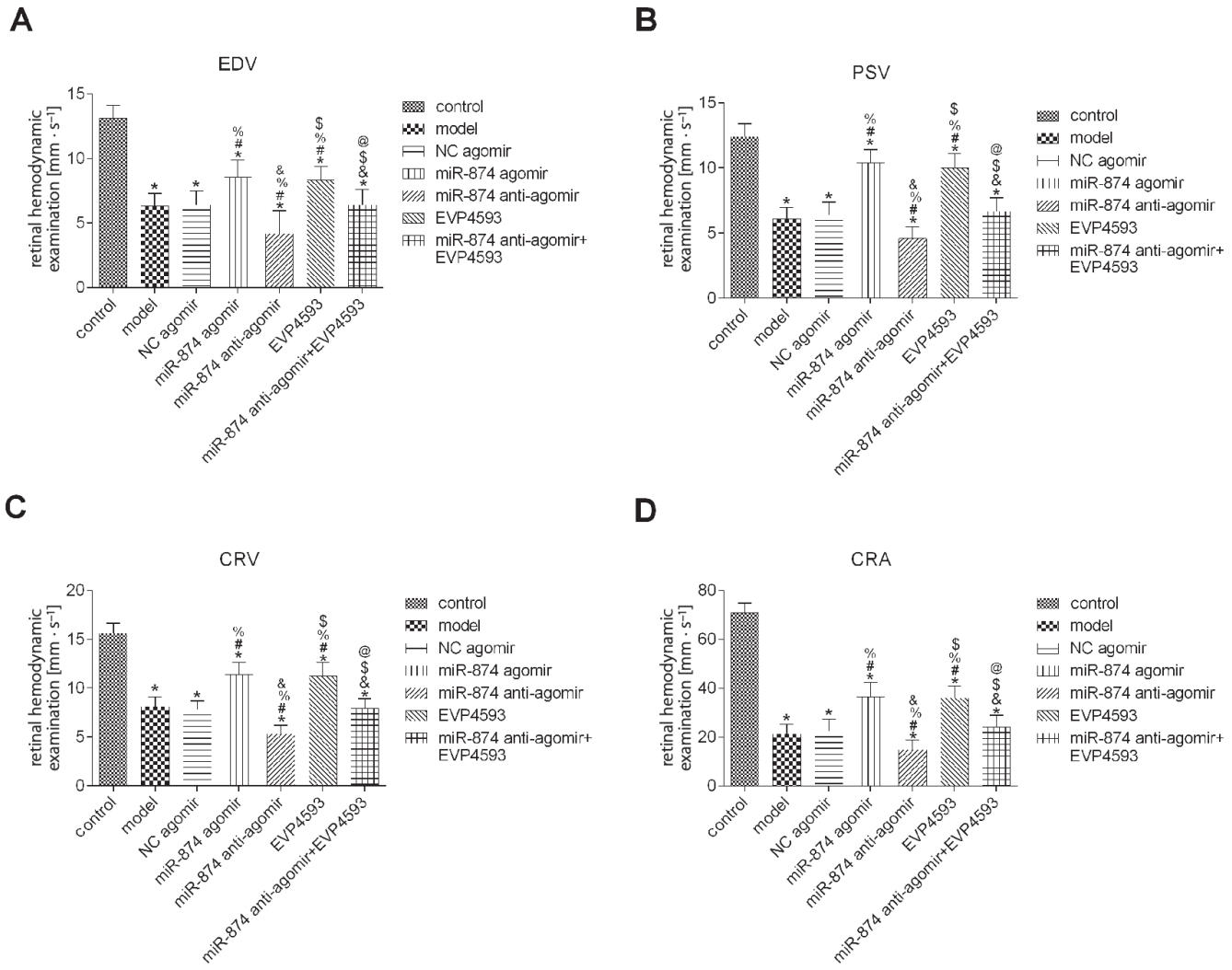

Fig. 5. Retinal hemodynamic examinations of diabetes rats

A. End-diastolic velocity; B. Peak systolic velocity of central retinal artery; C. Blood velocity of central retinal vein; D. Blood velocity of central retinal artery. Compared with the control group *p < 0.05; compared with the model group #p < 0.05; compared with the NC agomir group %p < 0.05; compared with the *miR-874* agomir group &p < 0.05; compared with the *miR-874* anti-agomir group $p < 0.05; compared with the EVP4593 group @p < 0.05; NC – negative control; EDV – end-diastolic velocity; PSV – peak systolic velocity; CRV – central retinal vein; CRA – central retinal artery.

blood supply in diabetic rats. Diabetic rats with *miR-874* agomir and EVP4593 treatment had increased EDV, PSV and CRV values, while the *miR-874* anti-agomir group showed opposite effects. EVP4593 neutralized the inhibitory effect of *miR-874* anti-agomir on the EDV, PSV and CRV values (all p < 0.05). Hence, it was shown that *miR-874* had an influence on the hemodynamic indices of rats with DR, and that *miR-874* could alleviate the retinopathy of diabetic rats.

Hemorheology indices in diabetic rats were also measured to further verify the alleviation of *miR-874* on DR (Fig. 6). Compared with the control group, BV, PV and ESR values were increased in the model group. Diabetic rats with *miR-874* agomir and EVP4593 treatment showed decreased BV, PV and ESR values, while the *miR-874* anti-agomir group exhibited opposite effects. EVP4593 neutralized the promoting effect of *miR-874* anti-agomir on BV, PV and ESR values at all shear rates (all p < 0.05). Thus, it was demonstrated that *miR-874* relieved retinopathy in diabetic rats.

The numbers of retinal capillary VECs and IPCs were also measured (Fig. 7). Compared with the control group, the numbers of IPCs were significantly reduced, and numbers of VECs significantly increased, in the retinal capillaries of the diabetic group. Diabetic rats treated with *miR-874* agomir and EVP4593 had increased numbers of IPCs and decreased VEC proliferation in the retinal capillaries, while the *miR-874* anti-agomir group showed opposite effects. EVP4593 partly reversed the IPC number decrease and the VEC proliferation increase caused by *miR-874* anti-agomir (all p < 0.05). Thus, *miR-874* relieved the retinopathy of diabetic rats.

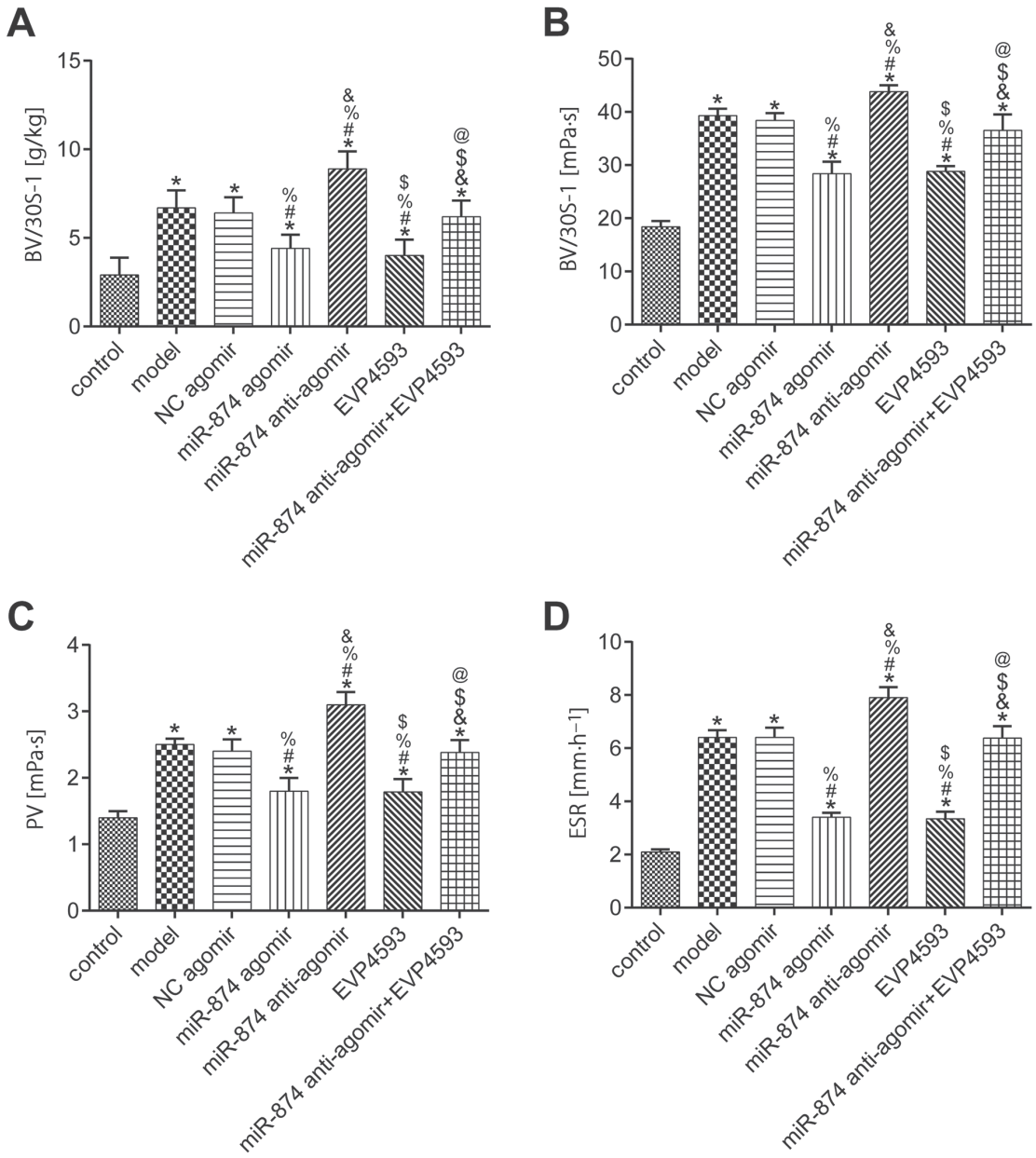

Fig. 6. Retinal hemorheology of diabetes rats

A. BV/30S-1; B. BV/1S-1; C. PV; D. ESR. Compared with the control group *$p < 0.05$; compared with the model group $^{\#}p < 0.05$; compared with the NC agomir group $^{\%}p < 0.05$; compared with the *miR-874* agomir group $^{\&}p < 0.05$; compared with the *miR-874* anti-agomir group $^{\$}p < 0.05$; compared with the EVP4593 group $^{@}p < 0.05$; NC – negative control; BV – blood viscosity; PV – plasma viscosity; ESR – erythrocyte sedimentation rate.

Discussion

The main treatment methods for DR are laser photocoagulation, hyperbaric oxygen and drug therapy.[26] However, these methods may lead to severe adverse side effects, including decreases in visual acuity and contrast sensitivity, and visual field damage. Therefore, safer therapeutic strategies need to be developed for DR patients.

Previous work has shown that NF-κB is activated in the retina of diabetics, and that the activated NF-κB increases capillary cell apoptosis.[27] These changes are observed prior to development of the histopathological features characteristic of DR.[28] Once NF-κB is activated early in the pathogenesis of DR, its effects could only be inhibited partially by early reconstruction. Moreover, if the hyperglycemia induced by diabetes was not well controlled for 7 months, it could be irreversible. In this study, there were heightened EDV, PSV of central retinal artery (CRA) and blood velocity of CRV, lowered PV, BV and ESR at all shear rates, an increased number of retinal capillary pericytes, decreased endothelial cell proliferation, and a significantly reduced p65 expression in the retina in the EVP4593 group as compared to the model group. These results indicate that inhibition of the NF-κB signaling pathway significantly improves the condition of DR in rats, which is consistent with the literature that we reviewed.

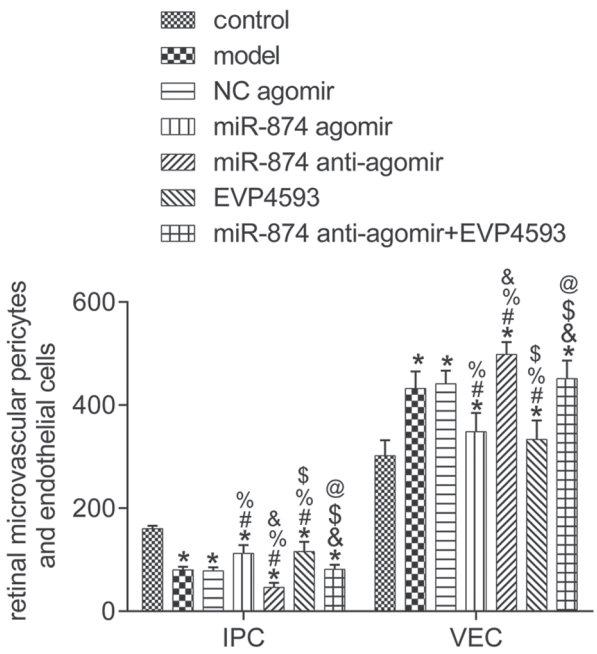

Fig. 7. Number of retinal microvascular pericytes and endothelial cells

Compared with the control group *p < 0.05; compared with the model group #p < 0.05; compared with the NC agomir group %p < 0.05; compared with the *miR-874* agomir group &p < 0.05; compared with the *miR-874* anti-agomir group $p < 0.05; compared with the EVP4593 group @p < 0.05; NC – negative control; IPC – pericytes; VEC – endothelial cells.

Recently, miRNA has been identified as a biomarker for the diagnosis of various diseases, including DR. Moreover, there is growing evidence that miRNAs play a key role in regulating NF-κB activation and its downstream functions. However, the effects of miRNA on NF-κB activation or inhibition in DR have not been fully revealed. *miR-874* plays a role in various diseases, including several types of cancers, such as colorectal, gastric and non-small cell lung cancers.[29] *miR-874* is significantly downregulated in the sertoli cells of diabetic rats and *miR-874* overexpression relieves renal injury in these animals.[30] However, there are no studies on the relationship between *miR-874* and DR.

In this study, we used bioinformatics prediction to identify a targeted site where *miR-874* binds to p65, which is the most important protein in the NF-κB signaling pathway. Moreover, a dual-luciferase reporter system assay confirmed that p65 is a target gene of *miR-874*. A DR rat model was successfully established to explore the relationship between *miR-874* and NF-κB signaling pathway. The results showed that, in DR rats, a *miR-874* mimic has similar therapeutic effects to the NF-κB signaling pathway antagonist EVP4593. In addition, DR was aggravated after treatment with a *miR-874* inhibitor in diabetic rats. EVP4593 also counteracted the aggravation of retinopathy that was caused by the *miR-874* inhibitor. These results indicate that *miR-874* upregulation inhibits the activity of the NF-κB signaling pathway, alleviating retinopathy in diabetic rats.

In addition, we found that blood glucose levels in the *miR-874* agomir and EVP4593 groups were the lowest for the diabetic rat groups. In this study, diabetes in rats was first established and then treated. Moreover, compared with the *miR-874* agomir and EVP4593 groups, the NF-κB signaling pathway in other groups of diabetic rats was not inhibited or only partially inhibited, and correspondingly their retinopathy was more severe. Therefore, the amelioration effect of *miR-874* on diabetic retinopathy was due not to low blood glucose levels, but to the fact that *miR-874* inhibited the abnormally high activity of the NF-κB signaling pathway (the NF-κB impairment) in the retinas of diabetic rats. As signaling pathways in the body are complicated, it remains to be elucidated whether the decrease in blood glucose is related to inhibition of the NF-κB signaling pathway.

Limitations

While the effects of *miR-874* on retinopathy in diabetic rats have been confirmed, the specific molecular mechanism between *miR-874* and NF-κB is not clear. Moreover, further experiments will be necessary to determine whether overexpressed *miR-874* mimic can be applied in clinical treatment.

Conclusions

miR-874 can inhibit p65, an important protein in the NF-κB signaling pathway, in the retina of diabetic rats, and further inhibit NF-κB signaling, leading to an alleviation of retinopathy. It may be a new drug target in the treatment of DR.

ORCID iDs

Rui Li https://orcid.org/0000-0001-6774-538X
Huimin Yuan https://orcid.org/0000-0002-5525-7909
Tao Zhao https://orcid.org/0000-0003-4833-3448
Yimin Yan https://orcid.org/0000-0002-3351-4732
Zhaochen Liu https://orcid.org/0000-0002-8298-2436
Jiayu Cai https://orcid.org/0000-0002-7041-0342
Chunli Qiu https://orcid.org/0000-0003-0797-2286
Chuanjing Li https://orcid.org/0000-0002-7188-1584

References

1. Brinchmann-Hansen O, Dahl-Jorgensen K, Hanssen KF, Sandvik L. The response of diabetic retinopathy to 41 months of multiple insulin injections, insulin pumps, and conventional insulin therapy. *Arch Opthalmol*. 1988;106(9):1242–1246. doi:10.1001/archopht.1988.01060140402041
2. Xie MY, Yang Y, Liu P, Luo Y, Tang SB. 5-aza-2′-deoxycytidine in the regulation of antioxidant enzymes in retinal endothelial cells and rat diabetic retina. *Int J Ophthamol*. 2019;12(1):1–7. doi:10.18240/ijo.2019.01.01
3. Obeid A, Su D, Patel SN, et al. Outcomes of eyes lost to follow-up with proliferative diabetic retinopathy that received panretinal photocoagulation versus intravitreal anti-vascular endothelial growth factor. *Ophthalmology*. 2019;126(3):407–413. doi:10.1016/j.ophtha.2018.07.027
4. Joussen AM, Poulaki V, Mitsiades N, et al. Nonsteroidal anti-inflammatory drugs prevent early diabetic retinopathy via TNF-alpha suppression. *FASEB J*. 2002;16(3):438–440. doi:10.1096/fj.01-0707fje

5. Zheng L, Szabo C, Kern TS. Poly(ADP-ribose) polymerase is involved in the development of diabetic retinopathy via regulation of nuclear factor-kappaB. *Diabetes*. 2004;53(11):2960–2967. doi:10.2337/diabetes.53.11.2960
6. Kamble VV, Kokate RD. Automatic identification and classification of microaneurysms, exudates and blood vessel for early diabetic retinopathy recognition. In: Sekhar Behera H, Nayak J, Naik B, Abraham A, eds. *Computational Intelligence in Data Mining*. Singapore: Springer Singapore; 2019. doi:10.1007/978-981-10-8055-5_38
7. Hemanth DJ, Deperlioglu O, Kose U. An enhanced diabetic retinopathy detection and classification approach using deep convolutional neural network. *Neural Comput Appl*. 2019;7398:1–15. doi:10.1007/s00521-018-03974-0
8. Thomas AA, Biswas S, Feng B, Chen S, Gonder J, Chakrabarti S. lncRNA H19 prevents endothelial–mesenchymal transition in diabetic retinopathy. *Diabetologia*. 2019;62(3):517–530. doi:10.1007/s00125-018-4797-6
9. Aeschlimann FA, Laxer RM. Response to: "A20 haploinsufficiency (HA20): Clinical phenotypes and disease course of patients with a newly recognised NF-kB-mediated autoinflammatory disease" by Aeschlimann et al. *Ann Rheum Dis*. 2019;78(5):e36. doi:10.1136/annrheumdis-2018-213359
10 Huang WJ, Wang Y, Liu S, et al. Retraction notice to "Silencing circular RNA hsa_circ_0000977 suppresses pancreatic ductal adenocarcinoma progression by stimulating *miR-874-3p* and inhibiting *PLK1* expression" [*Cancer Lett*. 422C (2018) 70–80]. *Cancer Lett*. 2018;438:232. doi:10.1016/j.canlet.2018.09.027
11. Tang W, Wang W, Zhao Y, Zhao Z. *MicroRNA-874* inhibits cell proliferation and invasion by targeting cyclin-dependent kinase 9 in osteosarcoma. *Oncol Lett*. 2018;15(5):7649–7654. doi:10.3892/ol.2018.8294
12. Liao H, Pan Y, Pan Y, et al. *MicroRNA874* is downregulated in cervical cancer and inhibits cancer progression by directly targeting ETS1. *Oncol Rep*. 2018;40(4):2389–2398. doi:10.3892/or.2018.6624
13. Zhang Y, Wang X, Zhao Y. *MicroRNA874* prohibits the proliferation and invasion of retinoblastoma cells by directly targeting metadherin. *Mol Med Rep*. 2018;18(3):3099–3105. doi:10.3892/mmr.2018.9295
14. Luo DW, Zheng Z, Wang H, et al. UPP mediated diabetic retinopathy via ROS/PARP and NF-kappaB inflammatory factor pathways. *Curr Mol Med*. 2015;15(8):790–799. doi:10.2174/1566524015666150921110500
15. Chen F, Zhang HQ, Zhu J, et al. Puerarin enhances superoxide dismutase activity and inhibits RAGE and VEGF expression in retinas of STZ-induced early diabetic rats. *Asian Pac J Trop Med*. 2012;5(11):891–896. doi:10.1016/S1995-7645(12)60166-7
16. Yin Y, Chen F, Wang W, Wang H, Zhang X. Resolvin D1 inhibits inflammatory response in STZ-induced diabetic retinopathy rats: Possible involvement of NLRP3 inflammasome and NF-kappaB signaling pathway. *Mol Vis*. 2017;23:242–250. PMID:28465656
17. Liang Z, Gao KP, Wang YX, et al. RNA sequencing identified specific circulating miRNA biomarkers for early detection of diabetes retinopathy. *Am J Physiol Endocrinol Metab*. 2018;315(3):E374–E385. doi:10.1152/ajpendo.00021.2018
18. Zhang J, Wu L, Chen J, et al. Downregulation of microRNA 29a/b exacerbated diabetic retinopathy by impairing the function of Muller cells via forkhead box protein O4. *Diab Vasc Dis Res*. 2018;15(3):214–222. doi:10.1177/1479164118756239
19. Wang W, Lo ACY. Diabetic retinopathy: Pathophysiology and treatments. *Int J Mol Sci*. 2018;19(6):1816. doi:10.3390/ijms19061816
20. Sorrentino FS, Matteini S, Bonifazzi C, Sebastiani A, Parmeggiani F. Diabetic retinopathy and endothelin system: Microangiopathy versus endothelial dysfunction. *Eye (London)*. 2018;32(7):1157–1163. doi:10.1038/s41433-018-0032-4
21. Meerson A, Eliraz Y, Yehuda H, et al. Obesity impacts the regulation of miR-10b and its targets in primary breast tumors. *BMC Cancer*. 2019;19(1):86. doi:10.1186/s12885-019-5300-6
22. Chen PJ, Shang AQ, Yang JP, Wang WW. *MicroRNA-874* inhibition targeting STAT3 protects the heart from ischemia-reperfusion injury by attenuating cardiomyocyte apoptosis in a mouse model. *J Cell Physiol*. 2019;234(5):6182–6193. doi:10.1002/jcp.27398
23. Yao T, Zha D, Gao P, Shui H, Wu X. *MiR-874* alleviates renal injury and inflammatory response in diabetic nephropathy through targeting toll-like receptor-4. *J Cell Physiol*. 2018;234(1):871–879. doi:10.1002/jcp.26908
24. Gong Q, Li F, Xie J, Su G. Upregulated VEGF and Robo4 correlate with the reduction of miR-15a in the development of diabetic retinopathy. *Endocrine*. 2019;65(1):35–45. doi:10.1007/s12020-019-01921-0
25. Wang G, Yan Y, Xu N, Hui Y, Yin D. Upregulation of microRNA-424 relieved diabetic nephropathy by targeting rictor through mTOR complex2/protein kinase B signaling. *J Cell Physiol*. 2019;234(7):11646–11653. doi:10.1002/jcp.27822
26. Berteau F, Rouviere B, Nau A, et al. A20 haploinsufficiency (HA20): Clinical phenotypes and disease course of patients with a newly recognised NF-kB-mediated autoinflammatory disease. *Ann Rheum Dis*. 2019;78(5):e35. doi:10.1136/annrheumdis-2018-213347
27. Antzelevitch C. Genetic, molecular and cellular mechanisms underlying the J wave syndromes. *Card Electrophysiol*. 2018;76(5):483–493. doi:10.1253/circj.cj-12-0284
28. Jiang T, Guan LY, Ye YS, Liu HY, Li R. *MiR-874* inhibits metastasis and epithelial–mesenchymal transition in hepatocellular carcinoma by targeting SOX12. *Am J Cancer Res*. 2017;7(6):1310–1321. PMID:28670493
29. Yang R, Li P, Zhang G, Lu C, Wang H, Zhao G. Long non-coding RNA XLOC_008466 functions as an oncogene in human non-small cell lung cancer by targeting *miR-874*. *Cell Physiol Biochem*. 2017;42(1):126–136. doi:10.1159/000477121
30. Leong KW, Cheng CW, Wong CM, Ng IO, Kwong YL, Tse E. *miR-874*-3p is downregulated in hepatocellular carcinoma and negatively regulates PIN1 expression. *Oncotarget*. 2017;8(7):11343–11355. doi:10.18632/oncotarget.14526

Phenalen-1-one-mediated photodynamic therapy inhibits keloid graft progression by reducing vessel formation and promoting fibroblast apoptosis

Wei Zheng[A,D,E], Haiyan Wu[A,B,D], Ying Li[A,B,E], Helin Li[B,E], Zhaojun Liu[B,E], Yongzhi Nie[C,E], Lingling Shi[C,E], Hongyu Wang[A,E,F]

Department of Burn Orthopedics, Xingtai People's Hospital, China

A – research concept and design; B – collection and/or assembly of data; C – data analysis and interpretation; D – writing the article; E – critical revision of the article; F – final approval of the article

Advances in Clinical and Experimental Medicine, ISSN 1899–5276 (print), ISSN 2451–2680 (online) *Adv Clin Exp Med*. 2021;30(4):431–439

Address for correspondence
Hongyu Wang
E-mail: uyv12254@126.com

Funding sources
None declared

Conflict of interest
None declared

Received on August 20, 2020
Reviewed on September 12, 2020
Accepted on November 18, 2020

Published online on April 29, 2021

Abstract

Background. Keloid is a unique refractory syndrome characterized by a proliferation disorder of the fibroblasts. Recently, photodynamic therapy (PDT) has become a promising technique to modulate fibroblasts. However, use of the photosensitizer Phenalen-1-one (Ph1) in PDT for keloid remains to be explored.

Objectives. This study investigated the efficacy of Ph1-PDT in the in vitro and in vivo models of keloid.

Materials and methods. Cell viability was assessed with a Cell Counting Kit-8 (CCK-8) analysis in keloid fibroblasts. The migrated and invaded keloid fibroblasts after Ph1-PDT were detected using scratch and matrigel invasion assays in vitro. Flow cytometry measured the apoptosis changes. The protein concentrations and the mRNA expression of inflammatory modulators (interleukin 8 (IL-8) and IL-1β) were determined using enzyme-linked immunosorbent assay (ELISA) and real-time quantitative polymerase chain reaction (RT-qPCR) methods, respectively. Nude mice were used to perform the transplantation of keloid grafts. Western blot analysis measured the protein expression of CD31, CD34, tumor growth factor β1 (TGF-β1), and collagen 1 in keloid fibroblasts and grafts.

Results. Our results revealed that Ph1-PDT significantly suppressed cell viability, migration and invasion, and enhanced the rate of cell apoptosis and caspase-3 expression in keloid fibroblasts. Moreover, in the nude mice model, Ph1-PDT decreased the volume of the graft and attenuated the vessel density by inhibiting the expression of vessel density biomarkers (CD31 and CD34) in keloid grafts. Furthermore, Ph1-PDT significantly inactivated the inflammatory mediators in keloid grafts. In addition, Ph1-PDT considerably attenuated the development of keloids by inhibiting TGF-β1 and collagen 1 proteins in keloid fibroblasts and grafts.

Conclusions. Ph1-PDT may suppress keloid progression by reducing vessel formation and inflammation, and promoting fibroblast apoptosis, suggesting a potential therapy method for keloid.

Key words: TGF-β1, photodynamic therapy, phenalen-1-one, keloid graft, collagen 1

Cite as
Zheng W, Wu H, Li Y. Phenalen-1-one-mediated photodynamic therapy inhibits keloid graft progression by reducing vessel formation and promoting fibroblast apoptosis. *Adv Clin Exp Med*. 2021;30(4):431–439. doi:10.17219/acem/130594

DOI
10.17219/acem/130594

Copyright
© 2021 by Wroclaw Medical University
This is an article distributed under the terms of the Creative Commons Attribution 3.0 Unported (CC BY 3.0) (https://creativecommons.org/licenses/by/3.0/)

Background

Keloid is a skin disorder that results in pathological scars. This condition is characterized by inflammation, abnormal deposition of collagen fibers, and excessive proliferation of fibroblasts with cancer-like properties that are usually invasive and often recur after excision.[1] The abnormal growth of keloid can be disfiguring, and cause pain and irritation.[2] Keloid also generally leads to psychological and physical anxiety in patients.[3] There are various treatments for keloids, such as radiation therapy, corticosteroid injections, surgical excision, pressure therapy, and silicone gel sheeting.[4] However, few of the current therapeutic modalities provide good clinical outcomes without side effects. Surgical excision is an efficient method compared to others, yet it might add to a higher risk of cancer years after the radiation exposure.[5] Therefore, it is urgent to explore an effective and safe therapy for keloid scarring.

Photodynamic therapy (PDT) is a promising therapeutic strategy used to treat skin lesions, including actinic keratosis, Bowen's disease and basal cell carcinoma.[6] The PDT has been widely used to treat keloid due to its accuracy and minimal side effects.[7] This method kills bacteria through an oxidative burst, leading to damage in biomolecules and cell structures.[8] It consists of 3 main components: molecular oxygen, light of a proper wavelength and a non-toxic dye (photosensitizer (PS)).[9] Briefly, the PS is absorbed into the target cells and exposed to the radiation of visible light with a wavelength of 400–750 nm. The abovementioned components of PDT cannot induce cytotoxic effects alone. However, when they are joined together, reactive oxygen (RO) occurs, inducing cellular apoptosis.[10] The accurate supply of light to the target cells enables PDT to eliminate a large number of cancer cells with minimal adverse effects.[11] An appropriate amount of light is required to activate the PS, as it is considered a light-absorbing molecule. The oxidation reactions of the radicals are promoted due to the excited PS, which leads to the generation of numerous RO derivatives, including peroxyl radical (ROO•), superoxide radical anion (O_2•$^-$) and hydroxyl radical (HO•).[12] The PS also transfers its energy to the molecular oxygen to generate singlet oxygen ($^1O_2$).[13] Previous research has revealed that HMME-PDT activates the apoptosis of keloid fibroblasts in vitro.[14] Also, PDT directly triggers apoptosis in targeted cells due to the formation of reactive oxygen species (ROS) in the proximity of, or in, the mitochondria of the cells.[15]

Optimal performance of PDT depends on the type of PS used and, recently, several PSs have been applied in clinical treatment. However, these PSs have certain limitations, including excessive potency and inadequate discernment of the site of the lesion. Therefore, a new PS that can improve the efficacy of PDT is urgently needed.[16] Phenalen-1-one (Ph1) is a newly developed PS that is extracted from *Scutellaria barbata*, an ethnopharmacological herb.[17] Ph1 exhibits ROS-mediated properties against plant-parasitic nematodes and vector mosquito larvae, which are increased in the presence of light.[18] In addition, Ph1 induces the photo-inactivation of key oral bacteria and acts as a potential dental drug.[19] However, the role and mechanism of Ph1-PDT in the treatment of keloids remain unknown.

Objectives

The current study aimed to explore the impacts of Ph1-PDT on the viability, invasion, migration, and apoptosis of keloid fibroblasts in vitro. Also, the effects of Ph1-PDT on keloid graft growth and vessel density were determined in vivo. Moreover, the efficiency and mechanism of Ph1-PDT for vascular remodeling was evaluated in a mouse model. Triamcinolone acetonide (TA) was used as a positive control in these latter experiments as it is widely recognized that this agent significantly suppresses keloid in vivo.[20] Furthermore, the impact of Ph1-PDT on inflammatory cytokines was examined in keloid grafts. The current findings may provide an efficient therapeutic strategy for the treatment of keloids.

Materials and methods

Keloid fibroblast culture

Human keloid fibroblasts were obtained from American Type Culture Collection (ATCC, Manassas, USA) and cultured in Dulbecco's modified Eagle's medium (DMEM; Thermo Fisher Scientific, Waltham, USA) with penicillin (100 U mL^{-1}), streptomycin (100 µg mL^{-1}) and 10% fetal bovine serum (FBS). The cells were incubated in humidified air conditions of 21% O_2 and 5% CO_2 at 37°C. The cells from 3 through 6 passages were used in the experiments.

Ph1-PDT in cells

The cells were collected and inoculated into the culture plates, followed by the addition of various dosages (1 µM, 3 µM, 10 µM, and 30 µM) of Ph1 into the medium. These cells were then cultured for 4 h in the dark. Green light with a wavelength of 532 nm was then applied upright on the culture plates for another 12 h. Non-light cell groups on the culture plate were covered with tinfoil, and the gaps in the culture plate were minimized by using sterilized gauze. After light treatment, the medium was instantly aspirated and rinsed with phosphate-buffered saline (PBS), followed by the addition of DMEM medium with 10% FBS.

CCK-8 assay

A Cell Counting Kit-8 (CCK-8; Beyotime, Shanghai, China) was used to measure the cell viability according to the manufacturer's protocols. More specifically, keloid

fibroblasts were seeded in 96-well plates (5×10^3 cells/well), followed by treatment with different concentrations (1 μM, 3 μM, 10 μM, and 30 μM) of Ph1, and exposure to a 100 mW cm^{-2} laser at a wavelength of 532 nm for 10 min. Cells were also selected for triamcinolone acetonide (TA) (1 mg/mL) or DMEM treatment. The TA group served as a positive control while the DMEM group served as a negative control. The CCK-8 solution (10 μL; Sigma-Aldrich, St. Louis, USA), 10% FBS and 100 μL of DMEM were added into each plate followed by incubation for 4 h at 37°C in a humidified incubator. A microplate reader (Bio-Rad, Hercules, USA) was used to read the optical density (OD) values at 450 nm at 0 h, 24 h, 48 h, and 72 h. All the measurements were repeated 3 times for each sample.

Scratch migration assay

Six-well plates were used to seed keloid fibroblasts and, after various treatments, the fibroblasts were scratched with pipette tips (100 μL) and then washed twice using PBS. The scratched cells were incubated in a humidified incubator with 5% CO_2 at 37°C. Wound closures were examined after different time intervals (0 h, 24 h and 48 h) and the wound healing rates of the cells were calculated.

Matrigel invasion assay

The 24-well transwell chambers containing 8 mm pores (Bioz, Inc., Los Altos, USA) were used to conduct the cell invasion assay. Matrigel (30 mL) was used to coat the inserts. The upper matrigel chamber, supplemented with serum-free medium (100 mL), was used to seed fibroblasts (5×10^3) after different treatments, followed by incubation for 24 h. Further, 10% FBS with 500 μL of DMEM was added into the lower chamber. Crystal violet (0.1%) was added to stain the cells, invaded cells were imaged, and the cell number was analyzed across 5 fields (×100 magnification) under a light microscope.

Flow cytometry

Six-well plates were used to inoculate the keloid fibroblasts of the logarithmic growth phase. After 1 day, a suspension of the culture was prepared with a cell density of 1×10^6 cells per milliliter. The cells were centrifuged (1000 rpm, 5 min, 4°C), supernatants were resuspended in buffer solution and 5 μL of Annexin V-FITC (Beyotime) was added. The culture was mixed gradually and incubated for 10 min in the dark. After centrifugation (1000 rpm, 5 min, 4°C), the supernatants were discarded and cells were suspended in 10 μL of propidium iodide and 190 μL of Annexin V-FITC for 15 min at room temperature. Flow cytometry (Biocompare, San Francisco, USA) was used to perform the quantitative analysis of apoptosis. All measurements were performed 3 times.

ELISA assay

Enzyme-linked immunosorbent assay (ELISA) was used to determine the concentrations of interleukin 1β (IL-1β; Human IL-1-beta ELISA Kit; Abcam, Cambridge, USA) and IL-8 (Human IL-8 ELISA Kit; Abcam) according to the manufacturer's protocol. The supernatants attained from the cell cultures were collected, and a microplate reader (BMG LabTech, Ortenberg, Germany) was used to detect absorbance at 450 nm. The concentration of cytokines was calculated based on a standard curve derived from the data of standard samples. All the measurements were repeated in triplicate.

RT-qPCR

RiboZol RNA extraction reagent (VWR, Toronto, Canada) was used to extract total RNA from keloid tissues, and the concentration of RNA was measured using a NanoDrop 2000 spectrophotometer (Thermo Fisher Scientific). The cDNA was reverse transcribed using a PrimeScript RT Master Mix Kit (TakaraBio, Gothenburg, Sweden), and the real-time quantitative polymerase chain reaction (RT-qPCR) was prepared following the manufacturer's instructions. Reactions were carried out in a Pikoreal 96 real-time PCR system (Thermo Fisher Scientific) to measure the mRNA levels of the genes. The primers used are given in the table below. Glyceraldehyde 3-phosphate dehydrogenase (GAPDH) was considered an internal control for mRNA, and the data was analyzed using the $2^{-\Delta\Delta Ct}$ method. All the measurements were repeated in triplicate (Table 1).

Table 1. Primer sequences

Primers	Sequence
Caspase-3 Forward	ACTGGACTGTGGCATTGAGA
Caspase-3 Reverse	GTTTCAGCATGGCACAAAGC
IL-8 Forward	GTGGTGGCAGATGTGCTTAG
IL-8 Reverse	TTCAGAGCCACAAACAAGGC
IL-1β Forward	CTCTCTCCTTTCAGGGCCAA
IL-1β Reverse	GCGGTTGCTCATCAGAATGT
GAPDH Forward	ACCCAGAAGACTGTGGATGG
GAPDH Reverse	TCAGCTCAGGGATGACCTTG

Keloid transplantation and treatment with Ph1-PDT

Male Bagg albino laboratory-bred (BALB) nude mice (18 ±2 g; 4–6 weeks old; 12 in each group) were kept in a pathogen-free environment. All the animals were provided by Tianjin Saierbio Co. (Tianjin, China). Prior to transplantation, all mice were acclimatized for 2 weeks (20 ±2 g). All the animal assays were performed strictly in accordance with the regulations of the 983rd PLA Hospital.

Eye scissors were used to make an incision (8 mm in length) for transplant of the keloid tissues (ATCC). The incision was stitched immediately after the keloid graft filled the gap between the subcutaneous tissues and the skin. Ph1 was injected into the nude rats via tail veins 15 days after the keloid implantation. A semiconductor laser with a 532 nm wavelength (model number FD532-5-A; Wuhan Lingyun Photoelectric Technology, Wuhan, China) was used on the keloid graft for 10 min. This laser equipment was selected as its wavelength is quite close to the oxyhemoglobin absorption peak (542 nm). Ph1-PDT group (100 mW cm^{-2} laser + 8 μg Ph1 per mouse) underwent irradiation again on day 7 and 14. The normal saline (NS) and TA (0.1 mg/mouse) group was not exposed to laser. The nude mice were treated with Ph1-PDT (100 mW cm^{-2} laser + 8 μg Ph1/mouse), NS and TA (0.1 mg/mouse without light) on day 7 and 14, respectively. The volume of NS and TA injected into the nude mice was 0.1 mL. The control group received no injection and no light.

Western blot analysis

Mice were anesthetized using a 10% chloral hydrate solution, the keloid blocks were removed surgically and stored at −80°C for 21 days. The frozen keloid tissues were defrosted, homogenized in lysis buffer and centrifuged at 4°C for 20 min at 12,000 rpm to gather supernatants. Sodium lauryl sulfate loading buffer was used to lyse the cells for immunoblot and samples were stored at −80°C until use. The supernatants were exposed to electrophoresis. After the proteins were separated and transferred to polyvinylidene fluoride (PVDF) membranes, the membranes were blocked for 2 h with bovine serum albumin (BSA, 1% w/v). This was followed by incubation with primary antibodies against CD31 (ab222783; 1 : 2000; Abcam), CD34 (ab81289; 1 : 10000; Abcam), tumor growth factor β1 (TGF-β1; ab215715; 1 : 1000; Abcam), collagen 1 (ab34710; 1 : 2000; Abcam), and GAPDH (ab8245; 1 : 2000; Abcam) at 4°C for 12 h. After washing with PBS 3 times for 5 min, the membranes were incubated with Goat Anti-Rabbit lgG H&L (horseradish peroxidase (HRP); ab205718; 1 : 2000; Abcam) secondary antibody for 2 h at 4°C. A Chemi Doc XRS system (Bio-Rad) was used to visualize the proteins.

Statistical analysis

SPSS v. 19.0 (IBM Corp., Armonk, USA) and GraphPad Prism v. 7.0 (GraphPad Software, San Diego, USA) were used for the analyses; all data are presented as mean ± standard deviation (SD). Differences between the groups were determined using Student's t-test (for 2 groups) and one-way analysis of variance (ANOVA) for multiple groups. Bonferroni's correction was used for the post hoc comparisons. An alpha value of $p < 0.05$ was regarded as statistically significant.

Results

Ph1-PDT suppresses keloid fibroblast viability, invasion and migration

To investigate the impact of Ph1-PDT on keloid in vitro, we examined the effects of different concentrations of Ph1-PDT on the cell viability of keloid fibroblasts using a CCK-8 assay. The results indicated that cell viability was significantly reduced in the PDT groups with Ph1 treatments ($p < 0.05–0.001$) compared to the control DMEM group without Ph1-PDT treatment (Fig. 1A). The 1 μM and 3 μM Ph1 groups were used for further experiments. In addition, we explored the impact of Ph1-PDT on the invasion and migration of keloid fibroblasts using scratch and invasion assays. The results revealed that the cells in the 1 μM Ph1, 3 μM Ph1, and TA groups showed a significantly weaker wound healing ability compared to the control group ($p < 0.05–0.01$; Fig. 1B). Moreover, invasion assays revealed that the 3 μM Ph1 and TA groups showed a significantly weaker invasion capability compared to the control group ($p < 0.05–0.01$), while there was no significant difference between the 1 μM Ph1 group and the control (not significant (ns); Fig. 1C). These data indicates that Ph1-PDT markedly reduces the migration and invasion of keloid fibroblasts.

Effect of Ph1-PDT on keloid fibroblast apoptosis

The impact of Ph1-PDT on keloid fibroblast apoptosis was determined using flow cytometry. Our results showed that the rate of apoptosis was enhanced in the 1 μM group ($p < 0.05$, compared to the control), which was less significant than that observed for the 3 μM Ph1 and TA groups ($p < 0.01$, compared to the control, Fig. 2A,B). In addition, the mRNA expression of caspase-3 in keloid fibroblasts was determined using RT-qPCR, and was found to be significantly higher in the cells treated with 1 μM Ph1 ($p < 0.05$), 3 μM Ph1 ($p < 0.01$) or TA ($p < 0.01$), compared to the control group (Fig. 2C) These data demonstrate that Ph1-PDT treatment promotes apoptosis in keloid fibroblasts.

Effect of Ph1-PDT on growth and vessel density in keloid grafts

Keloid tissues were transplanted into nude mice and the impact of Ph1-PDT on the growth of keloid in vivo was examined. Following the transplant, the mice were treated with Ph1-PDT, NS or TA, or remained untreated, as outlined above. It was found that Ph1-PDT treatment significantly decreased the volume of the graft ($p < 0.01$; Fig. 3A). In addition, to evaluate the vessel density in keloid grafts, the protein expression of CD31 and CD34 were determined using western blot analysis. Results showed

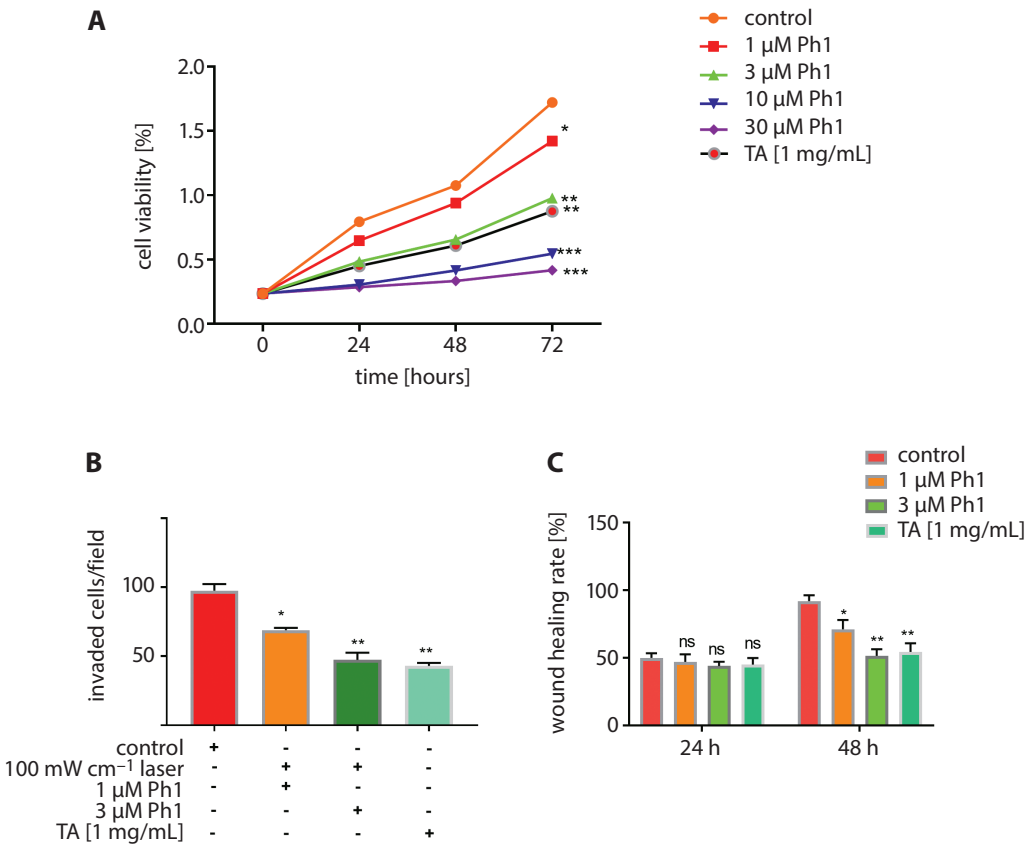

Fig. 1. Ph1-PDT suppressed keloid fibroblast viability, invasion and migration. A. CCK-8 assay was used to measure the viability of keloid fibroblast after different treatments; B. The number of migrated cells in keloid fibroblasts was determined using scratch migration assay; C. The wound healing rate of keloid fibroblast was detected after 24 h and 48 h. Compared the control group, which was treated with DMEM

*** $p < 0.001$; ** $p < 0.01$; * $p < 0.05$; ns – not significant.

that Ph1-PDT significantly reduced the protein expression of CD31 and CD34, implying that the vessel density was decreased by Ph1-PDT treatment in vivo ($p < 0.05–0.01$; Fig. 3B,C). Collectively, these data demonstrate that Ph1-PDT suppresses the growth and vessel density of keloid grafts in vivo.

Ph1-PDT inhibits the expression of TGF-β1 and collagen 1 in keloid fibroblasts and keloid grafts

Next, we determined the protein expression of TGF-β1 and collagen 1 in keloid fibroblasts and keloid grafts using western blot analysis. The results show that Ph1-PDT treatment significantly reduces the protein expression of TGF-β1 and collagen 1 both in vitro and in vivo ($p < 0.05–0.01$; Fig. 4A,B).

Effect of Ph1-PDT on inflammatory mediators in keloid grafts

Using ELISA assays and RT-qPCR, the 2 inflammatory modulators (IL-8 and IL-1β) were detected in the keloid grafts. The results revealed that Ph1-PDT treatment significantly reduces the protein concentration and the mRNA expression of IL-1β and IL-8 compared to the control (TA) group ($p < 0.01$; Fig. 5A,B).

Discussion

Keloid is characterized by the hyperproliferation of fibroblasts and excess collagen deposition due to an abnormal wound healing process after skin injury. Keloid acts like a tumor by invading the adjacent skin and spreading beyond the margins of the wound boundary.[21] Traditional therapies for keloids exhibit some drawbacks, including a high risk of palindromes, side effects and low efficacy.[22] Therefore, a more effective and safer technique for the treatment of keloid is urgently needed. The PDT, together with the photosensitizer 5-ALA, has previously been reported to induce apoptosis in fibroblasts and reduce the growth of a keloid graft.[23] It has also been observed previously that HMME-PDT treatment enhances the apoptosis rate of keloid fibroblasts.[23] In the current study, PDT and the photosensitizing agent Ph1 were investigated under different conditions and light powers both in vitro and in vivo.

Microvessel density is considered as a factor for angiogenesis and keloid maturation.[24] CD31 and CD34 are vascular endothelial markers and can be used as a reference for vessel density in differentiated endothelial cells,[25] as CD31 and CD34 promote angiogenesis and tumor growth.[26] A recent study demonstrated that the expression of CD31 and CD34 were inhibited by 5-ALA-mediated PDT in oral leukoplakia.[27] In the current study, it was observed that CD31 and CD34 protein expression were significantly decreased

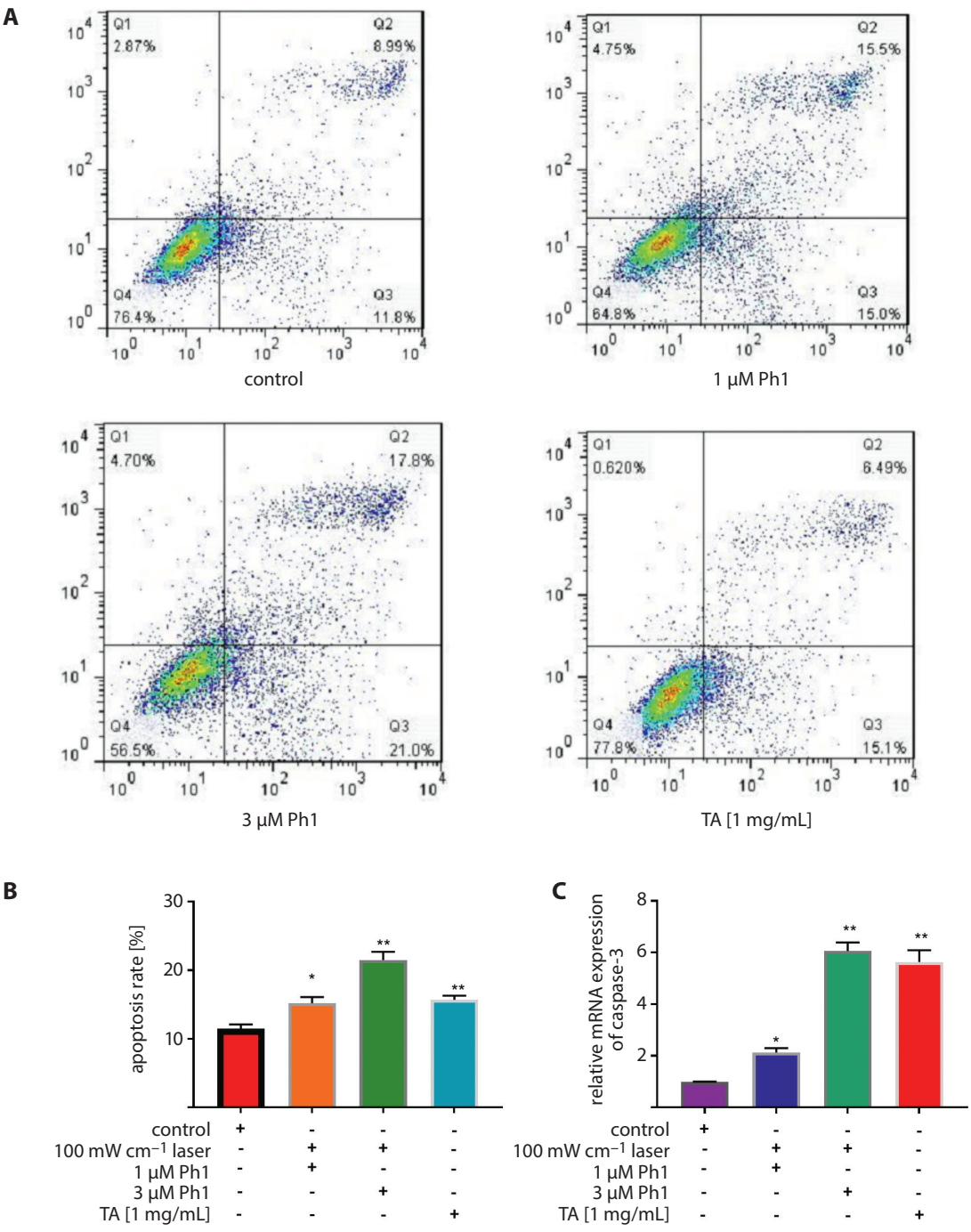

Fig. 2. Effect of Ph1-PDT on keloid fibroblast apoptosis. A and B. The rate of apoptosis of keloid fibroblasts was measured using flow cytometry after different treatments; C. RT-qPCR was used to determine the mRNA expression of caspase-3 in keloid fibroblasts after different treatments. Compared to the control group, which was treated with DMEM

*** $p < 0.001$; ** $p < 0.01$; * $p < 0.05$; ns – not significant.

and the volume of the keloid graft was reduced by Ph1-PDT treatment.

Previous work has shown that MPPa-PDT significantly reduces the invasion and migration of MCF-7 cells.[28] In addition, 5-ALA-PDT markedly suppresses cell migration and invasion in A431 cells by enhancing apoptosis in cutaneous squamous cell carcinoma.[29] It has also been reported that Ph1-PDT activates the apoptotic-related proteins caspase-3 and caspase-8, inducing cell apoptosis.[30] Interestingly, our findings showed that Ph1-PDT reduces keloid fibroblast migration and invasion, and promotes apoptosis. In combination with the abovementioned results, our findings suggest that Ph1-PDT might be a novel and efficient technique for keloid treatment.

The TGF-β1 is an important regulator in the progression of keloid due to its various biological functions in wound healing.[31] An earlier study elucidated the mechanism of 5-ALA-mediated PDT, and demonstrated that TGF-β1-mediated signaling and p53-related apoptosis might be an important factor for the treatment of hypertrophic scars.[32] The excessive accumulation of collagens (collagen 1 and collagen 3) and hypernomic development of fibroblasts are considered as the critical characteristics in the formation of keloid.[33] Our results showed

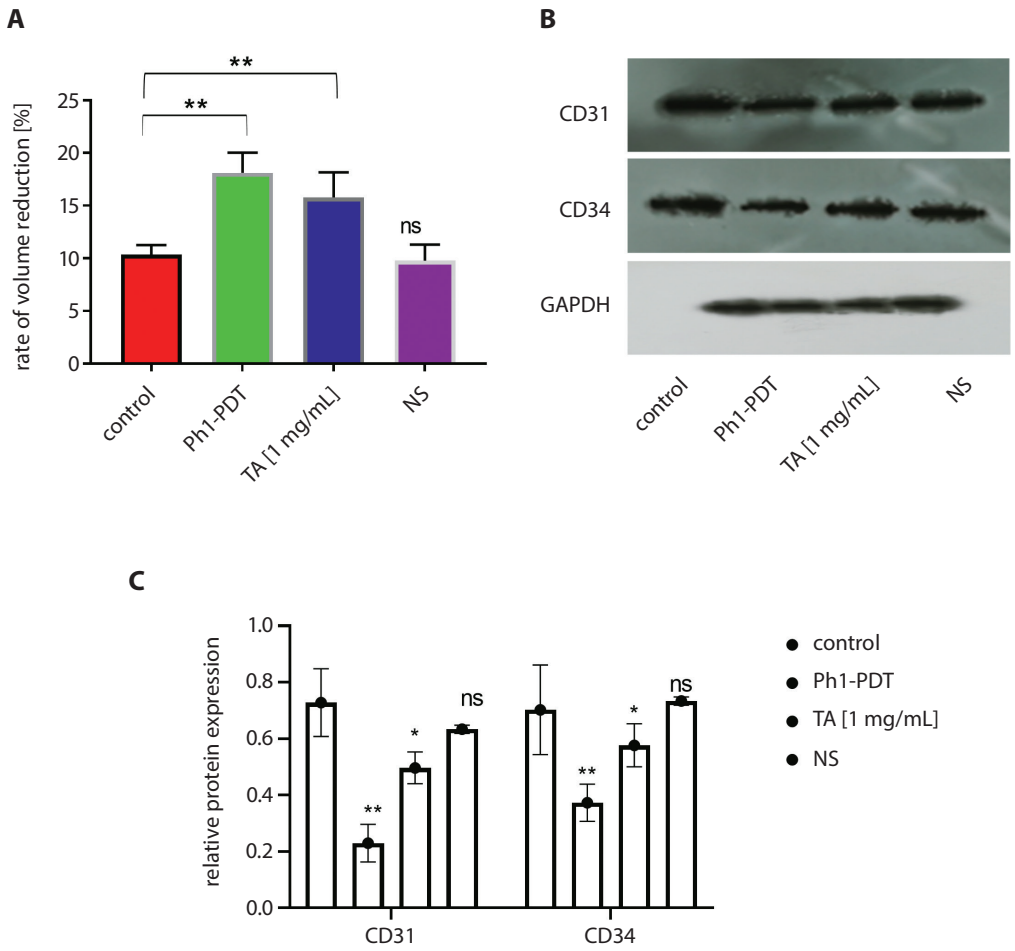

Fig. 3. Effect of Ph1-PDT on growth and vessel density in keloid grafts. A. The rate of keloid volume reduction was calculated based on that data collected by calipers in keloid graft. B and C. Western blot analysis was used to determine the protein expressions of CD31 and CD34 in keloid graft. Compared to control group in vivo, which was the group without treatment

*** $p < 0.001$; ** $p < 0.01$; * $p < 0.05$; ns – not significant.

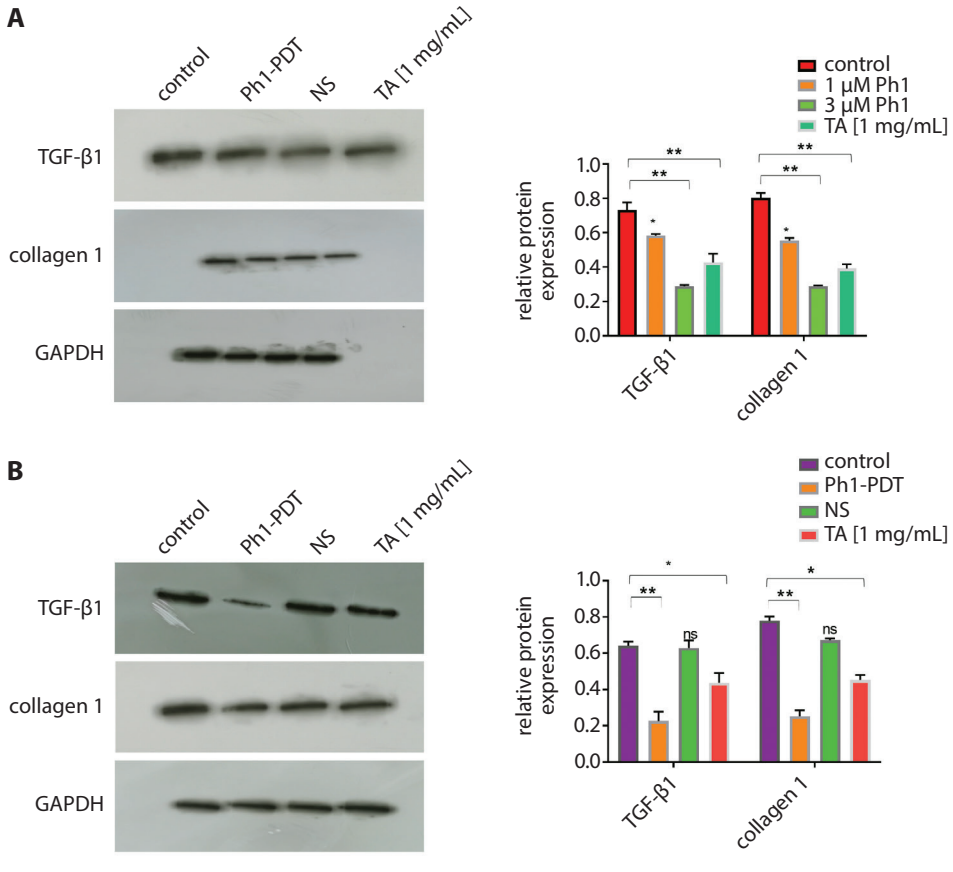

Fig. 4. Ph1-PDT inhibited the expression of TGF-β and collagen 1 in keloid fibroblasts and keloid graft. A and B. Western blot analysis was used to determine the protein expressions of TGF-β and collagen 1 in keloid fibroblasts and keloid graft after different treatments. Compared to control group in vivo, which was the group without treatment, and to control group in vitro, which was treated with DMEM

*** $p < 0.001$; ** $p < 0.01$; * $p < 0.05$; ns – not significant.

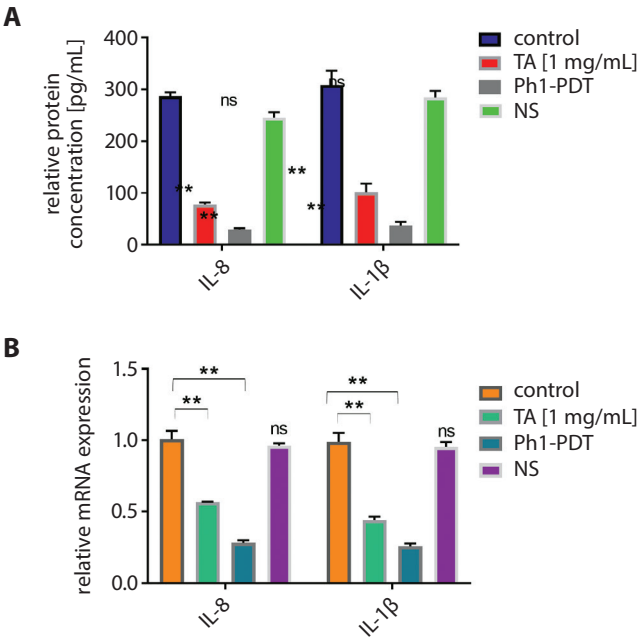

Fig. 5. Effect of Ph1-PDT on inflammatory mediators in keloid grafts: A and B. ELISA assay and RT-qPCR were used to determine the protein concentration and mRNA expression of IL-8 and IL-1β in keloid fibroblasts. Compared to control group in vivo, which was the group without treatment, and to control group in vitro, which was treated with DMEM

*** $p < 0.001$; ** $p < 0.01$; * $p < 0.05$; ns – not significant.

that Ph1-PDT downregulated the expression of TGF-β1 and collagen 1, indicating that Ph1-PDT dysregulated the TGF-β1/collagen 1 pathway involved the pathogenesis of keloid.

The basic healing process after PDT treatment is complex and dynamic, including biochemical, molecular and cellular actions that terminate in the re-development of impaired tissues.[23] Previous work has shown that the levels of pro-inflammatory cytokines (IL-6, IL-1β and IL-8) are markedly reduced after PDT in chronic periodontitis.[34] An earlier study has also observed the inhibition of inflammatory modulators (IL-6, IL-8 and tumor necrosis factor α (TNF-α)) after PDT in humans.[35] Furthermore, a study in an animal model of skin scars and striae distensae showed that pro-inflammatory cytokines were dramatically inhibited after PDT therapy.[36] Consistent with these previous studies, our findings demonstrate that Ph1-PDT significantly inhibits the protein concentration and the mRNA expression of the inflammatory cytokines IL-1β and IL-8 in keloid fibroblasts. Regardless of this, the suppression impact of PDT on keloid fibroblasts in lieu of inflammation stimulation was favorable for keloid treatment.

Limitations

Limitations of this study lie in the lack of further investigations into classical signaling pathways involved in this study.

Conclusions

The current study shows that Ph1-PDT inhibits keloid growth both in vitro and in vivo, suggesting that Ph1-PDT may potentially serve as a therapeutic strategy for keloid.

ORCID iDs

Wei Zheng https://orcid.org/0000-0001-6848-3537
Haiyan Wu https://orcid.org/0000-0002-0589-9663
Ying Li https://orcid.org/0000-0002-8247-7034
Helin Li https://orcid.org/0000-0002-4528-644X
Zhaojun Liu https://orcid.org/0000-0003-0419-7296
Yongzhi Nie https://orcid.org/0000-0003-0184-3846
Lingling Shi https://orcid.org/0000-0002-5506-746X
Hongyu Wang https://orcid.org/0000-0002-6657-8775

References

1. Kim SH, Jung SH, Chung H, et al. Annexin A2 participates in human skin keloid formation by inhibiting fibroblast proliferation. *Arch Dermatol Res*. 2014;306(4):347–357. doi:10.1007/s00403-014-1438-x
2. Smith OJ, McGrouther DA. The natural history and spontaneous resolution of keloid scars. *J Plast Reconst Aesthet Surg*. 2014;67(1):87–92. doi:10.1016/j.bjps.2013.10.014
3. Celli JP, Spring BQ, Rizvi I, et al. Imaging and photodynamic therapy: Mechanisms, monitoring, and optimization. *Chem Rev*. 2010;110(5):2795–2838. doi:10.1021/cr900300p
4. Kerwin LY, El Tal AK, Stiff MA, Fakhouri TM. Scar prevention and remodeling: A review of the medical, surgical, topical and light treatment approaches. *Int J Dermatol*. 2014;53(8):922–936. doi:10.1111/ijd.12436
5. McKeown SR, Hatfield P, Prestwich RJ, Shaffer RE, Taylor RE. Radiotherapy for benign disease: Assessing the risk of radiation-induced cancer following exposure to intermediate dose radiation. *Br J Radiol*. 2015;88(1056):20150405. doi:10.1259/bjr.20150405
6. Christensen E, Warloe T, Kroon S, et al. Guidelines for practical use of MAL-PDT in non-melanoma skin cancer. *J Eur Acad Dermatol Venereol*. 2010;24(5):505–512. doi:10.1111/j.1468-3083.2009.03430.x
7. Gu T, Cheng L, Gong F, et al. Upconversion composite nanoparticles for tumor hypoxia modulation and enhanced near-infrared-triggered photodynamic therapy. *ACS Appl Mater Interfaces*. 2018;10(18):15494–15503. doi:10.1021/acsami.8b03238
8. Maisch T. Anti-microbial photodynamic therapy: Useful in the future? *Lasers Med Sci*. 2007;22(2):83–91. doi:10.1007/s10103-006-0409-7
9. Alves E, Costa L, Carvalho CM, et al. Charge effect on the photoinactivation of Gram-negative and Gram-positive bacteria by cationic meso-substituted porphyrins. *BMC Microbiol*. 2009;9:70. doi:10.1186/1471-2180-9-70
10. Dougherty TJ, Gomer CJ, Henderson BW, et al. Photodynamic therapy. *J Natl Cancer Inst*. 1998;90(12):889–905. doi:10.1093/jnci/90.12.889
11. Kessel D, Oleinick NL. Cell death pathways associated with photodynamic therapy: An update. *Photochem Photobiol*. 2018;94(2):213–218. doi:10.1111/php.12857
12. Salmerón ML, Quintana-Aguiar J, De La Rosa JV, et al. Phenalenone-photodynamic therapy induces apoptosis on human tumor cells mediated by caspase-8 and p38-MAPK activation. *Mol Carcinog*. 2018;57(11):1525–1539. doi:10.1002/mc.22875
13. Foote CS. Definition of type I and type II photosensitized oxidation. *Photochem Photobiol*. 1991;54(5):659. doi:10.1111/j.1751-1097.1991.tb02071.x
14. Wang X, Li J, Li L, Li X. Photodynamic therapy-induced apoptosis of keloid fibroblasts is mediated by radical oxygen species in vitro. *Clin Lab*. 2015;61(9):1257–1266. doi:10.7754/clin.lab.2015.150222
15. Plaetzer K, Kiesslich T, Oberdanner CB, Krammer B. Apoptosis following photodynamic tumor therapy: Induction, mechanisms and detection. *Curr Pharm Des*. 2005;11(9):1151–1165. doi:10.2174/1381612053507648
16. Luna MC, Ferrario A, Wong S, Fisher AM, Gomer CJ. Photodynamic therapy-mediated oxidative stress as a molecular switch for the temporal expression of genes ligated to the human heat shock promoter. *Cancer Res*. 2000;60(6):1637–1644. PMID:10749134

17. Zheng Z, Zhu L, Zhang X, et al. RUNX3 expression is associated with sensitivity to pheophorbide a-based photodynamic therapy in keloids. *Lasers Med Sci*. 2015;30(1):67–75. doi:10.1007/s10103-014-1614-4
18. Song R, Feng Y, Wang D, Xu Z, Li Z, Shao X. Phytoalexin phenalenone derivatives inactivate mosquito larvae and root-knot nematode as type-II photosensitizer. *Sci Rep*. 2017;7:42058. doi:10.1038/srep42058
19. Späth A, Leibl C, Cieplik F, et al. Improving photodynamic inactivation of bacteria in dentistry: Highly effective and fast killing of oral key pathogens with novel tooth-colored type-II photosensitizers. *J Med Chem*. 2014;57(12):5157–5168. doi:10.1021/jm4019492
20. Chen AD, Chen RF, Li YT, et al. Triamcinolone acetonide suppresses keloid formation through enhancing apoptosis in a nude mouse model. *Ann Plast Surg*. 2019;83(4S Suppl 1):S50–S54. doi:10.1097/sap.0000000000002090
21. Jagadeesan J, Bayat A. Transforming growth factor beta (TGFbeta) and keloid disease. *Int J Surg*. 2007;5(4):278–285. doi:10.1016/j.ijsu.2006.04.007
22. Liu T, Ma X, Ouyang T, et al. Efficacy of 5-aminolevulinic acid-based photodynamic therapy against keloid compromised by downregulation of SIRT1-SIRT3-SOD2-mROS dependent autophagy pathway. *Redox Biol*. 2019;20:195–203. doi:10.1016/j.redox.2018.10.011
23. Cui X, Zhu J, Wu X, et al. Hematoporphyrin monomethyl ether-mediated photodynamic therapy inhibits the growth of keloid graft by promoting fibroblast apoptosis and reducing vessel formation. *Photochem Photobiol Sci*. 2020;19(1):114–125. doi:10.1039/c9pp00311h
24. Folkman J. Angiogenesis and breast cancer. *J Clin Oncol*. 1994;12(3):441–443. doi:10.1200/jco.1994.12.3.441
25. Poblet E, Gonzalez-Palacios F, Jimenez FJ. Different immunoreactivity of endothelial markers in well and poorly differentiated areas of angiosarcomas. *Virchows Arch*. 1996;428(4–5):217–221. doi:10.1007/bf00196693
26. Teo NB, Shoker BS, Jarvis C, Martin L, Sloane JP, Holcombe C. Vascular density and phenotype around ductal carcinoma in situ (DCIS) of the breast. *Br J Cancer*. 2002;86(6):905–911. doi:10.1038/sj.bjc.6600053
27. Rosin FC, Barcessat AR, Borges GG, Ferreira LG, Corrêa L. Vascular alterations after photodynamic therapy mediated by 5-aminolevulinic acid in oral leukoplakia. *Lasers Med Sci*. 2017;32(2):379–387. doi:10.1007/s10103-016-2127-0
28. Huang L, Lin H, Chen Q, Yu L, Bai D. MPPa-PDT suppresses breast tumor migration/invasion by inhibiting Akt-NF-κB-dependent MMP-9 expression via ROS. *BMC Cancer*. 2019;19(1):1159. doi:10.1186/s12885-019-6374-x
29. Chi YF, Qin JJ, Li Z, Ge Q, Zeng WH. Enhanced anti-tumor efficacy of 5-aminolevulinic acid-gold nanoparticles-mediated photodynamic therapy in cutaneous squamous cell carcinoma cells. *Braz J Med Biol Res*. 2020;53(5):e8457. doi:10.1590/1414-431x20208457
30. Zhuang S, Demirs JT, Kochevar IE. p38 mitogen-activated protein kinase mediates bid cleavage, mitochondrial dysfunction, and caspase-3 activation during apoptosis induced by singlet oxygen but not by hydrogen peroxide. *J Biol Chem*. 2000;275(34):25939–25948. doi:10.1074/jbc.M001185200
31. Lee TY, Chin GS, Kim WJ, Chau D, Gittes GK, Longaker MT. Expression of transforming growth factor beta 1, 2, and 3 proteins in keloids. *Ann Plast Surg*. 1999;43(2):179–184. PMID:10454326
32. Chang M, Ma X, Ouyang T, et al. Potential molecular mechanisms involved in 5-aminolevulinic acid-based photodynamic therapy against human hypertrophic scars. *Plast Reconstr Surg*. 2015;136(4):715–727. doi:10.1097/prs.0000000000001626
33. Lin L, Wang Y, Liu W, Huang Y. BAMBI inhibits skin fibrosis in keloid through suppressing TGF-β1-induced hypernomic fibroblast cell proliferation and excessive accumulation of collagen I. *Int J Clin Exp Med*. 2015;8(8):13227–13234. PMID:26550247
34. Luchesi VH, Pimentel SP, Kolbe MF, et al. Photodynamic therapy in the treatment of class II furcation: A randomized controlled clinical trial. *J Clin Periodontol*. 2013;40(8):781–788. doi:10.1111/jcpe.12121
35. Nesi-Reis V, Lera-Nonose D, Oyama J, et al. Contribution of photodynamic therapy in wound healing: A systematic review. *Photodiagnosis Photodyn Ther*. 2018;21:294–305. doi:10.1016/j.pdpdt.2017.12.015
36. Mendoza-Garcia J, Sebastian A, Alonso-Rasgado T, Bayat A. Ex vivo evaluation of the effect of photodynamic therapy on skin scars and striae distensae. *Photodermatol Photoimmunol Photomed*. 2015;31(5):239–251. doi:10.1111/phpp.12180

Standardization of the ultrasound examination of the masseter muscle with size-independent calculation of records

Krzysztof Gawriołek[1,A,C–E], Tomasz Klatkiewicz[1,A–D], Agnieszka Przystańska[1,C–E], Zofia Maciejewska-Szaniec[1,B–D], Tomasz Gedrange[2,A,C,E,F], Agata Czajka-Jakubowska[1,A,C,E,F]

[1] Department of Temporomandibular Disorders, Division of Prosthodontics, Poznan University of Medical Sciences, Poland
[2] Department of Dental Surgery, Wroclaw Medical University, Poland

A – research concept and design; B – collection and/or assembly of data; C – data analysis and interpretation; D – writing the article; E – critical revision of the article; F – final approval of the article

Advances in Clinical and Experimental Medicine, ISSN 1899–5276 (print), ISSN 2451–2680 (online) *Adv Clin Exp Med*. 2021;30(4):441–447

Address for correspondence
Krzysztof Gawriołek
k.gawriolek@gmail.com

Funding sources
None declared

Conflict of interest
None declared

Received on July 3, 2020
Reviewed on July 28, 2020
Accepted on November 11, 2020

Published online on April 29, 2021

Abstract

Background. As ultrasonography provides objective parameters and values, it is a reliable method of examining the structure and dimensions of the masseter muscle. Although the method is well known, there is no standardization in clinical examination and data analysis yet.

Objectives. The study aimed to measure masseter muscle thickness in designated areas to establish the most repeatable and clinically applicable method of ultrasound examination, and to assess differences in measurements in designated areas for clinical purposes by devising the size-independent parameter. The size-independent parameter may potentially be more clinically applicable than distance records, which are affected by the size of the subject.

Materials and methods. An ultrasound examination of 124 masseter muscles was performed. Axial examination in 3 horizontal regions (lower, middle and upper) and coronal examination in 2 vertical regions (proximal and distal) was carried out. Masseter muscle thickness was measured in every designated area when relaxed (muscle at rest (RMT)) and with clenched teeth (contracted muscle (CMT)). A morphological independent functional index of thickness difference (FITD) was calculated.

Results. The study revealed very high statistical differences between RMT and CMT ($p < 0.0001$) in all designated areas but with location variations. Masseter muscle thickness significantly differed depending on the examined area and transducer projection.

Conclusions. The ultrasound study showed that masseter muscle thickness significantly differs depending on the examined area. The authors emphasize the necessity to examine the masseter muscle in specified areas with both coronal and axial projections to achieve objective and repeatable examination. Notable clinical value is assigned to FITD, which is independent from the morphological dimensions of the muscle.

Key words: bruxism, tooth wear, masticatory muscles, masseter ultrasound measurements

Cite as
Gawriołek K, Klatkiewicz T, Przystańska A, Maciejewska-Szaniec Z, Gedrange T, Czajka-Jakubowska A. Standardization of the ultrasound examination of the masseter muscle with size-independent calculation of records. *Adv Clin Exp Med*. 2021;30(4):441–447. doi:10.17219/acem/130358

DOI
10.17219/acem/130358

Copyright
© 2021 by Wroclaw Medical University
This is an article distributed under the terms of the Creative Commons Attribution 3.0 Unported (CC BY 3.0) (https://creativecommons.org/licenses/by/3.0/)

Background

Ultrasound examination is considered to be useful for functional analysis of the masticatory organ[1,2] and diagnosis of alterations in the muscles of mastication.[3] It provides objective parameters and values; it is an effective, accurate, low-cost, and reliable method of examining the structure and dimensions of the masseter muscle.[4,5] The most often investigated parameter, because of its clinical value and ease of measurement, is masseter muscle thickness. Several ultrasound assessments of masseter muscle thickness in healthy individuals have been published.[5–8] The morphology of the muscle revealed a large variation in masseter muscle thickness among adult individuals during both relaxed and contracted conditions.[5] Moreover, significant positive correlations between masseter muscle thickness and some morphological features (i.e., anterior and posterior total face height, vertical jaw length, mandibular ramus height, mandibular length, mandibular inclination) were observed. Also, significant negative correlations with mandibular plane angle and gonial angle were observed.[9,10] It was also proved that masseter muscle thickness influences the growth of the jaws.[11]

The relation between masseter muscle thickness and clinical findings was proven in numerous studies. Some ultrasound studies were concerned with masseter muscle thickness in relation to dental procedures such as diagnostics and treatment of temporomandibular disorders (TMD),[12] oral submucous fibrosis,[13,14] prosthetic treatment,[15–18] and orthodontic treatment,[19] as well as general clinical findings (i.e., sarcopenia[20] and osteoporosis[21]). It was also believed that muscle thickness is an indicator of muscle function. Its significant correlation to bite force and occlusal tooth contact has been reported.[9]

Although attempts were made to introduce ultrasonography as a routine diagnostic procedure in TMD, the methodological aspects of the examination are unclear and not standardized.[22] A clear explanation of the examination method or description of the examined region was very rare. Some studies present no relation to examined and measured location, thus not taking under consideration masseter morphological differences in thickness. Others do not specify muscle activity or examine the masseter only at rest or contraction. There is also lack of studies describing differences in clinical ultrasound records at coronal and axial projections. Most current studies present examination using only 1 projection, with no explanation of the advantages of the chosen projection. No paper has presented relationships between the measurements taken and body size.

Our previous review[22] showed that there are no standards and population normal values. The need for standardization of methods and parameters has been previously reported.[7] It is believed that various factors can affect the accuracy of measurements of the masseter muscle, with even the use of different conduits a possible cause of inconsistent results.[23]

Objectives

In this paper, the authors attempted to present a method of standardization of masseter ultrasound examination for clinical needs, with specific regard to the dimensions of the studied muscle and how the examination protocol may affect clinical judgment. Thus, the aim of this ultrasound study was: 1) to establish the most repeatable and clinically applicable method of ultrasound examination of the masseter muscle; and 2) to assess differences in measurements in designated areas for clinical purposes by devising the size-independent parameter that potentially may be more clinically applicable than distance records.

Materials and methods

The study protocol was approved by the local university Bioethics Committee of Poznan University of Medical Sciences. It involved investigation of 80 consecutive asymptomatic participants who volunteered for the study by responding to an invitation (random volunteerns recruited verbally). The participants gave their written informed consent prior to participation in the study. The inclusion criteria were as follows: age 20–30 years, full dentition (except third molars) and no previous TMD treatment. Exclusion criteria were: no referred symptoms of TMDs in the patient's history (e.g., pain from the temporomandibular joint (TMJ) region, movement restriction, muscle weakness, or joint sounds (clicks) (DC/TMD II and III group), radiological and clinical signs of TMJ disc dislocation without reduction or degenerative joint disorders, tooth wear (according to tooth wear index (TWI)), prosthetic reconstructions, or the presence of a systemic disease (e.g., rheumatic or degenerative disease, systemic connective tissue disorders, myasthenia gravis).

All participants were examined with the Diagnostic Criteria for Temporomandibular Disorders (DC/TMD) form.[24] According to this protocol, 62 consecutive patients qualified for the study (30 men and 32 women). The average age of the patients was 25.4 years. Each individual underwent bilateral ultrasound examination of the masseter muscles. The muscles were examined with the Aloka-Hitachi F37 USG device with 12 MHz linear probe (Aloka-Hitachi, Tokyo, Japan). To achieve the most repeatable examination protocol, the muscle was virtually divided into 3 horizontal regions (lower, middle and upper) and 2 vertical regions (proximal and distal). The axial and coronal ultrasound examinations were carried out in the horizontal and vertical regions, respectively. The thickness of the masseter muscle was measured in every designated area when relaxed (muscle at rest (RMT)), with individuals resting comfortably and associated muscles in a state of minimal contractual activity, and with clenched teeth (contracted muscle (CMT)) in maximal intercuspal position (Fig. 1–3).

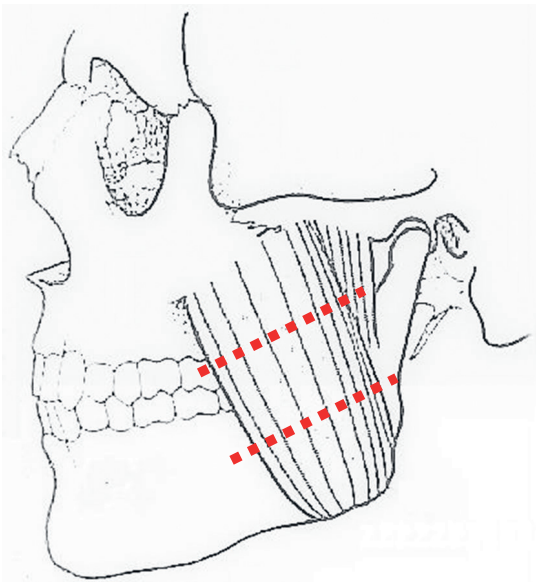

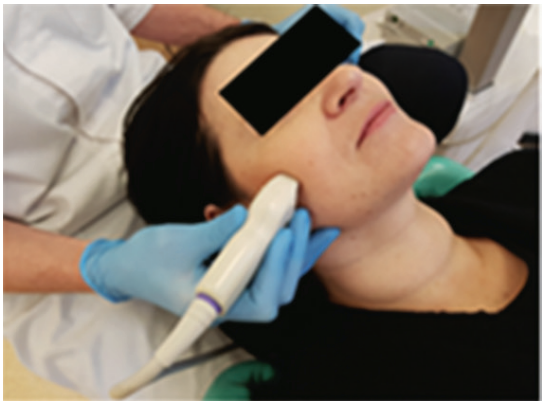

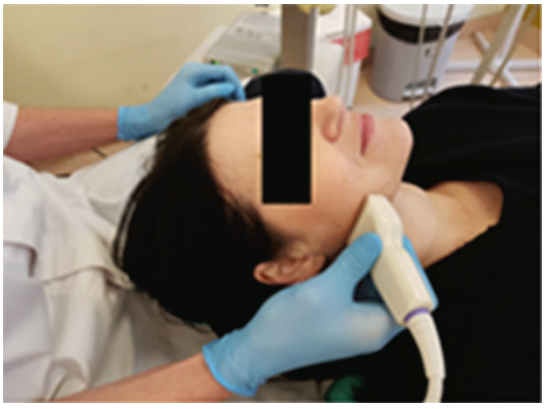

Fig. 1. Schematic diagram of the division into horizontal examination areas (upper, middle and lower), with the example of examination

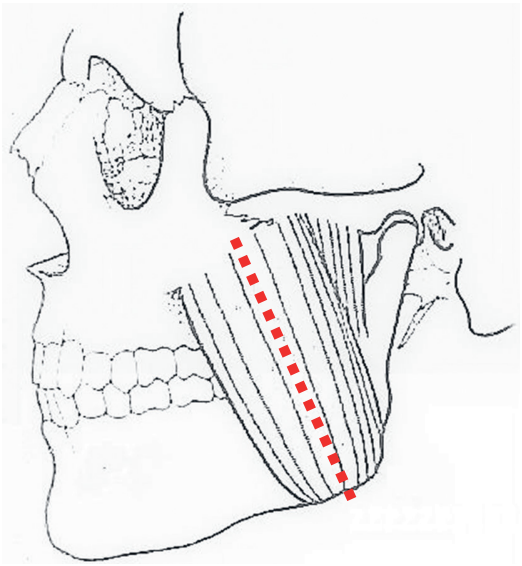

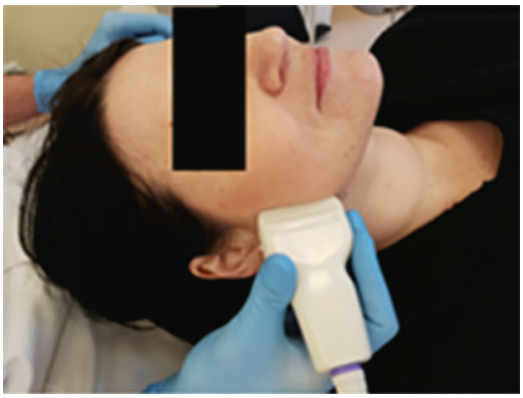

Fig. 2. Schematic diagram of the division to vertical examination areas (upper, middle and lower), with the example of examination

Two examiners were responsible for the recruitment and dental and ultrasound examination of the patients. Each patient was examined independently by both examiners. The measurements were taken 3 times and the mean results were used for the analysis.

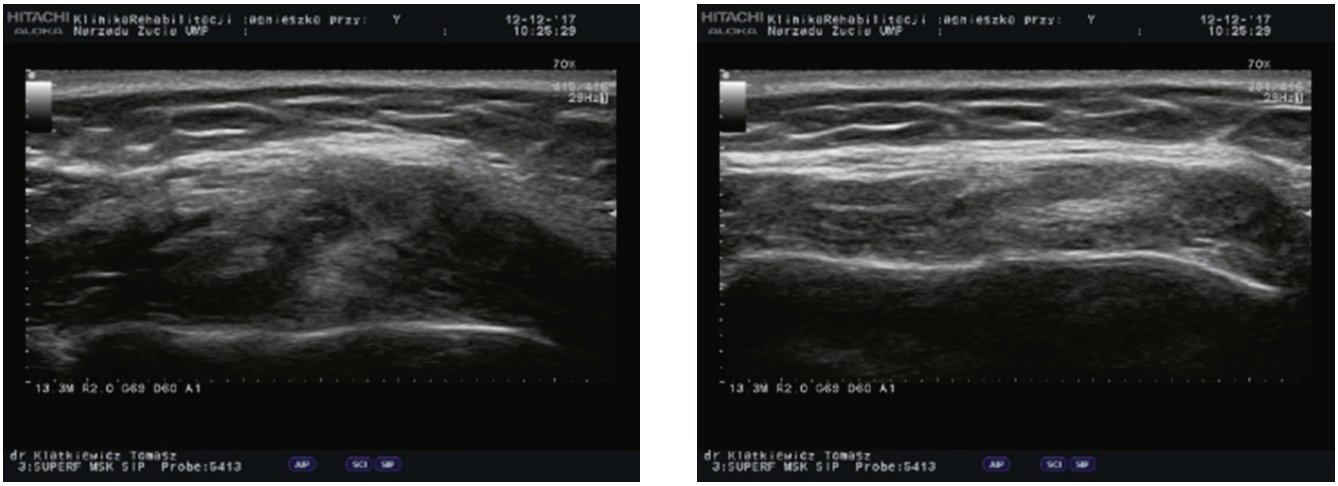

Fig. 3. Ultrasound image at relaxed muscle (RMT) (A) and clenched position (CMT) (B)

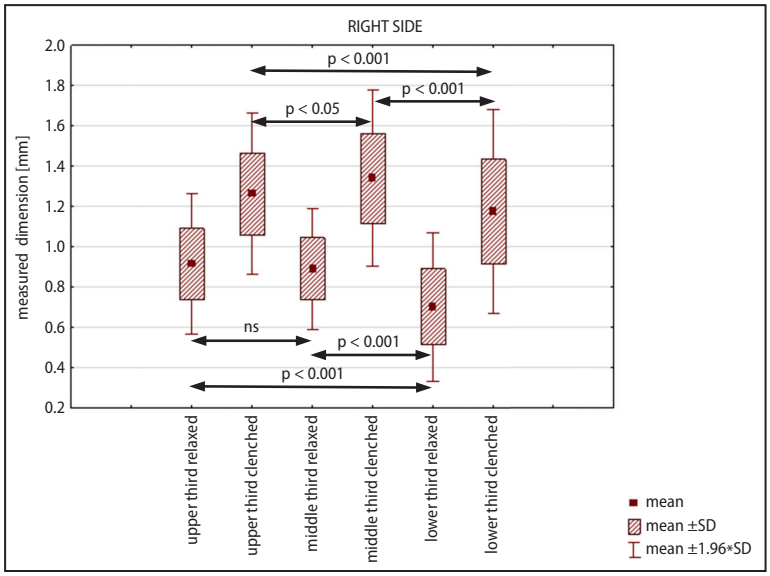

Fig. 4. Statistical imaging of ultrasound measurements at upper, middle and lower areas of masseter at RMT and CMT records, with the p-level on the right side

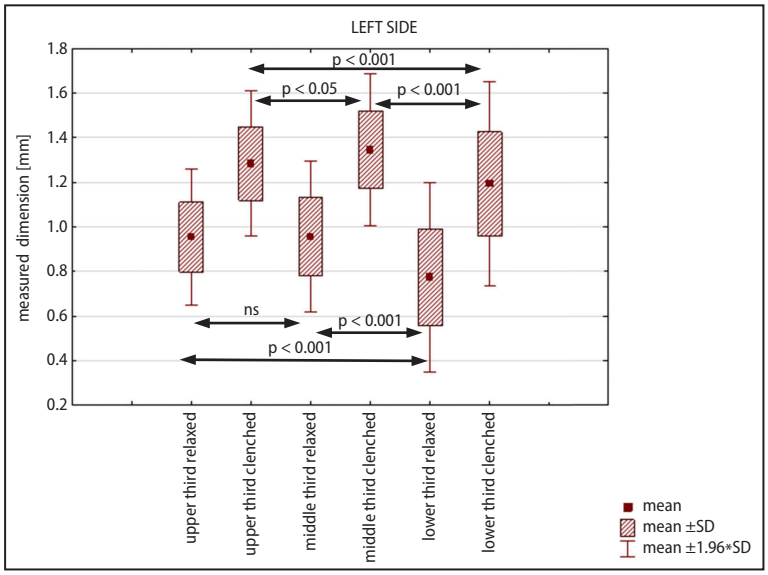

Fig. 5. Statistical imaging of ultrasound measurements at upper, middle and lower areas of masseter at RMT and CMT records, with the p-level on the left side

The authors' original method of calculations included the functional index of thickness difference (FITD). The index was devised to show the change in masseter muscle thickness between contraction and relaxation with no relation to muscle size. It was calculated as the quotient of the difference in values between CMT and RMT.

Data were analyzed using STATISTICA PL v. 12.0 (StatSoft Poland, Kraków, Poland). The analyzed variables expressed in the quantitative scale were presented using the number (N), mean, median, minimum and maximum value, lower and upper quartile, and standard deviation (SD). The Shapiro–Wilk test was used to test the distribution of analyzed variables. Because the analyzed variables significantly differed from the normal distribution, non-parametric tests were applied. The Friedman's test with a post hoc test (Dunn's test) was used to analyze the differences of investigated variables in relation to the muscle thickness examination region (upper, middle or lower), and the Wilcoxon's test was used to test for differences between investigated variables in relation to the masseter muscle thickness examination region (distal or proximal). The analysis was performed for the right and the left side. The assumed significance level was $p < 0.05$.

Results

The data obtained from every examined area were compared to other areas in the coronal and axial projections. The Friedman's test (axial projection) and Wilcoxon's test (coronal projection) showed statistically significant differences between most of the analyzed areas. No statistically significant differences were found

Table 1. The masseter muscle thickness [mm] measured in different regions of the muscle (n = 62)

Examination position/ region/side	Mean	Median	Min	Max	SD	Mean	Median	Min	Max	SD
	right side					left side				
RMT upper third	0.91	0.91	0.56	1.36	0.18	0.95	0.94	0.62	1.34	0.16
RMT middle third	0.89	0.89	0.57	1.22	0.15	0.96	0.95	0.57	1.52	0.17
RMT lower third	0.70	0.67	0.44	1.18	0.19	0.78	0.75	0.42	1.75	0.22
RMT proximal	1.00	1.01	0.62	1.30	0.16	1.03	1.03	0.70	1.35	0.16
RMT distal	0.96	0.95	0.57	1.31	0.18	0.97	0.95	0.57	1.28	0.17
CMT upper third	1.26	1.25	0.78	1.68	0.20	1.28	1.29	0.90	1.64	0.16
CMT middle third	1.34	1.33	0.94	1.99	0.22	1.34	1.33	0.93	1.73	0.17
CMT lower third	1.18	1.15	0.68	1.83	0.26	1.19	1.18	0.76	1.83	0.23
CMT proximal	1.42	1.43	0.97	1.89	0.21	1.43	1.44	1.09	1.79	0.18
CMT distal	1.32	1.37	0.82	1.70	0.22	1.34	1.35	0.97	1.78	0.21

RMT – rested muscle thickness; CMT – contracted muscle thickness; SD – standard deviation.

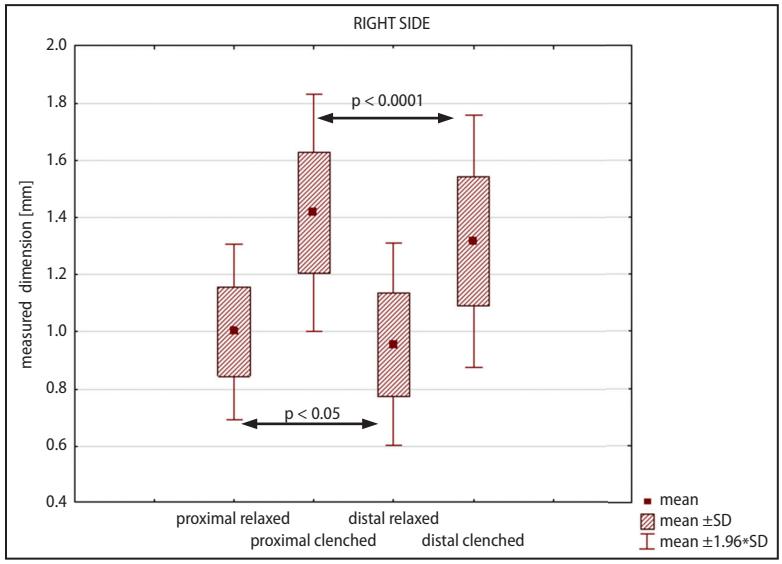

Fig. 6. Statistical imaging of ultrasound measurements at proximal and distal areas of masseter at RMT and CMT records, with the p-level on the right side

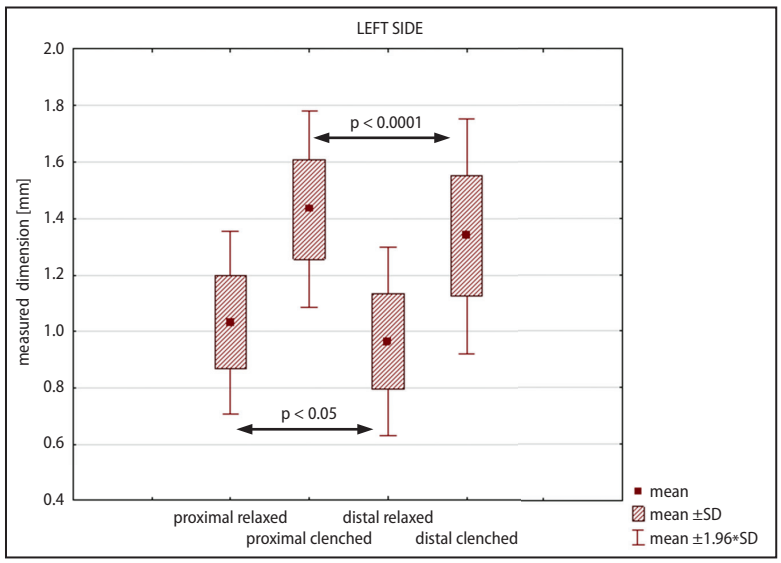

Fig. 7. Statistical imaging of ultrasound measurements at proximal and distal areas of masseter at RMT and CMT records, with the p-level on the left side

between masseter muscle thickness measured in the upper and middle areas during relaxation. No statistically significant differences were found between left and right sides or between males and females ($p > 0.05$). Expected morphological differences were found at ultrasound records. Clinically, the minimum mean masseter muscle thickness was recorded in the lower third of the muscle at rest (0.74 ±0.2 mm) and the maximum mean in the proximal part of contracted muscle (1.42 ±0.2 mm). The recorded masseter muscle thickness measurements are presented in Table 1.

The ultrasound study revealed very high ($p < 0.0001$) or high ($p < 0.001$) statistical differences between RMT and CMT in most designated areas. Only RMT measurement differences between upper and middle areas revealed no statistical difference, while the difference of proximal compared to distal region was significant at $p < 0.05$ (Fig. 4–7).

The difference between CMT and RMT was most significant in the lower third of the muscle. The greatest increase in recorded dimensions during contraction was found at the lower (54%) and anterior (41%) regions of the muscle. The results revealed that the difference between CMT and RMT results in higher statistical and clinical meaning than a single measurement. This emphasizes the meaning of the FITD calculation, which describes functional status and is not a size-relative diagnosis.

Discussion

The presented study recorded average results of 9.15 ±1.6 mm and 13.1 ±1.9 mm for RMT and CMT, respectively, with no significant

differences between the right and the left side or between women and men.

The results are in agreement with 2 previous ultrasound studies,[6,25] where no dimensional differences in the masseter muscle between women and men were observed. However, other studies showed significantly greater masseter muscle thickness in men than in women in both relaxed and contracted states.[11,26] In another study,[5] authors observed that masseter muscle thickness in women during both relaxed and contracted conditions was significantly lesser than in men. They also concluded that masseter muscle thickness during contraction in women was significantly related to body weight and body constitution.

The dimensions of the masseter muscle obtained in the present study are similar to those previously reported. Recorded mean contracted masseter muscle thickness was 15.1 ±1.9 mm in men and 13.0 ±1.8 mm in women.[5] Another study[24] reported masseter muscle thickness as 13.3 ±1.4 mm in men and 10.9 ±1.3 mm in women (when relaxed), and 15.5 ±1.8 mm in men and 13.0 ±1.2 mm in women (when contracted). A different study[9] examined only women and measured masseter muscle thicknesses from 8.83 mm to 11.08 mm with the muscle relaxed, and from 9.84 mm to 12.57 mm during contraction. An investigation of the thickness during contraction in 252 individuals[27] revealed an average of 12.3 ±2.7 mm.

In the present study, the maximum value of the masseter muscle thickness was recorded in the middle third of the contracted muscle. When both contracted and relaxed, the muscle was thickest in the middle region and thinnest in the lower region. When divided vertically, the proximal region was found to be thicker than the distal one in both contracted and relaxed muscles. Moreover, the greatest difference between RMT and CMT was found in the lower region of the muscle. These findings are in agreement with another study[26] where the thickest part of the masseter was recorded in the area between the inferior border of the mandible and the virtual line drawn from the angle of the mouth to the ear lobe.

These results encourage consideration of the anatomical and functional organization of the masseter muscle. Two parts of the muscle (superficial and deep) are commonly distinguished, but 3 well-differentiated parts (superficial, intermediate and deep) have been also reported.[28] A different study[29] showed no evidence for further subdivision of the superficial part into anterior, middle and posterior regions, contrary to an earlier report[30] where the authors proved that the anterior fibers were considerably longer (35%) than the posterior fibers. Apparently, a difference in fiber length may be evidence for muscle organization into anterior and posterior parts. This finding was a highly significant result in this study.

Surprisingly, the use of FITD allowed for different results. The analysis of all parameters with the difference between RMT and CMT revealed high statistical significance. The FITD seems to be clinically more objective than regular measurements of muscle dimensions that can present wide differences relative to the size of the subject. The FITD is thought to be independent from muscle thickness and describes functional increases in muscle dimensions. It correlates strongly with the location of the ultrasound measurement. The clinician must be aware of the fact that a single measurement, particularly in relaxed muscle position, may not reveal hypothetical pathology of muscle thickness as strongly as an increase in the difference between RMT and CMT.

The authors proved that the region of examination and the position of the probe influenced the final result of the measurement. The statistically significant differences were observed between series of measurements in different areas. Our results did not allow the best position for examination to be indicated.

Recently, other ultrasound techniques, such as elastography, have been introduced.[31] This method potentially allows assessment of not only morphological or functional changes in dimensions but also function of the muscle fibers. However, this method is still under investigation for improved diagnosis of TMD and for monitoring the effects of management.

The ultrasound examination is cost-effective, repeatable (unlike electromyography (EMG)), free from contraindications (unlike magnetic resonance imaging (MRI)), and more objective than clinical examination because it does not reflect the patient's self-reported data. The presented protocol emphasizes clinical use, makes it reliable for functional diagnostics, and enables objective examination of muscle strength and muscle bilateral symmetry. We are convinced that the authors' original method of examination standardizes the clinical protocol, and allows objective comparison of the population. The presented FITD calculation allows size-independent data to be recorded and can be easily introduced into clinical examination. Further studies describing the relationship of FITD to clinical disorders seem to be needed in the future.

Limitations

This method could include age- and weight-related statistics as well as occlusion related morphological relations in masseter US findings.

Conclusions

The ultrasound study showed that masseter muscle thickness significantly differs depending on the examined area. The authors emphasize the necessity to examine the masseter muscle in specified areas with both coronal and axial projections to achieve objective and repeatable examination. Notable clinical value is assigned to FITD, which is independent from morphological dimensions of the muscle.

ORCID iDs

Krzysztof Gawriołek https://orcid.org/0000-0002-2590-2372
Tomasz Klatkiewicz https://orcid.org/0000-0002-4994-7612
Agnieszka Przystańska https://orcid.org/0000-0003-0012-9819
Zofia Maciejewska-Szaniec https://orcid.org/0000-0002-1965-0498
Tomasz Gedrange https://orcid.org/0000-0002-3551-6467
Agata Czajka-Jakubowska https://orcid.org/0000-0002-1692-2910

References

1. Busato A, Balconi G, Vismara V, Bertelè L, Tonti G, Pedrizzetti G. Strain analysis of masseter muscle by ultrasound. *J Biol Regul Homeost Agents*. 2015;29(3 Suppl 1):74–81. PMID:26511184
2. Busato A, Balconi G, Vismara V, Bertelè L, Garo G, De Gregorio D. Ultrasound and analysis of the deformation patterns of the masseter muscle: Comparing surgical anatomy, ultrasound and functional anatomy. *Oral Implantol (Rome)*. 2017;9(Suppl 1/2016 to N 4/2016):28–37. doi:10.11138/orl/2016.9.1S.028
3. Serra MD, Duarte Gavião MB, dos Santos Uchôa MN. The use of ultrasound in the investigation of the muscles of mastication. *Ultrasound Med Biol*. 2008;34(12):1875–1884. doi:10.1016/j.ultrasmedbio.2008.05.009
4. Dimova-Gabrovska M, Dimitrova D. Ultrasound diagnostic of musculus masseter. *Journal of IMAB*. 2017;23(2):1611–1615. doi:10.5272/jimab.2017232.1611
5. Kiliaridis S, Kalebo P. Masseter muscle thickness measured by ultrasonography and its relation to facial morphology. *J Dent Res*. 1991;70(9):1262–1265. doi:10.1177/00220345910700090601
6. Prabhu NT, Munshi AK. Measurement of masseter and temporalis muscle thickness using ultrasonographic technique. *J Clin Pediatr Dent*. 1994;19(1):41–44. PMID:7865422
7. Reis Durão AP, Morosolli A, Brown J, Jacobs R. Masseter muscle measurement performed by ultrasound: A systematic review. *Dentomaxillofac Radiol*. 2017;46(6):20170052. doi:10.1259/dmfr.20170052
8. Naser-ud-Din S, Thoirs K, Sampson WJ. Ultrasonography, lateral cephalometry and 3D imaging of the human masseter muscle. *Orthod Craniofac Res*. 2011;14(1):33–43. doi:10.1111/j.1601-6343.2010.01505.x
9. Bakke M, Tuxen A, Vilmann P, Jensen BR, Vilmann A, Toft M. Ultrasound image of human masseter muscle related to bite force, electromyography, facial morphology, and occlusal factors. *Scand J Dent Res*. 1992;100(3):164–171. doi:10.1111/j.1600-0722.1992.tb01734.x
10. Rani S, Ravi MS. Masseter muscle thickness in different skeletal morphology: An ultrasonographic study. *Indian J Dent Res*. 2010;21(3):402–407. doi:10.4103/0970-9290.70812
11. Tircoveluri S, Singh JR, Rayapudi N, Karra A, Begum M, Challa P. Correlation of masseter muscle thickness and intermolar width: An ultrasonography study. *J Int Oral Health*. 2013;5(2):28–34. PMID:24155588
12. Aldemir K, Üstüner E, Erdem E, Demiralp AS, Oztuna D. Ultrasound evaluation of masseter muscle changes in stabilization splint treatment of myofascial type painful temporomandibular diseases. *Oral Surg Oral Med Oral Pathol Oral Radiol*. 2013;116(3):377–383. doi:10.1016/j.oooo.2013.06.011
13. Chakarvarty A, Panat SR, Sangamesh NC, Aggarwal A, Jha PC. Evaluation of masseter muscle hypertrophy in oral submucous fibrosis patients: An ultrasonographic study. *J Clin Diagn Res*. 2014;8(9):ZC45–ZC47. doi:10.7860/JCDR/2014/8892.4857
14. Kant P, Bhowate RR, Sharda N. Assessment of cross-sectional thickness and activity of masseter, anterior temporalis and orbicularis oris muscles in oral submucous fibrosis patients and healthy controls: An ultrasonography and electromyography study. *Dentomaxillofac Radiol*. 2014;43(3):20130016. doi:10.1259/dmfr.20130016
15. Bhoyar PS, Godbole SR, Thombare RU, Pakhan AJ. Effect of complete edentulism on masseter muscle thickness and changes after complete denture rehabilitation: An ultrasonographic study. *J Investig Clin Dent*. 2012;3(1):45–50. doi:10.1111/j.2041-1626.2011.0088.x
16. Müller F, Hernandez M, Grütter L, Aracil-Kessler L, Weingart D, Schimmel M. Masseter muscle thickness, chewing efficiency and bite force in edentulous patients with fixed and removable implant-supported prostheses: A cross-sectional multicenter study. *Clin Oral Implants Res*. 2012;23(2):144–150. doi:10.1111/j.1600-0501.2011.02213.x
17. Sathasivasubramanian S, Venkatasai PM, Divyambika CV, et al. Masseter muscle thickness in unilateral partial edentulism: An ultrasonographic study. *J Clin Imaging Sci*. 2017;7:44. doi:10.4103/jcis.JCIS_50_17
18. Schimmel M, Loup A, Duvernay E, Gaydarov N, Muller F. The effect of mandibular denture abstention on masseter muscle thickness in a 97-year-old patient: A case report. *Int J Prosthodont*. 2010;23(5):418–420. PMID:20859556
19. Trawitzki LV, Dantas RO, Elias-Júnior J, Mello-Filho FV. Masseter muscle thickness three years after surgical correction of class III dentofacial deformity. *Arch Oral Biol*. 2011;56(8):799–803. doi:10.1016/j.archoralbio.2011.01.012
20. Umeki K, Watanabe Y, Hirano H, et al. The relationship between masseter muscle thickness and appendicular skeletal muscle mass in Japanese community-dwelling elders: A cross-sectional study. *Arch Gerontol Geriatr*. 2018;78:18–22. doi:10.1016/j.archger.2018.05.014
21. Vasconcelos PB, de Sousa LG, Regalo SC, et al. The influence of maxillary and mandibular osteoporosis on maximal bite force and thickness of masticatory muscles. *Acta Odontol Latinoam*. 2015;28(1):22–27. doi:10.1590/S1852-48342015000100003
22. Klatkiewicz T, Gawriołek K, Pobudek-Radzikowska M, Czajka-Jakubowska A. Ultrasonography in the diagnosis of temporomandibular disorders: A meta-analysis. *Med Sci Monit*. 2018;24:812–817. doi:10.12659/msm.908810
23. Oliveira J, Filho M, Melo T, Lima N, Filho M, Silva H. Evidence of measures of normalcy for thickness of masseter muscle evaluated with ultrasound. *Revista CEFAC: actualização científica em fonoaudiologia*. 2015;17(1):238–252. https://doi.org/10.1590/1982-021620150514
24. Schiffman E, Ohrbach R, Truelove E, et al; International RDC/TMD Consortium Network; International Association for Dental Research; Orofacial Pain Special Interest Group; International Association for the Study of Pain. Diagnostic Criteria for Temporomandibular Disorders (DC/TMD) for clinical and research applications: Recommendations of the International RDC/TMD Consortium Network and Orofacial Pain Special Interest Group. *J Oral Facial Pain Headache*. 2014;28(1):6–27. doi:10.11607/jop.1151
25. Pereira LJ, Gavião MB, Bonjardim LR, Castelo PM, van der Bilt A. Muscle thickness, bite force, and craniofacial dimensions in adolescents with signs and symptoms of temporomandibular dysfunction. *Eur J Orthod*. 2007;29(1):72–78. doi:10.1093/ejo/cjl055
26. Strini PJ, Strini PJ, de Sousa Barbosa T, Gavião MB. Assessment of thickness and function of masticatory and cervical muscles in adults with and without temporomandibular disorders. *Arch Oral Biol*. 2013;58(9):1100–1108. doi:10.1016/j.archoralbio.2013.04.006
27. Xie Y, Zhou J, Li H, Cheng C, Herrler T, Li Q. Classification of masseter hypertrophy for tailored botulinum toxin type A treatment. *Plast Reconstr Surg*. 2014;134(2):209e–218e. doi:10.1097/PRS.0000000000000371
28. Gaudy JF, Zouaoui A, Bravetti P, Charrier JL, Guettaf A. Functional organization of the human masseter muscle. *Surg Radiol Anat*. 2000;22(3–4):181–190. doi:10.1007/s00276-000-0181-5
29. Zwijnenburg AJ, Lobbezoo F, Kroon GW, Naeije M. Mandibular movements in response to electrical stimulation of superficial and deep parts of the human masseter muscle at different jaw positions. *Arch Oral Biol*. 1999;44(5):395–401. doi:10.1016/s0003-9969(99)00016-3
30. van Eijden TM, Raadsheer MC. Heterogeneity of fiber and sarcomere length in the human masseter muscle. *Anat Rec*. 1992;232(1):78–84. doi:10.1002/ar.1092320109
31. Olchowy A, Wieckiewicz M, Winocur E, et al. Great potential of ultrasound elastography for the assessment of the masseter muscle in patients with temporomandibular disorders: A systematic review. *Dentomaxillofac Radiol*. 2020;49(8):20200024. doi:10.1259/dmfr.20200024

Is home-based therapy in Fabry disease the answer to compelling patients' needs during the COVID-19 pandemic? Survey results from the Polish FD Collaborative Group

Mariusz Kusztal[1,A–D], Mariusz Kłopotowski[2,A,B,F], Stanisława Bazan-Socha[3,A,C,E], Beata Błażejewska-Hyżorek[4,B,C,E], Krzysztof Pawlaczyk[5,6,A,E,F], Andrzej Oko[5,E,F], Magdalena Krajewska[1,E,F], Michał Nowicki[7,A,B,E,F]

[1] Department of Nephrology and Transplantation Medicine, Wroclaw Medical University, Poland
[2] Department of Interventional Cardiology and Angiology, Institute of Cardiology, Warszawa, Poland
[3] Department of Internal Medicine, Jagiellonian University Medical College, Kraków, Poland
[4] 2nd Department of Neurology, Institute of Psychiatry and Neurology, Warszawa, Poland
[5] Department of Nephrology, Transplantology, and Internal Diseases, Poznan University of Medical Sciences, Poland
[6] Department of Nephrology, University Hospital of Karol Marcinkowski, Zielona Góra, Poland
[7] Department of Nephrology, Hypertension, and Kidney Transplantation, Medical University of Lodz, Poland

A – research concept and design; B – collection and/or assembly of data; C – data analysis and interpretation; D – writing the article; E – critical revision of the article; F – final approval of the article

Advances in Clinical and Experimental Medicine, ISSN 1899–5276 (print), ISSN 2451–2680 (online) *Adv Clin Exp Med*. 2021;30(4):449–454

Address for correspondence
Mariusz Kusztal
E-mail: mariusz.kusztal@umed.wroc.pl

Funding sources
None declared

Conflict of interest
The following authors declare potential conflict of interest: M.K. – consultation fees/speaker fees from Sanofi Genzyme and Takeda/Shire; B. B-H. – consultation fees/speaker fees from Sanofi Genzyme and Takeda/Shire; M.N. – consultation fees/speaker fees from Sanofi Genzyme, Takeda/Shire, symposium fee from Amicus. The other authors declare no conflict of interest.

Received on December 14, 2020
Reviewed on December 15, 2020
Accepted on December 30, 2020

Published online on April 28, 2021

Cite as
Kusztal M, Kłopotowski M, Bazan-Socha S, et at. Is home-based therapy in Fabry disease the answer to compelling patients' needs during the COVID-19 pandemic? Survey results from the Polish FD Collaborative Group. *Adv Clin Exp Med*. 2021;30(4):449–454. doi:10.17219/acem/132038

DOI
10.17219/acem/132038

Copyright
© 2021 by Wroclaw Medical University
This is an article distributed under the terms of the Creative Commons Attribution 3.0 Unported (CC BY 3.0) (https://creativecommons.org/licenses/by/3.0/)

Abstract

Background. Fabry disease (FD) is an X-linked disorder related to a deficiency of the lysosomal enzyme alpha-galactosidase A. In Poland, enzyme replacement therapy (ERT) for FD is offered by the National Health Fund only at selected hospital infusion centers. Patients with FB are considered at a high risk of developing complications from COVID-19. Some patients omitted infusions due to fear of infection or outbreaks in hospitals. Lack of alternative infusion sites hampered the situation.

Objectives. To analyze the impact of the SARS-CoV-2 pandemic on FD patients, especially their fears and expectations, the Polish FD Collaborative Group collaborated on a survey project.

Materials and methods. Between September and November 2020, we distributed a customized survey exploring expectations and fears among FD subjects.

Results. Fifty-five individuals (35 receiving ongoing ERT) from different FD centers completed the study. The median age was 40 years [IQR 25; 50], and gender distribution was almost equal (27 F; 28 M). One-fourth of FD patients reported severe disability limiting transportation for infusions that, in the opinion of the other 25% of responders, consumed >4 h. Forty-four (80%) of all would prefer home infusions performed by a nurse (n = 37, 67.3%) or by a trained non-medical person (n = 7, 12.7%), while 8 (14.5%) patients would choose a local hospital. As expected, transportation time (in one direction) was longer in those preferring home infusions (89.4 ±63 vs 36.2 ±67 min; p = 0.02). Also, those with more severe FD manifestation would prefer home infusions to treatment in FD centers (p = 0.03). The vast majority of respondents (n = 46; 83%) would not change their preferences after pandemic termination.

Conclusions. To maintain ERT, FD patients prefer home infusions or those given in the nearest hospital, especially during a pandemic.

Key words: COVID-19, enzyme replacement therapy, Fabry disease, home therapy, hospital infusion

Background

Fabry disease (FD) is a rare lysosomal disorder characterized by deficiency of α-galactosidase A activity resulting from mutations in the *GLA* gene (FD; OMIM #301500; ORPHA: 324). In FD, progressive accumulation of lipids, primarily globotriaosylceramide (Gb3) and its deacylated derivative globotriaosylsphingosine (lyso-Gb3), lead to cell, tissue and multiorgan damage, and eventual failure.[1]

In Europe, FD has an estimated incidence of 1 in 100,000 inhabitants. While the exact prevalence in Poland is unknown, numbers provided by the association of families with FD indicate 73 patients, likely a major underestimation. Since September 2019, the only FD therapy offered by the Polish National Health Fund (NFZ) has been based on a two-enzyme replacement therapy (ERT) provided at hospitals' infusions centers (hospital-based ERT). Prior to 2019, most FD patients received ERT either in clinical trials or as a part of a compassionate drug therapy program provided by the pharmaceutical companies.[2] At present, no patients in Poland receive home-based ERT.

The outbreak of the coronavirus disease 2019 (COVID-19) pandemic has become a major threat for humanity. The World Health Organization (WHO) declared the outbreak of COVID-19 a worldwide pandemic in March 2020. Globally, as of December 3, 2020, there have been 64.5 million confirmed cases of COVID-19, including 1.5 million deaths, reported to the WHO.[3]

The lessons learned from the disease outbreak in China,[4,5] Italy and New York City[6] showed that patients with comorbidities, particularly those with cardiovascular disease, are at a higher risk of complications and mortality. Regarding FD and other ultra-rare diseases, there are no reliable data indicating their predisposition to SARS-CoV-2 infection. Most adult FD patients, in fact, have chronic illnesses caused by the chronic accumulation of glycosphingolipids found in the lysosomes of most cell types and tissues, leading in time to dysfunction. The most common manifestations are heart failure, chronic kidney disease, recurrent/transient brain ischemia, gastrointestinal symptoms, hypertension, and skin edema/cellulitis.[7] Therefore, a delay of therapy[8] due to the collateral damage done by the pandemic, including the postponement of procedures or rescheduled hospital visits, places FD adults at risk of worsening their condition. Patients' fear of contact with other people and hospital workers has also been exaggerated by lockdown media news and the stay-at-home order.

The situation during the first coronavirus wave in the spring was less dramatic for Polish FD patients, as the majority of patients avoided COVID-19. However, increased numbers during the current second wave indicate a more serious situation. By December 3, 2020, more than 1 million people in Poland had been infected with SARS-CoV-2 and 18,828 had died. Thus, a real risk of treatment discontinuation for FD patients appeared. SARS-CoV-2-infected patients with FD may be isolated or admitted to COVID-19-dedicated hospitals where ERT is not available. In a few FD centers, visits were rescheduled due to the appearance of outbreaks of infection in the hospital. Due to these circumstances, increased numbers of FD patients began to ask in the FD centers why the treatment is not provided closer to their homes, or in their homes with or without nurse assistance. The social impact and the fear of recurrence of viral infections have put pressure on clinicians to change strategies in order to avoid therapy interruptions for patients.

Objectives

To analyze the impact of the SARS-CoV-2 pandemic on FD patients, especially their fears and expectations, the Polish FD Collaborative Group collaborated on a survey project. The results are presented below.

Materials and methods

Survey and statistical analysis

A customized survey (available as supplementary material) containing 24 questions was created. The anonymous survey was distributed to all FD patients visiting Fabry centers in Poland between September 20 and November 1, 2020. The patients provided verbal consent prior to filling out the survey and left it in a drop-box after completion. Anonymization allowed for quicker survey distribution (no data protection needed by our country law) and hopefully more honest answers, especially for some questions referring to the change of treating facility and place of infusion.

Demographic and clinical data, and all survey responses were entered into a database for this study. Descriptive analyses, the frequency distribution of variables, and comparative tests (Mann–Whitney U test, χ^2 test, Student's t-test) were performed.

Results

Patient characteristics

Fifty-five patients responded by returning the filled survey. Four surveys were incompletely filled, but eventually considered useful as omissions were <30% of the questions. Participating patients were from most Polish centers for FD located in Kraków, Łódź, Wrocław, Gdańsk, Warszawa, and Poznań.

Demographic and clinical characteristics are displayed in Table 1. The median age of the surveyed patients was 40 years [IQR 25;50], and gender distribution was almost

Table 1. Demographic and clinical characteristics of patients

Parameter	Total; n = 55	Receiving ERT; n = 35
Age [years] [IQR] Under 18 years	38.2; [25; 50]); median 40 3	39.6; [26; 51]; median 37 2
Gender	27F/28M	13F/22M
Educational level • elementary/basic vocational school • high school/technical college • university/college • no response	 10 27 17 1	 7 15 12 1
Employment/learning • employed • unemployed • disability pension • retirement • learning/studying • no response	 28 1 13 4 10 1	 15 1 10 3 7
Self-reliance • complete • with some effort • incomplete (frequent help of the other person) • total dependence	 25 (45.5%) 19 (34.5%) 7 (12.7%) 4 (7.3%)	 10 (28.6%) 16 (45.7%) 7 (20%) 2 (5.7%)
General health perception (scale 1–10; 10– best)	6.3; [5; 8] median 6	5.7; [4; 7] median 6
Mean age at symptoms onset [years] [IQR]	14.0; [7; 18] median 9	13.5; [7; 16] median 9
Mean age at diagnosis [years] [IQR]	28.2; [17; 40] median 28	27.8; [14.5; 41.5] median 24
Number of affected organs/systems (brain/heart/kidney/arteries/skin/eyes/ears/digestive tract/nervous system/severe pain)	2.7; [1; 4] median 2	3.4; [2; 4] median 3.5
Severity of cases among affected family members (multiple choice) • mild • severe (heart/kidney failure, stroke, severe pain) • unknown	 9 (16.3%) 47 (85.5%) 3 (5.4%)	 6 (17.1%) 26 (74.3%) 3 (8.5%)
Treatment • ERT • Oral chaperon No treatment: no or minor symptoms • I don't want to be treated • I have nowhere to be treated • I've been treated, but I'm no longer • waiting for the drug • no response	 35 1 11 2 2 1 2 1	 35

ERT – enzyme replacement therapy.

equal (27 women and 28 men). Four surveys were completed by someone other than the patient (i.e., 3 by parents and 1 by a caregiver). The majority of FD patients (63.3%) were receiving ERT-hospital infusions. In 20 FD patients,

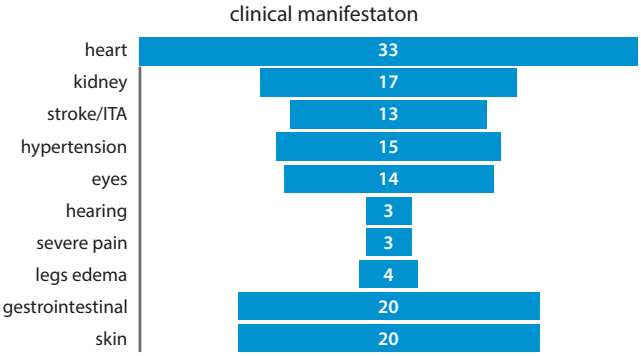

Fig. 1. Clinical manifestation of Fabry disease in entire cohort (n = 55)

treatment was not provided mainly due to minor symptoms or a lack of symptoms.

The disease characteristics of the surveyed group are shown in Fig. 1. The median age of symptoms onset was 9 years [IQR 7;18] and the age of diagnosis 28 years [IQR 17;40]. Patients treated with ERT began therapy relatively late, namely at a median age of 30 years [IQR 16; 47]. The family burden by created FD was prominent – the vast majority (85.5%) reported to have at least 1 member with a severe course (heart/kidney failure, stroke, severe pain).

General health perception (1–10 points; 10 – means best) was 6.3 in total, and 5.7 in ERT-treated patients. This was in line with the median number of affected organs – 2 [IQR 1;4] and 3.5 [IQR 2;4], respectively.

Functioning and reaching hospitals for infusions

The majority (69%) of patients were active workers (50.9% employed, 18.1% studying). Self-reliance was reported by 45.5%, and partial independence by 34%. Disability of various degrees was reported by 20% of the whole group, and in 25.7% of those already receiving ERT.

The median time to reach the hospital (in one direction) for infusions was 60 min [IQR 20; 120]; however, 1/4 of patients spent 4 or more hours on transportation. If we add a few hours for the infusion and hospital visit, it takes the whole day for these patients, and sometimes their caregivers (up to 25%), to receive treatment. More than half of the surveyed FD patients never experienced infusion-related reactions, while 40% experienced a few episodes (Table 2).

Home infusions as a potential therapy option

Most patients on ERT (82.9%) believed that therapy provided closer to home would be more convenient. However, some of them (22.6%) admitted that a disadvantage of treatment closer to home is that local doctors know less about FD management (Table 2). From all the surveyed cohort, 37 patients (67.3%) would choose home infusions performed

Table 2. Experienced obstacles in transportation and infusions of FD patients receiving enzyme replacement therapy (ERT; n = 35)

Mean time to reach the hospital (in 1 direction; minutes) [IQR] • ≥20 min • <30 min • 30–59 min • 60–119 min	75; [20; 120], median 60 9 (25.7%) 9 9 7
Means of transport to the hospital/center (multiple choice) • public transport • own car • friend or family member car • by bike/walk	 9 (25.7%) 17 7 2
Difficult peripheral cannulation • no • yes (including 2 with ports)	 24 11 (31.4%)
History of infusion-related reaction • few episodes • frequently • never	 14 (40%) 1 19 (54.3%)
Is it better to be treated closer or further from place of residence? (multiple choice) • treatment closer to home is more convenient • the weak side of treatment closer to home is the fact that local doctors know less about FD • it doesn't matter to me where I'm treated	 29 (82.9%) 8 (22.6%) 4 (11.4%)

by a nurse, at a local hospital (n = 8, 14.5%), or at home by a trained non-medical person (n = 7, 12.7%). Interestingly, less experienced patients with fewer symptoms (and not on ERT) would more often choose home-based infusions than those receiving ERT (Table 3). Regardless of treatment experience, the time spent on transportation for hospital-based infusions may be decisive. Namely, transportation time (in one direction) varied significantly between patients choosing infusions at home and the remainder (89.4 ±63 compared to 36.2 ±67 min; p = 0.02). Another factor distinguishing those preferring home-based from other sites is more severe FD manifestation defined by the presence of at least 1 of the following conditions: heart/kidney failure, stroke or severe pain. Those with severe FD would more frequently opt for home therapy than the others (p = 0.03).

With regard to possible problems and worries associated with home infusions, our respondents indicated mainly vascular access (10–17%), infusion-related reactions (11–20%) and getting to the nearest hospital within an hour (5–8.5%) as concerns.

Table 3. Home infusions as therapy option in the opinion of both treated and untreated FD patients

Survey question	In total (n = 55)	Receiving ERT (n = 35)	Untreated (n = 20)
Preferred place of therapy infusion (multiple choice)* • university hospital/institute • hospital in the place of residence • local clinic in the place of residence • infusions at home by a doctor and nurse • infusions at home by a nurse • infusions at home by a trained person • no opinion	 3 8 (14.5) 1 1 37 (67.3%) 7 (12.7%) 2	 2 7 (20%) 1 1 19 (54.2%) 9 (16.4%) 1	 1 1 (5%) 0 0 18 (90%) 2 (10%) 1
Worried about potential problems during home infusions (multiple choice) • none • difficult vein cannulation • infusion related reactions • getting to the nearest hospital within an hour • remote visit with indications of vital signs (not applicable to telephone advice)	 35 (63.6%) 8 (14.5%) 8 (14.5%) 4 (7.3%) 2 (3.6%)	 21 (60%) 6 (17.1%) 4 (11.4%) 3(8.5%) 2 (5.7%)	 14 (70%) 2 (10%) 4 (20%) 1 (5%) 0
If the SARS-CoV-2 pandemic will be over or an effective vaccine appears I will change my preferences regarding where the infusions are to be made • yes • no • no response	 5 48 (87.3%) 2	 3 31 (88.6%) 1	 2 17 (85%) 1
Transportation and administration of hospital-based therapy during an epidemic may increase the risk of infection • Yes, regardless of protective measures maintained • Yes, but only when protective measures are omitted • No, while maintaining protective measures • No, regardless of protective measures maintained	 33 (60%) 8 (14.5%) 11 (20%) 3 (5.5%)	 21(60%) 5 (14.3%) 8 (22.9%) 1 (2.8%)	 12 (60%) 3 (15%) 3 (15%) 2 (10%)
I am afraid that coronavirus may affect my health condition • No, infection is often asymptomatic • Yes, like any other infection • Yes, coronavirus if more dangerous than other infections	 3 (5.5%) 24 (43.6%) 28 (50.9%)	 2 (5.8%) 11(31.4%) 22 (62.8%)**	 1 (5%) 13 (65%) 6 (30%)

*43 responders chose one option; ** chi-square p < 0.05.

Impact of SARS-CoV-2 on FD patients' expectations regarding infusion sites

To verify whether the preferences are situational and transient, we asked the following question: "Would you change preferences regarding infusion site if the SARS-CoV-2 pandemic will be finished or an effective vaccine will be available?" The vast majority of subjects (87.3%) responded negatively (Table 3).

From all the surveyed patients, 41 (74.5%) expressed concern that transportation and administration of hospital-based therapy during an epidemic may increase infection risk. That is, a generalized fear of potentially infected people further compounded concerns, regardless of protective measures maintained (Table 3).

Furthermore, anxiety that infection with SARS-CoV-2 may affect the health condition of FD patients is common. More ERT-treated than non-treated patients believed that SARS-CoV-2 is more dangerous than other infections (62.8% compared to 30%; $p < 0.05$). This difference may be due to a higher burden of the disease in the ERT group.

Discussion

Nowadays, besides mortality, patient-reported outcomes (PRO) and patients' quality of life are considered significant treatment endpoints. This refers to all chronic illnesses, including FD, which need to be diagnosed on time and adequately treated for relatively normal functioning. Fortunately, ERT, substrate reducing therapy and chaperone drugs show effectiveness in treating this disease. As of November 2020, the only reimbursed therapy in Poland was agalsidase infusions carried out in hospital. Due to the SARS-CoV-2 pandemic, the risk of ERT discontinuation emerged and an increase in patients' anxiety raised the question of optional home-based treatment. The pandemic additionally revealed to us the needs of severely affected patients. The FD Collaborative group survey showed a significant burden for patients and their families when getting hospital infusions, especially for those with a physical disability. Based on a customized survey, it was revealed that 25% of FD patients receiving ERT spend 4 or more hours only for transportation, plus an additional few hours for the hospital visit and infusion. Moreover, 25% of them need frequent or full support from others, which produces an additional family burden.

The majority of ERT receiving patients expressed the opinion that therapy provided at home or closer to home would be more convenient. Among the factors indicating a strong preference for home infusions were transportation time to the hospital and a more severe FD course.

Based the on survey results, we found that anxiety related to infection risk with SARS-CoV-2 is common in FD patients and even more expressed among ERT patients. However, interestingly, patients' preferences and needs are somewhat not situational due to the coronavirus pandemic – the vast majority of them declared that they would not change infusion site after pandemic termination or in a case of adequate vaccination availability. This suggests that the pandemic is not the primary motive for choosing the place of ERT administration.

Well-organized home-therapy seems to be the most efficient way to maintain ERT access during the SARS-CoV-2 pandemic in many European countries. For instance, an Italian experience with a home infusion of agalsidase during the COVID-19 pandemic has demonstrated no increase in infection during the first wave in the spring.[9] The absence of disease in the Naples's example could be due to the particular attention that this category of patients pays to respecting hygiene and infection prevention measures, and previously practiced and proven home-therapy with telemedicine for monitoring and supervision.

Regarding other lysosomal storage disorders like Gaucher disease (GD), where ERT is widely practiced, similar observations were made during the coronavirus pandemic. Patients with GD receiving oral therapy did not suffer problems with the medicine supply; 1 of the 16 patients receiving ERT in a home-based manner missed 1 dose, and 49% of the patients receiving therapy at hospitals experienced a treatment disruption.[10]

Limitations

Our data strongly suggest that we should offer home-based infusions or at least infusions in nearby facilities for FD patients. However, as it has been reported, home infusions have several limitations. They require dedicated training and several requirements before starting.[11–13] Nonetheless, we estimate that currently 30–50% of Polish FD patients would be eligible for ERT home infusions. We might relate 10–15% of further discontinuation due to vascular access problems or infusion-related reactions.

Conclusions

Our findings reflecting FD patients' needs and expectations underline the necessity of new ways to ensure therapy regarding patient burden and safety. It seems that home-based therapies need to be considered in most FD patients and should be an option for a specific group of patients.

ORCID iDs

Mariusz Kusztal https://orcid.org/0000-0002-6502-0374
Mariusz Kłopotowski https://orcid.org/0000-0002-4316-5417
Stanisława Bazan-Socha https://orcid.org/0000-0001-9634-0963
Beata Błażejewska-Hyżorek https://orcid.org/0000-0002-6096-2952
Krzysztof Pawlaczyk https://orcid.org/0000-0001-6237-0814
Andrzej Oko https://orcid.org/0000-0002-3394-7140
Magdalena Krajewska https://orcid.org/0000-0002-2632-2409
Michał Nowicki https://orcid.org/0000-0002-0823-5440

References

1. Germain DP. Fabry disease. *Orphanet J Rare Dis*. 2010;5:30. doi:10.1186/1750-1172-5-30
2. Bazan-Socha S, Kuczia P, Musiał J, Błażejewska-Hyżorek B. Fabry disease in Poland. *Pol Arch Intern Med.* 2018;128:567–568. doi:10.20452/pamw.4342
3. World Health Organisation (WHO) Coronavirus Disease (COVID-19) Dashboard, 2020. https://covid19.who.int/. Updated December 3, 2020 (7 PM CET).
4. Zhou F, Yu T, Du R, et al. Clinical course and risk factors for mortality of adult inpatients with COVID-19 in Wuhan, China: A retrospective cohort study. *Lancet.* 2020;395:1054–1062.
5. Guan WJ, Ni Z, Hu Y, et al. Clinical characteristics of coronavirus disease 2019 in China. *N Engl J Med.* 2020;382:1708–1720. doi:10.1056/NEJMoa2002032
6. Cummings MJ, Baldwin MR, Abrams D, at al. Epidemiology, clinical course, and outcomes of critically ill adults with COVID-19 in New York City: a prospective cohort study. *Lancet.* 2020;395:1763–1770. doi:10.1016/S0140-6736(20)31189-2
7. MacDermot KD, Holmes A, Miners AH. Anderson-Fabry disease: clinical manifestations and impact of disease in a cohort of 60 obligate carrier females. *J Med Genet*. 2001;38:769–775. doi:10.1136/jmg.38.11.769
8. Palmer K, Monaco A, Kivipelto M, et al. The potential long-term impact of the COVID-19 outbreak on patients with non-communicable diseases in Europe: consequences for healthy ageing. *Aging Clin Exp Res*. 2020;32:1189–1194. doi:10.1007/s40520-020-01601-4
9. Sechi A, Macor D, Valent S, et al. Impact of COVID-19 related healthcare crisis on treatments for patients with lysosomal storage disorders, the first Italian experience. *Mol Genet Metab*. 2020;130:170–171. doi:10.1016/j.ymgme.2020.04.002
10. Politei J. Fabry disease during the COVID-19 pandemic. Why and how treatment should be continued. *Mol Genet Metab.* 2020;130:227–229. doi:10.1016/j.ymgme.2020.06.002
11. Milligan A, Hughes D, Goodwin S, Richfield L, Mehta A. Intravenous enzyme replacement therapy: better in home or hospital? Spotlight on agalsidase beta in Fabry disease. *Br J Nurs*. 2006;15:330–333. doi:10.12968/bjon.2006.15.6.20681
12. Linthorst GE, Vedder AC, Ormel EE, Aerts JM, Hollak CE. Home treatment for Fabry disease: practice guidelines based on 3 years experience in The Netherlands. *Nephrol Dial Transplant.* 2006;21:355–360. doi:10.1093/ndt/gfi221
13. Kisinovsky I, Cáceres G, Coronel C, Reisin R. Home infusion program for Fabry disease: experience with agalsidase alfa in Argentina. *Medicina (B Aires).* 2013;73:31–34.

Meta-analysis of the diagnostic value of procalcitonin in adult burn sepsis

Zhao Chen[1,A–C,E], Nurlan Turxun[1,B–D], Fangyan Ning[2,A,E,F]

[1] Department of Burns, People's Hospital of Xinjiang Uygur Autonomous Region, China
[2] Intensive Care Unit, People's Hospital of Xinjiang, Uygur Autonomous Region, China

A – research concept and design; B – collection and/or assembly of data; C – data analysis and interpretation;
D – writing the article; E – critical revision of the article; F – final approval of the article

Advances in Clinical and Experimental Medicine, ISSN 1899–5276 (print), ISSN 2451–2680 (online) *Adv Clin Exp Med*. 2021;30(4):455–463

Address for correspondence
Zhao Chen
E-mail: mn35241@126.com

Funding sources
None declared

Conflict of interest
None declared

Received on June 2, 2020
Reviewed on September 1, 2020
Accepted on December 17, 2020

Published online on April 28, 2021

Abstract

Sepsis is one of the main causes of death in burn patients, and many studies have suggested that procalcitonin (PCT) is a biomarker for the early diagnosis of sepsis, but the results are controversial. The aim of this study was to evaluate the diagnostic value of serum PCT in adult burn sepsis by conducting a meta-analysis of published studies. The PubMed, Embase, Web of Science, CNKI and China Wanfang databases were searched, and studies on PCT as a marker for the diagnosis of adult burn sepsis from the establishment of the database, to February 1, 2020 were screened. The data were analyzed using Stata v. 15.0 software. A total of 10 studies and 704 patients were included. The combined sensitivity, specificity, positive likelihood ratio (PLR), negative likelihood ratio (NLR) and diagnostic odds ratio (DOR) were 0.67 (95% CI: 0.48–0.81), 0.87 (95% CI: 0.72–0.95), 5.20 (95% CI: 2.49–10.84), 0.38 (95% CI: 0.24–0.61) and 13.70 (95% CI: 5.72–32.82), respectively. The area under the summary receiver operating characteristic curve (SROC) was 0.85 (95% CI: 0.82–0.88), and the diagnostic threshold was the main source of heterogeneity. Results demonstrate that serum PCT may be used as a useful biomarker for the early diagnosis of burn sepsis in adults, and may be combined with other diagnostic indexes to further improve the sensitivity and specificity.

Key words: sepsis, burn, procalcitonin, meta-analysis

Cite as
Chen Z, Turxun N, Ning F. Meta-analysis of the diagnostic value of procalcitonin in adult burn sepsis. *Adv Clin Exp Med*. 2021;30(4):455–463. doi:10.17219/acem/131755

DOI
10.17219/acem/131755

Copyright
© 2021 by Wroclaw Medical University
This is an article distributed under the terms of the Creative Commons Attribution 3.0 Unported (CC BY 3.0) (https://creativecommons.org/licenses/by/3.0/)

Background

Burns are common injuries in life and war. Although there are many strategies for the prevention and treatment of infection in burns, burn sepsis is still one of the common causes of death in patients with severe burns.[1] Burns, especially severe burns, can lead to extensive damage to the skin tissue, the body's first defense barrier, resulting in serious damage to the body's internal homeostasis, a decrease in immunity, and a large volume of necrotic wound tissue. These changes provide good conditions for the growth and reproduction of bacteria. Therefore, infection in patients with severe burns is difficult to avoid.[2,3] Septic shock and multiple organ failure can develop rapidly from burn sepsis, which can lead to death.[4] Therefore, early detection of high-risk groups prone to burn sepsis, early diagnosis, and prediction of the prognosis of burn sepsis are key to reducing the mortality of patients with this condition. Bacterial blood culture is an important aspect of clinical etiological detection and diagnosis of burn sepsis, however blood culture does not enable a rapid diagnosis of burn sepsis, as it may take 3 days or more to produce a result. The use of prophylactic antibiotics in severe burn patients leads to a low positive rate of blood culture, which leads to a delay in the diagnosis of burn sepsis and an increase in antibiotic resistance.[5] Patients with severe burns often have similar symptoms to infection, such as increased respiratory rate, increased heart rate, and an obvious increase of white blood cells. The commonly used clinical indicators such as blood pressure, heart rate, respiratory rate, white blood cells, neutrophils, liver, and kidney function have low specificity and sensitivity in the diagnosis of burn sepsis, and these indexes cannot accurately estimate the prognosis of burn sepsis patients. Therefore, it is necessary to identify a rapidly detectable indicator, with high specificity and sensitivity, to enable the early prediction, diagnosis, and prognosis of burn sepsis. Such an indicator would facilitate timely treatment measures, guide the use of antibiotics, and increase the survival rate of patients with burn sepsis.

In recent years, various studies have shown that serum procalcitonin (PCT) plays an important role in the diagnosis of sepsis.[6,7] Serum PCT is a non-hormone active glycoprotein composed of 116 amino acids, which is a propeptide of calcitonin (CT).[8] The content of serum PCT in the blood of healthy people is very low, generally less than 0.1 ng/mL.[9] It has been shown that the release of serum PCT is closely related to the release of endotoxins and inflammatory mediators.[10] Serum PCT level has been demonstrated to be increased in differing degrees of bacterial and fungal infections, burns, trauma, surgery, and other conditions, but the increase in patients with systemic bacterial infection was the most significant.[11,12] The level of serum PCT in patients with systemic bacterial infection increased rapidly in 6–8 h and reached a peak at about 24 h. The level of serum PCT can change from low to high with severity of infection, i.e., local infection, sepsis, severe sepsis, septic shock. The level of serum PCT can always be at a high level or can increase continuously with persistent infection or aggravation of infection, so there is a significant correlation between serum PCT level and the severity of infection.[11]

Objectives

At present, there is still a debate regarding the significance of PCT in burn sepsis, so this study uses the method of meta-analysis to comprehensively analyze the relationship between serum PCT level and the diagnosis of sepsis in adult burn patients, to provide medical evidence for its diagnostic value.

Materials and methods

Literature search

PubMed, Embase, Web of Science, CNKI, China Wanfang, and other databases were searched for literature related to PCT and burn sepsis, published from the establishment of each database, to February 1, 2020. The key words used were: PCT, sepsis, burn, diagnosis. The search language was limited to Chinese and English. A detailed study flow chart is shown in Fig. 1, as per PRISMA guidelines.

Inclusion and exclusion criteria

Inclusion criteria: 1) the purpose of the study was to evaluate and explore the value of PCT in the diagnosis of sepsis in burn patients over 18 years old; 2) they can directly obtain four-grid data or provide sufficient information to construct four-grid data; 3) sepsis was diagnosed using accurate definition criteria: according to the American Society of Chest Physicians (ACCP)/Society of Critical Care Medicine (SCCM) meeting definition or the American Burn Association (ABA) meeting definition; 4) there were comparative data on clinical diagnosis and blood culture results. The literature was screened independently by 2 researchers according to the inclusion criteria, and the data were extracted according to a designed data extraction table. Finally, the data extraction was cross-compared, and if any differences were solved through discussion and negotiation.

Exclusion criteria: 1) poor experimental design or implementation of the study, unable to extract accurate data to construct a 2 × 2 four-grid table; 2) the subjects included children; 3) the Quality Assessment Of Diagnostic Accuracy Studies (QUADAS) score was less than 10.

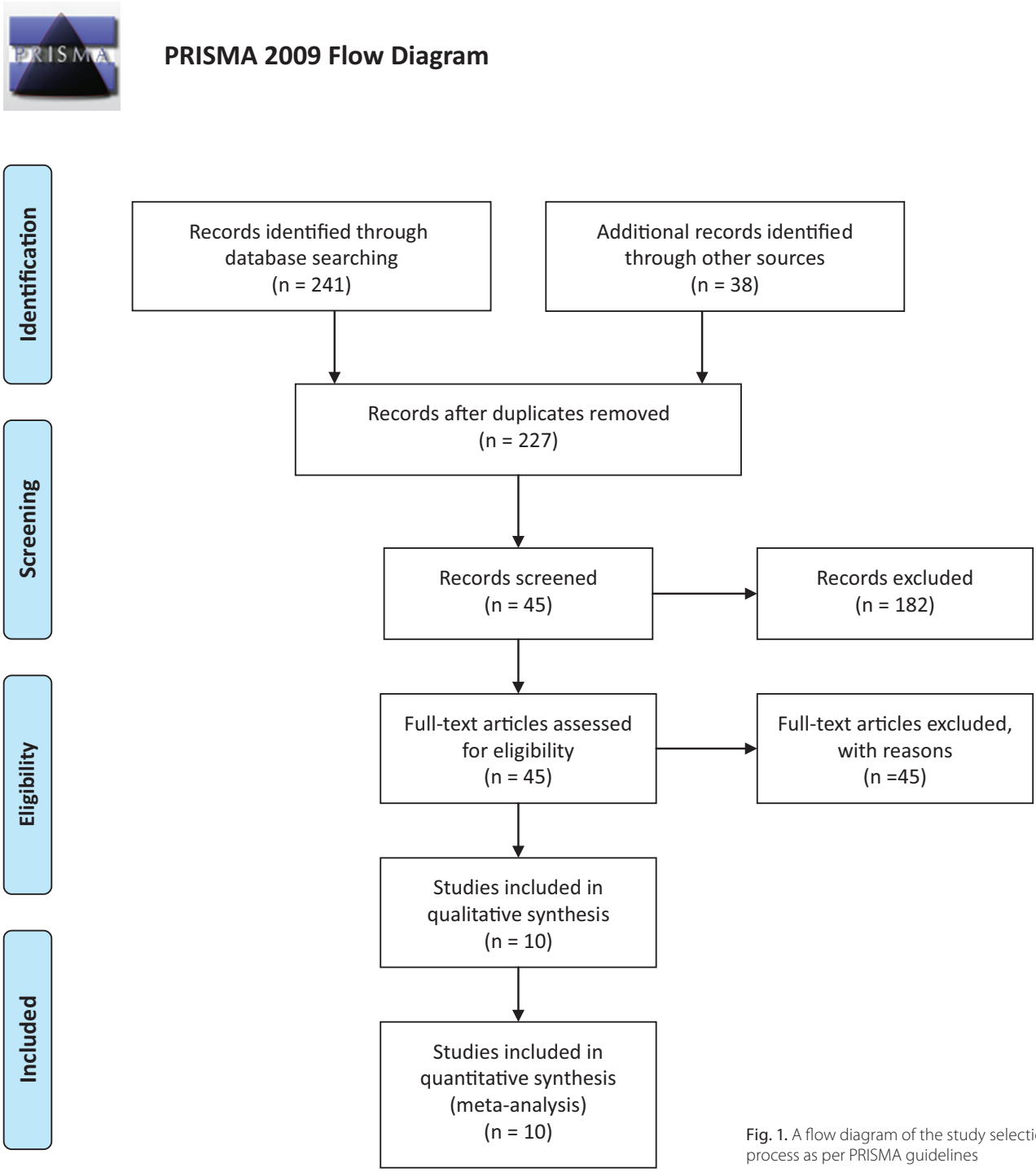

Fig. 1. A flow diagram of the study selection process as per PRISMA guidelines

Data extraction

Literature extraction: first author, publication time, country, experimental design, sample number of patients, age, burn area, critical value of PCT, sensitivity/specificity, and other indicators for the diagnosis of burn sepsis were extracted. When we observed a significant difference between the data reported in the study and the calculated data, we contacted the first or last author of the individual study by email to request clarification of the original data for the patient group.

Document quality evaluation

The QUADAS tool[13] was used for quality assessment, which included 14 items covering multiple dimensions of research quality. The QUADAS score was the sum of the 14 items. The scores for each item were discussed by two researchers. The highest available QUADAS score was 14, and to ensure the quality of the study, all included projects scored greater than 70% of the maximum QUADAS score (QUADAS score ≥ 10).

Statistical analyses

Stata v. 15.0 software was used to analyze the data. Cochran Q and Higgins' I^2 statistics were used to test the heterogeneity between the studies. The diagnostic threshold effect was evaluated by the receiver operating curve (ROC) and the Spearman's correlation coefficient was used to determine sensitivity and specificity. The typical shoulder-arm representation in ROC space and a strong positive correlation between the logarithm of sensitivity and the logarithm of 1-specificity were used to indicate the existence of the threshold effect. The bivariate mixed-effect regression model was used, combined with 95% confidence interval (CI), to calculate the sensitivity, specificity, positive likelihood ratio (PLR), negative likelihood ratio (NLR) and diagnostic odds ratio (DOR) aggregate statistics, and to draw the corresponding forest plot. Deeks' test was used to detect publication bias, and finally; sensitivity analysis was carried out. The area under the summary receiver operating curve (SROC), (AUC) was obtained. The AUC value varies from 0.5 to 1.0, with a value close to 0.5 indicating poor diagnostic performance, and AUC value close to 1.0 indicating good diagnostic performance. Where there was heterogeneity, meta-regression was used to analyze the source.

Results

Literature retrieval and quality evaluation

When retrieving statistics related to vital signs and blood samples collected at a specific time point, according to the diagnostic criteria of sepsis, each time point was defined as either sepsis or non-sepsis, and divided into a sepsis group and non-sepsis group accordingly. Initially, 227 articles were retrieved through keywords and all titles and abstracts were reviewed, resulting in exclusion of 182 articles. Full text and data integrity were then reviewed,

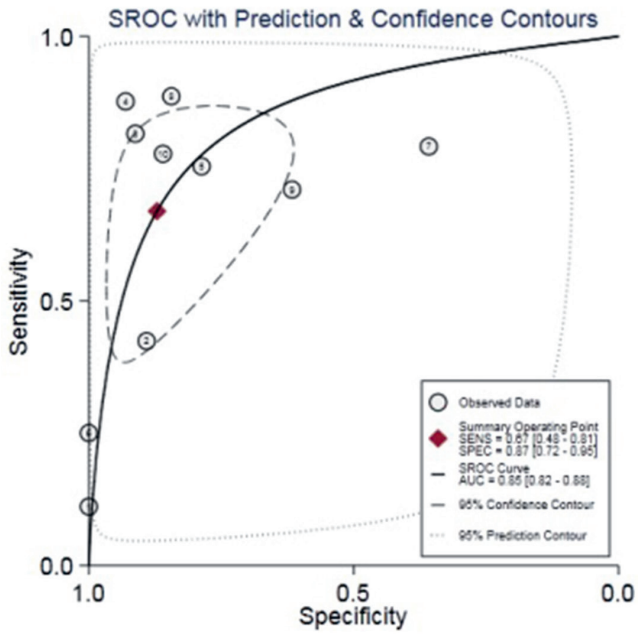

Fig. 2. SROC curve for the accuracy of PCT in the diagnosis of adult burn sepsis

and a further 35 were excluded. Finally, 10 studies met all the inclusion criteria[14–23], with a total of 704 patients, and 6062 time points. The information on the screening flow chart is shown in Fig. 1, which was prepared as per PRISMA guidelines.[24] The basic characteristics and quality score of the included literature are shown in Table 1.

The results of diagnostic accuracy analysis showed that significant heterogeneity was observed in the studies of sensitivity ($p = 0.00$, $I^2 = 93.40$), specificity ($p = 0.00$, $I^2 = 98.66\%$), PLR ($p = 0.00$, $I^2 = 97.13\%$), and DOR ($p = 0.00$, $I^2 = 100.0\%$). There was no obvious threshold effect in the current meta-analysis because the ROC curve was not a typical "shoulder-arm" pattern (Fig. 2). The Spearman correlation coefficient between the logarithm of sensitivity and the logarithm of 1-specificity was −0.2857, and the difference was not statistically significant. Overall, the diagnostic accuracy

Table 1. Characters of included studies

First author	Year	Country	Design	PCT cut-off	Age [years]	TBSA [%] burned	Time points	Sample size	TP	FP	FN	TN	QUADAS score
Heimburg et al.[15]	1998	Germany	PS	3	37.3 (18–65)	51 (20–91)	27	27	2	0	16	9	10
Bargues et al.[14]	2007	France	PS	0.534	40 ±14	40 ±17	359	25	39	29	53	237	11
Lavrentieva et al.[16]	2007	Greece	PS	1.5	45.6 ±20.1	41.4 ±22	934	43	93	72	21	748	13
Lavrentieva et al.[17]	2012	Greece	PS	1.5	48.2 ±18.3	38.8 ±18	145	145	64	5	9	67	13
Cakir et al.[18]	2013	Turkey	PS	0.759	40 ±17	36.1 ±23.4	611	37	181	79	59	292	11
Seoane et al.[20]	2014	Spain	RS	1.7	52.5 ±17.2	37.6 ±22.9	34	34	4	0	12	18	10
Paratz et al.[19]	2014	Australia	PS	1.4	40.16 (18–60)	40.1 ±16.0	344	54	38	190	10	106	11
Mokline et al.[21]	2015	Tunisia	PS	0.69	37 ±17	23 ± 17	121	121	39	12	5	65	11
Cabral et al.[22]	2017	Portugal	RS	0.5	40.8 ±79.0	16.0–38.8	3419	150	463	1062	189	1705	12
Zhou M et al. [23]	2020	China	PS	4.05	30.93–54.31	40.6–53.7	68	68	14	7	4	43	10

TP – true positive; FP – false positive; FN – false negative; TN – true negative; QUADAS – Quality Assessment Of Diagnostic Accuracy Studies; PS – prospective; RS – retrospective; TBSA – total body surface area; PCT – procalcitonin.

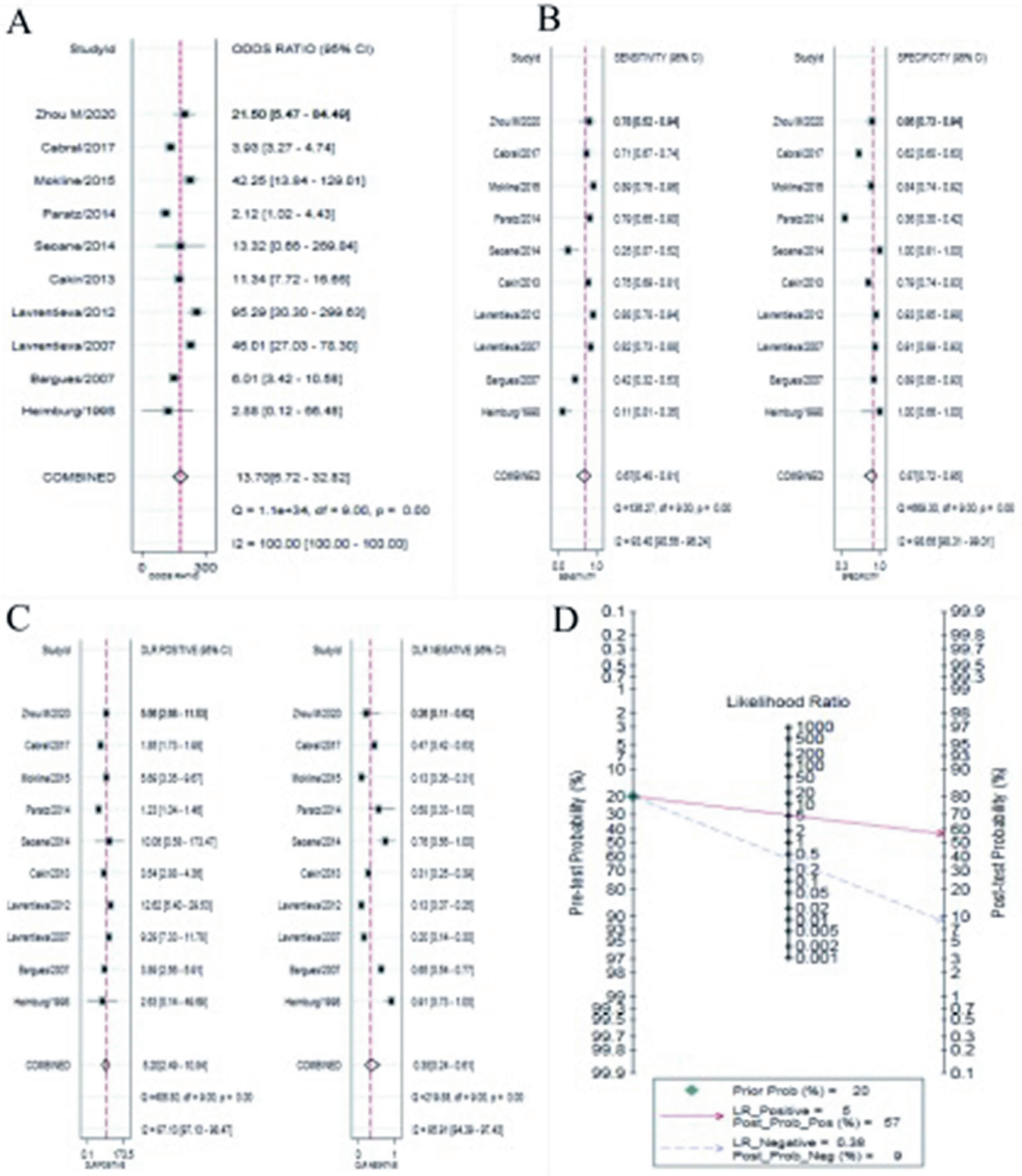

Fig. 3. Forest plot of PCT in the diagnosis of adult burn sepsis

A – DOR; B – sensitivity and specificity; C – PLR and NLR; D – Fagan's nomogram.

of PCT in adult burn sepsis was: combined sensitivity = 0.67 (95% CI: 0.48–0.81), combined specificity = 0.87 (95% CI: 0.72–0.95), PLR = 5.20 (95% CI: 2.49–10.84), NLR = 0.38 (95% CI: 0.24–0.61), DOR = 13.70 (95% CI: 5.72–32.82). The forest plot of DOR is shown in Fig. 3A, the sensitivity and specificity of the forest plot are shown in Fig. 3B, and the forest plot of PLR and NLR are shown in Fig. 3C. The SROC is shown in Fig. 2 (AUC = 0.85, 95% CI: 0.82–0.88). Fagan's nomogram result showed that when the pre-test probability ratio was 20%, the post-test probability of PLR was 57% and

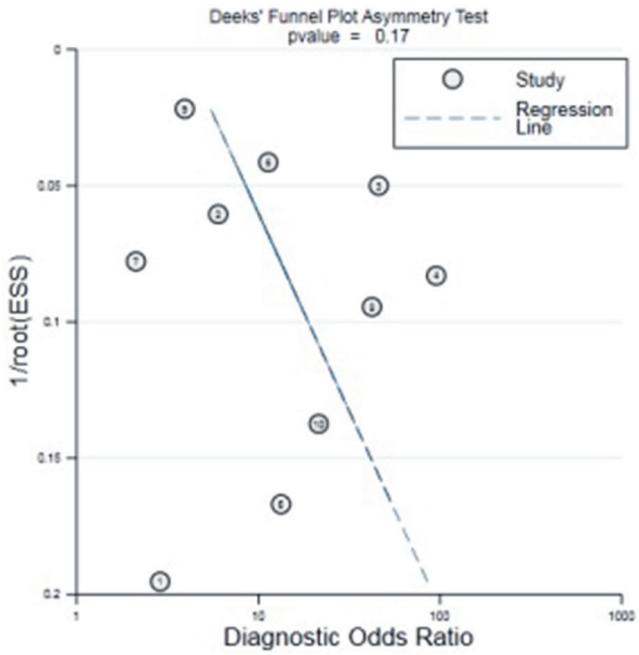

Fig. 4. Funnel plot of PCT in the diagnosis of adult burn sepsis

the post-test probability of NLR was 9% (Fig. 3D). This shows that PCT has a good diagnostic performance for adult burn sepsis. The Deeks' funnel plot in Fig. 4 shows that the p-value was 0.61, which can be considered as a lack of publication bias. The results of the meta-regression analysis are shown in Table 2, which shows that the ethnicity of the study population and experimental design did not affect the source of heterogeneity, and the diagnostic threshold was the main source of heterogeneity.

Sensitivity analysis

The result of the sensitivity analysis is shown in Fig. 5. Goodness-of-fit and bivariate normal analysis (Fig. 5A,B) show that the bivariate mixed-effect model was robust for meta-analysis. Also, through sensitivity analysis (Fig. 5C) and outlier detection (Fig. 5D), a study that deviated from the others was identified, that may affect the robustness of meta-analysis. After excluding this study, in the overall analysis with or without outliers, there was no significant change in sensitivity (0.67 vs 0.73), specificity (0.87 vs 0.84), PLR (5.20 vs 4.60), NLR (0.38 vs 0.32), DOR (13.70 vs 14.00) and AUC (0.85 vs 0.85), indicating that the meta-analysis of diagnostic value in this study was robust.

Discussion

Burns are tissue injuries caused by thermal, chemical, electrical, or radiation factors, which can damage the physiological barriers of the body surface of burn patients. When an extensive area of this physiological barrier is destroyed, the resulting large wound becomes a suitable medium for the growth of bacteria, and as the body surface has the temperature and humidity suitable for the reproduction and growth of bacteria, the proliferation of bacteria is promoted within the wound. The immune function of the patient after burns is impaired and maladjusted, and the anti-infection ability of the whole body is low. Therefore, burn patients have a higher incidence of sepsis. Severe sepsis and septic shock are common causes of death in burn patients, accounting for 30% of hospital mortality.[25]

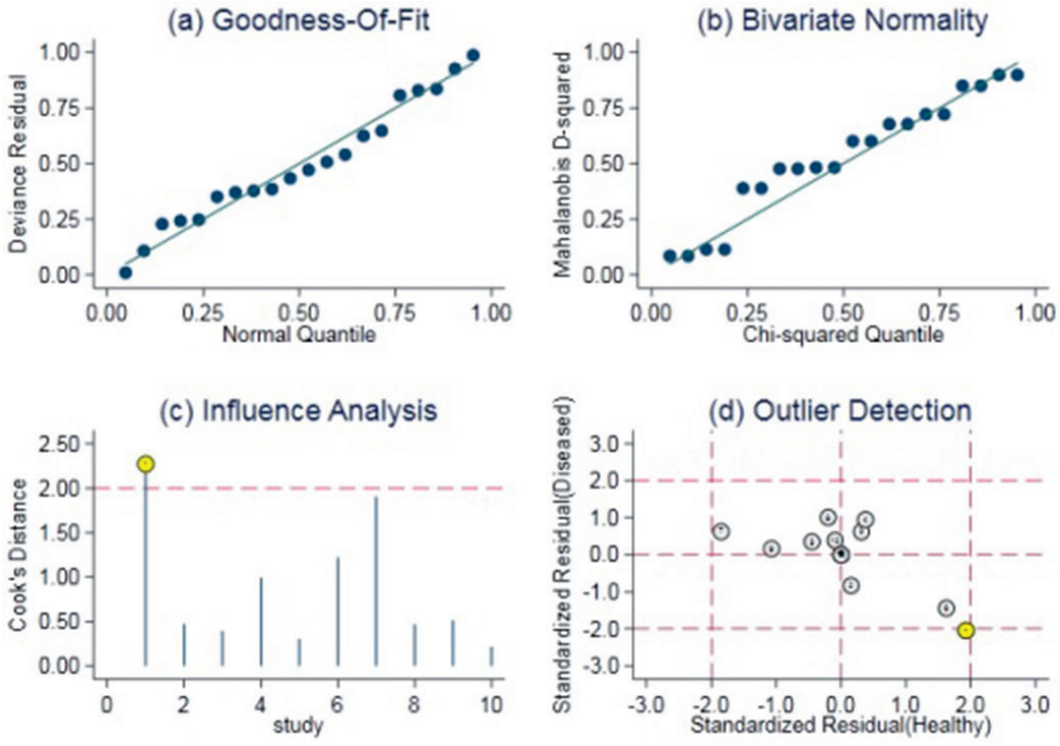

Fig. 5. The results of sensitivity analysis

Table 2. Results of meta-regression analysis

Parameter	Category	Studies	Sen (95% CI)	p-value for Sen	Spe (95% CI)	p-value for Spe
Ethnicity	Non-Caucasian	2	0.85 (0.64–1.00)	0.22	0.86 (0.62–1.00)	0.94
	Caucasian	8	0.62 (0.43–0.81)		0.88 (0.76–0.99)	
Design	RS	2	0.48 (0.07–0.89)	0.29	0.88 (0.65–1.00)	0.65
	PS	8	0.71 (0.55–0.88)		0.87 (0.75–0.98)	
PCT cut-off	>1.5 ng/mL	3	0.35 (0.09–0.62)	0.02	0.97 (0.90–1.00)	0.04
	≤1.5 ng/mL	7	0.77 (0.65–0.89)		0.80 (0.67–0.93)	

Sen – sensitivity; Spe – specificity; PS – prospective; RS – retrospective; PCT – procalcitonin.

Although interventions for the treatment of sepsis have been improving, such as anti-infective treatment and efforts to follow the development of supportive methods such as immunotherapy from the surviving sepsis guidelines, prognosis remains not optimistic for patients with sepsis.[26] Burn sepsis is a severe systemic inflammatory response syndrome (SIRS) reaction caused by a bacterial infection, which occurs and develops rapidly. When the course of burn sepsis progresses to septic shock or multiple organ dysfunction syndrome (MODS), there are no clear, effective, and specific treatment measures, and this condition carries a poor prognosis and high mortality. Early diagnosis of sepsis and appropriate treatment can reduce the mortality of burn sepsis.[27] Therefore, the early diagnosis of sepsis in burn patients becomes particularly critical, and there is an urgent need for more effective markers for early diagnosis. Mann et al.[28] in 2011 and Ren et al.[29] in 2015 systematically reviewed the relationship of PCT and the diagnostic value of burn sepsis, until then there was little systematic analysis on the topic. Therefore, we carried out a meta-analysis to comprehensively evaluate the diagnostic value of PCT in adult burn sepsis.

The date of literature retrieval included in this study was from the establishment of each relevant database to February 1, 2020. A total of 10 studies, 704 patients, and 6062 time points were included. There were strict inclusion and exclusion criteria for the included literature. To ensure the quality of the literature, each paper was scored by QUADAS, and studies with a score of less than 10 were not included. In the data collection, we carefully read the original literature, and through the sensitivity and specificity reported in the original literature, and other values, obtained four-grid table data. In this process, we found that some of the study designs were not rigorous enough to extract accurate data from the original data, and such papers were also excluded. To more accurately evaluate the role of PCT in the diagnosis of adult burn sepsis, this study also imposed a strict age limit, with all subjects being over 18 years old, which reduced the heterogeneity to some extent. Besides patient age, there are many factors that may affect the heterogeneity of the diagnostic value of PCT, such as detection method, burn severity etc. Therefore, this study conducted a meta-analysis including ethnicity of the study, experimental design and diagnostic threshold to analyze the source of heterogeneity. The results of this study showed that the AUC was 0.85, and combined sensitivity and specificity of SROC were 0.67 and 0.87 respectively. In terms of sensitivity, the ability of serum PCT to detect sepsis in adult burn patients was weaker, and the ability to detect non-sepsis in adult burn patients was stronger. The PLR was 5.20 and the NLR was 0.38. Where the likelihood ratio is more than 1, it means that the result of the diagnostic test is related to the disease; and where the likelihood ratio is less than 1, it means that the result of the diagnostic test is not related to the disease. In our results, the PLR was 5.20, which means that sepsis patients with positive diagnostic tests were 5.20 times more likely to develop sepsis than non-sepsis patients with positive diagnostic tests. The results of the likelihood ratio showed that serum PCT could be used to distinguish adult burn patients with sepsis from those without sepsis. DOR combines the results of sensitivity and specificity, which is an ideal independent index. When the lower limit of 95% CI of its value is more than 1, the difference is considered statistically significant, and the larger the value is, the more obvious the diagnostic effect is. In our study, DOR = 13.70 (95% CI: 5.72–32.82), therefore this showed that serum PCT had good accuracy in the diagnosis of adult burn sepsis. The analysis of publication bias showed that there was no obvious publication bias in this study. The results of the sensitivity analysis showed that the results of this study were robust.

The diagnostic criteria of sepsis are defined by the ACCP/SCCM, but in patients with burn sepsis, there is a higher incidence of local bacterial colonization and more obvious SIRS, which will affect the diagnosis of burn sepsis. The ABA meeting in 2007 proposed new diagnostic criteria for SIRS and sepsis in burn patients, which were more suitable for this group of patients.[29,30] Meta-regression analysis showed that the main source

of heterogeneity may be the threshold of PCT, and was not related to race or experimental design. The criteria of Bargues et al.[14] for the diagnosis of sepsis were based on the ACCP/SCCM consensus, in which the proportion of respiratory system infection and wound infection was higher, which tend to mislead or exaggerate the diagnosis of sepsis, combined with the relatively conservative diagnostic threshold of 0.534 ng/mL. There was reason to suspect that the subjects were patients with mild to moderate infection rather than severe burns, so it was recommended to adopt the ABA sepsis criteria in future studies to avoid exaggerating the diagnosis of sepsis.

The results of this study suggest that PCT may not be the most ideal biomarker for early diagnosis of burn sepsis in adult patients. In fact, an ideal biomarker may not exist, due to the complex pathophysiological processes in sepsis that cannot be described by a single biomarker. However, it may be a useful and promising biomarker of sepsis in burn patients. In practical application, PCT may be combined with other biomarkers to aid in the early diagnosis of burn sepsis, which may achieve higher diagnostic accuracy.

Limitations

Of course, inevitably, this study had some limitations:

1) There were relatively few studies included, and only 10 articles met the criteria. We aimed to collect all studies that met the requirements, but some of them were of low quality or the data was not accurate, which were therefore excluded from our study.

2) There is a certain heterogeneity in the study. Although we have carried out meta-regression according to the diagnostic threshold, ethnicity and experimental design, and come to the conclusion that the diagnostic threshold has the greatest influence on the heterogeneity, it is still inevitable that there is still a certain heterogeneity, which may be caused by different ages or burn areas, but cannot be further stratified. As a result, it is impossible for us to conduct further research on it.

3) This study only considers published studies in Chinese and English, which may mean important data obtained from unpublished studies and studies written in other languages was excluded.

Conclusions

Procalcitonin is useful in the diagnosis of burn sepsis in adult burn patients. This index can be used in early diagnosis of adult burn sepsis. At the same time, it is necessary to combine PCT with other diagnostic indexes to further improve the diagnostic sensitivity and specificity of burn sepsis. Sepsis leads to a complex inflammatory response, and clinicians should understand the diagnostic efficiency and limitations of PCT and other inflammatory indicators. Combination of a variety of inflammatory indicators for comprehensive evaluation is often more reliable than relying solely on one diagnostic threshold.

ORCID iDs

Zhao Chen https://orcid.org/0000-0003-3239-8642
Nurlan Turxun https://orcid.org/0000-0003-1476-4629
Fangyan Ning https://orcid.org/0000-0002-8569-8385

References

1. Nitzschke S, Offodile AC, Cauley RP, et al. Long term mortality in critically ill burn survivors. *Burns.* 2017;43(6):1155–1162. doi:10.1016/j.burns.2017.05.010
2. Calvano TP, Hospenthal DR, Renz EM, Wolf SE, Murray CK. Central nervous system infections in patients with severe burns. *Burns.* 2010;36(5):688–691. doi:10.1016/j.burns.2009.08.004
3. Yoon J, Kym D, Hur J, et al. Comparative usefulness of sepsis-3, burn sepsis, and conventional sepsis criteria in patients with major burns. *Crit Care Med.* 2018;46(7):e656–e662. doi:10.1097/CCM.0000000000003144
4. Belba MK, Petrela EY, Belba AG. Epidemiology and outcome analysis of sepsis and organ dysfunction/failure after burns. *Burns.* 2017;43(6):1335–1347. doi:10.1016/j.burns.2017.02.017
5. Hidalgo F, Mas D, Rubio M, Garcia-Hierro P. Infections in critically ill burn patients. *Med Intensiva.* 2016;40(3):179–185. doi:10.1016/j.medin.2016.02.001
6. Rao L, Song Z, Yu X, et al. Progranulin as a novel biomarker in diagnosis of early-onset neonatal sepsis. *Cytokine.* 2020;128:155000. doi:10.1016/j.cyto.2020.155000
7. Solé-Ribalta A, Bobillo-Pérez S, Valls A, et al. Diagnostic and prognostic value of procalcitonin and mid-regional pro-adrenomedullin in septic paediatric patients. *Eur J Pediatr.* 2020;179(7):1089–1096. doi:10.1007/s00431-020-03587-7
8. Sakr Y, Sponholz C, Tuche F, Brunkhorst F, Reinhart K. The role of procalcitonin in febrile neutropenic patients: Review of the literature. *Infection.* 2008;36(5):396–407. doi:10.1007/s15010-008-7374-y
9. Ozmen M, Oktay E, Tarhan EF, Aslan O, Oflazoglu U, Koseoglu MH. Serum procalcitonin levels in patients with ankylosing spondylitis. *Int J Rheum Dis.* 2016;19(5):500–505. doi:10.1111/1756-185X.12386
10. Nakae H, Inaba H, Endo S: Usefulness of procalcitonin in Pseudomonas burn wound sepsis model. *Tohoku J Exp Med.* 1999;188(3):271–273. doi:10.1620/tjem.188.271
11. Wirz Y, Meier MA, Bouadma L, et al. Effect of procalcitonin-guided antibiotic treatment on clinical outcomes in intensive care unit patients with infection and sepsis patients: A patient-level meta-analysis of randomized trials. *Crit Care.* 2018;22(1):191. doi:10.1186/s13054-018-2125-7
12. Schneider HG, Lam QT. Procalcitonin for the clinical laboratory: A review. *Pathology.* 2007;39(4):383–390. doi:10.1080/00313020701444564
13. Whiting P, Rutjes AW, Reitsma JB, Bossuyt PM, Kleijnen J. The development of QUADAS: A tool for the quality assessment of studies of diagnostic accuracy included in systematic reviews. *BMC Med Res Methodol.* 2003;3:25. doi:10.1186/1471-2288-3-25
14. Bargues L, Chancerelle Y, Catineau J, Jault P, Carsin H. Evaluation of serum procalcitonin concentration in the ICU following severe burn. *Burns.* 2007;33(7):864. doi:10.1016/j.burns.2006.10.401
15. Heimburg DV, Stieghorst W, Khorram-Sefat R, Pallua N. Procalcitonin– a sepsis parameter in severe burn injuries. *Burns.* 1998;24(8):750. doi:10.1016/s0305-4179(98)00109-0
16. Lavrentieva A, Kontakiotis T, Lazaridis L, et al. Inflammatory markers in patients with severe burn injury. What is the best indicator of sepsis? *Burns.* 2007;33(2):189–194. doi:10.1016/j.burns.2006.07.001
17. Lavrentieva A, Papadopoulou S, Kioumis J, Kaimakamis E, Bitzani M. PCT as a diagnostic and prognostic tool in burn patients. Whether time course has a role in monitoring sepsis treatment. *Burns.* 2012;38(3):363. doi:10.1016/j.burns.2011.08.021
18. Cakır Madenci Ö, Yakupoğlu S, Benzonana N, Yücel N, Akbaba D, Orçun Kaptanağası A. Evaluation of soluble CD14 subtype (presepsin) in burn sepsis. *Burns.* 2014;40(4):664–669. doi:10.1016/j.burns.2013.08.024

19. Paratz JD, Lipman J, Boots RJ, Muller MJ, Paterson DL. A new marker of sepsis post burn injury? *Crit Care Med.* 2014;42(9):2029–2036. doi:10.1097/CCM.0000000000000400
20. Seoane L, Pértega S, Galeiras R, Astola I, Bouza T. Procalcitonin in the burn unit and the diagnosis of infection. *Burns*. 2014;40(2):223–229. doi:10.1016/j.burns.2013.11.018
21. Mokline A, Garsallah L, Rahmani I, et al. Procalcitonin: A diagnostic and prognostic biomarker of sepsis in burned patients. *Ann Burns Fire Disasters*. 2015;28(2):116–120. PMID: 27252609
22. Cabral L, Afreixo V, Santos F, Almeida L, Paiva JA. Procalcitonin for the early diagnosis of sepsis in burn patients: A retrospective study. *Burns*. 2017;43(7):1427–1434. doi:10.1016/j.burns.2017.03.026
23. Zhou M, Wang XC, Guo L, Chen H, Huang DP, Wang LJ. Value of soluble myeloid cell trigger receptor-1,CD64 and procalcitonin in diagnosis of burn patients complicated with sepsis. *Chin J Nosocomiol.* 2020;30:216–219.
24. Moher D, Liberati A, Tetzlaff J, Altman DG, The PRISMA Group. Preferred reporting items for systematic reviews and meta-analyses: The PRISMA statement. *PLoS Med*. 2009;6(7):e1000097. doi:10.1371/journal.pmed1000097
25. Levy MM, Dellinger RP, Townsend SR, et al. The Surviving Sepsis Campaign: Results of an international guideline-based performance improvement program targeting severe sepsis. *Intensive Care Med*. 2010;36(2):222–231. doi:10.1007/s00134-009-1738-3
26 Veach RA, Liu Y, Zienkiewicz J, et al. Survival, bacterial clearance and thrombocytopenia are improved in polymicrobial sepsis by targeting nuclear transport shuttles. PLOS ONE 2017;12:e179468. https://doi.org/10.1371/journal.pone.0179468
27 Wineberg D, Moore R, Kruger D. Procalcitonin and bacterial sepsis in burn patients in south africa. *J Surg Res*. 2020;246:490–498. doi:10.1016/j.jss.2019.09.040
28 Mann EA, Wood GL, Wade CE. Use of procalcitonin for the detection of sepsis in the critically ill burn patient: A systematic review of the literature. Burns. 2011;37(4):549–558. doi:10.1016/j.burns.2010.04.013
29. Ren H, Li Y, Han C, Hu H. Serum procalcitonin as a diagnostic biomarker for sepsis in burned patients: A meta-analysis. *Burns*. 2015;41(3):502–509. doi:10.1016/j.burns.2014.08.019
30. Vandijck DM, Brusselaers N, Blot SI. Inflammatory markers in patients with severe burn injury: What is the best indicator of sepsis? *Burns*. 2007;33(7):940. doi:10.1016/j.burns.2007.02.003

Interleukin 6: biological significance and role in inflammatory bowel diseases

Agnieszka Pawłowska-Kamieniak[A,C–E], Paulina Krawiec[A,E], Elżbieta Pac-Kożuchowska[E,F]

Department of Pediatric and Gastroenterology, Medical University of Lublin, Poland

A – research concept and design; B – collection and/or assembly of data; C – data analysis and interpretation;
D – writing the article; E – critical revision of the article; F – final approval of the article

Advances in Clinical and Experimental Medicine, ISSN 1899–5276 (print), ISSN 2451–2680 (online) *Adv Clin Exp Med*. 2021;30(4):465–469

Address for correspondence
Agnieszka Pawłowska-Kamieniak
E-mail: agnieszkapawlowskakamieniak@umlub.pl

Funding sources
None declared

Conflict of interest
None declared

Received on July 4, 2020
Reviewed on September 23, 2020
Accepted on November 11, 2020

Published online on April 28, 2021

Abstract

Cytokines affect a number of processes in the living body. Interleukin 6 (IL-6) is a cytokine involved in inflammation, infection response and also regulation of metabolism. It stimulates target cells through a membrane-bound IL-6 receptor. Inflammatory bowel diseases (IBD) are autoimmune diseases whose incidence and prevalence are increasing worldwide. It is a group of chronic gastrointestinal disorders characterized by multifactorial, still unknown pathogenesis, varied symptomatology, course with periods of exacerbation and remission, and polymorphic infiltration in histopathological examination. As it is known, pro-inflammatory cytokines, including IL-6, in IBD initiate, intensify and support the development of the inflammatory process in the intestine. Our knowledge of IL-6 biology has important consequences for therapeutic strategies. Elevation of IL-6 concentration can be considered as an early and sensitive, although non-specific marker for various inflammatory conditions and may be used in the diagnosis and monitoring of patients with IBD.

Key words: inflammatory bowel disease, pro-inflammatory cytokines, interleukin 6, interleukin 6 receptor

Cite as
Pawłowska-Kamieniak A, Krawiec P, Pac-Kożuchowska E. Interleukin 6: Biological significance and role in inflammatory bowel diseases. *Adv Clin Exp Med*. 2021;30(4):465–469. doi:10.17219/acem/130356

DOI
10.17219/acem/130356

Copyright
© 2021 by Wroclaw Medical University
This is an article distributed under the terms of the Creative Commons Attribution 3.0 Unported (CC BY 3.0) (https://creativecommons.org/licenses/by/3.0/)

Introduction

Cytokines are glycoproteins with molecular weights ranging from a few to a dozen or so kilodaltons (kDa). These molecules affect a number of processes in the living body, such as proliferation, differentiation and migration of cells. Cytokines are produced mainly by immune cells and may act in 3 different manners. They may have an influence on the same cells that produced them (autocrine action), on nearby cells (paracrine action) or on distant cells (endocrine action).[1] Thus, by affecting many cells, cytokines are mediators of immune reactions and they also participate in hematopoietic processes. Currently, more than 100 distinct types of cytokines are known, and due to continuing progress in the field of immunology, this number is steadily growing. The immune response of a particular cytokine depends on its concentration, presence of appropriate effector cells, and the expression of specific receptors for cytokines on target cells.[1–4]

The currently known types of cytokines include interleukins, interferons, chemokines, superfamily of tumor necrosis factor alfa (TNF-α) molecules, macrophage migration inhibiting factor (MIF), and transforming growth factor beta (TGF-β).[2,4]

To date, 39 interleukins are known and some of them consist of several subtypes. Based on specific properties, interleukins may be divided into pro-inflammatory and anti-inflammatory cytokines.[1,2,4]

Inflammatory bowel diseases: immunological background

Inflammatory bowel diseases (IBD) are autoimmune diseases whose incidence and prevalence are increasing worldwide. They are a group of chronic gastrointestinal disorders characterized by multifactorial, still unknown pathogenesis, varied symptomatology, course with periods of exacerbation and remission, and polymorphic infiltration in histopathological examination. They include Crohn's disease (CD), ulcerative colitis (UC) and IBD of unclassified type (IBD-U).[2,4–12]

The etiopathogenesis of these diseases is unknown and multifactorial. There have been several factors suggested to be involved in the development of IBD, including genetic susceptibility, environmental factors and immune response dysregulation.[2,5,6,8–10,12–14] The action of environmental factors may lead to damage of the mucosal barrier, development of local inflammatory reaction with the release of many mediators of the inflammatory process, and infiltration of many inflammatory cells.[15] It is considered that IBD could result from dysregulation of the intestinal barrier and a pathologic activation of the intestinal immune response toward environmental antigens.

It has been shown that CD results from abnormal response of the intraepithelial T lymphocytes (Th1), triggered by environmental factors, which induces a cascade of pro-inflammatory cytokines, particularly TNF-α. Increased activation of CD4 T cells (Th2) lymphocytes, which are responsible for interleukin production and increased production of antibodies, is observed in UC.[16–18]

It is believed that disorders of intestinal immune mechanisms may be caused by imbalance between pro-inflammatory cytokines and anti-inflammatory cytokines, resulting in a chronic inflammatory process in the intestinal wall.[2,5,6,19]

As it is known, pro-inflammatory cytokines in IBD initiate, intensify and support the development of the inflammatory process in the intestine. In patients with IBD, the intestinal wall is infiltrated with inflammatory cells, including monocytes and macrophages which are the source of pro-inflammatory cytokines. Cytokines, which play a role in the pathogenesis of IBD, may represent a new biomarker for the intensity of inflammatory changes in gastrointestinal tract.[6,7,9,17,18]

Interleukin 6 and its role in transmission of the activation signal

Interleukin 6 (IL-6) is a prominent cytokine with a pleiotropic effect on inflammation and immunity. Interestingly, IL-6 can both boost and reduce inflammation. It is one of the pro-inflammatory cytokines and it also has many regenerative and anti-inflammatory properties.[20–24] The pro- or anti-inflammatory effect depends on the target cells and this dual activity of IL-6 has been the subject of many studies.[25]

Interleukin 6 is a four-helical protein of 184 amino acids.[1] It is involved in anti-infective response, acute phase reaction and hematopoiesis. It is believed to be one of the main factors regulating the immune defense mechanism of the body.[25] Interleukin 6 is mainly produced by monocytes and macrophages, but also by endothelial cells, activated Th2 lymphocytes and fibroblasts.[15,23,24] The main factor inducing the production of IL-6 is interleukin 1β (IL-1β), while less important stimulating factors include TNF-α, interferons and lipopolysaccharides (LPS).[26] Interleukin 6 is also produced during viral infections.

The cytokines are characterized by binding with the appropriate receptors, thereby activating the transmission of the appropriate signal in the effector cell. The interleukin 6 receptor (IL-6R) consists of 2 subunits: a 80-kDa glycoprotein (IL-6R, gp80) and the signal transducing subunit 130-kDa glycoprotein (gp130).[1,4,23] Interleukin 6 belongs to a family of 10 cytokines, which act through receptor complexes containing the cytokine receptor subunit gp130.[15,22,25] In addition to IL-6, members of this family of cytokines include interleukin 11 (IL-11), leukemia inhibitory factor (LIF), ciliary inhibitory factor (CNTF), oncostatin M (OSM), cardiotrophin-1

(CT-1), cardiotrophin-like cytokine (CLC), neutropoietin (NPN), interleukin 27 (IL-27), and interleukin 31 (IL-31).[1,13,20,21,23,24,27,28] Gp130 is expressed by most cells in the body, while the IL-6R is mainly expressed by hepatocytes and some leukocytes, such as neutrophils, monocytes and some lymphocytes. As previously mentioned, the pro- or anti-inflammatory effect of IL-6 depends on the target cells. The dual nature of IL-6 is associated with different receptor activation: classical and trans-signaling.[17,18,20–22,25,27,28] Anti-inflammatory messages are transmitted by binding of IL-6 to IL-6R in the cell membrane and this complex interacts with 2 molecules of gp130, leading to the signal activation. The IL-6-dependent activation through the membrane-bound IL-6R is called classic signaling.[4,13,29] Interleukin 6 classical signaling induces the acute-phase response and is considered to have anti-inflammatory effects (Fig. 1). In body fluids, these receptors are present in the soluble form of soluble IL-6 receptor (sIL-6R) and soluble glycoprotein 130 (sgp130). Pro-inflammatory messages are transmitted by binding of IL-6 to sIL-6R and this process is called trans-signaling (Fig. 2).[4,13,29] This second activation through binding of complex IL-6 with sIL-6R induces trans-signaling, also via gp130. This trans-signaling transmission is the primary activation mechanism in chronic inflammatory processes.[13,17,25,29,30]

The subunit of gp130 present in the cell membrane enhances the action of IL-6. The sIL-6R is agonistic and has signal transmission ability in the cell through

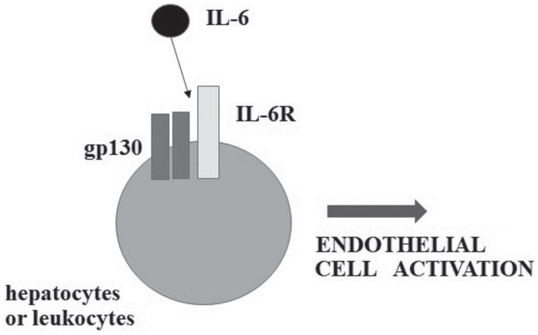

Fig. 1. Classical IL-6 activation (classic signaling)

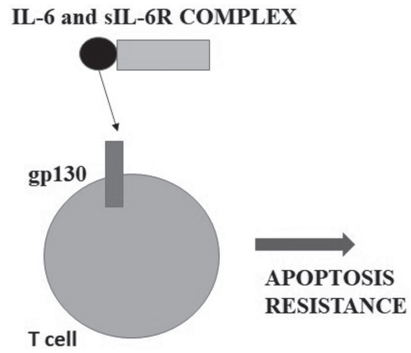

Fig. 2. sIL-6 R-mediated cell signaling (IL-6 trans-signaling)

interaction with the gp130. The IL-6/sIL-6R complex stimulates target cells, which are unresponsive to IL-6 alone due to lack of expression membrane-bound IL-6R. As mentioned earlier, gp130 is expressed in many cells, thus trans-signaling via complex IL-6 and sIL-6R can activate many cells of the body. In both classical signaling and trans-signaling, responses are elicited through the engagement with the membrane-bound gp130, a subunit of IL-6R.[8,25,27,31,32]

The sIL-6R is the result of the enzymatic action of a disintegrin and metalloproteinase ADAM 10 and ADAM 17 on the IL-6R membrane receptor. In contrast to other cytokines, sIL-6R does not neutralize IL-6, and IL-6/sIL-6R complexes activate cells, like IL-6 alone. Therefore, the combination of IL-6 with sIL-6R acts agonistically and intensifies the inflammatory process. Constant stimulation and maintenance of this process leads to tissue damage.[1,8,10,25,31,32] Under physiological conditions, the transactivation by IL-6/sIL-6R complexes is limited by sgp130, which captures these complexes and prevents their attachment to the membrane gp130. In healthy people, the concentration of sgp130 is significantly higher than the concentration of IL-6/sIL-6R. It is different in autoimmune diseases, which include IBD. Classical IL-6 signaling is unaffected by sgp130, but soluble form of gp130 is the inhibitor of IL-6 trans-signaling responses (Fig. 3).[1,25,29,33]

Apoptosis plays an important role in regulating growth, tissue homeostasis, development and immune responses. The induction of apoptosis is mediated by extrinsic and

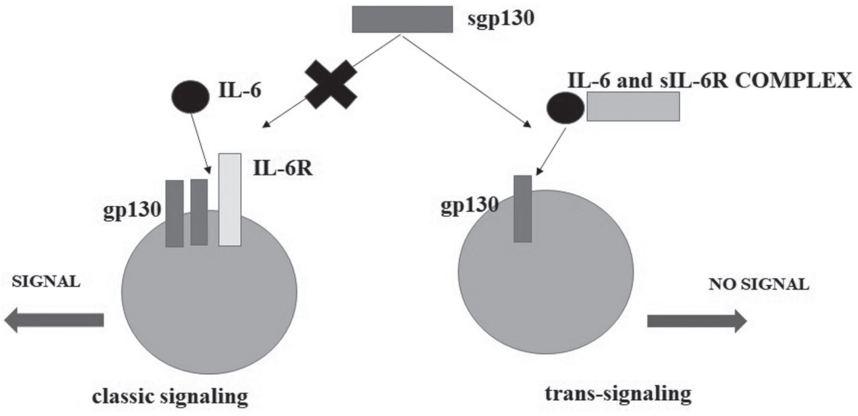

Fig. 3. Selective inhibition of trans-signaling by sgp130

intrinsic pathways, which require the cooperation of a series of molecules. Trans-signaling response plays important role in resolution of inflammatory responses.[30,34] Interleukin 6 trans-signaling is involved in the maintenance of the state of chronic inflammatory disease, among others IBD.[8,17]

Interleukin 6 associated with the receptor in trans-signaling process makes use of JAK tyrosine kinases (Janus kinases) and STAT proteins (signal transducers and activators of transcription), and activates the STAT3 transcription factor, which stimulates the inflow of granulocytes and lymphocytes to the intestinal epithelium, inhibits the apoptosis of damaged cells and repairs the intestinal tissue.[1,10,11,13,14,27,32,34,35] It is believed that the inhibition of T lymphocyte apoptosis is due to STAT3 induction of anti-apoptotic Bcl members, Bcl-2 and Bcl-xL, which leads to the accumulation of these lymphocytes in the tissue and the formation of chronic inflammatory process.[1,10,16,30] Thus, antibodies against IL-6R, such as tocilizumab, may be used in inhibition of the inflammatory response in rheumatology.[1,9,16,18,28,29,31]

It is well known that one of the basic functions of IL-6 is the influence on the proliferation and differentiation of B lymphocytes into cells releasing immunoglobulins of different classes. Furthermore, it is known that IL-6, together with interleukin 1 (IL-1), is involved in the stimulation of T lymphocytes recognizing the antigen.[4] Similarly to IL-1 and interferons, IL-6 plays an important role in inducing a response to a fever. It may also be responsible for the development of many inflammatory conditions and diseases. It participates in the stimulation of the production of acute-phase proteins, involved in the development of an inflammatory response to infection, injury or tissue damage, in the liver. It is believed that in inflammatory states, the concentration of IL-6 (as well as of acute-phase proteins) in body fluids increases significantly.[25,26] Interleukin 6 also affects appetite suppression, as the cytokines of the IL-6 group include leptin, which is an anorexigenic hormone.

Interleukin 6, as mentioned above, is the main factor inducing the synthesis of acute-phase proteins in the liver. Moreover, STAT3 induces liver transcription of the hepcidin, which regulates iron metabolism. Hepcidin inhibits the release of iron from macrophages and other cells, as well as inhibits its absorption in the intestine, which leads to anemia associated with chronic inflammation.[10,25,26]

The participation of interleukin 6 in IBD

In IBD, the innate immune response plays an important role. It is known that IL-6 signaling plays an important role in maintenance of chronic intestinal inflammation in IBD. Many studies have shown, that IL-6 is a main inducer of C-reactive protein (CRP), and IL-6 and sIL-6R levels are positively associated with elevated levels in IBD.[23,33] As already mentioned, IL-6 has been found to use an alternative pathway to activate target cells lacking the membrane-bound IL-6 receptor through a naturally occurring soluble form of the IL-6R. Although mostly regarded as a pro-inflammatory cytokine, IL-6 also has many regenerative functions as an anti-inflammatory cytokine. The availability of IL-6, membrane-bound IL-6R, soluble IL-6R, and gp130 determines the trans- or classic signaling response. Different expression of IL-6 and sIL-6R in healthy and diseased individuals has been demonstrated. In inflammatory conditions, serum concentration of sIL-6R increases. Increased availability of sIL-6R and a high inflammation-induced concentration of IL-6 increase the strength of the cellular response towards IL-6. In the body, the ratio of sgp130 in contrast to sIL-6R is an antagonist of IL-6-induced signaling. Sgp130 together with sIL-6R act as a buffer system that, in the excess of sIL-6R, favors trans-signaling and, in the excess of sgp130, blocks IL-6-induced classic signaling.[21,33] Interleukin 6 controls the balance between pro-inflammatory T cells and immunosuppressive regulatory T cells. The cytokines such as IL-6 or TNF-α are elevated in most of the inflammatory conditions and therefore have been recognized as targets of therapeutic intervention.

Clinical trials using anti-IL-6 therapy (PF-04236921) by subcutaneous injection in IBD, especially in patients with moderate to severe CD who previously failed treatment with anti-TNF therapy, appear to be promising.[35] Elevation of IL-6 concentration can be considered as an early and sensitive, although non-specific, marker for various inflammatory conditions.[26,33] Diagnosis, monitoring and evaluation of the severity and intensity of intestinal lesions in the course of IBD is based on clinical, endoscopic and histopathological assessment. The aim of many studies was to identify novel biomarkers assessing the intensity of inflammation in the course of IBD.

In many available studies, it has been shown that serum levels of IL-6 are elevated in patients with exacerbation of UC or CD, and decreased in IBD remission.[5,8,9,11,12,14,19,33] Moreover, it has been presented that IL-6 level correlates with the severity of inflammatory changes in the intestine.[2,7] A similar relationship, according to Ciećko-Michalska et al., exists in patients with CD.[5] Vasilyeva et al. also showed an increase of IL-6 levels in adolescent patients with active CD compared to those in disease remission and to the control group.[12] Lochhead et al. in prospective cohort studies found higher levels of IL-6 and high-sensitivity CRP (hsCRP) in patients with IBDs.[19]

Nikolaus et al. demonstrated an increase of IL-6 concertation in the active form of both UC and CD, without significant increase of the sIL-6R and sgp130 receptor concentrations.[9] In a study by Mitsuyama et al., elevated concentrations of both IL-6 and sIL-6R were found in patients with active forms of UC and CD.[8] In another study, Mitsuyama et al. demonstrated elevated concentration of IL-6 as well as sIL-6R and sgp130 in the exacerbation of IBD.[33] Takač et al. demonstrated statistically higher serum levels

of IL-6 in patients with CD and UC than in a control group. At the same time, no statistically significant differences of IL-6 were found in both groups of patients.[11]

It is known that the determination of the level of pro-inflammatory cytokines, including IL-6, may be used in the diagnosis and monitoring of patients with IBD. Several studies have provided evidence for the important role of IL-6 in inflammatory disorders, including IBD. Interleukin 6 has become a non-invasive marker of the assessment of activity and severity of inflammation in the course of IBD. The assessment of serum concentration of IL-6 and other cytokines, and evaluation of their correlation with IBD activity may contribute to the identification of reliable non-invasive markers of IBD and identification of novel therapeutic targets.

ORCID iDs

Agnieszka Pawłowska-Kamieniak https://orcid.org/0000-0002-7747-420X
Paulina Krawiec https://orcid.org/0000-0002-2197-2197
Elżbieta Pac-Kożuchowska https://orcid.org/0000-0002-3204-2235

References

1. Rose-John S. Interleukin-6 family cytokines. *Cold Spring Harb Perspect Biol*. 2018;10(2):a028415. doi:10.1101/cshperspect.a028415
2. Polińska B, Matowicka-Karna J, Kemona H. The cytokines in inflammatory bowel disease [in Polish]. *Postepy Hig Med Dosw (Online)*. 2009; 63:389–394. PMID:19724079
3. Lee SH, Kwon J, Cho ML. Immunological pathogenesis of inflammatory bowel disease. *Intest Res*. 2018;16(1):26–42. doi:10.5217/ir.2018.16.1.26
4. Turner MD, Nedial B, Hurst T, Pennington DJ. Cytokines and chemokines: At the crossroads of cell signaling and inflammatory disease. *Biochim Biophys Acta*. 2014;1843(11):2563–2582. doi:10.1016/j.bbamcr.2014.05.014
5. Ciećko-Michalska I, Wierzbicka-Tutka I, Szczepanek M, Fedak D, Mach T. Could the cytokines concentration be a marker of IBD activity and be useful in evaluation of IBD differentiation? [in Polish]. *Przegl Lek*. 2016;73(5):301–304. PMID:29629745
6. Eder P, Stawczyk K, Krela-Kaźmierczak I, Linke K. Chosen markers of inflammation in inflammatory bowel disease. *Gastroentereol Pol*. 2007;14(6):429–431.
7. Neubauer K, Bednarz-Misa I, Walecka-Zacharska E, et al. Oversecretion and overexpression of nicotinamide phosphoribosyltransferase/Pre-B colony-enhancing factor/visfatin in inflammatory bowel disease reflects the disease activity, severity of inflammatory response and hypoxia. *Int J Mol Sci*. 2019;4;20(1):166. doi:10.3390/ijms20010166
8. Mitsuyama K, Toyonaga A, Sasaki E, et al. Soluble interleukin-6 receptors in inflammatory bowel disease: Relations to circulating interleukin-6. *Gut*. 1995;36(1):45–49. doi:10.1136/gut.36.1.45
9. Nikolaus S, Waetzing GH, Butzin S, et al. Evaluation of interleukin-6 and its soluble receptor components sIL-6R and sgp 130 as markers of inflammation in inflammatory bowel diseases. *Int J Colorectal Dis*. 2018;33(7):927–936. doi:10.1007/s00384-018-3069-8
10. Sanchez-Muñoz F, Dominguez-Lopez A, Yamamoto-Furusho JK. Role of cytokines in inflammatory bowel disease. *World J Gastroenterol*. 2008;14(27):4280–4288. doi:10.3748/wjg.14.4280
11. Takač B, Mihaljević S, Štefanić M, Glavas-Obrovac L, Kibel A, Samardzija M. Importance of interleukin 6 in pathogenesis of inflammatory bowel disease. *Coll Antropol*. 2014;38(2):659–664. PMID:25145003
12. Vasilyeva E, Abdulkhakov S, Cherepnev G, et al. Serum cytokine profiles in children with Crohn's disease. *Mediators Inflamm*. 2016;2016: 7420137. doi:10.1155/2016/7420127
13. Nguyen PM, Putoczki TL, Ernst M. STAT3-activating cytokines: A therapeutic opportunity for inflammatory bowel disease? *J Interferon Cytokine Res*. 2015;35(5):340–350. doi:10.1089/jir.2014.0225
14. Carey R, Jurickova I, Ballard E, et al. Activation of an IL-6: STAT3-dependent transcriptome in pediatric-onset inflammatory bowel disease. *Inflamm Bowel Dis*. 2008;14(4):446–457. doi:10.1002/ibd.20342
15. Xue X, Falcon DM. The role of immune cells and cytokines in intestinal wound healing. *Int J Mol Sci*. 2019;20(23):6097. doi:10.3390/ijms20236097
16. Ahluwalia B, Moraes L, Magnusson MK, Öhman L. Immunopathogenesis of inflammatory bowel disease and mechanisms of biological therapies. *Scand J Gastroenterol*. 2018;53(4):379–389. doi:10.1080/00365521.2018.1447597
17. Neurath MF. Cytokines in inflammatory bowel disease. *Nat Rev Immunol*. 2014;14(5):329–342. doi:10.1038/nri3661
18. Sanchez-Muñoz F, Dominguez-Lopez A, Yamamoto-Furusho JK. Role of cytokines in inflammatory bowel disease. *World J Gastroenterol*. 2008;14(27):4280–4288. doi:10.3748/wjg.14.4280
19. Lochhead P, Khalili H, Ananthakrishnan AN, Richer JM, Chan AT. Association between circulating levels of C-reactive protein and interleukin-6 and risk of inflammatory bowel disease. *Clin Gastroenterol Hepatol*. 2016;14(6):818–824. doi:10.1016/j.cgh.2016.01.016
20. Scheller J, Chalaris A, Schmidt-Arras D, Rose-John S. The pro- and anti-inflammatory properties of the cytokine interleukin-6. *Biochim Biophys Acta*. 2011;1813(5):878–888. doi:10.1016/j.bbamcr.2011.01.034
21. Rose-John S. IL-6 trans-signaling via the soluble IL-6 receptor: Importance for the pro-inflammatory activities of IL-6. *Int J Biol Sci*. 2012; 8(9):1237–1247. doi:10.7150/ijbs.4989
22. Baran P, Hansen S, Waetzig GH, et al. The balance of interleukin (IL)-6, IL-6:soluble IL-6 receptor (IL-6R) and IL-6:sIL-6R:sgp130 complexes allows simultaneous classic and trans-signaling. *J Biol Chem*. 2018; 293(18):6762–6775. doi:10.1074/jbc.RA117.001163
23. Kishimoto T. Interleukin-6: Discovery of a pleiotropic cytokine. *Arthritis Res Ther*. 2006;8(Suppl 2):S2. doi:10.1186/ar1916
24. Hirano T. Interleukin 6 in autoimmune and inflammatory diseases: A personal memoir. *Proc Jpn Acad Ser B Phys Biol Sci*. 2010;86(7):717–730. doi:10.2183/pjab.86.717
25. Liu X, Jones GW, Choy EH, Jones SA. The biology behind interleukin-6 targeted interventions. *Curr Opin Rheumatol*. 2016;28(2):152–160. doi:10.1097/BOR.0000000000000255
26. Narazaki M, Kishimoto T. The two-faced cytokine IL-6 in host defense and diseases. *Int J Mol Sci*. 2018;19(11):3528. doi:10.3390/ijms19113528
27. Scheller J, Ohnesorge N, Rose-John S. Interleukin-6 trans-signalling in chronic inflammation and cancer. *Scand J Immunol*. 2006;63(5): 321–329. doi:10.1111/j.1365-3083.2006.01750.x
28. Jones GW, Hill DG, Cardus A, Jones SA. IL-27: A double agent in the IL-6 family. *Clin Exp Immunol*. 2018;193(1):37–46. doi:10.1111/cei.13116
29. Lokau J, Agthe M, Garbers C. Generation of soluble interleukin-11 and interleukin-6 receptors: A crucial function for proteases during inflammation. *Mediators Inflamm*. 2016;2016:1785021. doi:10.1155/2016/1785021
30. Lee MJ, Lee JK, Choi JW, et al. Interleukin-6 induces S100A9 expression in colonic epithelial cells through STAT3 activation in experimental ulcerative colitis. *PLoS One*. 2012;7(9):e38801. doi:10.1371/journal.pone.0038801
31. Desreumaux P. Specific targeting of IL-6 signalling pathway: A new way to treat IBD? *Gut*. 2000;47(4):465–466. doi:10.1136/gut.47.4.465
32. Neuman MG. Signaling for inflammation and repair in inflammatory bowel disease. *Rom J Gastroenterol*. 2004;13(4):309–316. PMID: 15624029
33. Mitsuyama K, Mitsuyama K, Tomlyasu N, et al. A form of circulating interleukin-6 receptor component soluble gp130 as a potential interleukin-6 inhibitor in inflammatory bowel disease. *Clin Exp Immunol*. 2006;143(1):125–131. doi:10.1111/j.1365-2249.2005.02960
34. Lee SD, Choe JW, Lee BJ, et al. Butein effects in colitis and interleukin-6/signal transducer and activator of transcription 3 expression. *World J Gastroenterol*. 2015;21(2):465–474. doi:10.3748/wjg.v21.i2.465
35. Danese S, Vermeire S, Hellstern P, et al. Randomised trial and open-label extension study of an anti-interleukin-6 antibody in Crohn's disease (ANDANTE I and II). *Gut*. 2019;68(1):40–48. doi:10.1136/gutjnl-2017-314562

The significance of the gut microbiome in children with functional constipation

Monika Kwiatkowska[A–F], Aneta Krogulska[A–F]

Department of Pediatrics, Allergology and Gastroenterology, Ludwik Rydygier Collegium Medicum in Bydgoszcz, Nicolaus Copernicus University in Toruń, Poland

A – research concept and design; B – collection and/or assembly of data; C – data analysis and interpretation;
D – writing the article; E – critical revision of the article; F – final approval of the article

Advances in Clinical and Experimental Medicine, ISSN 1899–5276 (print), ISSN 2451–2680 (online) *Adv Clin Exp Med*. 2021;30(4):471–480

Address for correspondence
Monika Kwiatkowska
E-mail: monikasobecka5@gmail.com

Funding sources
None declared

Conflict of interest
None declared

Received on July 28, 2020
Reviewed on October 12, 2020
Accepted on December 6, 2020

Published online on April 28, 2021

Abstract

Constipation is a widespread problem in pediatric practice, affecting almost 30% of pediatric population. As much as 90–95% of constipation cases have a functional basis, and although the pathogenesis of functional constipation remains unclear, its etiology is considered to be multifactorial. Its growing prevalence has been attributed to the occurrence of disorders in the homeostasis of gastrointestinal microbiota. In humans, the best known microbiome is that of the intestines, which has been the subject of a number of studies based on recognition of the *16S rRNA* gene sequence. Microbiota are believed to influence the pathogenesis of functional constipation by affecting peristalsis, relationship with diet, and physical activity. The paper evaluates the role of intestinal microbiota in functional constipation and describes its contribution to the onset of disease. Determining the importance of the microbiome in the pathogenesis of functional constipation creates hope for the development of new prevention and treatment methods.

Key words: microbiota, *16S rRNA*, peristalsis, childhood

Cite as
Kwiatkowska M, Krogulska A. The significance of the gut microbiome in children with functional constipation. *Adv Clin Exp Med*. 2021;30(4):471–480. doi:10.17219/acem/131215

DOI
10.17219/acem/131215

Copyright
© 2021 by Wroclaw Medical University
This is an article distributed under the terms of the Creative Commons Attribution 3.0 Unported (CC BY 3.0) (https://creativecommons.org/licenses/by/3.0/)

Introduction

Constipation is a troublesome condition characterized by the production of hard, compact stool which requires great effort to pass. Consequently, stool is passed less frequently than would be typical for a given age. The norms of defecation frequency depending on age are presented in Table 1.[1] Constipation is one of the most common childhood complaints, being reported by up to 29.6% of the population of pediatric population.[2–4] It is slightly more common in boys than in girls.[5] The condition accounts for 3–5% of visits to pediatricians and 10–25% of visits to pediatric gastroenterologists.[3,6] In addition to its widespread prevalence, constipation is also becoming more common; this rise has been attributed to a range of causes, such as poor diet, reduced physical activity, rapidly progressing socio-cultural changes, increasing stress levels, and inappropriate parental attitude.[7,8] In as many as a quarter of children, the problem of constipation persists into adulthood.[9] In addition, it is a clinical problem that generates high costs for healthcare: the number of children hospitalized due to constipation in the USA increased by 112% in the period 1997–2009, and the costs associated with hospitalization increased by 221.5%.[7] The importance of constipation is demonstrated by its significant impact on the quality of life of both children and their families.[3,7]

Table 1. Normal frequency of bowel movements in infants and children[1]

Age	Mean number of bowel movements per week	Mean number of bowel movements per day
0–3 months (breastfed)	5–40	2.9
0–3 months (formula-fed)	5–28	2.0
6–12 months	5–28	1.8
1–3 years	4–21	1.4
Over 3 years	3–14	1.0

Constipation can cause a number of symptoms, such as abdominal pain, bloating, painful bowel movements, lack of appetite, fecal staining of underwear, vomiting, and even intestinal obstruction and perforation.[3,8] In addition, children with constipation are more likely to suffer from urinary tract infections and bedwetting,[10] and this cohort demonstrates an increased risk of various emotional disorders, such as anxiety and irritability.[8] When left untreated, or inadequately treated, long-term constipation can adversely affect child's development.

It is believed that 5% of cases of constipation may be organic in origin, while the other 95% are functional. Prevalence rates for functional constipation in children aged 0–18 years range from 0.5% to 32.2%.[11] The prevalence varies according to age groups, with the highest prevalence reported in toddlers.[11] The differential diagnosis of constipation depending on age is presented in Table 2.[12] The bases for recognizing functional constipation according to the Rome IV criteria are presented in Table 3.[13,14]

Table 2. Differential diagnosis of constipation according to age in children[12]

Cause of constipation	Infants	Children older than 1 year
Functional constipation	rare (prevalence 3–12.1%)	more than 95% of cases (prevalence 0.5–32.2%)
Hirschsprung's disease	yes	yes
Congenital anorectal malformations	yes	rarely
Neurological disorders	yes	rarely
Encephalopathy	yes	rarely
Spinal cord abnormalities: myelomeningocele, spina bifida, tethered cord	yes	rarely
Cystic fibrosis	yes	yes
Metabolic causes: hypothyroidism, hypercalcemia, hypokalemia, diabetes insipidus	yes	yes
Heavy metal poisoning	yes	yes
Medication side effects	yes	yes
Gluten enteropathy	no	yes
Spinal cord trauma	no	yes
Neurofibromatosis	rarely	yes
Developmental delay	rarely	yes
Sexual abuse	rarely	yes

Etiology of functional constipation

Although the etiology of functional constipation is believed to be multifactorial, it remains poorly understood.[7,15–17] The basic causative factor is believed to be conscious stopping of defecation due to pain or fear, thus resulting in a "vicious circle".[15] Such withholding of stool is believed to be the cause of constipation in 50% of younger children.[7] The prolonged stasis and accumulation of fecal mass leads to an enlargement of the rectum and a decrease in anal muscle contraction efficiency, resulting in pelvic floor muscle fatigue, weakness of anal sphincter function and fecal incontinence.[7,16] Almost 30% of children with functional constipation soil their underwear.[17]

Functional constipation is typically categorized into normal transit constipation (NTC), slow transit constipation (STC), and defecatory or rectal evacuation disorders. Defecatory or rectal evacuation disorders are caused by pelvic floor dyssynergia (PFD) as well as a reduction in intra-abdominal pressure, rectal sensory perception and rectal contraction.[18]

Table 3. Rome IV criteria for functional constipation[13,14]

Criteria	Children <4 years *	Children >4 years **
Rome IV criteria	• 2 or fewer defecations per week	• 2 or fewer defecations in the toilet per week
	• history of excessive stool retention	• at least 1 episode of fecal incontinence per week
	• history of painful or hard bowel movements	• history of retentive posturing or excessive volitional stool retention
	• history of large-diameter stools	• history of painful or hard bowel movements
	• presence of a large fecal mass in the rectum	• presence of a large fecal mass in the rectum
	In toilet-trained children, the following additional criteria may be used:	• history of large-diameter stools that can obstruct the toilet
	• at least 1 episode/week of incontinence after the acquisition of toileting skills	
	• history of large-diameter stools that may obstruct the toilet	

* Must fulfil ≥2 criteria at least once per week for a minimum of 1 month with insufficient criteria for a diagnosis of irritable bowel syndrome.
** Must fulfil ≥2 criteria at least once per week for a minimum of 1 month with insufficient criteria for a diagnosis of irritable bowel syndrome. After appropriate evaluation, the symptoms cannot be fully explained by another medical condition.

Rao et al. showed that dyssynergic defecation was detected in 27–59% of patients, slow colonic transit in 3–47%, and an overlap of dyssynergic defecation and slow colonic transit or constipation-predominant irritable bowel syndrome (IBS-C) was commonly present.[19] Dyssynergic defecation is common and affects up to ½ of patients with chronic constipation.[19] The PFD prevalence varies between 11% and 74%; it is typically present in about 50% of patients. The exact prevalence of PFD in children is unknown. According to Whitehead et al., PFD is found in 25–50% of both children and adults.[20] Another study showed slow transit constipation in 60% of the children with constipation, and among them, 13% had pelvic floor dysfunction.[21] Zar-Kessler at al. completed a retrospective chart review over 15 months of patients aged 5–18 years with chronic constipation. They showed that <50% of all studied patients met criteria for dyssynergic defecation

In addition, it has been found that children with motility disorders tend to display normal or slow bowel motor function. In addition, peristalsis may be slowed throughout the entire large intestine, resulting in inefficient movement of fecal masses and stool retention. Such problems, occurring as a result of slow passage of stools though the intestine, has been reported in 25% of older children by Rajindrajith et al.[7] and in 13–25% of children by Nurko et al.[23] A relationship has also been noted between motility disorders and intestinal microbiota. In contrast, defecatory and rectal evacuation disorders do not appear to be related to gut microbiota.[18]

Constipation can also occur due to abnormalities of the anorectum region which impede excretion of fecal masses, such as spastic pelvic floor spasm.[17] In a study of 1400 adult patients with functional constipation, 65% demonstrated constipation with normal intestinal passage time and 5% with a longer time, while 30% had problems with fecal excretion from the end of the bowel.[24]

Constipation may also be caused by low fiber intake[25] and lack of physical activity.[26] In addition, obesity, closely related to physical activity and diet, is commonly associated with a higher risk of constipation,[27] although no such relationship has been confirmed.[28] Other lifestyle factors that increase the risk of constipation include poor socioeconomic conditions and low maternal education.[4] Stress has also been found to be associated with constipation in children,[29] which can lead to permanent changes in gastrointestinal motility, visceral sensitivity and hypothalamic–pituitary–adrenal dysfunction.[7,26] In addition, constipation has been found to be more common in children who receive less attention from parents, and who may get insufficient sleep.[29]

In addition to environmental factors, genetic factors may also be important in the development of constipation, since it has been shown that a positive family history has prognostic value[30]; however, no mutations in genes potentially related to functional constipation have been identified.[31]

One group of factors that has demonstrated increasing significance in constipation is that of disorders in the homeostasis of the intestinal microbiota.[2,15]

Diversity of the intestinal microbiota at different levels of the digestive tract

The intestines are the most widely colonized organ in the human body, with colonization mainly with bacteria of the *Firmicutes*, *Bacteroidetes*, *Proteobacteria*, and *Actinobacteria*, but also by fungi, viruses and archaea.[32] The total mass of bacteria in the intestine is believed to range from 1.5 kg to 2 kg. Due to the variation in their conditions and function, each section of the digestive system is characterized by a unique microbial community. The oral cavity is typically inhabited by 108 CFU (colony forming units) per gram of fecal content, with the genera

Actinobacteria, *Saccharibacteria*, *Proteobacteria* (class beta), *Fusobacteria*, *Firmicutes* (mainly *Negativicutes* and *Bacilli*), and *Bacteroides* (*Flavobacteria*, *Prevotella*) predominating. The esophagus and upper gastrointestinal tract are characterized by a relatively fast transport of gastrointestinal content, which is not conducive to the development of microorganisms; similarly, the stomach and the initial section of the small intestine have very low pH and high passage speed, and hence typically demonstrate 101–103 bacteria/gram of fecal matter, with acid-resistant *Lactobacilli* predominating. In comparison, a more diverse microbiota is found in the distal section of the small intestine, where 105 bacteria/gram of fecal matter is typically found. The most numerous, and most active, microorganism complex can be found in the large intestine, with 1011–1012 microbes/gram of fecal content; this higher number is most likely due to the slower passage of feces.[32] This region has been shown to be dominated by anaerobic bacteria.[33]

The significance of the microbiota of the digestive tract for health

The microbiota creates a unique ecosystem that performs many functions important for maintaining homeostasis, i.e., it is responsible for the energy balance of the body,[34] and is involved in digestion, fermentation of nutrients and the storage of energy obtained from food by transformation to short-chain fatty acids (SCFAs).[34] It is also responsible for the production of polyamines and vitamins B and K, as well as for mineral management.[34] The microbiota also plays an important role in the proper functioning of the immune system.[35] By releasing neurotransmitters and neuromodulators, such as dopamine, noradrenaline, acetylcholine, gamma aminobutyric acid, and serotonin, it also affects the function of the brain–gut axis.[36] It has been demonstrated that direct contact of intestinal epithelial cells with the probiotic *Lactobacillus acidophilus* induces the expression of opioid and cannabinoid receptors in the intestine and is involved in the modulation of visceral pain perception.[37]

Although previous research has examined the significance of microbiota in a range of specific diseases, including allergic diseases,[38] mental and neurodevelopmental disorders,[39,40] diabetes, obesity, hypertension, cardiovascular disorders,[41] coeliac disease, rheumatoid arthritis, inflammatory bowel disease (IBD), and colorectal cancer,[8,35] the largest number of studies concerns functional disorders of the gastrointestinal tract.[8] It is also important to note that although the microbiomes of various body compartments have been studied, most previous research has focused on the digestive tract.[8]

It is possible that the microbiota may play a direct or indirect role in the pathogenesis of functional constipation by influencing peristalsis, or by a relationship with diet and physical activity.

The pathomechanisms behind the relationship between intestinal microbiota, peristaltic disorders and constipation

Changes in the composition of the microbiota play an important role in the pathogenesis of many gastrointestinal functional disorders, including constipation. It has been observed that the composition of the gastrointestinal microbiota of individuals with constipation differs considerably from those without.[6,15,39,40] Constipation is a disorder resulting from changes in the peristalsis of the digestive tract. The function of the intestine is maintained by a number of factors that play significant roles, including the nervous system, the immune system, bile acid metabolism, and the microbiota of the digestive tract. The cause–effect relationship between alterations in gut microbiota and gut dysmotility remains unclear. Some changes in the composition of the gut microbiota may be secondary to slower gastrointestinal transit.

In addition, the microbiota can influence intestinal peristalsis by various mechanisms described below.

Changes in pH in the intestine

Disruptions in the normal intestinal microbiota can result in changes in the fermentation of dietary fiber to SCFA, preventing the effective control of pH in the intestine and thus disrupting its peristalsis. In addition, abnormal pH prevents the development of certain components of the microbiota, particularly *Lactobacillus* and *Bifidobacterium*. Therefore, the composition of the microbiota both influences, and is influenced by, constipation.[8,16]

Regulation of butyric acid concentration

The proper composition of the microbiota maintains the concentration of butyric acid in the colon at an optimal level, maintaining the correct rhythm of bowel movements. The correct concentration of butyrate facilitates contractions of the smooth muscle in the colon, thus supporting intestinal motility and preventing constipation. However, at excessive concentrations, it inhibits muscle contraction and slows peristalsis. In addition, excessive concentrations of butyrate may favor the development of constipation by inhibiting mucin secretion from intestinal goblet cells, and decreasing stool volume by disturbing water and electrolyte absorption. This explains the occurrence of smaller numbers of *Prevotella* species (including *P. veroralis*, *P. corporis* and *P. ruminicola*), which do not produce butyric acid, in patients with constipation, and the greater number of butyric acid-producing *Coprococcus*, *Roseburia* and *Faecalibacterium*. Interestingly, while the presence of bacteria that produce butyrate in the intestinal mucosa

(e.g., *Faecalibacterium*) is associated with a higher likelihood of constipation, the presence of those that produce butyric acid in the feces (e.g., *Faecalibacterium*, *Roseburia* and *Coprococcus*) actually increase the rate of peristalsis in the colon.[39]

Production of methane in the intestinal lumen

Disturbances in the composition of the microbiota influences the production of methane in the intestinal lumen, causing intestinal distension, reduction of smooth muscle contractility and a slowing of peristalsis.[42]

Modulation of gene expression

Experimental studies in mice have shown that microbes can modulate the expression of genes involved in regulating motility: colonization of *Bacteroides thetaiotaomicron* resulted in an increase in mRNA encoding the L-glutamate transporter, glutamate decarboxylase (which converts L-glutamate to gamma-aminobutyric acid), synaptobrevin binding protein (which is involved in the release of neurotransmitters), and intestinal g-actin. These findings suggest that the microbiota may directly influence the intestinal nervous system and therefore motility.[43] In addition, SCFA produced by intestinal microbiota was observed to induce a phase of muscle contraction dependent on GPR41 (G protein-coupled receptor 41) level, with the highest affinity being observed for propionate, followed by butyrate and acetate. GPR41, also known as free fatty acid receptor 3 (FFAR3), is a free fatty acid receptor coupled to a G protein, encoded by the *FFAR3* gene. GPR41 has an affinity to both ethanoic and propionic acid, and a lower affinity for butyric acid. To a small extent, it also recognizes caproic and valeric acid.[25]

Neuroendocrine factors

The microbiota of the digestive tract affects peristalsis by stimulating the sympathetic nervous system and relaxing the smooth muscle of the intestine. Microorganisms stimulate cholinergic pathways directly through their ability to synthesize neurotransmitters. It has been found that *Lactococcus*, *Streptococcus*, *Escherichia*, and *Candida* effectively increase the concentration of serotonins, *Lactobacillus* and *Bifidobacterium* increase gamma-aminobutyric acid, and *Bacillus* spp., *Escherichia* spp. and *Saccharomyces* spp. increase norepinephrine. The gastrointestinal microbiota can also stimulate cholinergic pathways indirectly through the synthesis of metabolites such as SCFAs (e.g., butyrate), thus stimulating the release of serotonin. It has also been shown that *Faecalibacterium*, *Roseburia* and *Coprococcus* produce butyrate, and thus increase serotonin levels.[2,39]

Role in bile acid metabolism

The intestinal microbiota can also affect intestinal motility by modulating the composition and size of the bile acid pool. The microorganisms colonizing the colon participate in the deconjugation and dehydroxylation of primary bile acids (cholic and chenodeoxycholic acid) which are absorbed in the ileum. Secondary bile acids, such as deoxycholic and lithocholic acid, are formed. The conjugation of primary bile acids in the large intestine is facilitated by bacterial 7α-dehydroxylase, the activity of which has been observed in *Clostridium leptum*, *Clostridium bifermentans*, *Clostridium sordellii*, *Eubacterium* spp., *Escherichia coli*, and *Bacteroides* spp.

Lithocholic acid, the most potent TGR5 membrane receptor activator conjugated to G protein, is also involved in the regulation of metabolism. Studies on mice overexpressing TGR5 identified a 2.2-fold reduction in colonic transit time and a 2.6-fold increase in the number of bowel movements compared to normal mice.

It is also possible that intestinal motility is affected by cholic acid, which is found to be present at higher levels in obese people. Obesity also influences the specific composition of the intestinal microbiota; e.g., obese people tend to demonstrate a greater abundance of *Firmicutes* compared to *Bacteroidetes*, which is associated with a faster peristalsis.[39]

The influence of particular bacterial strains on peristalsis and the prevention of constipation

A great deal of research has been conducted to determine the effect of individual bacterial strains on intestinal motility and the occurrence of constipation, and the results are varied and often contradictory. These differences may result from the fact that children with constipation constitute a highly heterogeneous phenotypical group, and the fact that previous studies use a wide range of diagnostic criteria, methods of patient classification, patient diets, and research methods used to identify the microbiome. Unfortunately, research into microbiota composition has long been limited by the need to use traditional bacterial culture. However, the recent development of *16S rRNA* gene pyrosequencing and specific gene primers, and the ability to assess the DNA sequence of each taxon in the intestinal microbiome, has provided a clearer view of the molecular basis of constipation.

Changes in intestinal barrier permeability and systemic resistance observed in adults with constipation have been associated with the presence of a reduced number of *Bifidobacteria*, *Lactobacillus* and *Prevotella.*[40]

A study of the fecal microbiota in 50 adult female patients (25 with constipation and 25 without) by *16S rRNA* sequencing found that the fecal microbiota profile was

associated with colonic transit time: the presence of *Firmicutes* bacteria (*Faecalibacterium*, *Lactococcus* and *Roseburia*) was correlated with faster digestive passage.[39] Another study found significantly reduced numbers of *Bacteroides fragilis*, *Bacteroides ovatus*, *Bifidobacterium longum*, and *Alistipes finegoldi*, as well as an increased number of *Parabacteroides* species, in 76 children aged 4–18 years with functional constipation.[15] Another study of children aged 6–36 months found a lower number of *Lactobacillus* bacteria per milligram of feces in a group of 39 children with constipation compared to a group of 40 children without constipation; however, the number of *Bifidobacterium* did not differ between the 2 groups.[6]

Another study based on *16S rRNA* gene pyrosequencing compared the microbiological composition of feces of obese children and the occurrence of constipation. It was found that the number of *Bacteroides* was significantly reduced in children with constipation; this was mainly accounted for by a reduced number of *Prevotella* and an increased number of *Firmicutes* in the children without constipation. The children with obesity did not demonstrate any changes in the *Lactobacillus* or *Bifidobacteria* fractions.[2] It is worth emphasizing that obesity is characterized by a particular microbiota composition of the digestive tract, and that it is possible that such changes may explain the greater likelihood of functional constipation in obese children.[2]

According to Vandeputte et al., stool consistency is strongly associated with the composition and richness of the intestinal microbiota.[44] Stool consistency, assessed using the Bristol stool scale (where a low score indicates hard stool and slow passage through the colon, and a high score indicates loose consistency and a short passage through the colon), was negatively correlated with species richness and positively related to the *Bacteroides* : *Firmicutes* ratio.[44]

Children with functional constipation (mean age: 9.5 years) had a significantly higher level of *Clostridium* and *Bifidobacterium* species than healthy subjects (mean age: 7.9 years).[46] In this study, it was also proved that *C. sporogenes*, *C. paraputrificum*, *C. fallax*, and *C. innocuum* were dominant among the *Clostridium* species.[46]

Reports of gut microbiota in functional constipation according to age

Reports of gut microbiota in functional constipation in relation to age are inconsistent and there is currently no consensus as to which gut microbiota are involved, mainly because the gut microbiota naturally changes according to age.[45] There are some reports which analyzed gut microbiota in children and in adults with functional constipation. Zhu et al.[2] used *16S rRNA* gene pyrosequencing to demonstrate that children with functional constipation (mean age: 11.8 years) had a significantly lower level of *Bacteroidetes*, in particular *Prevotella*, and an increased level of several species of *Firmicutes*, including *Lactobacillus*. They also demonstrated that the levels of *Lactobacillus* and *Bifidobacteria* species were not reduced. Khalif et al. analyzed gut microbiota in adults with functional constipation and showed a reduced level of *Bifidobacterium*, *Lactobacillus*, *Bacteroides* and *Clostridium* species, and an increased level of *Enterobacteriaceae*, such as *Escherichia coli*, as well as *Staphylococcus aureus* and fungi.[40] In another study, it was demonstrated that adult patients with functional constipation had a significantly lower level of *Bifidobacterium* and *Bacteroides*.[47] Parthasarathy et al. demonstrated that although no difference was present in the amount of bacterial species at the genus level between functional constipation adults and healthy control groups, patients with constipation, including those with IBS, had increased levels of *Bacteroidetes* in their mucosa.[39]

The results of the studies are varied and do not allow the determination of patterns of gut microbiota in children as opposed to adults. More studies are required to reach any conclusions.

The influence of diet on the composition of the gut microbiota and the occurrence of constipation

Eating habits play an important role in the etiology of constipation. Diet affects the occurrence of constipation directly, by directly altering stool weight and water content, therefore potentially slowing passage through the intestines and preventing excretion, as well as indirectly, by modulating the composition of the intestinal microbiota.

Various elements of the diet (discussed below) can affect the occurrence of functional constipation.

Effect of fiber consumption

Consumption of low levels of fiber-rich products (water-soluble and water-insoluble fiber) such as vegetables and fruit, can significantly hasten the pathogenesis of functional constipation. Water-insoluble fiber, such as cellulose and lignans that build plant cell walls, absorb water. This causes the stool to expand and soften, making bowel movements easier and more frequent. Soluble fiber includes pectins, mucilages and gums. Fiber cannot be hydrolyzed directly by the human gut: intestinal microbiota, more specifically saccharolytic bacteria such as *Bifidobacterium* and *Lactobacillus* spp., are needed to ferment dietary water-soluble fiber to SCFAs and lactic acid, thus reducing intestinal pH.[6] Low intestinal pH stimulates smooth muscle and increases the speed of peristalsis, thus reducing

intestinal transit time. In addition, low intestinal pH promotes the growth of beneficial intestinal microbes, especially *Bifidobacterium* and *Lactobacillus* spp. Therefore, a diet with the correct water-soluble fiber content facilitates colonization of the intestines by live microorganisms. These properties of soluble fiber are used in the treatment of patients with functional constipation. Children consuming higher amounts of fruit and vegetables tend to have higher numbers of *Bifidobacterium* in the intestine, and those who do not consume as much are more likely to suffer from constipation.[6]

It has also been shown that higher fiber intake is significantly associated with 4 or more bowel movements per week. In addition, regular consumption of potatoes, legumes, vegetables, and fruit among children has been shown to reduce the incidence of infrequent bowel movements, i.e., less than 3 bowel movements per week.[48] De Filippo et al. report that children with a high fiber content in their diet tend to have microbiomes richer in *Bifidobacteria* than children on lower fiber diets.[49] Similar results were obtained by Bernal et al.[50] It has been proposed that children on a low-fiber diet are more likely to suffer from constipation because such a diet hinders colonization of the intestines by beneficial microorganisms.[6]

Dietary advice currently recommends consuming an optimal amount of fiber and fluids, and advises against excessive fibre.[51] A meta-analysis conducted in 2017 found insufficient evidence for the inclusion of fiber supplementation in the treatment of constipation in children and adolescents.[52]

Impact of dairy products and sweets

Research has found that high consumption of simple sugars, fatty acids and proteins in children aged 3–18 years is associated with low *Lactobacillus* content in feces and a frequent occurrence of constipation. Cow's milk protein intake has been positively associated with intestinal constipation in children aged 3–12 years.[53] Kocaay et al. also note a positive relationship between the occurrence of constipation and cow's milk consumption exceeding 250 mL per day.[54] The mechanism behind this correlation has not been fully explained. Protein intake is thought to modulate the intestinal microbiota and it has been proposed that the greater occurrence of constipation observed in such children may be associated with the fact that children who consume larger amounts of cow's milk and sweets tend to consume less fiber-rich products.[54]

The data on the relationship between cow's milk protein allergy (CMPA) and the development of functional constipation are inconsistent. It has been shown that children with CMPA are significantly more likely to show symptoms of gastrointestinal disorders meeting the Rome IV criteria (45%) compared to controls without CMPA (15%). In addition, conventional treatment of constipation combined with elimination of cow's milk protein was found to be more effective than therapy without an elimination diet.[55] Iacono et al. reported that 68% of children with chronic constipation demonstrated improvement after eliminating cow's milk from the diet; however, all children developed constipation after re-inclusion of milk into the diet.[56] Daher et al. also reported a relationship between CMPA and constipation.[57] However, no such relationship was observed in other studies: Simeone et al. found that the incidence of atopy among children with functional constipation was similar to that in the general population, and that constipation was not improved by a four-week elimination of cow's milk protein from the diet.[58]

Impact of fat intake

Vakili at al. demonstrated that a high dietary saturated fat intake is associated with a significant increase in the prevalence of constipation.[59] The authors showed that after a high-fat meal, healthy people demonstrate a lengthening phase of the peristaltic waves of the intestine. In studies on rodents, a high-fat diet was associated with lower availability of serotonin in the large intestine and dysbiosis, which resulted in delayed colon motility.[48] A high-fat diet delayed intestinal transit, which was associated with increased apoptosis and loss of colonic myenteric neurons.[60,61] Saturated fatty acids such as palmitate have also been shown to cause apoptosis of enteric neuronal cells,[60] while unsaturated fatty acids such as oleic acid stimulate peristalsis and prevent neuronal damage.[61] Sayegh et al. demonstrated that intra-intestinal infusion of oleate has been shown to activate myenteric neurons in the duodenum and jejunum, but not the ileum.[62]

Physical activity, functional constipation and the microbiome

Constipation may be caused by low physical activity. Physical activity is thought to stimulate intestinal peristalsis, thus shortening the duration of food passage through the colon and rectum.[63] This effect has been attributed to hormonal changes.[64] Physical activity affects the level of endogenous sex hormones, which regulate the passage of food through the colon. However, fluctuations of sex hormone levels do not seem to significantly affect colonic motility in children before puberty. Reduced progesterone levels in postmenopausal women has been shown to shorten the time for food to pass through the digestive tract.[65] Transient variations in blood supply to the gastrointestinal tract and changes in the balance between sympathetic and parasympathetic innervation have also been shown to affect digestive transit.[70]

Driessen et al. report that increased physical activity (as measured by an accelerometer) was associated with a reduced risk of functional constipation in Dutch preschool children.[66] Similarly, high levels of physical activity

have been found to be significantly associated with a lower rick of constipation in a group of 5000 Japanese preschoolers,[67] and in 234 Romanian children aged 4–18 years.[68] In addition, an analysis of 14,626 Taiwanese teenagers found that encouraging greater physical activity can be helpful in preventing constipation,[69] and insufficient physical activity, i.e., less than 1 h of activity per day, and an excessively sedentary lifestyle, i.e., over 4 h per day, were associated with constipation in a group of 33,692 Hong Kong students.[3]

Currently, a study involving 338 Japanese adults examining whether a decrease in physical activity may contribute to the development of constipation by disturbing the gastrointestinal microbiota is ongoing. The available results indicate a statistically significant difference in the mean frequency of defecation (i.e., less than once per day or less than once per week) between more and less physically active people, with activity measured throughout the day using an accelerometer: intestinal peristalsis was about 10% faster in older people who completed 7000 steps per day or spent 15 min per day engaged in activity >3 MET (metabolic equivalents) compared with those who completed <7000 steps/day or engaged in <15 min/day activity >3 MET. However, no relationship was found between physical activity and the composition of the intestinal microbiota. The authors conclude that moderate daily physical activity reduces the risk of infrequent bowel movements mainly through mechanical stimulation of intestinal motility, without changing the composition of the microbiota.[70]

It has also been found that the structure and abundance of butyrate-producing microorganisms in the colon did not change significantly after cessation of physical activity. This may suggest that the intestinal microbiota is resistant to short-term changes in host level of exercise or hypoxia. Nevertheless, defecation difficulties were observed shortly after cessation of physical activity, most probably due to slowed intestinal motility.[71]

Conclusions

The wide prevalence and the growing problem of constipation suggests that existing therapeutic methods require improvement; therefore, new therapeutic possibilities are constantly being sought. The exiting literature indicates that the structure of the intestinal microbiota may be associated with the occurrence of functional constipation, hence new therapeutic solutions are being sought in the modulation of microbiota. Further research is needed to clarify the composition of the intestinal microbiota in patients with functional constipation and to determine its importance in the pathogenesis of the disease.

ORCID iDs

Monika Kwiatkowska https://orcid.org/0000-0002-7057-3248
Aneta Krogulska https://orcid.org/0000-0002-5280-1876

References

1. Biggs WS, Dery WH. Evaluation and treatment of constipation in infants and children. *Am Fam Physician*. 2006;73(3):469–477. PMID:16477894
2. Zhu L, Liu W, Alkhouri R, et al. Structural changes in the gut microbiome of constipated patients. *Physiol Genomics*. 2014;46(18):679–686. doi:10.1152/physiolgenomics.00082.2014
3. Huang R, Hu J. Positive effect of probiotics on constipation in children: A systematic review and meta-analysis of six randomized controlled trials. *Front Cell Infect Microbiol*. 2017;7:153. doi:10.3389/fcimb.2017.00153
4. Pawłowska K, Umławska W, Iwańczak B. A link between nutritional and growth states in pediatric patients with functional gastrointestinal disorders. *J Pediatr*. 2018;199:171–177. doi:10.1016/j.jpeds.2018.02.069
5. Lewis ML, Palsson OS, Whitehead WE, van Tilburg MAL. Prevalence of functional gastrointestinal disorders in children and adolescents. *J Pediatr*. 2016;177:39–43.e3. doi:10.1016/j.jpeds.2016.04.008
6. Gomes de Moraes J, Farias de Almeida Motta ME, Ferraz de Sa Beltrão M, Salviano TL, Alves Pontes da Silva G. Fecal microbiota and diet of children with chronic constipation. *Int J Pediatr*. 2016;2016:6787269. doi:10.1155/2016/6787269
7. Rajindrajith S, Devanarayana NM, Crispus Perera BJ, Benninga MA. Childhood constipation as an emerging public health problem. *World J Gastroenterol*. 2016;22(30):6864–6875. doi:10.3748/wjg.v22.i30.6864
8. Huang L, Zhu Q, Qu X, Qin H. Microbial treatment in chronic constipation. *Sci China Life Sci*. 2018;61(7):744–752. doi:10.1007/s11427-017-9220-7
9. Bongers MEJ, van Wijk MP, Reitsma JB, Benninga MA. Long-term prognosis for childhood constipation: Clinical outcomes in adulthood. *Pediatrics*. 2010;126(1):e156–e162. doi:10.1542/peds.2009-1009
10. Dehghani SM, Basiratnia M, Matin M, Hamidpour L, Haghighat M, Imanieh MH. Urinary tract infection and enuresis in children with chronic functional constipation. *Iran J Kidney Dis*. 2013;7(5):363–366. PMID:24072148
11. Steutel NF, Zeevenhooven J, Scarpato E, et al. Prevalence of functional gastrointestinal disorders in European infants and toddlers. *J Pediatr*. 2020;221:107–114. doi:10.1016/j.jpeds.2020.02.076
12. Fontana M, Bianchi C, Cataldo F, et al. Bowel frequency in healthy children. *Acta Paediatr Scand*. 1989;78(5):682–684. doi:10.1111/j.1651-2227.1989.tb11126.x
13. Benninga MA, Nurko S, Faure C, Hyman PE, St. James Roberts I, Schechter NL. Childhood functional gastrointestinal disorders: Neonate/toddler. *Gastroenterology*. 2016;150(6):1443–1455.e2. doi:10.1053/j.gastro.2016.02.016
14. Hyams JS, Di Lorenzo C, Saps M, Shulman RJ, Staiano A, van Tilburg M. Childhood functional gastrointestinal disorders: Child/adolescent. *Gastroenterology*. 2016;150(6):1456–1468.e2. doi:10.1053/j.gastro.2016.02.015
15. de Meij TGJ, de Groot EFJ, Eck A, et al. Characterization of microbiota in children with chronic functional constipation. *PLoS One*. 2016;11(10):e0164731. doi:10.1371/journal.pone.0164731
16. van Mill MJ, Koppen IJN, Benninga MA. Controversies in the management of functional constipation in children. *Curr Gastroenterol Rep*. 2019;21(6):23. doi:10.1007/s11894-019-0690-9
17. Amendola S, De Angelis P, Dall'Oglio L, di Abriola GF, Di Lorenzo M. Combined approach to functional constipation in children. *J Pediatr Surg*. 2003;38(5):819–823. doi:10.1016/jpsu.2003.50174
18. Ohkusa T, Koido S, Nishikawa Y, Sato N. Gut microbiota and chronic constipation: A review and update. *Front Med*. 2019;6:19. doi:10.3389/fmed.2019.00019
19. Rao SSC, Patcharatrakul T. Diagnosis and treatment of dyssynergic defecation. *J Neurogastroenterol Motil*. 2016;22(3):423–435. doi:10.5056/jnm16060
20. Whitehead WE, Wald A, Diamant NE, Enck P, Pemberton JH, Rao SSC. Functional disorders of the anus and rectum. *Gut*. 1999;45(Suppl 2):ii55–ii59. doi:10.1136/gut.45.2008.ii55
21. Rajindrajith S, Devanarayana NM. Constipation in children: Novel insight into epidemiology, pathophysiology and management. *J Neurogastroenterol Motil*. 2011;17(1):35–47. doi:10.5056/jnm.2011.17.1.35
22. Zar-Kessler C, Kuo B, Cole E, Benedix A, Belkind-Gerson J. Benefit of pelvic floor physical therapy in pediatric patients with dyssynergic defecation constipation. *Dig Dis*. 2019;37(6):478–485. doi:10.1159/000500121

23. Nurko S, Scott SM. Coexistence of constipation and incontinence in children and adults. *Best Pract Res Clin Gastroenterol*. 2011;25(1): 29–41. doi:10.1016/j.bpg.2010.12.002
24. Nullens S, Nelsen T, Camilleri M, et al. Regional colon transit in patients with dys-synergic defaecation or slow transit in patients with constipation. *Gut*. 2012;61(8):1132–1139. doi:10.1136/gutjnl-2011-301181
25. Morais MB, Vítolo MR, Aguirre ANC, Fagundes-Neto U. Measurement of low dietary fiber intake as a risk factor for chronic constipation in children. *J Pediatr Gastroenterol Nutr*. 1999;29(2):132–135. doi:10.1097/00005176-199908000-00007
26. Yamada M, Sekine M, Tatsuse T. Psychological stress, family environment, and constipation in Japanese children: The Toyama Birth Cohort Study. *J Epidemiol*. 2019;29(6):220–226. doi:10.2188/jea.JE20180016
27. vd Baan-Slootweg OH, Liem O, Bekkali N, et al. Constipation and colonic transit times in children with morbid obesity. *J Pediatr Gastroenterol Nutr*. 2011;52(4):442–445. doi:10.1097/MPG.0b013e3181ef8e3c
28. Koppen IJN, Velasco-Benítez CA, Benninga MA, Di Lorenzo C, Saps M. Is there an association between functional constipation and excessive bodyweight in children? *J Pediatr*. 2016;171:178–182.e1. doi:10.1016/j.jpeds.2015.12.033
29. Tam YH, Li AM, So HK, et al. Socioenvironmental factors associated with constipation in Hong Kong children and Rome III Criteria. *J Pediatr Gastroenterol Nutr*. 2012;55(1):56–61. doi:10.1097/MPG.0b013e31824741ce
30. Ostwani W, Dolan J, Elitsur Y. Familial clustering of habitual constipation: A prospective study in children from West Virginia. *J Pediatr Gastroenterol Nutr*. 2010;50(3):287–289. doi:10.1097/MPG.0b013e3181a0a595
31. Peeters B, Benninga MA, Hennekam RC. Childhood constipation; An overview of genetic studies and associated syndromes. *Best Pract Res Clin Gastroenterol*. 2011;25(1):73–88. doi:10.1016/j.bpg.2010.12.005
32. Simrén M, Barbara G, Flint HJ, et al. Intestinal microbiota in functional bowel disorders: A Rome Foundation report. *Gut*. 2013;62(1):159–176. doi:10.1136/gutjnl-2012-302167
33. Mezzasalma V, Manfrini E, Ferri E, et al. A randomized, double-blind, placebo-controlled trial: The efficacy of multispecies probiotic supplementation in alleviating symptoms of irritable bowel syndrome associated with constipation. *Biomed Res Int*. 2016;2016:4740907. doi:10.1155/2016/4740907
34. Ramakrishna BS. Role of the gut microbiota in human nutrition and metabolism: Role of the gut microbiota. *J Gastroenterol Hepatol*. 2013; 28:9–17. doi:10.1111/jgh.12294
35. de Oliveira GLV, Leite AZ, Higuchi BS, Gonzaga MI, Mariano VS. Intestinal dysbiosis and probiotic applications in autoimmune diseases. *Immunology*. 2017;152(1):1–12. doi:10.1111/imm.12765
36. Asano Y, Hiramoto T, Nishino R, et al. Critical role of gut microbiota in the production of biologically active, free catecholamines in the gut lumen of mice. *Am J Physiol Gastrointest Liver Physiol*. 2012; 303(11):G1288–G1295. doi:10.1152/ajpgi.00341.2012
37. Rousseaux C, Thuru X, Gelot A, et al. *Lactobacillus acidophilus* modulates intestinal pain and induces opioid and cannabinoid receptors. *Nat Med*. 2007;13(1):35–37. doi:10.1038/nm1521
38. Pothmann A, Illing T, Wiegand C, Hartmann AA, Elsner P. The microbiome and atopic dermatitis: A review. *Am J Clin Dermatol*. 2019;20(6): 749–761. doi:10.1007/s40257-019-00467-1
39. Parthasarathy G, Chen J, Chen X, et al. Relationship between microbiota of the colonic mucosa vs feces and symptoms, colonic transit, and methane production in female patients with chronic constipation. *Gastroenterology*. 2016;150(2):367–379.e1. doi:10.1053/j.gastro.2015.10.005
40. Khalif I, Quigley E, Konovitch E, Maximova I. Alterations in the colonic flora and intestinal permeability and evidence of immune activation in chronic constipation. *Dig Liver Dis*. 2005;37(11):838–849. doi:10.1016/j.dld.2005.06.008
41. Tang WHW, Kitai T, Hazen SL. Gut microbiota in cardiovascular health and disease. *Circ Res*. 2017;120(7):1183–1196. doi:10.1161/CIRCRESAHA.117.309715
42. Ojetti V, Petruzziello C, Migneco A, Gnarra M, Gasbarrini A, Franceschi F. Effect of *Lactobacillus reuteri* (DSM 17938) on methane production in patients affected by functional constipation: A retrospective study. *Eur Rev Med Pharmacol Sci*. 2017;21(7):1702–1708. PMID: 28429333
43. Hooper LV. Molecular analysis of commensal host–microbial relationships in the intestine. *Science*. 2001;291(5505):881–884. doi:10.1126/science.291.5505.881
44. Vandeputte D, Falony G, Vieira-Silva S, Tito RY, Joossens M, Raes J. Stool consistency is strongly associated with gut microbiota richness and composition, enterotypes and bacterial growth rates. *Gut*. 2016;65(1):57–62. doi:10.1136/gutjnl-2015-309618
45. Yatsunenko T, Rey FE, Manary MJ, et al. Human gut microbiome viewed across age and geography. *Nature*. 2012;486(7402):222–227. doi:10.1038/nature11053
46. Zoppi G, Cinquetti M, Luciano A, Benini A, Muner A, Minelli EB. The intestinal ecosystem in chronic functional constipation. *Acta Paediatr*. 2007;87(8):836–841. doi:10.1111/j.1651-2227.1998.tb01547.x
47. Kim SE, Choi SC, Park KS, et al. Change of fecal flora and effectiveness of the short-term VSL#3 probiotic treatment in patients with functional constipation. *J Neurogastroenterol Motil*. 2015;21(1):111–120. doi:10.5056/jnm14048
48. Fujitani A, Sogo T, Inui A, Kawakubo K. Prevalence of functional constipation and relationship with dietary habits in 3- to 8-year-old children in Japan. *Gastroenterol Res Pract*. 2018;2018:3108021. doi:10.1155/2018/3108021
49. De Filippo C, Cavalieri D, Di Paola M, et al. Impact of diet in shaping gut microbiota revealed by a comparative study in children from Europe and rural Africa. *Proc Nat Acad Sci*. 2010;107(33):14691–14696. doi:10.1073/pnas.1005963107
50. Bernal MJ, Periago MJ, Martínez R, et al. Effects of infant cereals with different carbohydrate profiles on colonic function: Randomised and double-blind clinical trial in infants aged between 6 and 12 months. Pilot study. *Eur J Pediatr*. 2013;172(11):1535–1542. doi:10.1007/s00431-013-2079-3
51. Southwell BR. Treatment of childhood constipation: A synthesis of systematic reviews and meta-analyses. *Exp Rev Gastroenterol Hepatol*. 2020;14(3):163–174. doi:10.1080/17474124.2020.1733974
52. Piccoli de Mello P, Eifer DA, Daniel de Mello E. Use of fibers in childhood constipation treatment: Systematic review with meta-analysis. *J Pediatr (Rio J)*. 2018;94(5):460–470. doi:10.1016/j.jped.2017.10.014
53. Crowley E, Williams L, Roberts T, Dunstan R, Jones P. Does milk cause constipation? A crossover dietary trial. *Nutrients*. 2013;5(1):253–266. doi:10.3390/nu5010253
54. Kocaay P, Egritas O, Dalgic B. Normal defecation pattern, frequency of constipation and factors related to constipation in Turkish children 0–6 years old. *Turk J Gastroenterol*. 2011;22(4):369–375. doi:10.4318/tjg.2011.0238
55. Feng BW, Fu SM, Zhang QS, et al. Influence of cow's milk protein allergy on the diagnosis of functional gastrointestinal diseases based on the Rome IV standard in infants and young children [in Chinese]. *Zhongguo Dang Dai Er Ke Za Zhi*. 2018;20(1):56–59. doi:10.7499/j.issn.1008-8830.2018.01.012
56. Iacono G, Cavataio F, Montalto G, et al. Intolerance of cow's milk and chronic constipation in children. *N Engl J Med*. 1998;339(16):1100–1104. doi:10.1056/NEJM199810153391602
57. Daher S, Tahan S, Sole D, et al. Cow's milk protein intolerance and chronic constipation in children. *Pediatr Allergy Immunol*. 2001;12(6): 339–342. doi:10.1034/j.1399-3038.2001.0o057.x
58. Simeone D, Miele E, Boccia G, Marino A, Troncone R, Staiano A. Prevalence of atopy in children with chronic constipation. *Arch Dis Childhood*. 2008;93(12):1044–1047. doi:10.1136/adc.2007.133512
59. Taba Taba Vakili S, Nezami BG, Shetty A, Chetty VK, Srinivasan S. Association of high dietary saturated fat intake and uncontrolled diabetes with constipation: Evidence from the National Health and Nutrition Examination Survey. *Neurogastroenterol Motil*. 2015;27(10): 1389–1397. doi:10.1111/nmo.12630
60. Nezami BG, Mwangi SM, Lee JE, et al. MicroRNA 375 mediates palmitate-induced enteric neuronal damage and high-fat diet-induced delayed intestinal transit in mice. *Gastroenterology*. 2014;146(2): 473–483.e3. doi:10.1053/j.gastro.2013.10.053
61. Mushref MA, Srinivasan S. Effect of high fat-diet and obesity on gastrointestinal motility. *Ann Transl Med*. 2013;1(2):14. doi:10.3978/j.issn.2305-5839.2012.11.01
62. Sayegh AI, Covasa M, Ritter RC. Intestinal infusions of oleate and glucose activate distinct enteric neurons in the rat. *Autonom Neurosci*. 2004;115(1–2):54–63. doi:10.1016/j.autneu.2004.08.006

63. De Schryver AM, Keulemans YC, Peters HP, et al. Effects of regular physical activity on defecation pattern in middle-aged patients complaining of chronic constipation. *Scand J Gastroenterol*. 2005;40(4): 422–429. doi:10.1080/00365520510011641
64. Mugie SM, Benninga MA, Di Lorenzo C. Epidemiology of constipation in children and adults: A systematic review. *Best Pract Res Clin Gastroenterol*. 2011;25(1):3–18. doi:10.1016/j.bpg.2010.12.010
65. Chan MF, Dowsett M, Folkerd E, et al. Usual physical activity and endogenous sex hormones in postmenopausal women: The European Prospective Investigation into Cancer – Norfolk Population Study. *Cancer Epidemiol Biomarkers Prevent*. 2007;16(5):900–905. doi:10.1158/1055-9965.EPI-06-0745
66. Driessen LM, Jong JCK, Wijtzes A, et al. Preschool physical activity and functional constipation: The Generation R Study. *J Pediatr Gastroenterol Nutr*. 2013;57(6):768–774. doi:10.1097/MPG.0b013e3182a313fc
67. Asakura K, Masayasu S, Sasaki S. Dietary intake, physical activity, and time management are associated with constipation in preschool children in Japan. *Asia Pac J Clin Nutr*. 2017;26(1):118–129. doi:10.6133/apjcn.112015.02
68. Olaru C, Diaconescu S, Trandafir L, et al. Some risk factors of chronic functional constipation identified in a pediatric population sample from Romania. *Gastroenterol Res Pract*. 2016;2016:3989721. doi:10.1155/2016/3989721
69. Chien LY, Liou YM, Chang P. Low defaecation frequency in Taiwanese adolescents: Association with dietary intake, physical activity and sedentary behavior. *J Paediatr Child Health*. 2011;47(6):381–386. doi:10.1111/j.1440-1754.2010.01990.x
70. Aoyagi Y, Amamoto R, Park S, et al. Independent and interactive effects of habitually ingesting fermented milk products containing *Lactobacillus casei* strain Shirota and of engaging in moderate habitual daily physical activity on the intestinal health of older people. *Front Microbiol*. 2019;10:1477. doi:10.3389/fmicb.2019.01477
71. Šket R, Treichel N, Debevec T, et al. Hypoxia and inactivity related physiological changes (constipation, inflammation) are not reflected at the level of gut metabolites and butyrate producing microbial community: The PlanHab Study. *Front Physiol*. 2017;8:250. doi:10.3389/fphys.2017.00250